

# COMPUTED TOMOGRAPHY *of* PROSTHETIC HEART VALVES



Jesse Habets

## **Computed Tomography of Prosthetic Heart Valves**

PhD thesis, Utrecht University, the Netherlands

ISBN/EAN: 978-90-393-5806-1

© Jesse Habets, Utrecht, 2012

The copyright of the articles that have been published or accepted for publication has been transferred to the respective journals

The research in this thesis was conducted at the departments of Cardiology, Cardiothoracic surgery and Radiology of the University Medical Center Utrecht, the Netherlands and the Academic Medical Center, Amsterdam, the Netherlands. It was financially supported by the department of Radiology of the University Medical Center Utrecht and by a grant of the Dutch Heart Foundation (DHF- 2009B014).

Lay-out: Karin van Rijnbach

Cover art: ©Kay Habets, Maastricht, 2012

Printed by: PrintSupport4U, Meppel, the Netherlands

# COMPUTED TOMOGRAPHY *of* PROSTHETIC HEART VALVES

CT van kunsthartkleppen

(met een samenvatting in het Nederlands)

**Proefschrift**

ter verkrijging van de graad van doctor aan de Universiteit Utrecht  
op gezag van de rector magnificus, prof. dr. G.J. van der Zwaan,  
ingevolge het besluit van het college voor promoties  
in het openbaar te verdedigen  
op donderdag 5 juli 2012 des middags te 2.30 uur

door

**Jesse Habets**

geboren op 17 mei 1985 te Beek

**Promotor:** Prof. dr. W.P.Th.M. Mali

**Co-promotor:** Dr. R.P.J. Budde

The research described in this thesis was supported by a grant of the Dutch Heart Foundation (DHF-2009B014).

Additional financial support for the reproduction of this thesis was generously provided by: Philips Healthcare, Bayer B.V., and the Röntgen Stichting Utrecht



**Passionate multidisciplinary cooperation results in.....**

## CONTENTS

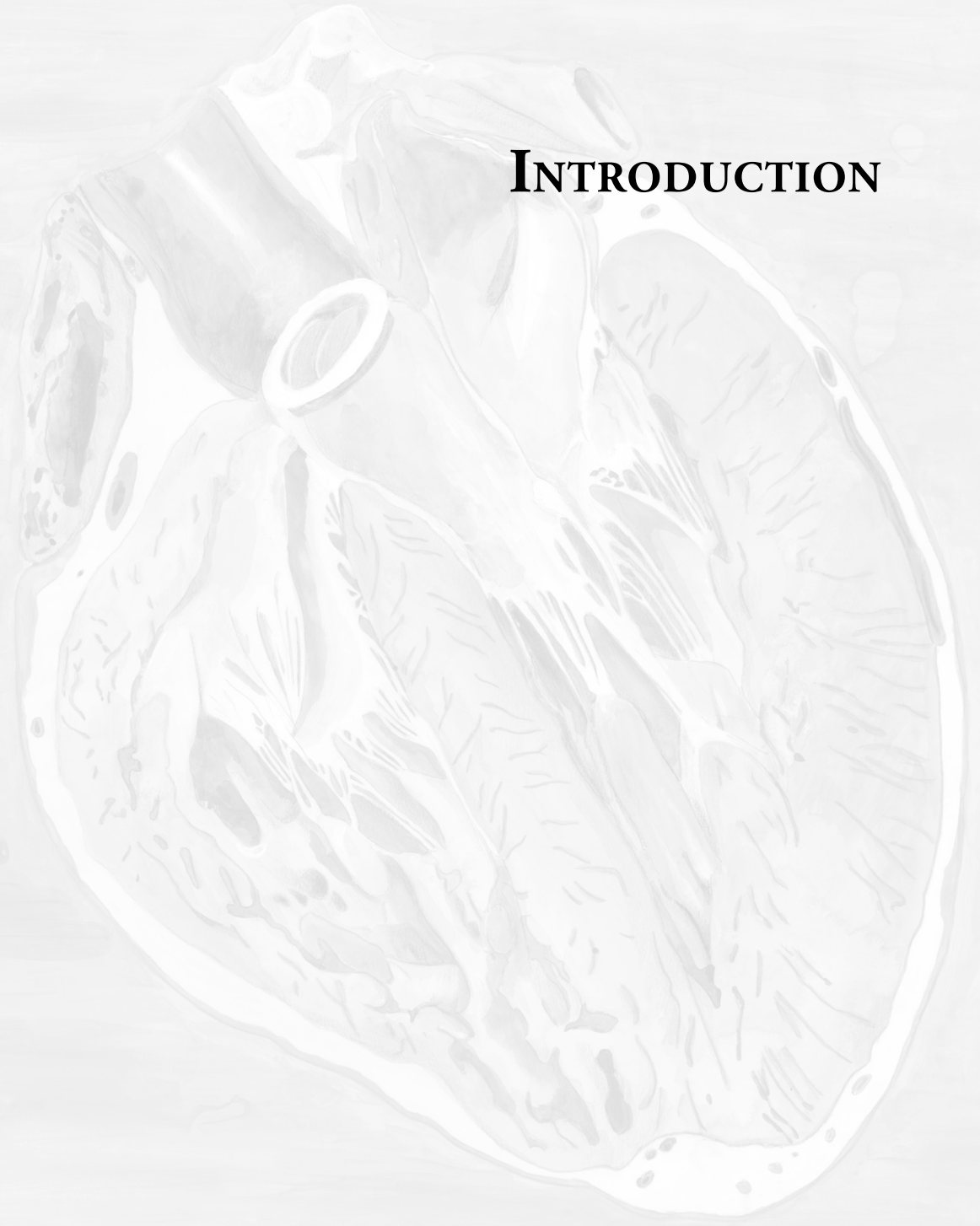
INTRODUCTION	9
CHAPTER I GENERAL INTRODUCTION	11
CHAPTER II DIAGNOSTIC EVALUATION <i>of</i> LEFT-SIDED PROSTHETIC HEART VALVE DYSFUNCTION	17
CHAPTER III NON-INVASIVE IMAGING <i>of</i> LEFT-SIDED PROSTHETIC HEART VALVE DYSFUNCTION: <i>a</i> SYSTEMATIC REVIEW <i>and</i> META-ANALYSIS	43
IN VITRO PART	61
CHAPTER IV A NOVEL ITERATIVE RECONSTRUCTION ALGORITHM ALLOWS REDUCED DOSE MULTIDETECTOR-ROW CT IMAGING <i>of</i> MECHANICAL PROSTHETIC HEART VALVES	63
CHAPTER V ARTIFACT REDUCTION STRATEGIES <i>for</i> PROSTHETIC HEART VALVE CT IMAGING	75
CHAPTER VI PROSPECTIVE ECG TRIGGERING REDUCES PROSTHETIC HEART VALVE INDUCED-ARTIFACTS COMPARED <i>with</i> RETROSPECTIVE ECG GATING <i>on</i> 256-SLICE CT	87
CHAPTER VII LOW-DOSE MULTIDETECTOR-ROW CT <i>of</i> PROSTHETIC HEART VALVES USING PROSPECTIVE TRIGGERING <i>and</i> ITERATIVE RECONSTRUCTION	97
IN VIVO PART	109
CHAPTER VIII MULTISLICE CT ANGIOGRAPHY <i>of</i> PROSTHETIC HEART VALVES: NORMAL <i>and</i> DYSFUNCTIONAL PROSTHETIC HEART VALVE IMAGING CHARACTERISTICS	111
CHAPTER IX IMAGING <i>of</i> PROSTHETIC HEART VALVE DYSFUNCTION: COMPLEMENTARY DIAGNOSTIC VALUE <i>of</i> TRANSESOPHAGEAL ECHOCARDIOGRAPHY <i>and</i> MULTIDETECTOR COMPUTED TOMOGRAPHY	131
CHAPTER X PROSTHETIC HEART VALVE ASSESSMENT <i>with</i> MULTIDETECTOR-ROW CT: IMAGING CHARACTERISTICS <i>of</i> 91 VALVES <i>in</i> 83 PATIENTS	143
CHAPTER XI CT ATTENUATION MEASUREMENTS <i>are</i> VALUABLE <i>to</i> DISCRIMINATE PTFE FELT PLEDGETS <i>used in</i> PROSTHETIC HEART VALVE IMPLANTATION <i>from</i> PARAVALVULAR LEAKAGE	155

CHAPTER XII	CORONARY ARTERY ASSESSMENT <i>with</i> MULTIDETECTOR COMPUTED TOMOGRAPHY <i>in</i> PATIENTS <i>with</i> PROSTHETIC HEART VALVES	165
CHAPTER XIII	OPTIMAL SYSTOLIC <i>and</i> DIASTOLIC RECONSTRUCTION PHASE <i>for</i> AORTIC PROSTHETIC HEART VALVE IMAGING <i>with</i> ECG-GATED MULTIDETECTOR-ROW CT	179
CHAPTER XIV	AORTIC PROSTHETIC HEART VALVE MOTION DURING <i>the</i> CARDIAC CYCLE: IMPLICATIONS <i>for</i> CT IMAGING	193
CHAPTER XV	SERIAL COMPUTED TOMOGRAPHY IMAGING <i>of</i> PROSTHETIC HEART VALVE ENDOCARDITIS <i>in a</i> PEDIATRIC PATIENT	205
CHAPTER XVI	IMPACT STUDY PROTOCOL	213
CHAPTER XVII	GENERAL DISCUSSION	229
	NEDERLANDSE SAMENVATTING	239
	DANKWOORD	249
	CURRICULUM VITAE	257
	LIST <i>of</i> PUBLICATIONS	261
APPENDIX		265





# INTRODUCTION







CHAPTER I

GENERAL INTRODUCTION



The prevalence and incidence of valvular heart disease is increasing worldwide because of increasing age and the problem of rheumatic cardiac disease in the developing countries.<sup>1,2</sup> Valvular heart disease is treated with prosthetic heart valve (PHV) implantation or native valve repair in symptomatic patients with an indication for cardiothoracic surgery. In 2003, 290,000 heart valve operations were performed worldwide, and this number will rise in the next decades mainly due to increasing age of the world population.<sup>1</sup>

Prosthetic heart valves are implanted in the decalcified annulus with sutures, and often polytetrafluorethylene (PTFE) pledgets are used to disperse the pressure on single sutures to prevent suture loosening. The PHV type (mechanical or biological PHV) that is implanted depends on the patient characteristics, and patient and surgeon preferences.

In the postoperative period, it is important to assess PHV function by non-invasive imaging techniques. The primary imaging modality for postoperative assessment of PHV function is the transthoracic echocardiography (TTE). TTE is fast, bedside available, patient friendly and relatively cheap compared to more advanced non-invasive imaging techniques. Essential echocardiographic parameters are maximum and mean pressure transprosthetic pressure gradients, prosthetic orifice area and the presence of pathological valvular or paravalvular leakage. After a normal postoperative echocardiographic examination, subsequent TTE is only performed in patients with a clinical indication according to the guidelines of the European Society of Cardiology.<sup>3</sup> In patients with biological PHVs, however, annual TTE evaluation has to be performed starting five years after PHV implantation to assess for the presence of valve degeneration.<sup>3</sup>

PHV dysfunction is a rare but potentially life-threatening pathological entity with incidence of 0.01-6.0% per year and a heterogeneous clinical presentation. Three major subtypes are distinguished: PHV obstruction, PHV endocarditis and PHV regurgitation. Patients with PHV dysfunction can present with symptoms of congestive heart failure (dyspnea, fatigue, edema), fever, angina pectoris, dizziness during exercise or non-specific complaints (e.g. stroke).

The first screening tool to detect PHV dysfunction is TTE. Anatomical B-mode imaging and Doppler evaluation is often able to determine the presence of PHV dysfunction. However, TTE often fails to determine the exact cause of the PHV dysfunction. Echocardiographic assessment can be inconclusive owing to poor transthoracic echocardiographic windows (i.e. obesity and chronic obstruction pulmonary disease) or acoustic shadowing due to the metal components present in valve prostheses.

Transesophageal echocardiography (TEE) has incremental value to TTE especially in patients with suspected mitral PHV dysfunction.<sup>4</sup> Fluoroscopy has diagnostic value in patients with suspected mechanical PHV obstruction by assessing valve leaflet opening and closure.<sup>5</sup> In patients with suspected biological PHV dysfunction, fluoroscopy is not useful since valve leaflets are not visible.

Even combined, the routine non-invasive imaging modalities (TTE, TEE and fluoroscopy) may fail to detect the exact cause of PHV dysfunction especially in patients with mechanical aortic PHVs.<sup>6</sup> The identification of the exact cause of PHV dysfunction is crucial because different causes require different treatment strategies.<sup>7</sup>

The introduction of multidetector-row computed tomography (MDCT) has resulted in the capability of computed tomography to diagnostically assess cardiac structures owing to increased spatial and temporal resolution compared to conventional computed tomography.

The CT image quality of PHVs mainly depends on the presence of artifacts.<sup>8</sup> The occurrence of artifacts is multifactorial.<sup>8</sup> First, the heart is a lively moveable structure in the human thorax. To reduce motion artifacts, it is important to freeze this cardiac movement. Retrospective ECG-gating and prospective ECG triggering are CT acquisition techniques to achieve this freezing. Retrospective

ECG-gated helical acquisition compromises data acquisition during several different heart beats (RR intervals) and is associated with a considerable radiation dose exposure. Retrospective ECG-gating enables dynamic cardiac evaluation. In contrast in prospective triggering (volume scanning), CT data acquisition occurs during a predefined ECG-phase which substantially decreases radiation exposure. However, volume scanning is more sensitive for higher heart rates and arrhythmia (often present in patients with suspected PHV dysfunction) and dynamic cardiac assessment is not possible.

Second, heart rate control is important for diagnostic CT imaging. Increasing heart rate results in non-proportional shortening of the diastolic imaging phases compared to the systolic imaging phases, and decreases CT image quality. It is advisable to reduce heart rate to  $\leq 60$  beats per minute for optimal CT image quality with administration of oral and/or intravenous  $\beta$ -blockers in patients without contraindications for  $\beta$ -blockers. Third, breathing artifacts can decrease CT image quality. For optimal cardiac CT imaging, scanning during breath hold in inspiration is advisable. Besides artifact reduction, optimal cardiac contrast enhancement is important for anatomical assessment of cardiac structures. Bi- and triphasic contrast administration protocols with saline chasers are commonly used to reach optimal left-sided contrast administration and reduce streak artifacts in the right ventricle.<sup>8,9</sup>

Raw data are reconstructed with reconstruction algorithms (standard filtered back projection) into imaging datasets for each scanned phase of the RR-interval. In dedicated cardiac analysis software, these imaging datasets can be reconstructed in every desired imaging plane. Furthermore, in patients after retrospective ECG-gating acquisition cine movies can be reconstructed. These data are sent to PACS for archiving and diagnostic assessment.

Cardiac MDCT is an established non-invasive imaging technique to evaluate patients with an intermediate risk for coronary artery disease.<sup>3,10</sup> Initial reports demonstrate promising results of MDCT as a non-invasive imaging technique for PHV imaging.<sup>11-16</sup>

## OUTLINE OF THIS THESIS

This thesis focuses on the development of MDCT for PHV imaging, and is subdivided in three parts: introduction, in vitro part and in vivo part.

### INTRODUCTION

**Chapter II** presents a comprehensive overview of the role of non-invasive imaging modalities (echocardiography, fluoroscopy and MDCT) in the diagnosis of left-sided PHV dysfunction, and provides a proposed diagnostic algorithm for non-invasive PHV imaging. In **Chapter III**, the literature on the role of non-invasive imaging modalities for the diagnosis of PHV obstruction and endocarditis is systematically reviewed and a meta-analysis is performed to provide insights in the diagnostic accuracy of the different non-invasive imaging modalities.

### IN VITRO PART

In vitro MDCT imaging of different prosthetic heart valves was performed: (1) to optimize CT acquisition protocols for clinical purposes, (2) to decrease radiation exposure, and (3) to provide insights in the occurrence of PHV-related artifacts which may dramatically decrease CT image quality. **Chapter IV** presents the application of a novel iterative reconstruction algorithm to reduce radiation exposure in MDCT PHV imaging without increasing image noise and PHV-related

artifacts. **Chapter V** describes the effectiveness of three different artifact reduction strategies in PHV MDCT imaging: higher tube voltages, novel iterative reconstruction and metal artifact reduction filters. **Chapter VI** provides insights in the potential role of prospective triggering in PHV MDCT imaging by PHV-related artifact and radiation exposure reduction. **Chapter VII** explores different acquisition and reconstruction techniques to determine the optimal low-dose MDCT acquisition protocol.

## IN VIVO PART

The diagnostic process of patients with suspected PHV dysfunction requires a multidisciplinary approach. Different medical specialists have to be involved including cardiologists, cardiothoracic surgeons and radiologists. **Chapter VIII** provides insights on MDCT acquisition, interpretation and reporting in patients imaged to assess PHV function for radiologists. In **Chapter IX**, the potential complementary role of MDCT to echocardiography and fluoroscopy is illustrated with TEE MDCT views.

Clinical PHV MDCT imaging is a promising non-invasive imaging modality to evaluate PHV dysfunction.<sup>11-16</sup> **Chapter X** provides normal MDCT imaging characteristics for different mechanical and biological PHVs. **Chapter XI** presents a method to distinguish the presence of contrast material and the presence of polytetrafluorethylene (PTFE) pledgets based on Hounsfield measurement. This differentiation is clinically relevant because paravalvular leakage (presence of intravascular contrast outside the annulus) and PTFE pledgets both presents as hyperdense structures on MDCT images which can result in diagnostic dilemmas.

Besides PHV dysfunction, MDCT is performed to evaluate the presence of coronary artery disease in patients with an intermediate risk of coronary artery disease. In patients with PHVs, non-invasive evaluation of coronary arteries is desirable especially in patients with PHV endocarditis which will undergo reoperation to avoid the risk of embolization during invasive coronary angiography. **Chapter XII** describes the suitability of MDCT to evaluate coronary artery segments in patients with different mechanical and biological PHVs. **Chapter XIII** provides insights in the optimal systolic and diastolic MDCT imaging reconstruction phase for aortic mechanical and biological PHVs. In **Chapter XIV**, the role of annular movement and velocity on MDCT image quality in patients with aortic PHVs is described.

**Chapter XV** demonstrates the promising complementary diagnostic value of MDCT to echocardiography in a pediatric patient with PHV endocarditis. **Chapter XVI** presents the IMPACT (Imaging of Prosthetic Heart Valves) study protocol, a prospective diagnostic cross-sectional study to evaluate the complementary diagnostic role of MDCT in the evaluation of patients with suspected PHV dysfunction, and to obtain normal CT references values of PHVs. The last chapter, **Chapter XVII** encloses the general discussion and future perspectives.

In summary, this thesis aims to develop and improve MDCT imaging as a non-invasive complementary imaging modality to assess patients with prosthetic heart valves.

## REFERENCES

1. Yacoub MH, Takkenberg JJ. Will heart valve tissue engineering change the world? *Nat Clin Pract Cardiovasc Med* 2005; 2:60-61.
2. Carapetis JR, Currie BJ, Mathews JD. Cumulative incidence of rheumatic fever in an endemic region: a guide to the susceptibility of the population? *Epidemiol Infect* 2000; 124:239-244.
3. Vahanian A, Baumgartner H, Bax J, et al. Guidelines on the management of valvular heart disease: The Task Force on the Management of Valvular Heart Disease of the European Society of Cardiology. *Eur Heart J* 2007; 28:230-268.
4. Chaudhry FA, Herrera C, DeFrino PF, et al. Pathologic and angiographic correlations of transoesophageal echocardiography in prosthetic heart valve dysfunction. *Am Heart J* 1991; 122:1057-1064.
5. Montorsi P, De Bernardi F, Muratori M, et al. Role of cine-fluoroscopy, transthoracic, and transoesophageal echocardiography in patients with suspected prosthetic heart valve thrombosis. *Am J Cardiol* 2000; 85:58-64.
6. Girard SE, Miller FA, Jr., Orszulak TA, et al. Reoperation for prosthetic aortic valve obstruction in the era of echocardiography: trends in diagnostic testing and comparison with surgical findings. *J Am Coll Cardiol* 2001; 37:579-584.
7. Guiar-Souto P, Mirelis JG, Silva-Melchor L. Guidelines on the management of valvular heart disease. *Eur Heart J* 2007; 28:1267-1268.
8. Prokop M. Radiation Dose and Image Quality. In: Prokop M, Galanski M (eds). *Spiral and Multislice Computed Tomography of the Body*. Stuttgart, Thieme, 2003.
9. Weininger M, Barraza JM, Kemper CA, et al. Cardiothoracic CT Angiography: Current Contrast Medium Delivery Strategies. *Am J Roentgenol*. 2011; 196:W260-W272.
10. Meijboom WB, Meijs MF, Schuijf JD, et al. Diagnostic accuracy of 64-slice computed tomography coronary angiography: a prospective, multicenter, multivendor study. *J Am Coll Cardiol* 2008; 52:2135-2144.
11. Konen E, Goitein O, Feinberg MS, et al. The role of ECG-gated MDCT in the evaluation of aortic and mitral mechanical valves: initial experience. *Am J Roentgenol*. 2008; 191:26-31.
12. Teshima H, Hayashida N, Fukunaga S, et al. Usefulness of a multidetector-row computed tomography scanner for detecting pannus formation. *Ann Thorac Surg* 2004; 77:523-526.
13. Symersky P, Budde RP, de Mol BA, et al. Comparison of multidetector-row computed tomography to echocardiography and fluoroscopy for evaluation of patients with mechanical prosthetic valve obstruction. *Am J Cardiol* 2009; 104:1128-1134.
14. Tsai IC, Lin YK, Chang Y, et al. Correctness of multi-detector-row computed tomography for diagnosing mechanical prosthetic heart valve disorders using operative findings as a gold standard. *Eur Radiol* 2009; 19:857-867.
15. Feuchtner GM, Stolzmann P, Dichtl W et al. Multislice computed tomography in infective endocarditis: comparison with transoesophageal echocardiography and intraoperative findings. *J Am Coll Cardiol* 2009; 53:436-444.
16. Chenot F, Montant P, Goffinet C et al. Evaluation of anatomic valve opening and leaflet morphology in aortic valve bioprosthesis by using multidetector CT: comparison with transthoracic echocardiography. *Radiology* 2010; 255:377-385.





## CHAPTER II

# DIAGNOSTIC EVALUATION *of* LEFT-SIDED PROSTHETIC HEART VALVE DYSFUNCTION

J.Habets  
R.P.J. Budde  
P. Symersky  
R.B.A. van den Brink  
B.A.J.M. de Mol  
W.P.Th.M. Mali  
L.A. van Herwerden  
S.A.J. Chamuleau

**ABSTRACT**

Prosthetic heart valve (PHV) dysfunction is a rare, but potentially life-threatening complication. In clinical practice, PHV dysfunction poses a diagnostic dilemma. Echocardiography and fluoroscopy are the imaging techniques of choice and are routinely used in daily practice. However, these techniques sometimes fail to determine the specific cause of PHV dysfunction, which is crucial to the selection of the appropriate treatment strategy. Multidetector-row CT (MDCT) can be of additional value in diagnosing the specific cause of PHV dysfunction and provides valuable complementary information for surgical planning in case of reoperation. Cardiac magnetic resonance imaging (CMR) has limited value in the evaluation of biological PHV dysfunction. In this review, we discuss the use of established imaging modalities for the detection of left-sided mechanical and biological PHV dysfunction and discuss the complementary role of MDCT in this context.

**Key points**

- Echocardiography and fluoroscopy are the 'gold standard' for the evaluation of mechanical prosthetic heart valve (PHV) dysfunction
- Echocardiography is the preferred imaging technique to assess biological PHV dysfunction.
- Determining the exact cause of PHV dysfunction is essential for optimal patient treatment, but echocardiography and fluoroscopy sometimes may fail to identify the exact cause of the PHV dysfunction
- Multislice CT can complement echocardiography and fluoroscopy particularly in patients with mechanical heart valve obstruction and infective endocarditis
- Multislice CT can provide specific anatomical information assisting the cardiothoracic surgeon during the planning of reoperation

In 2003, approximately 290,000 patients worldwide underwent heart-valve replacement and received a prosthetic heart valve (PHV).<sup>1</sup> Valve repair is currently the preferred method in mitral-valve surgery, but the other valves, particularly the aortic valve, often require replacement with biological or mechanical valve prostheses in the majority of patients. Mechanical PHVs have proven to be durable, but structural and nonstructural prosthesis dysfunction, or valve-related complications such as PHV thrombosis can occur with a reported incidence of between 0.01% and 6.0% per year.<sup>2–6</sup> The variation in the frequency of such complications depends on the design of the study and the year that the data were published, the type and position of the implanted valve, as well as the adequacy of oral anticoagulation therapy.<sup>2–6</sup> By contrast, biological valve dysfunction usually occurs as a consequence of valve degeneration, which requires reoperation approximately 15 years after PHV implantation.<sup>7</sup> Besides biological PHV degeneration, endocarditis and thrombosis are a common complication after biological PHV implantation.

PHV dysfunction is associated with substantial morbidity and mortality, and determining the appropriate treatment necessitates elucidation of the specific underlying cause of the dysfunction, such as pannus (tissue in-growth into the PHV, supporting structures, or both) or thrombus formation, biological valve degeneration, patient–prosthesis mismatch (PPM), pathologic regurgitation, or infective endocarditis. Three imaging techniques currently have a key role in PHV assessment and the detection of PHV dysfunction: transthoracic echocardiography (TTE), transesophageal echocardiography (TEE), and fluoroscopy. Over the past 2 years, multidetector-row CT (MDCT) also has shown potential for PHV assessment.<sup>8–14</sup> In patients with biological PHV dysfunction, cardiac magnetic resonance imaging (CMR) might have complementary diagnostic value.<sup>15–17</sup>

In this review, we discuss the principles and relative merits and shortcomings of TTE, TEE, fluoroscopy, MDCT, and CMR. Our aim is to describe their complementary roles in the diagnosis of left-sided mechanical and biological PHV dysfunction, and to illustrate principal imaging findings for various common pathological entities, including PHV obstruction, regurgitation, and infective endocarditis.

## IMAGING TECHNIQUES

In patients with suspected PHV dysfunction, TTE is the primary screening tool, followed by TEE, fluoroscopy, or both. MDCT has shown potential as a complementary diagnostic imaging technique.<sup>8–10,13,14</sup> CMR has a limited role in the assessment of biological PHV dysfunction. The various imaging techniques with their relative merits and shortcomings are discussed in detail in the following sections.

### **Transthoracic echocardiography**

TTE is noninvasive, fast, readily available at the bedside, and cost-effective.<sup>18</sup> Imaging in adults is performed with transducers operating at 2–3.5 MHz, providing a spatial resolution of 0.6–1.0 mm and an excellent temporal resolution of 15–60 ms.<sup>19</sup> Anatomical information is obtained by B-mode imaging. Doppler ultrasonography is an essential part of PHV evaluation, as it visualizes direction and velocity of blood flow. The transprosthetic mean pressure gradient can be determined using the modified Bernoulli equation.<sup>18,20</sup> An increased transvalvular pressure can be a sign of PHV obstruction. In the measurement of pressure gradients, aligning the ultrasound beam as parallel as possible to the transprosthetic flow is important. The transvalvular gradient is determined by the effective orifice area (EOA) and the blood-flow rate, which, in turn, depends on the tissue oxygen demand related to body surface area (BSA). Therefore, knowing the size of the prosthesis, heart rate, and BSA is important

to correctly interpret the transvalvular pressure gradient measured by TTE.<sup>21</sup> Normal maximum and mean pressure gradients of commonly implanted mechanical PHVs are shown in Table 1 and Table 2, which can be of help in daily clinical practice. An increased transprosthetic pressure gradient might be caused by high stroke volume (because of low heart rate or paravalvular leakage), PPM, or obstruction by thrombus, pannus, or vegetations.<sup>21</sup> Calculating the effective prosthetic valve area using the continuity equation is also important because multiple echocardiographic parameters will result in a more confident diagnosis.<sup>18,21,22</sup> Limitations of TTE include operator-dependency and poor acoustic windows resulting from either acoustic shadowing caused by the PHV material or TTE being performed in the early postoperative phase (within 1 week after PHV implantation) owing to postoperative influences such as pericardial effusion, or in specific patient groups, such as those with emphysema and obese individuals. Left-ventricular dysfunction and concomitant valvular disease can also influence the echocardiographic parameters.<sup>21,23</sup> Furthermore, the pressure recovery phenomenon and complex, fast, local blood flow can result in unreliably high measurements of transvalvular pressure gradient, which do not reflect the actual transvalvular pressure gradient and prosthetic EOA for diagnostic assessment of PHVs.<sup>24–26</sup> However, an increased transvalvular gradient and/or decreased prosthetic EOA compared with baseline TTE Doppler measurements (Table 1 and Table 2) remain indicators for further evaluation of suspected PHV dysfunction, as stated in the consensus guidelines for evaluation of PHV with echocardiography.<sup>18</sup> Three-dimensional (3D) TTE might have additional diagnostic value to two-dimensional (2D) TTE evaluation for PHV evaluation and can be considered in patients with inconclusive 2D TTE evaluation.<sup>27</sup>

### Transesophageal echocardiography

TEE is a semi-invasive imaging technique for the evaluation of suspected PHV dysfunction. The proximity of the esophagus to the heart enables the TEE probe to be positioned close to the heart, without the interference of the lungs. Owing to its semi-invasive nature, a few absolute contraindications to TEE should be taken into account, including esophageal spasm, stricture, laceration, perforation, and diverticula. Although TEE is less convenient for patients than TTE, TEE offers better spatial resolution (0.2 mm) because the transducer operates at a higher frequency (usually 3.5–7.0 MHz). The high spatial resolution, close proximity of the probe to the anatomical structures, and the use of various probe angulations in TEE allow better visualization of anatomical abnormalities related to the PHV than with TTE.<sup>21,28</sup> TEE can also be combined with visualization techniques using Doppler ultrasound. TEE is superior to TTE in the detection of leaflet thickening, leaflet prolapse, and flail cusps.<sup>29–32</sup> Complementary to TTE, TEE can be useful for evaluation of PHV leaflet motion and assessment of regurgitation, especially in the mitral position.<sup>33</sup> Acquisition and interpretation of TEE images are operator-dependent and require considerable experience.

3D TEE has been introduced in the past decade and has the potential to be of additional diagnostic value for evaluation of patients with PHV dysfunction. However, only case studies involving the use of this modality have been published thus far.<sup>34</sup>

### Fluoroscopy

Fluoroscopy enables the noninvasive evaluation of the opening and closing angles of mechanical PHV leaflet(s), the motion of the leaflets and the PHV base ring, and the integrity of mechanical PHV components. Each mechanical type of PHV has a characteristic appearance on X-ray images, with specific opening and closing angles (Table 1 and Table 2). For adequate fluoroscopic evaluation, the patient must be positioned so that the leaflets of the mechanical PHV are positioned perpendicular to the X-ray tube—a process that can be cumbersome, depending on specific valve

**Table 1** | Reference values for mechanical heart valves in the aortic position\*

Valve manufacturer	Valve type	Leaflet opening angle <sup>‡</sup>	Leaflet closing angle <sup>‡</sup>	Normal Doppler echocardiographic peak gradient (mmHg)	Normal Doppler echocardiographic mean gradient (mmHg)
ATS Open Pivot® (Medtronic ATS Medical, Minneapolis, MN, USA) <sup>81,82</sup>	Bileaflet	85°	25°	11.0–47.7 <sup>§</sup>	8.0–27.0 <sup>§</sup>
Carbomedics® (Sorin Group USA Inc., Arvada, CO, USA) <sup>83–89</sup>	Bileaflet	78°	25°	12.5–33.4 <sup>§</sup>	5.8–20.1 <sup>§</sup>
Duromedics (Baxter Healthcare Corp, Santa Ana, CA, USA) <sup>90–92</sup>	Bileaflet	78°	20°	13.0–22.5 <sup>§</sup>	3.4–9.0 <sup>§</sup>
On-X® (On-X Life Technologies Inc., Austin, TX, USA) <sup>93</sup>	Bileaflet	90°	40°	11.4–21.3 <sup>§</sup>	5.6–11.8 <sup>§</sup>
Sorin® Bicarbon (Sorin Biomedica Cardio, Milan, Italy) <sup>94–96</sup>	Bileaflet	80°	20°	9.0–29.5 <sup>§</sup>	5.0–16.3
St. Jude Medical® (St. Jude Medical, St. Paul, MN, USA) <sup>96–107</sup>	Bileaflet	85° (19–25mm) 85° (27–31mm)	30° (19–25mm) 25° (27–31mm)	16.0–35.2 <sup>§</sup>	9.9–19.0 <sup>§</sup>
Björk-Shiley spherical (Shiley inc.; Irvine, CA, USA) <sup>99,108,109</sup>	Tilting disc	60° <sup>  </sup>	0° <sup>  </sup>	19.4–38.9 <sup>§</sup>	10.7–21.8 <sup>§</sup>
Medtronic® Hall (Medtronic, Minneapolis, MN, USA) <sup>91,98,110–113</sup>	Tilting disc	75°	0°	17.1–34.4 <sup>§</sup>	8.7–17.1 <sup>§</sup>
Omniscience (Medical Inc, St Paul, MN, USA) <sup>112</sup>	Tilting disc	60°	0°	39.8–50.8 <sup>§</sup>	20.1–28.2 <sup>§</sup>
Sorin® Allcarbon (Sorin Biomedica Cardio, Milan, Italy) <sup>113,114</sup>	Tilting disc	60°	0°	13.0–44.0 <sup>§</sup>	8.0–29.0 <sup>§</sup>

\*For the interpretation of the transvalvular pressure gradients, it is important to be aware that several factors, such as left-ventricular dysfunction and concomitant valvular disease, can influence the echocardiographic measurements. <sup>§</sup>Depending on valve size. <sup>‡</sup>Opening and closing angles based on manufacturer data. <sup>||</sup>Before 1981.

**Table 2** | Reference values for mechanical heart valves in the mitral position\*

Valve manufacturer	Valve type	Leaflet opening angle <sup>‡</sup>	Leaflet closing angle <sup>‡</sup>	Normal Doppler echocardiographic peak gradient (mmHg)	Normal Doppler echocardiographic mean gradient (mmHg)
Carbomedics® (Sorin Group USA Inc., Arvada, CO, USA) <sup>87,115,116</sup>	Bileaflet	78°	25°	8.8–10.3 <sup>§</sup>	3.3–4.8 <sup>§</sup>
Duromedics (Baxter Healthcare Corp, Santa Ana, CA, USA) <sup>92,110</sup>	Bileaflet	73°	20°	10.0–13.0 <sup>§</sup>	2.5–5.0 <sup>§</sup>
On-X® (On-X Life Technologies Inc., Austin, TX, USA) <sup>93</sup>	Bileaflet	90°	40°	9.8–11.5 <sup>§</sup>	4.5–5.3 <sup>§</sup>
Sorin® Bicarbon (Sorin Biomedica Cardio, Milan, Italy) <sup>95</sup>	Bileaflet	80°	20°	10.0–15.0 <sup>§</sup>	4.0 <sup>§</sup>
St. Jude Medical® (St Jude Medical, St Paul, MN, USA) <sup>20,103,111</sup>	Bileaflet	85° (19–25mm) 85° (27–31mm)	30° (19–25mm) 25° (27–31mm)	10.0–12.0 <sup>§</sup>	2.5–5.0 <sup>§</sup>
Björk-Shiley spherical (Shiley Inc., Irvine, CA, USA) <sup>109,110,117</sup>	Tilting disc	60° <sup>  </sup> 70° <sup>‡</sup>	0° <sup>  </sup> 0° <sup>‡</sup>	6.0–12.0 <sup>§</sup>	2.0–6.0 <sup>§</sup>
Sorin® Allcarbon (Sorin Biomedica Cardio, Milan, Italy) <sup>114</sup>	Tilting disc	60°	0°	9.0–15.0 <sup>§</sup>	4.0–5.0 <sup>§</sup>

\*For the interpretation of the transvalvular pressure gradients, it is important to be aware that several factors, such as left-ventricular dysfunction and concomitant valvular disease, can influence the echocardiographic measurements. <sup>§</sup>Depending on valve size. <sup>‡</sup>Opening and closing angles based on manufacturer data. <sup>||</sup>Before 1981. <sup>‡</sup>After 1981.

orientations.<sup>23</sup> Radiation exposure is limited (less than 1 mSv per session), as only a few heartbeats need to be visualized. Fluoroscopy is superior to TTE and TEE for visualization of leaflet motion in the aortic position. In the mitral position, where more extreme tube angulations are needed, TEE and fluoroscopy demonstrate comparable results.<sup>35</sup> Fluoroscopy has no role in biological PHV assessment because of the radiolucent aspect of the biological PHV leaflets.

### **Multidetector- row CT**

Contrast-enhanced, electrocardiographically (ECG)-gated MDCT is of increasing value as an imaging modality complementary to echocardiography and fluoroscopy in the evaluation of PHV but experience with MDCT is limited thus far. In a series of initial studies<sup>8–13,36</sup>, a total of 182 mechanical PHVs were evaluated by MDCT, including 133 in the aortic position and 49 in the mitral position. Biological PHVs can also be assessed using MDCT; a series of 49 biological valves was described in 2010.<sup>14</sup> Retrospectively ECG-gated MDCT scans visualize the PHV in the different phases of the cardiac cycle. In most cases, the cardiac cycle is reformatted into ten evenly spaced phases. Leaflet motion can be evaluated in cine mode by looping images of the various reconstruction phases. The spatial resolution of MDCT (0.6 mm) is superior to TTE, but not to TEE. The temporal resolution of MDCT (90–180 ms for a 64-slice MDCT), however, is inferior to both TTE and TEE (15–60 ms). Postprocessing of the acquired CT data set allows static and dynamic reconstructions in every desired imaging plane.

Commonly implanted mechanical bileaflet PHVs (St. Jude Medical® [St. Jude Medical, St Paul, MN, USA], On-X® [On-X Life Technologies, Inc., Austin, TX, USA] and Carbomedics® [Sorin Group USA Inc., Delaware, CO, USA]) and biological PHVs show only few artifacts when visualized with MDCT.<sup>12,38</sup> Whereas Björk-Shiley (Shiley Inc., Irvine, CA, USA) tilting disc valves demonstrate extensive artifacts that prohibit valve assessment, other tilting disc valves, such as the Medtronic® Hall valve (Medtronic Inc.; Minneapolis, MN, USA) can be visualized with good image quality.<sup>38</sup> With MDCT, opening and closing angles can be measured as accurately as with fluoroscopy.<sup>8,10–12</sup> MDCT planimetry can measure the effective prosthetic orifice area in biological PHVs as accurately as TTE. Biological leaflet thickening or calcification and leaflet restriction can also be detected.<sup>14</sup>

Disadvantages of CT include radiation exposure, which can be as high as 15 mSv in retrospectively ECG-gated scans, and the need for contrast injection. However, modern equipment allows for much lower radiation doses. ECG-triggered radiation-dose modulation and optimized low-dose scan protocols are currently being evaluated and might reduce radiation dose by up to 50–70%, depending on patient characteristics.<sup>39</sup> Arrhythmias, which are often present in patients with PHVs<sup>40</sup>, and heart rates higher than 75 beats per minute can cause motion artifacts. In these patients, higher-dose, retrospectively ECG-gated CT image acquisition and reconstructions in all ten phases of the cardiac cycle remains necessary. In the absence of contraindications,  $\beta$ -blockers are commonly administered to reduce heart rate and improve image quality. As the morbidity and mortality associated with PHV dysfunction is high and CT can help to establish the exact cause of the dysfunction, we feel the radiation exposure is justified given a good clinical indication for CT scanning.

### **Cardiac magnetic resonance**

CMR allows both anatomical and functional cardiac assessment. The technique has little to no role in mechanical PHV assessment owing to valve-induced image artifacts. CMR can accurately assess the prosthetic orifice area and transvalvular flow in normal biological PHVs, particularly in valves that do not have a supporting framework. However, CMR imaging cannot be used if patients with a PHV also have a pacemaker or converter-defibrillator implanted, or if they suffer from claustrophobia.<sup>15–17</sup>

**Table 3 |** Routine clinical follow-up after prosthetic AVR or MVR\*

Follow-up schedule	Content
First follow-up visit (3–4 weeks after AVR/MVR)	Clinical history and physical examination; laboratory tests (including hemoglobin, lactate dehydrogenase and haptoglobin); TTE (baseline)
Second follow-up visit (6 months after AVR/MVR)	Outpatient clinic visit; clinical history and physical examination
Further follow-up (annually)	Outpatient clinic visit; TTE on indication, such as new murmur, concerns about left-ventricular function, questions about PHV integration or function, clinical deterioration, other clinical indications for MHV dysfunction (for example stroke). Annual TTE in patients with a biological PHV, starting 5 years after implantation‡

\*Based on European Society for Cardiology guidelines.<sup>40</sup> ‡Based on ACC/AHA guidelines.<sup>69</sup> Abbreviations: AVR: aortic valve replacement; MVR: mitral valve replacement; PHV: prosthetic heart valve; TTE: Transthoracic echocardiography.

### PHV dysfunction

PHV dysfunction can be subdivided into structural and nonstructural valve dysfunction.<sup>6</sup> Structural valve dysfunction refers to changes intrinsic to the valve, such as degeneration, wear, fracture, and disc escape. Nonstructural dysfunction refers to any abnormality not intrinsic to the valve itself. Examples of nonstructural dysfunction include entrapment (because of pannus formation or the presence of sutures), paravalvular leak, inappropriate sizing or positioning of the PHV, residual leak or obstruction after valve implantation, and clinically important intravascular, hemolytic anemia.

The European Society of Cardiology (ESC) has developed guidelines for a standardized and appropriate clinical follow-up of patients who have undergone valve-replacement surgery (Table 3).<sup>40</sup> PHV dysfunction can develop in the immediate postoperative phase or many years after implantation. Clinical presentations of PHV dysfunction include a new heart murmur, signs of heart failure (left-sided, right-sided, or on both sides), dizziness while doing exercise, angina pectoris, or nonspecific complaints (such as palsy owing to stroke caused by a cardiac embolus).

## MECHANICAL PHV DYSFUNCTION

### Obstruction

Mechanical PHV obstruction is a life-threatening complication with an incidence of 0.5–6.0% per year.<sup>41,42</sup> Mechanical PHV obstruction can be caused by thrombosis, pannus formation, interference by sutures, infectious vegetations, PPM, and structural PHV dysfunction. Suspected PHV obstruction requires TTE evaluation to document an increased transprosthetic pressure gradient. Assessment of peak velocity and Doppler ultrasound velocity index are also important in determining PHV obstruction.<sup>18,22</sup>

In patients with aortic PHV prostheses, the differentiation between real PHV obstruction and subvalvular obstruction is important. Systolic obliteration of the left ventricle, for instance, causes a dynamic gradient with the typical dagger-shaped flow-signal with late-systolic, high velocities. This appearance is in contrast to the early-systolic, high velocities that are seen in case of a fixed obstruction to flow caused, for example, by a prosthetic valve.<sup>21</sup> Apart from an increased pressure gradient and the presence of a pathological mass on or near the valve, PHV obstruction can also simply present as restricted leaflet motion.



**Pannus or thrombus?**

Pannus tissue seems to originate from the neointima in the periannulus of the left ventricular septum and consists of myofibroblasts and extracellular matrix molecules, such as collagen fibers.<sup>12,43</sup> The incidence of pannus formation varies between 0.2–4.5% per patient year.<sup>44</sup>

Thrombus formation in patients with PHV is a major complication, estimated to occur annually in 0.1–0.4% of patients with mechanical valves, depending on valve type and location, and on the adequacy of anticoagulation therapy.<sup>2,3</sup> Thrombotic emboli are a clinically important complication with an incidence of 2.5–3.7% per year in patients with mechanical PHVs.<sup>3</sup> Clinical risk factors for PHV thrombosis include inadequate anticoagulation therapy, a short interval (<6 months) between PHV implantation and development of heart failure symptoms, and reoperation (secondary PHV replacement).<sup>7,42,45</sup>

The differentiation between pannus and thrombus formation is crucial because pannus must be removed surgically in symptomatic patients, whereas patients with thrombus formation can be treated primarily with heparin or other thrombolytic drugs without the need to undergo surgery.<sup>46</sup> The location of the mass can also be helpful to differentiate between pannus and thrombus. Pannus formation occurs more often on the ventricular side, whereas thrombus formation is often localized on the atrial side of the mitral PHV. For the aortic PHVs, pannus formation is often localized on the ventricular side, whereas thrombus formation often occurs on the aortic side. In most cases, thrombus formation occurs earlier after PHV implantation than pannus formation.<sup>47</sup> Typically, pannus develops several months to years after PHV implantation.<sup>41,48</sup> Contrary to pannus, PHV thrombosis can also occur in the immediate postoperative phase (within 1 week) and the first months after PHV implantation.

TTE is the primary screening tool to evaluate PHV obstruction. TTE is important to detect an increased transprosthetic pressure gradient and decreased effective prosthetic valve area, but the technique cannot be reliably used for anatomical classification of the pathological mechanism of PHV obstruction.<sup>7,45</sup> TEE is superior to TTE for establishing the pathological causes of PHV obstruction in both the aortic and mitral position (Figure 1).<sup>49</sup> Girard et al.<sup>7</sup> reported that the mechanism of mechanical PHV obstruction could be identified more often with TEE (49%) than with TTE (10%) in 49 patients reoperated for PHV obstruction, using intraoperative findings as the ‘gold standard’ for determination of the cause of the obstruction. However, even TEE could not differentiate between thrombus and pannus in the majority of the patients. Barbetseas et al.<sup>45</sup> demonstrated that TEE can be of additional diagnostic value to TTE to differentiate between pannus and thrombus formation. Patients with thrombus formation had significantly greater valve motion restriction and increased mass length compared with patients with pannus formation. Moreover, compared with pannus formation, thrombus formation was associated on TEE with a softer mass video intensity, and a lower ultrasound video intensity ratio (defined as the ultrasound video intensity of the mass divided by that of the prosthetic valve).<sup>45</sup> However, the findings from this single-center experience were not reproduced by other research groups. Lin et al. described four independent predictors that favored thrombus as the cause of obstruction and that can help to differentiate between pannus and thrombus formation: firstly, an increased gradient (aortic Pmax  $\geq$ 50 mmHg, Pmean of mitral prosthesis  $\geq$ 10 mmHg), secondly, a mobile mass on the prosthetic valve; thirdly, a mass attached to the occluder; and, fourthly, an international normalized ratio  $\leq$ 2.5.<sup>41</sup> In most cases, however, differentiation between pannus and thrombus formation solely on the basis of echocardiographic findings remains difficult.<sup>7,21,41,42,45</sup>

If PHV obstruction presents as leaflet restriction, fluoroscopy can have additional diagnostic value to both TTE and TEE.<sup>7,33,50,51</sup> The combination of an increased transprosthetic pressure gradient and reduced effective prosthetic valve area, without pathologic regurgitation and a normal

leaflet motion at fluoroscopy, can suggest pannus formation.<sup>42</sup> Thrombus formation might present with leaflet-motion restriction at fluoroscopy.

MDCT offers unique anatomical information to the routine clinical work-up in patients with PHV with restricted leaflet motion.<sup>8–10,36,52</sup> MDCT seems to be a promising technique to localize the anatomical abnormalities causing PHV obstruction, especially in case of pannus (Figure 2 and Figure 3).<sup>8,10</sup> Several investigators have suggested that MDCT might enable the differentiation between a pannus and a thrombus on the basis of their CT attenuation, which is quantified in Hounsfield units (HU). Pannus tissue might have the same HU value as the ventricular septum, and both pannus and the septum attenuate X-rays more than a thrombus. However, no cut-off values in HU values for the distinction of pannus from thrombus are established yet.<sup>8–10</sup> We demonstrated that MDCT provided additional pathological information compared with echocardiography and fluoroscopy in nine of 13 patients (69%) with suspected PHV dysfunction. In six of these 13 patients, subvalvular tissue, which caused the PHV obstruction, was identified by MDCT and missed with the preferred imaging techniques in four of the six cases.<sup>10</sup> However, the scarcity of detailed data on normal MDCT imaging findings of PHV needs to be kept in mind when interpreting abnormal CT findings. In patients with mechanical PHV obstruction, we recommend initial evaluation using TTE, followed by TEE. Fluoroscopy can be considered, especially in patients with suspected aortic PHV obstruction, to assess leaflet opening and closing angles which can be difficult with echocardiography. In patients with inconclusive echocardiography, MDCT should be considered, particularly for the differentiation between pannus and thrombus. If MDCT is performed, fluoroscopy can be omitted (Figure 4).

### Patient–prosthesis mismatch

PPM means that a PHV is too small for the size of a patient's body.<sup>21</sup> An important parameter to diagnose PPM is the EOA index which is defined as the EOA divided by the BSA. An EOA index  $>0.85 \text{ cm}^2/\text{m}^2$  is considered normal. For patients with aortic PHVs, an EOA index of  $0.65\text{--}0.85 \text{ cm}^2/\text{m}^2$  indicates moderate PPM, whereas values  $<0.65 \text{ cm}^2/\text{m}^2$  are defined as severe PPM.<sup>53,54</sup> The reported prevalence of moderate and severe PPM varies widely between 20–70% and 2–11%, respectively.<sup>55–57</sup> The wide prevalence range is probably caused by a diagnostic gray zone with patients with high-normal or low-abnormal transvalvular pressure gradients. In these patients with clinical symptoms, cardiologist might diagnose PPM more often than in patients without symptoms. PPM can be caused by several factors. Firstly, PPM can arise because of patient-related factors, such as a small annular diameter owing to an altered cardiac anatomy with left ventricular hypertrophy, annulus calcifications, and fibrosis. Secondly, the PHV design can promote PPM, especially when the PHV contains supportive structures that decrease EOA compared with the native valve, or when an implanted PHV is too small for the patient's body size. PPM occurs most frequently in patients with large BSA or pre-existing valvular stenosis, in old patients, and when small PHVs ( $<21 \text{ mm}$ ) are used in adults.<sup>56</sup> PPM is associated with inferior hemodynamics, left ventricular dysfunction, worse NYHA functional class status, and reduced exercise capacity.<sup>53,58,59</sup> Patients with severe PPM, or with moderate PPM plus left-ventricular dysfunction, have increased short-term and long-term mortality.<sup>54</sup>

PPM presents as an increased transprosthetic pressure gradient and small effective prosthetic valve area during echocardiographic evaluation shortly (within 1 week) after surgery.<sup>21,56</sup> The presence of high pressure gradients by Doppler echocardiography, with normal opening angles by fluoroscopy, and without masses on echocardiography, support the diagnosis of PPM.<sup>33</sup> Although more common in the aortic position, PPM can also occur in the mitral position.<sup>54,60</sup> MDCT can be of additional value to the routine clinical work-up in the evaluation of suspected PPM, especially by excluding pannus formation, and by providing information on the geometry of the left ventricle outflow tract (LVOT).<sup>61</sup>

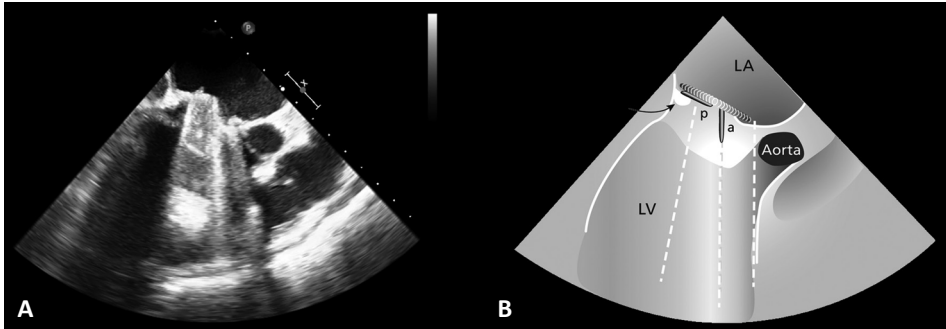


**Figure 1** | Assessment of PHV dysfunction with TEE. **A** | TEE image and **B** | schematic illustration of the heart of a patient with a mechanical PHV (St. Jude Medical® [St. Jude Medical, St Paul, MN, USA]) in the mitral position with thrombosis. The posterior leaflet (p) of the PHV is not opening because of the presence of a thrombus (black arrow). The anterior leaflet (a) opens normally. Abbreviations: LA = left atrium; LV = left ventricle; PHV = prosthetic heart valve; TEE = transesophageal echocardiography.



**Figure 2** | CT images of a thrombosed Carbomedics® (Sorin Group USA Inc., Arvada, CO, USA) bileaflet prosthetic heart valve in the aortic position. Transthoracic echocardiography (not shown) demonstrated an increased pressure gradient over the valve and raised suspicion of a thrombus. **A** | CT imaging revealed severe leaflet opening restriction in systole. The right valve leaflet does not open and the left leaflet opens incompletely. **B** | The thrombus (arrows) on the valve leaflet and ring is clearly visualized by CT. After thrombolysis, this hypodensity disappeared and the valve opened normally, supporting the diagnosis of a thrombosed prosthetic valve.

Results of one study demonstrated that the LVOT, analyzed by MDCT, has an elliptical shape in most people.<sup>62</sup> TTE underestimates EOA by assuming a circular LVOT shape. Actual planimetry of the LVOT by MDCT is potentially more accurate than TTE.<sup>62</sup> In patients with suspected PPM, anatomical information obtained by MDCT can have a role in the planning of subsequent surgical treatment, including annuloplasty, supra-annular implantation, and implantation of stentless valves. Further prospective evaluation of MDCT in patients with suspected PPM is necessary to determine the exact role of the technique in the diagnosis of PPM. At present, the determination of the EOA index with echocardiography remains the gold standard.

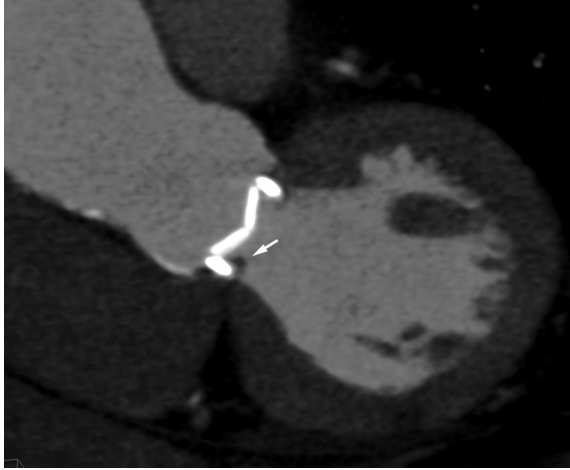


**Figure 3** | CT image of a Carbomedics® (Sorin Group USA Inc., Arvada, CO, USA) prosthetic bileaflet heart valve in the aortic position with pannus formation. Transthoracic echocardiography (not shown) demonstrated an increased pressure gradient over the valve. CT revealed a hypodense area (arrow) directly underneath the valve ring extending from the left-ventricular wall. The CT findings are compatible with pannus formation as the cause of the prosthetic heart valve obstruction.

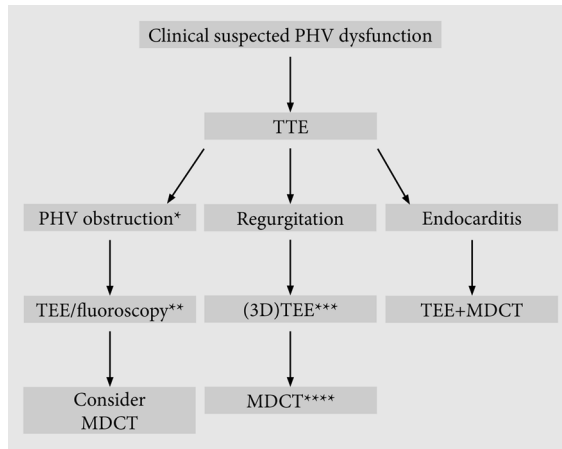


**Figure 4** | Flowchart for suggested non-invasive imaging protocol in the diagnostic work-up of patients with suspected PHV dysfunction. \* If increased transprosthetic gradient pressure is found on TTE examination. \*\* Consider skipping fluoroscopy when MDCT is performed because of the comparable diagnostic accuracy of MDCT for the evaluation of leaflet motion. Fluoroscopy is not a diagnostic imaging modality for patients with biological PHVs. \*\*\* 3D TEE can often be diagnostic for pathologic regurgitation. When TEE is inconclusive, consider MDCT. \*\*\*\* MDCT can have additional diagnostic value after TEE evaluation of regurgitation in case of inconclusive TEE, additional PHV obstruction, questions about leaflet closure, and to identify the exact location of the valvular or paravalvular leakage.

Abbreviations: 3D = three-dimensional; MDCT = multidetector CT; PHV = prosthetic heart valve; TEE = transesophageal echocardiography; TTE = transthoracic echocardiography.

## REGURGITATION

Regurgitation is defined as blood flow in the opposite direction to the normal physiological flow. In evaluating PHVs, it is important to realize that every mechanical PHV exhibits closure backflow, which is necessary to close the valve, and leakage backflow, which starts after valve closure. Both these phenomena are considered normal for mechanical PHVs (Figure 5A). A limited amount of backflow is desired to prevent thromboembolism and is often referred to as the ‘washing volume’. The closure and leakage backflow pattern is dependent on the design of the prosthesis.<sup>21,63</sup> Regurgitation becomes pathologic when the regurgitant volume exceeds physiological volumes, or regurgitation occurs in an abnormal location such as outside the suture ring. Normal closure and leakage backflow jets are low-velocity, nonaliasing, and homogeneous in color upon Doppler ultrasound examination. By contrast, pathologic backflow jets are more turbulent, often eccentric, and adherent to the left atrial wall in the case of mitral valves.<sup>21</sup>

In clinical practice, the differentiation between physiologic and pathologic regurgitation is important. Pathologic regurgitation can be caused by PHV dehiscence or abnormal structures that prevent complete leaflet closure, such as a thrombi, pannus, sutures, or vegetations, and is further categorized into paravalvular or valvular regurgitation.<sup>21</sup> Paravalvular regurgitation occurs with an incidence of  $\leq 2.75\%$  per year and can result in congestive heart failure and hemolytic anemia (Figure 5B).<sup>4</sup> Valvular regurgitation is often caused by interference of abnormal structures with disc closure.<sup>21</sup>

TTE is the primary screening modality to detect pathologic regurgitation.<sup>18</sup> TEE is more suitable than TTE to determine the anatomical cause of pathologic regurgitation, especially in the mitral position.<sup>32,64</sup> 3D TTE and 3D TEE can be of additional value by providing more exact information on the location and size of paravalvular leakage, particularly 3D TEE imaging of mitral PHVs.<sup>27,34</sup> Fluoroscopy can show leaflet restriction, as a sign of valvular regurgitation, in patients with pathologic valvular regurgitation. In patients with inconclusive echocardiographic findings, paravalvular leakage and its exact location might be visualized by MDCT in selected cases, but the diagnostic accuracy of MDCT in the setting of regurgitation is unknown (Figure 5B). At present, Doppler echocardiography remains the first choice of modality for the evaluation of pathologic regurgitation.

In patients with PHV regurgitation, we suggest a diagnostic work-up with echocardiography

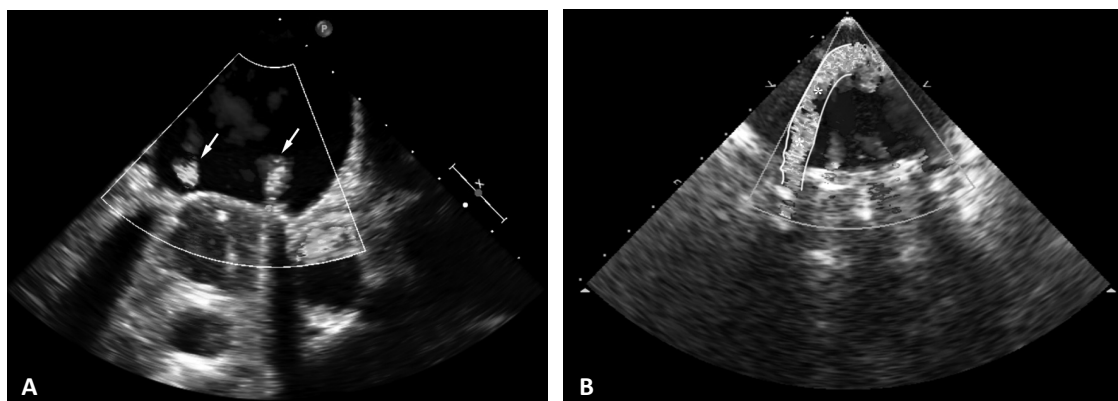


**Figure 5** | Transesophageal echocardiography of mechanical bileaflet prosthetic heart valves. **A** | Color Doppler image demonstrating normal leakage backflow (white arrows). **B** | Image showing paravalvular leakage in addition to normal leakage backflow.

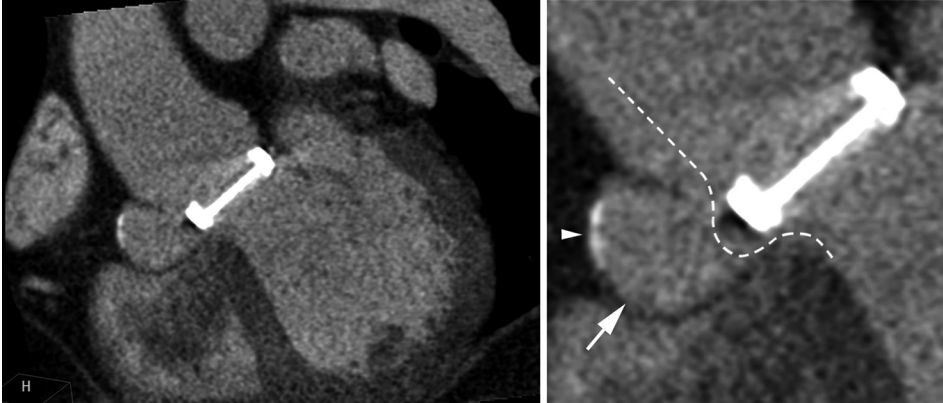


**Figure 6** | MDCT images of a Carbomedics® (Sorin Group USA Inc., Arvada, CO, USA) valve in a patient with infective endocarditis. TEE had been inconclusive, only showing a paravalvular leakage with no specific signs of prosthetic heart valve endocarditis. The enlarged MDCT image shows an aortic root cavity (arrow) with a calcified wall (arrowhead). The calcifications indicate a nonrecent origin. Also, note the small paravalvular leak as shown by the contrast-enhanced blood around the valve ring (dotted line).

Abbreviations: MDCT = multidetector CT; TEE = transesophageal echocardiography.

(both TTE and TEE). MDCT can be considered in case of inconclusive TEE, additional PHV obstruction, questions about leaflet closure and potentially more exact location of the valvular or paravalvular regurgitation (Figure 4).

## INFECTIVE ENDOCARDITIS

An estimated 15,000 new cases of infective endocarditis are reported annually in the USA, and this severe disease has a mortality of up to 40%.<sup>65</sup> The presence of mechanical heart valves is a strong risk factor for infective endocarditis, as 10–30% of all patients with this disease have a PHV.<sup>65</sup> The risk of infective endocarditis is highest in the first 5 years after PHV implantation (1.4–5.7%) and is comparable in the aortic and mitral positions.<sup>65</sup> Infective endocarditis is associated with severe and potential fatal complications, including congestive heart failure, PHV dehiscence, periprosthetic abscesses, and embolism. For the best clinical outcome, diagnosing these complications as early as possible is essential.

In the diagnosis of infective endocarditis, which can be difficult to establish, the modified Duke criteria are the diagnostic criteria of choice.<sup>66,67</sup> According to these criteria, the diagnosis of endocarditis is supported by echocardiographic findings including vegetations, paravalvular leakage, abscess formation, PHV dehiscence, and ruptured abscess or fistula. TEE can be of additional value for the timing of surgical intervention according to the ESC and AHA guidelines in patients with large vegetations (>1 cm), PHV dehiscence, paravalvular leakage owing to loosening of sutures, leaflet perforation, or periprosthetic abscess.<sup>13,21,40,68,69</sup> Importantly, all imaging techniques can only confirm the clinical diagnosis of infective endocarditis, but cannot exclude it.

Imaging plays a key role in the timing of surgical therapy for PHV-related infective endocarditis. TEE is superior to TTE for evaluation of vegetations in patients with infective endocarditis in both the aortic and mitral position.<sup>13,67,70</sup> However, PHVs might hamper TEE by producing valve-induced artifacts (acoustic shadowing). In patients with inconclusive TTE and TEE, MDCT can

be of additional diagnostic value.<sup>13</sup> MDCT is suitable for visualization of vegetations and may produce results comparable with TEE when assessing vegetation mobility and size.<sup>13</sup> TEE offers better diagnostic performance for assessment of small vegetations (<3 mm) than MDCT, because of its better temporal and spatial resolution.<sup>13</sup> However, MDCT can provide additional diagnostic information about the anatomy of the valve, of coronary arteries and, especially, of the aortic root that is valuable for preoperative surgical planning.<sup>13,39,74,75</sup>

Periprosthetic abscess formation occurs in approximately 10–40% of patients with PHV-related infective endocarditis. In most cases, TEE is required to diagnose periprosthetic abscesses, which is superior to TTE in this regard.<sup>73–76</sup> TEE has a sensitivity of 87% for detection of infective endocarditis abscesses that would be identified in surgery or autopsy.<sup>73</sup> The diagnostic performance of MDCT is similar to TEE for the evaluation of perivalvular abscesses and pseudoaneurysms.<sup>13</sup> MDCT can exactly locate and determine the extent of the abscess in relation to the cardiac structures, including the coronary arteries (Figure 6). 3D volume-rendered CT images are valuable for preoperative surgical planning. MDCT can provide additional information in evaluation of ruptured aneurysm of Valsalva and fistula as a complication of PHV-related infective endocarditis.<sup>72</sup> We therefore advise performing MDCT in addition to TEE in patients with infective endocarditis, particularly when abscess or mycotic aneurysm formation are suspected (Figure 4).

## BIOLOGICAL PHV DYSFUNCTION

### Obstruction

Mechanisms of biological PHV dysfunction differ markedly from those of mechanical PHV dysfunction. Most notably, all biological PHVs degenerate after a variable time period (10–20 years). To detect biological PHV dysfunction, which can present as obstruction or regurgitation, yearly routine echocardiographic surveillance is recommended commencing 5 years after implantation (Table 3).<sup>40,69,77</sup>

TTE and TEE are the preferred imaging techniques to investigate suspected biological PHV dysfunction, but both techniques can fail to identify the exact cause of the PHV obstruction.<sup>7,32</sup> Girard et al. evaluated 43 cases of biological PHV obstruction with TTE and TEE, correlating imaging results with intraoperative findings and autopsy reports.<sup>7</sup> PHV obstruction was caused by structural degeneration in 37 patients (86%), by thrombosis in three patients (7%), by PPM in two patients (5%) and by pannus formation in one patient (2%). TEE proved superior to TTE in the identification of the exact cause of biological PHV obstruction. The difference in diagnostic accuracy between TTE and TEE (63% versus 81%) was evidently smaller than in patients with mechanical PHV obstruction (10% versus 49%).<sup>7</sup> 3D TTE might offer additional diagnostic value, but can miss pannus formation.<sup>27</sup> In patients with inconclusive echocardiographic results, MDCT can have complementary value, especially by identifying pannus tissue or subvalvular obstruction.

### Regurgitation

As opposed to mechanical PHVs, biological PHVs do not have a normal closing backflow. TTE is the primary imaging technique for evaluation of regurgitation in biological PHVs. Additional TEE can be considered, as TEE is superior to TTE for the evaluation of pathologic regurgitation and discrimination between paravalvular and valvular leakage in both aortic and mitral positions.<sup>29,31,32,64,78</sup> In patients with inconclusive echocardiography, 3D TTE or CMR can have additional diagnostic value to discriminate paravalvular from pathologic valvular regurgitation.<sup>27,79</sup> MDCT can show

**Table 4** | Reference values for biological prosthetic heart valves in the aortic position\*

Valve manufacturer	Normal Doppler echocardiographic peak gradient (mmHg)	Normal Doppler echocardiographic mean gradient (mmHg)
Biocor® stentless (St. Jude Medical, St. Paul, MN, USA) <sup>97,118,119</sup>	22.0–36.0 <sup>‡</sup>	15.0–20.0 <sup>‡</sup>
Extended Biocor® (St. Jude Medical, St. Paul, MN, USA) <sup>120</sup>	14.0–17.5 <sup>‡</sup>	7.4–9.7 <sup>‡</sup>
Bioflow pericardial (Biomedical, Glasgow, UK) <sup>121,122</sup>	20.7–37.3 <sup>‡</sup>	12.5–24.2 <sup>‡</sup>
Carpentier Edwards® bovine (Edwards Lifesciences, Irvine, CA, USA) <sup>121,123–131</sup>	22.0–43.5 <sup>‡</sup>	9.9–25.6 <sup>‡</sup>
Carpentier-Edwards® pericardial (Edwards Lifesciences, Irvine, CA, USA) <sup>128,130,132</sup>	16.5–32.1 <sup>‡</sup>	5.6–24.2 <sup>‡</sup>
Hancock® I (Medtronic, Minneapolis, MN, USA) <sup>123,124,133</sup>	15.0–19.1 <sup>‡</sup>	10.0–12.4 <sup>‡</sup>
Hancock® II (Medtronic, Minneapolis, MN, USA) <sup>134–136</sup>	14.0–34.0 <sup>‡</sup>	8.2–16.6 <sup>‡</sup>
Ionescu-Shiley (Shiley inc, Irvine, CA, USA) <sup>121,131,132,137–140</sup>	14.8–42.0 <sup>‡</sup>	7.3–21.1 <sup>‡</sup>
Medtronic® Freestyle (Medtronic, Minneapolis, MN, USA) <sup>141–150</sup>	11.0 <sup>‡</sup>	4.6–13.0 <sup>‡</sup>
Medtronic® Intact (Medtronic, Minneapolis, MN, USA) <sup>128,129,151–154</sup>	25.0–40.9 <sup>‡</sup>	15.0–24.5 <sup>‡</sup>
Medtronic® Mosaic (Medtronic, Minneapolis, MN, USA) <sup>155,155–166</sup>	22.5–23.8 <sup>‡</sup>	9.0–14.2 <sup>‡</sup>
Mitroflow® (Mitroflow, Richmond, Canada) <sup>121,132,139</sup>	13.0–20.2 <sup>‡</sup>	6.6–13.1 <sup>‡</sup>

\*For the interpretation of the transvalvular pressure gradients, it is important to be aware that several factors, such as left-ventricular dysfunction and concomitant valvular disease, can influence the echocardiographic measurements. <sup>‡</sup>Depending on valve size. <sup>‡</sup>Valve size 23 mm

non-coaptation of the valve leaflets as well as leaflet thickening as a sign of regurgitation, but the role of this imaging technique in assessing regurgitation of biological PHVs is limited. In patients with biological PHV regurgitation, without an indication for surgery, repeated TTE every 3–6 months is advised to monitor deterioration of the valve.<sup>69</sup>

### Infective endocarditis

Biological PHVs are less susceptible to early PHV-related infective endocarditis than mechanical PHVs. Infective endocarditis in biological PHVs is often restricted to the leaflets, which can make differentiation between valve degeneration and vegetations (infective endocarditis) difficult, because both entities can present with leaflet thickening, leaflet prolapse, and antegrade extension of the leaflets.<sup>80</sup> The combination of the clinical presentation, laboratory findings, and imaging are essential to differentiate between valve degeneration and infective endocarditis.<sup>80</sup> TTE is the primary imaging technique to evaluate suspected PHV-related infective endocarditis and to detect vegetations in



**Table 5** | Reference values for biological prosthetic heart valves in the mitral position\*

Valve manufacturer	Normal Doppler echocardiographic peak gradient (mmHg)	Normal Doppler echocardiographic mean gradient (mmHg)
Biocor® stentless (St Jude Medical, St Paul, MN, USA) <sup>119</sup>	11.5–13 <sup>‡</sup>	NR
Bioflow pericardial (Biomedical, Glasgow, UK) <sup>122</sup>	4.0–10.0	2.0–6.3
Carpentier-Edwards® (Edwards Lifesciences, Irvine, CA, USA) <sup>127,167</sup>	NR	4.4–6.0
Carpentier-Edwards® pericardial (Edwards Lifesciences, Irvine, CA, USA) <sup>132</sup>	NR	1.0–5.3
Hancock® I (Medtronic, Minneapolis, MN, USA) <sup>133,167</sup>	3.0–10.0	2.5–5.0
Ionescu-Shiley (Shiley inc, Irvine, CA, USA) <sup>132</sup>	NR	3.2–4.9
Medtronic Intact® (Medtronic, Minneapolis, MN, USA) <sup>151</sup>	NR	3.2–4.2
Mitroflow® (Sorin Group Canada, Burnaby, Canada) <sup>132</sup>	NR	3.1–6.9

\*For the interpretation of the transvalvular pressure gradients, it is important to be aware that several factors, such as left-ventricular dysfunction and concomitant valvular disease, can influence the echocardiographic measurements. <sup>‡</sup>Depending on valve size. Abbreviation: NR = not reported.

biological PHVs. Compared with normal 2D TTE, 3D TTE can more accurately evaluate vegetation size, location, and extensiveness of infective endocarditis.<sup>27</sup> However, TEE is superior to TTE for the detection of vegetations in both the mitral and aortic position.<sup>29,76</sup> Infection of the sewing ring occurs less often than in mechanical PHVs, but can result in perivalvular abscesses.<sup>79</sup> Daniel et al. assessed TTE and TEE for the detection of perivalvular abscesses in 16 patients with biological PHVs, using intraoperative findings or autopsy reports as the reference standard. TEE was superior to TTE in the detection of perivalvular abscesses and PHV dehiscence, especially in the mitral position.<sup>27,76</sup> The latter was confirmed in other studies.<sup>29,31,76</sup> In patients with inconclusive echocardiographic results, 3D TTE, CMR, and MDCT can offer additional diagnostic value for the detection of perivalvular abscesses and for surgical planning.<sup>13,27,79</sup>

## CHOICE OF IMAGING TECHNIQUE

In the evaluation of biological PHV dysfunction, CMR might play a diagnostic role in patients with inconclusive echocardiographic windows, such as obese individuals, or patients with previous median sternotomy, pulmonary disease, or those displaying biological PHV artifacts.<sup>16,17</sup> Supporting structures such as struts can result in PHV-related artifacts. Further prospective research is required, however, to determine the exact diagnostic value of CMR.

We suggest that TTE should be the primary imaging technique to evaluate suspected biological PHV dysfunction, but can be followed by TEE, in particular for evaluation of PHV dysfunction

in the mitral position. Normal maximum and mean pressure gradients of commonly implanted biological PHVs are listed in Table 4 and Table 5. In patients with inconclusive findings from 2D echocardiography, 3D TTE or 3D TEE, MDCT, and CMR might have complementary value, especially in case of obstruction and infective endocarditis (Figure 4).<sup>13,14,27</sup>

## CONCLUSIONS

Noninvasive imaging techniques have an important role in the evaluation of PHV dysfunction and in therapeutic decision making. Nevertheless, evaluation of PHV dysfunction can result in diagnostic dilemmas. Primary echocardiographic evaluation, preferably using 3D techniques, followed by fluoroscopy in the case of mechanical PHVs, might fail to determine the cause of PHV dysfunction. CMR might have additional diagnostic value in patients with suspected biological PHV dysfunction. MDCT has shown to be of additional diagnostic value in the evaluation of PHV dysfunction in patients with an inconclusive routine diagnostic work-up and allows for more complete assessment of the cause of PHV dysfunction and the surrounding anatomy. Moreover, MDCT can have a key role in proper preoperative surgical planning and exclusion of coronary artery disease. In the clinical evaluation of patients with suspected PHV dysfunction, we propose the following diagnostic algorithm (Figure 4). However more studies are needed to determine the specific, additional diagnostic value of MDCT, 3D echocardiography and CMR to the routine diagnostic work-up with standard imaging techniques and intraoperative findings.

## REFERENCES

1. Yacoub MH, Takkenberg, JJ. Will heart valve tissue engineering change the world? *Nat Clin Pract Cardiovasc Med.* 2005; 2:60–61.
2. Cannegieter SC, Rosendaal FR, Briet E. Thromboembolic and bleeding complications in patients with mechanical heart valve prostheses. *Circulation* 1994; 89:635–641.
3. Khan S. Long-term outcomes with mechanical and tissue valves. *J Heart Valve Dis.* 2002; 11:S8–14.
4. Grunkemeier GL, Li HH, Naftel DC, et al. Long-term performance of heart valve prostheses. *Curr Probl Cardiol.* 2000; 25:73–154.
5. Hammermeister K, Sethi GK, Henderson WG, et al. Outcomes 15 years after valve replacement with a mechanical versus a bioprosthetic valve: final report of the Veterans Affairs randomized trial. *J Am Coll Cardiol* 2000; 36:1152–1158.
6. Akins CW, Miller DC, Turine MI, et al. Guidelines for reporting mortality and morbidity after cardiac valve interventions. *J Thorac Cardiovasc Surg.* 2008; 135:732–738.
7. Girard SE, Miller FA, Orszulak TA, et al. Reoperation for prosthetic aortic valve obstruction in the era of echocardiography: trends in diagnostic testing and comparison with surgical findings. *J Am Coll Cardiol.* 2001; 37:579–584.
8. Tsai IC, Lin YK, Chang Y, et al. Correctness of multi-detector-row computed tomography for diagnosing mechanical prosthetic heart valve disorders using operative findings as a gold standard. *Eur. Radiol.* 2009; 19:857–867.
9. Teshima H, Hayashida N, Fukunaga S, et al. Usefulness of a multidetector-row computed tomography scanner for detecting pannus formation. *Ann Thorac Surg.* 2004; 77:523–526.
10. Symersky P, Budde RP, de Mol BA et al. Comparison of multidetector-row computed tomography to echocardiography and fluoroscopy for evaluation of patients with mechanical prosthetic valve obstruction. *Am J Cardiol* 2009; 104:1128–1134.
11. LaBounty TM, Agarwal PP, Chughtai A, et al. Evaluation of mechanical heart valve size and function with ECG-gated 64-MDCT. *Am J Roentgenol.* 2009; 193:389–W396.
12. Konen E, Goitein O, Feinberg MS, et al. The role of ECG-gated MDCT in the evaluation of aortic and mitral mechanical valves: initial experience. *Am J Roentgenol.* 2008; 191:26–31.
13. Feuchtner GM, Stolzmann P, Dichtl W, et al. Multislice computed tomography in infective endocarditis: comparison with transesophageal echocardiography and intraoperative findings. *J Am Coll Cardiol.* 2009; 53:436–444.
14. Chenot F, Montant P, Goffinet C, et al. Evaluation of anatomic valve opening and leaflet morphology in aortic valve bioprosthesis by using multidetector CT: comparison with transthoracic echocardiography. *Radiology* 2010; 255:377–385.
15. Soulen RL, Budinger TF, Higgins CB. Magnetic resonance imaging of prosthetic heart valves. *Radiology* 1985; 154:705–707.
16. von Knobelsdorff-Brenkenhoff, F, Rudolph, A, Wassmuth, R, et al. Assessment of mitral bioprostheses using cardiovascular magnetic resonance. *J Cardiovasc Magn Reson* 2010; 12:36.
17. von Knobelsdorff-Brenkenhoff F, Rudolph A, Wassmuth R, et al. Feasibility of cardiovascular magnetic resonance to assess the orifice area of aortic bioprostheses. *Circ Cardiovasc Imaging* 2009; 2:397–404.
18. Zoghbi WA, Chambers JB, Dumesnil JG, et al. Recommendations for evaluation of prosthetic valves with echocardiography and doppler ultrasound: a report from the American Society of Echocardiography's Guidelines and Standards Committee and the Task Force on Prosthetic Valves, developed in conjunction with the American College of Cardiology Cardiovascular Imaging Committee, Cardiac Imaging Committee of the American Heart Association, the European Association of Echocardiography, a registered branch of the European Society of Cardiology, the Japanese Society of Echocardiography and the Canadian Society of Echocardiography, endorsed by the American College of Cardiology Foundation, American Heart Association, European Association of Echocardiography, a registered branch of the European Society of Cardiology, the Japanese Society of Echocardiography, and Canadian Society of Echocardiography. *J Am Soc Echocardiogr.* 2009; 22:975–1014.
19. Feigenbaum H, Armstrong WF, Thomas R. Page 11-21. In: Feigenbaum H, Armstrong WF, Thomas R (eds). *Feigenbaum's echocardiography.* Philadelphia, Lippincott Williams & Wilkins, 2005.
20. Bitar JN, Lechin ME, Salazar G, et al. Doppler echocardiographic assessment with the continuity equation of St. Jude Medical mechanical prostheses in the mitral valve position. *Am J Cardiol.* 1995; 76:287–293.
21. van den Brink RB. Evaluation of prosthetic heart valves by transesophageal echocardiography: problems, pitfalls, and timing of echocardiography. *Semin Cardiothorac Vasc Anesth* 2006; 10:89–100.

22. Garcia D, Kadem L. What do you mean by aortic valve area: geometric orifice area, effective orifice area, or gorlin area? *J Heart Valve Dis.* 2006; 15:601–608.
23. Steiner RM, Mintz G, Morse D, et al. The radiology of cardiac valve prostheses. *Radiographics* 1988; 8:277–298.
24. Chambers J, Coppack F, Deverall P, et al. The continuity equation tested in a bileaflet aortic prosthesis. *Int J Cardiol.* 1991; 31:149–154.
25. Keser N, Nanda NC, Miller AP, et al. Hemodynamic evaluation of normally functioning Sulzer Carbomedics prosthetic valves. *Ultrasound Med. Biol.* 2003; 29:649–657.
26. Hage FG, Nanda NC. Guidelines for the evaluation of prosthetic valves with echocardiography and Doppler ultrasound: value and limitations. *Echocardiography* 2010; 27:91–93.
27. Singh P, Inamdar V, Hage FG, et al. Usefulness of live/real time three-dimensional transthoracic echocardiography in evaluation of prosthetic valve function. *Echocardiography* 2009; 26, 1236–1249.
28. Feigenbaum H, Armstrong WF, Thomas R. Page 59–61 In: Feigenbaum H, Armstrong WF, Thomas R (eds). *Feigenbaum's echocardiography*. Philadelphia, Lippincott Williams & Wilkins, 2005.
29. Zabalgoitia M, Herrera CJ, Chaudhry FA, et al. Improvement in the diagnosis of bioprosthetic valve dysfunction by transesophageal echocardiography. *J Heart Valve Dis.* 1993; 2:595–603.
30. Daniel LB, Grigg LE, Weisel RD, et al. Comparison of transthoracic and transesophageal assessment of prosthetic valve dysfunction. *Echocardiography* 1990; 7:83–95.
31. Karalis DG, Chandrasekaran K, Ross JJ Jr, et al. Single-plane transesophageal echocardiography for assessing function of mechanical or bioprosthetic valves in the aortic valve position. *Am J Cardiol.* 1992; 69:1310–1315.
32. Chaudhry FA, Herrera C, DeFrino PF, et al. Pathologic and angiographic correlations of transesophageal echocardiography in prosthetic heart valve dysfunction. *Am Heart J* 1991; 122:1057–1064.
33. Cianciulli TE, Lax JA, Beck MA, et al. Cinefluoroscopic assessment of mechanical disc prostheses: its value as a complementary method to echocardiography. *J Heart Valve Dis.* 2005; 14:664–673.
34. Singh P, Manda J, Hsiung MC, et al. Live/real time three-dimensional transesophageal echocardiographic evaluation of mitral and aortic valve prosthetic paravalvular regurgitation. *Echocardiography* 2009; 26:980–987.
35. Muratori M, Montorsi P, Teruzzi G, et al. Feasibility and diagnostic accuracy of quantitative assessment of mechanical prostheses leaflet motion by transthoracic and transesophageal echocardiography in suspected prosthetic valve dysfunction. *Am J Cardiol.* 2006; 97:94–100.
36. Faletra FF, Alain M, Moccetti, T. Blockage of bileaflet mitral valve prosthesis imaged by computed tomography virtual endoscopy. *Heart* 2007; 93:324.
37. Symersky P, Budde RPJ, Prokop M, et al. Multidetector-row computed tomography imaging characteristics of mechanical prosthetic valves. *J Heart Valve Dis.* 2011; 20:216–222.
38. Habets J, Symersky P, van Herwerden LA, et al. Prosthetic heart valve assessment with multidetector-row CT: imaging characteristics of 91 valves in 83 patients. *Eur Radiol.* 2011; 21:1390–1396.
39. Symersky P, Budde RP, Prokop M, et al. Abstract 541: prosthetic valve evaluation using prospective triggering with 256-detector row computed tomography reduces radiation dose [abstract]. *Circulation* 2009; 120:S355.
40. Vahanian A, Baumgartner H, Bax J, et al. Guidelines on the management of valvular heart disease: The Task Force on the Management of Valvular Heart Disease of the European Society of Cardiology. *Eur Heart J* 2007; 28:230–268.
41. Lin SS, Tiong IY, Asher CR, et al. Prediction of thrombus-related mechanical prosthetic valve dysfunction using transesophageal echocardiography. *Am J Cardiol.* 2000; 86:1097–1101.
42. Licata A, Matthai WH Jr. Evaluating the etiology of mechanical valve obstruction: use of clinical parameters, fluoroscopy, and echocardiography. *Catheter Cardiovasc Interv.* 2002; 55:495–500.
43. Teshima H, Hayashida N, Yano H, et al. Obstruction of St Jude Medical valves in the aortic position: histology and immunohistochemistry of pannus. *J Thorac Cardiovasc Surg.* 2003; 126:401–407.
44. Deviri E, Sareli P, Wisenbaugh T, et al. Obstruction of mechanical heart valve prostheses: clinical aspects and surgical management. *J Am Coll Cardiol.* 1991; 17:646–650.
45. Barbetseas J, Nagueh SF, Pitsavos C, et al. Differentiating thrombus from pannus formation in obstructed mechanical prosthetic valves: an evaluation of clinical, transthoracic and transesophageal echocardiographic parameters. *J Am Coll Cardiol.* 1998; 32:1410–1417.
46. Guiar-Souto P, Mirelis JG, Silva-Melchor L. Guidelines on the management of valvular heart disease. *Eur Heart J* 2007; 28:1267–1268.

47. Vitale N, Renzulli A, Agozzino L, et al. Obstruction of mechanical mitral prostheses: analysis of pathologic findings. *Ann Thorac Surg.* 1997; 63:1101–1106.
48. Kondruweit M, Flachskampf FA, Weyand M, et al. Early failure of a mechanical bileaflet aortic valve prosthesis due to pannus: a rare complication. *J Thorac Cardiovasc Surg.* 2008; 136:213–214.
49. Daniel WG, Mügge A, Grote J, et al. Comparison of transthoracic and transesophageal echocardiography for detection of abnormalities of prosthetic and bioprosthetic valves in the mitral and aortic positions. *Am J Cardiol.* 1993; 71:210–215.
50. Montorsi P, De Bernardi F, Muratori M. Role of cine-fluoroscopy, transthoracic, and transesophageal echocardiography in patients with suspected prosthetic heart valve thrombosis. *Am J Cardiol.* 2000; 85:58–64.
51. Aoyagi S, Nishimi M, Tayama E, et al. Obstruction of St Jude medical valves in the aortic position: a consideration for pathogenic mechanism of prosthetic valve obstruction. *Cardiovasc Surg.* 2002; 10:339–344.
52. Chan J, Marwan M, Schepsis T, et al. Images in cardiovascular medicine. Cardiac CT assessment of prosthetic aortic valve dysfunction secondary to acute thrombosis and response to thrombolysis. *Circulation* 2009; 120:1933–1934.
53. Bleiziffer S, Eichinger WB, Hettich I, et al. Prediction of valve prosthesis-patient mismatch prior to aortic valve replacement: which is the best method? *Heart* 2007; 93:615–620.
54. Urso S, Sadaba R, Aldamiz-Echevarria G. Is patient-prosthesis mismatch an independent risk factor for early and mid-term overall mortality in adult patients undergoing aortic valve replacement? *Interact Cardiovasc Thorac Surg.* 2009; 9:510–518.
55. Blais C, Dumesnil JG, Baillet R, et al. Impact of valve prosthesis-patient mismatch on short-term mortality after aortic valve replacement. *Circulation* 2003; 108:983–988.
56. Pibarot P, Dumesnil JG. Hemodynamic and clinical impact of prosthesis-patient mismatch in the aortic valve position and its prevention. *J Am Coll Cardiol.* 2000; 36:1131–1141.
57. Tasca G, Brunelli F, Cirillo M, et al. Impact of valve prosthesis-patient mismatch on left ventricular mass regression following aortic valve replacement. *Ann Thorac Surg.* 2005; 79:505–510.
58. Pibarot P, Dumesnil JG. Prevention of valve prosthesis—patient mismatch before aortic valve replacement: does it matter and is it feasible? *Heart* 2007; 93:549–551.
59. Pibarot P, Dumesnil JG. Prosthesis-patient mismatch in the mitral position: old concept, new evidences. *J Thorac Cardiovasc Surg.* 2007; 133:1405–1408.
60. Yazdanbakhsh AP, van den Brink RB, Dekker E, et al. A. Small valve area index: its influence on early mortality after mitral valve replacement. *Eur J Cardiothorac Surg.* 2000; 17:222–227.
61. LaBounty TM, Agarwall PP, Chughtai A, et al. Hemodynamic and functional assessment of mechanical aortic valves using combined echocardiography and multidetector computed tomography. *J Cardiovasc Comput Tomogr.* 2009; 3:161–167.
62. Doddamani S, Grushko MJ, Makaryus AN, et al. Demonstration of left ventricular outflow tract eccentricity by 64-slice multi-detector CT. *Int J Cardiovasc Imaging* 2009; 25:175–181.
63. Van den Brink RB, Visser CA, Basart DC, et al. Comparison of transthoracic and transesophageal color Doppler flow imaging in patients with mechanical prostheses in the mitral valve position. *Am. J Cardiol.* 1989; 63:1471–1474.
64. Daniel LB, Grigg LE, Weisel RD, et al. Comparison of transthoracic and transesophageal assessment of prosthetic valve dysfunction. *Echocardiography* 1990; 7:83–95.
65. Bashore TM, Cabell C, Fowler V Jr. Update on infective endocarditis. *Curr Probl Cardiol.* 2006; 31:274–352.
66. Li JS, Sexton DJ, Mick N. Proposed modifications to the Duke criteria for the diagnosis of infective endocarditis. *Clin Infect Dis.* 2000; 30:633–638.
67. Hanrath P. Imaging techniques: transoesophageal echo-doppler in cardiology. *Heart* 2001; 86:586–592.
68. Jacob S, Tong AT. Role of echocardiography in the diagnosis and management of infective endocarditis. *Curr Opin Cardiol.* 2002; 17:478–485.
69. Bonow RO, Carabello BA, Chatterjee K, et al. 2008 focused update incorporated into the ACC/AHA 2006 guidelines for the management of patients with valvular heart disease: a report of the American College of Cardiology/American Heart Association Task Force on Practice Guidelines (Writing Committee to revise the 1998 guidelines for the management of patients with valvular heart disease). Endorsed by the Society of Cardiovascular Anesthesiologists, Society for Cardiovascular Angiography and Interventions, and Society of Thoracic Surgeons. *J Am Coll Cardiol* 2008; 52:e1–e142.

70. Daniel WG, Mügge A, Grote J, et al. Comparison of transthoracic and transesophageal echocardiography for detection of abnormalities of prosthetic and bioprosthetic valves in the mitral and aortic positions. *Am J Cardiol.* 1993; 71:210–215.
71. Meijboom WB, Mollet NR, Van Mieghem CA, et al. Pre-operative computed tomography coronary angiography to detect significant coronary artery disease in patients referred for cardiac valve surgery. *J Am Coll Cardiol.* 2006; 48:1658–1665.
72. Ro TK, Cotter BR, Simsir SA, et al. Complicated ruptured sinus of Valsalva: cardiac computed tomographic angiography (64 slice) predicts surgical appearance and obviates need for invasive cardiac catheterization. *Interact Cardiovasc Thorac Surg.* 2009; 9:888–890.
73. Daniel WG, Mügge A, Martin RP, et al. Improvement in the diagnosis of abscesses associated with endocarditis by transesophageal echocardiography. *N Engl J Med* 1991; 324:795–800.
74. Lerakis S, Robert Taylor W, Lynch M, et al. The role of transesophageal echocardiography in the diagnosis and management of patients with aortic perivalvular abscesses. *Am J Med Sci.* 2001; 321: 152–155.
75. Leung DY, Cranney GB, Hopkins AP, et al. W. F. Role of transoesophageal echocardiography in the diagnosis and management of aortic root abscess. *Br Heart J* 1994; 72:175–181.
76. Daniel WG, Mügge A, Grote J, et al. Comparison of transthoracic and transesophageal echocardiography for detection of abnormalities of prosthetic and bioprosthetic valves in the mitral and aortic positions. *Am J Cardiol.* 1993; 71:210–215.
77. Teoh KH, Ivanov J, Weisel RD, et al. Clinical and Doppler echocardiographic evaluation of bioprosthetic valve failure after 10 years. *Circulation* 1990; 82:IV110–IV116.
78. Chen YT, Kan MN, Chen JS, et al. Detection of prosthetic mitral valve leak: a comparative study using transesophageal echocardiography, transthoracic echocardiography, and auscultation. *J Clin Ultrasound* 1990; 18:557–561.
79. Mahesh B, Angelini G, Caputo M, et al. Prosthetic valve endocarditis. *Ann Thorac Surg.* 2005; 80:1151–1158.
80. Effron MK, Popp RL. Two-dimensional echocardiographic assessment of bioprosthetic valve dysfunction and infective endocarditis. *J Am Coll Cardiol.* 1983; 2:597–606.
81. Kirzner CF, Vinals B, Moya J, et al. Hemodynamic performance evaluation of small aortic ATS Medical valves by Doppler echocardiography. *J Heart Valve Dis.* 1997; 6:661–665.
82. Karpuz H, Jeanrenaud X, Hurni M, et al. Doppler echocardiographic assessment of the new ATS medical prosthetic valve in the aortic position. *Am J Card Imaging* 1996; 10:254–260.
83. De Paulis R, Sommariva L, Russo F, et al. Doppler echocardiography evaluation of the CarboMedics valve in patients with small aortic anulus and valve prosthesis-body surface area mismatch. *J Thorac Cardiovasc Surg.* 1994; 108:57–62.
84. Chakraborty B, Quek S, Pin DZ, et al. Doppler echocardiographic assessment of normally functioning Starr-Edwards, carbomedics and Carpentier-Edwards valves in aortic position. *Angiology* 1996; 47:481–489.
85. Chambers J, Cross J, Deverall P, et al. Echocardiographic description of the CarboMedics bileaflet prosthetic heart valve. *J Am Coll Cardiol.* 1993; 21:398–405.
86. De Paulis R, Sommariva L, De Matteis GM, et al. Hemodynamic performances of small diameter carbomedics and St. Jude valves. *J Heart Valve Dis.* 1996; 5:S339–S343.
87. Globits S, Rödler S, Mayr H, et al. Doppler sonographic evaluation of the CarboMedics bileaflet valve prosthesis: one-year experience. *J Card Surg.* 1992; 7:9–16.
88. Ihlen H, Mølsted P, Simonsen S, et al. Hemodynamic evaluation of the CarboMedics prosthetic heart valve in the aortic position: comparison of noninvasive and invasive techniques. *Am Heart J* 1992; 123:151–159.
89. Izzat MB, Birdi I, Wilde P, et al. Evaluation of the hemodynamic performance of small CarboMedics aortic prostheses using dobutamine-stress Doppler echocardiography. *Ann Thorac Surg.* 1995; 60:1048–1052.
90. Gibbs JL, Wharton GA, Williams GJ. Doppler echocardiographic characteristics of the Carpentier-Edwards xenograft. *Eur Heart J* 1986; 7:353–356.
91. Wiseth R, Levang OW, Sande E, et al. Hemodynamic evaluation by Doppler echocardiography of small (less than or equal to 21 mm) prostheses and bioprostheses in the aortic valve position. *Am J Cardiol.* 1992; 70:240–246.
92. Gioia G, Rutsch W. Normal echo-Doppler values in Duromedics valvular prostheses [Italian]. *G Ital Cardiol.* 1988; 18:213–217.
93. Chambers J, Ely JL. Early postoperative echocardiographic hemodynamic performance of the On-X prosthetic heart valve: a multicenter study. *J Heart Valve Dis.* 1998; 7:569–573.

94. Noera G, Pensa P, Lamarra M, et al. Hemodynamic evaluation of the Carbomedics R, St Jude Medical HP and Sorin-Bicarbon valve in patients with small aortic annulus. *Eur J Cardiothorac Surg.* 1997; 11:473–475.
95. Badano L, Mocchegiani R, Bertoli D, et al. Normal echocardiographic characteristics of the Sorin Bicarbon bileaflet prosthetic heart valve in the mitral and aortic positions. *J Am Soc Echocardiogr.* 1997; 10:632–643.
96. Flameng W, Vandeplas A, Narine K, et al. Postoperative hemodynamics of two bileaflet heart valves in the aortic position. *J Heart Valve Dis.* 1997; 6:269–273.
97. Bech-Hanssen O, Wallentin I, Larsson S, et al. Reference Doppler echocardiographic values for St. Jude Medical, Omnicarbon, and Biocor prosthetic valves in the aortic position. *J Am Soc Echocardiogr.* 1998; 11:466–477.
98. Aris A, Ramirez I, Camara ML, et al. The 20 mm Medtronic Hall prosthesis in the small aortic root. *J Heart Valve Dis.* 1996; 5:459–462.
99. Henneke KH, Pongratz G, Pohlmann M, et al. Doppler echocardiographic determination of geometric orifice areas in mechanical aortic valve prostheses. *Cardiology* 1995; 86:508–513.
100. Cooper DM, Stewart WJ, Schiavone WA, et al. Evaluation of normal prosthetic valve function by Doppler echocardiography. *Am Heart J* 1987; 114:576–582.
101. Chafizadeh ER, Zoghbi WA. Doppler echocardiographic assessment of the St. Jude Medical prosthetic valve in the aortic position using the continuity equation. *Circulation* 1991; 83:213–223.
102. Kadir I, Izzat MB, Birdi I, et al. Hemodynamics of St. Jude Medical prostheses in the small aortic root: *in vivo* studies using dobutamine Doppler echocardiography. *J Heart Valve Dis.* 1997; 6:123–129.
103. Panidis IP, Ross J, Mintz GS. Normal and abnormal prosthetic valve function as assessed by Doppler echocardiography. *J Am Coll Cardiol.* 1986; 8:317–326.
104. Perin EC, Jin BS, de Castro CM, et al. Doppler echocardiography in 180 normally functioning St. Jude Medical aortic valve prostheses. Early and late postoperative assessments. *Chest* 1991; 100: 988–990.
105. Ren JF, Chandrasekaran K, Mintz GS, et al. Effect of depressed left ventricular function on hemodynamics of normal St. Jude Medical prosthesis in the aortic valve position. *Am J Cardiol.* 1990; 65:1004–1009.
106. Carrel T, Zingg U, Jenni R, et al. Early *in vivo* experience with the Hemodynamic Plus St. Jude Medical heart valves in patients with narrowed aortic annulus. *Ann Thorac Surg.* 1996; 61:1418–1422.
107. Laske A, Jenni R, Maloigne M, et al. Pressure gradients across bileaflet aortic valves by direct measurement and echocardiography. *Ann Thorac Surg.* 1996; 61:48–57.
108. Kenny A, Woods J, Fuller CA, et al. Hemodynamic evaluation of the Monostrut and spherical disc Bjork-Shiley aortic valve prosthesis with Doppler echocardiography. *J Thorac Cardiovasc Surg.* 1992; 104:1025–1028.
109. Sagar KB, Wann LS, Paulsen WH, et al. Doppler echocardiographic evaluation of Hancock and Bjork-Shiley prosthetic valves. *J Am Coll Cardiol.* 1986; 7:681–687.
110. Gibbs JL, Wharton GA, Williams GJ. Doppler ultrasound of normally functioning mechanical mitral and aortic valve prostheses. *Int J Cardiol.* 1988; 18:391–398.
111. Habib G, Bénichou M, Gisbert MP, et al. Contribution of Doppler echocardiography in the evaluation of normal and pathologic aortic valve prosthesis. *Arch Mal Coeur Vaiss.* 1990; 83:937–945.
112. Mikhail A. A hemodynamic comparison of Omniscience and Medtronic Hall aortic prostheses. *J Heart Valve Dis.* 1996; 5:675–677.
113. Raisaro A, Caizzi V, Roda G, et al. Doppler evaluation of the Sorin and Medtronic-Hall prostheses in the aortic position. *G. Ital. Cardiol.* 1988; 18:206–212.
114. Badano L, Bertoli D, Astengo D, et al. Doppler haemodynamic assessment of clinically and echocardiographically normal mitral and aortic Allcarbon valve prostheses. Valve Prostheses Ligurian Cooperative Doppler Study. *Eur Heart J* 1993; 14:1602–1609.
115. Soo CS, Ca M, Tay M, et al. Doppler-echocardiographic assessment of Carbomedics prosthetic valves in the mitral position. *J Am Soc Echocardiogr.* 1994; 7:159–164.
116. Bjørnerheim R, Ihlen H, Simonsen S, et al. Hemodynamic characterization of the CarboMedics mitral valve prosthesis. *J Heart Valve Dis.* 1997; 6:115–122.
117. Mohan JC, Agrawal R, Arora R, et al. Improved Doppler assessment of the Bjork-Shiley mitral prosthesis using the continuity equation. *Int J Cardiol.* 1994; 43:321–326.
118. Eriksson M, Brodin LA, Ericsson A, et al. Doppler-derived pressure differences in normally functioning aortic valve prostheses. Studies in Bjork-Shiley monostrut and Biocor porcine prostheses. *Scand J Thorac Cardiovasc Surg.* 1993; 27:93–97.
119. Mykén PS, Berggren HE, Larsson S, et al. Long-term Doppler echocardiographic results of aortic or mitral valve replacement with Biocor porcine bioprosthesis. *J Thorac Cardiovasc Surg.* 1998; 116:599–608.

120. Eriksson MJ, Brodin LA, Dellgren GN, et al. Rest and exercise hemodynamics of an extended stentless aortic bioprosthesis. *J Heart Valve Dis.* 1997; 6:653–660.
121. Gonzalez-Juanatey JR, García-Acuña JM, Vega Fernandez M, et al. Hemodynamics of various designs of 19 mm pericardial aortic valve bioprosthesis. *Eur J Cardiothorac Surg.* 1996; 10:201–206.
122. Gonzalez-Juanatey JR, García-Bengochea JB, Vega M, et al. Doppler echocardiographic evaluation of the Bioflo pericardial bioprosthesis. *J Heart Valve Dis.* 1993; 2:315–319.
123. Ramirez ML, Wong M, Sadler N, et al. Doppler evaluation of bioprosthetic and mechanical aortic valves: data from four models in 107 stable, ambulatory patients. *Am Heart J* 1988; 115: 418–425.
124. Habib G, Bénichou M, Gisbert MP, et al. Contribution of Doppler echocardiography in the evaluation of normal and pathologic aortic valve prosthesis. *Arch. Mal. Coeur Vaiss.* 1990; 83:937–945.
125. Chakraborty B, Quek S, Pin DZ, et al. Doppler echocardiographic assessment of normally functioning Starr-Edwards, carbomedics and Carpentier-Edwards valves in aortic position. *Angiology* 1996; 47:481–489.
126. Bojar RM, Rastegar H, Payne DD, et al. Clinical and hemodynamic performance of the 19-mm Carpentier-Edwards porcine bioprosthesis. *Ann Thorac Surg.* 1993; 56:1141–1147.
127. Gibbs JL, Wharton GA, Williams GJ. Doppler echocardiographic characteristics of the Carpentier-Edwards xenograft. *Eur Heart J* 1986; 7:353–356.
128. McDonald ML, Daly RC, Schaff HV, et al. Hemodynamic performance of small aortic valve bioprostheses: is there a difference? *Ann Thorac Surg.* 1997; 63:362–366.
129. Mullany CJ, Schaff HV, Orszulak TA, et al. Early clinical and hemodynamic evaluation of the aortic intact porcine bioprosthesis. *J Heart Valve Dis.* 1994; 3:641–647.
130. Wiseth R, Levang OW, Sande E, et al. Hemodynamic evaluation by Doppler echocardiography of small (less than or equal to 21 mm) prostheses and bioprostheses in the aortic valve position. *Am J Cardiol.* 1992; 70:240–246.
131. Cooper DM, Stewart WJ, Schiavone WA, et al. Evaluation of normal prosthetic valve function by Doppler echocardiography. *Am Heart J* 1987; 114:576–582.
132. Lesbre JP, Chassat C, Lespérance J, et al. Evaluation of new pericardial bioprostheses by pulsed and continuous Doppler ultrasound. *Arch Mal Coeur Vaiss.* 1986; 79:1439–1448.
133. Sagar KB, Wann LS, Paulsen WH, et al. Doppler echocardiographic evaluation of Hancock and Bjork-Shiley prosthetic valves. *J Am Coll Cardiol.* 1986; 7:681–687.
134. David TE, Armstrong S, Sun Z. Clinical and hemodynamic assessment of the Hancock II bioprosthesis. *Ann Thorac Surg.* 1992; 54:661–667.
135. Eichinger WB, Schütz A, Simmerl D, et al. The mosaic bioprosthesis in the aortic position: hemodynamic performance after 2 years. *Ann Thorac Surg.* 1998; 66:S126–S129.
136. Ius P, Totis O, Chirillo F, et al. Hemodynamic evaluation of 23 mm Pericarbon and 23 mm Hancock II bioprostheses in the aortic position at mid-term follow up. *J Heart Valve Dis.* 1996; 5: 656–661.
137. Bojar RM, Diehl JT, Moten M, et al. Clinical and hemodynamic performance of the Ionescu-Shiley valve in the small aortic root. Results in 117 patients with 17 and 19 mm valves. *J Thorac Cardiovasc Surg.* 1989; 98:1087–1095.
138. Simpson IA, Reece IJ, Houston AB, et al. Non-invasive assessment by Doppler ultrasound of 155 patients with bioprosthetic valves: a comparison of the Wessex porcine, low profile Ionescu-Shiley, and Hancock pericardial bioprostheses. *Br Heart J* 1986; 56:83–88.
139. Gonzalez-Juanatey JR, García-Bengochea JB, Garcia-Acuña JM, et al. The influence of the design on the medium to long-term hemodynamic behavior of 19 mm pericardial aortic valve prostheses. *J Heart Valve Dis.* 1996; 5:S317–S323.
140. Bojar RM, Diehl JT, Moten M, et al. Clinical and hemodynamic performance of the Ionescu-Shiley valve in the small aortic root. Results in 117 patients with 17 and 19 mm valves. *J Thorac Cardiovasc Surg.* 1989; 98:1087–1095.
141. Cartier PC, Dumesnil JG, Métras J, et al. Clinical and hemodynamic performance of the Freestyle aortic root bioprosthesis. *Ann Thorac Surg.* 1999; 67:345–349.
142. Baur LH, Jin XY, Houdas Y, et al. Echocardiographic parameters of the freestyle stentless bioprosthesis in aortic position: the European experience. *J Am Soc Echocardiogr.* 1999; 12:729–735.
143. Yun KL, Jamieson WR, Khonsari S, et al. Prosthesis-patient mismatch: hemodynamic comparison of stented and stentless aortic valves. *Semin Thorac Cardiovasc Surg.* 1999; 11:98–102.
144. Dumesnil JG, LeBlanc MH, Cartier PC, et al. Hemodynamic features of the freestyle aortic bioprosthesis compared with stented bioprosthesis. *Ann Thorac Surg.* 1998; 66:S130–S133.



145. Dagenais F, Cartier P, Dumesnil JG, et al. A single center experience with the freestyle bioprosthesis: midterm results at the Quebec Heart Institute. *Semin Thorac Cardiovasc Surg.* 2001; 13:156–162.
146. Yun KL, Sintek CF, Fletcher AD, et al. Aortic valve replacement with the freestyle stentless bioprosthesis: five-year experience. *Circulation* 1999; 100: II17–II23.
147. Kappetein AP, Braun J, Baur LH, et al. Outcome and follow-up of aortic valve replacement with the freestyle stentless bioprosthesis. *Ann Thorac Surg.* 2001; 71:601–607.
148. Baur LH, Jin XY, Houdas Y, et al. Echocardiographic parameters of the freestyle stentless bioprosthesis in aortic position: the European experience. *J Am Soc Echocardiogr.* 1999; 12: 729–735.
149. Del Rizzo DF, Abdoh A. Clinical and hemodynamic comparison of the Medtronic Freestyle and Toronto SPV stentless valves. *J Card Surg.* 1998; 13:398–407.
150. Fries R, Wendler O, Schieffer H, et al. Comparative rest and exercise hemodynamics of 23-mm stentless versus 23-mm stented aortic bioprostheses. *Ann Thorac Surg.* 2000; 69:817–822.
151. Jaffe, WM, Barratt-Boyes BG, Sadri A. Early follow-up of patients with the Medtronic Intact porcine valve. A new cardiac bioprosthesis. *J Thorac Cardiovasc Surg.* 1989; 98:181–192.
152. Etienne Y, Jobic Y, Genet L, et al. Evaluation of the normal bioprosthetic Intact aortic valve by Doppler echocardiography. *Arch Mal Coeur Vaiss.* 1990; 83:2039–2044.
153. Ricou F, Brun A, Lerch R. Hemodynamic comparison of Medtronic intact bioprostheses and bileaflet mechanical prostheses in aortic position. *Cardiology* 1996; 87:212–215.
154. Dumesnil JG, Honos GN, Lemieux M, et al. Validation and applications of indexed aortic prosthetic valve areas calculated by Doppler echocardiography. *J Am Coll Cardiol.* 1990; 16:637–643.
155. Thomson DJ, Jamieson WR, Dumesnil JG, et al. Medtronic mosaic porcine bioprosthesis satisfactory early clinical performance. *Ann Thorac Surg.* 1998; 66:S122–S125.
156. Jamieson WR, Janusz MT, MacNab J, et al. Hemodynamic comparison of second- and third-generation stented bioprostheses in aortic valve replacement. *Ann Thorac Surg.* 2001; 71:S282–S284.
157. Eichinger W, Günzinger R, Botzenhardt F, et al. The Mosaic bioprosthesis in the aortic position at five years. *J Heart Valve Dis.* 2000; 9:653–660.
158. Corbineau H, Lelong B, Langanay T, et al. Echocardiographic assessment and preliminary clinical results after aortic valve replacement with the Medtronic Mosaic bioprosthesis. *J Heart Valve Dis.* 2001; 10:171–176.
159. Fradet GJ, Bleese N, Burgess J, et al. Mosaic valve international clinical trial: early performance results. *Ann Thorac Surg.* 2001; 71:S273–S277.
160. Fradet G, Bleese N, Busse E, et al. The mosaic valve clinical performance at seven years: results from a multicenter prospective clinical trial. *J Heart Valve Dis.* 2004; 13:239–246.
161. Yun KL, Jamieson WR, Khonsari S, et al. Prosthesis-patient mismatch: hemodynamic comparison of stented and stentless aortic valves. *Semin. Thorac. Cardiovasc. Surg* 1999; 11:98–102.
162. Wong SP, Legget ME, Greaves SC, et al. Early experience with the mosaic bioprosthesis: a new generation porcine valve. *Ann Thorac Surg.* 2000; 69:1846–1850.
163. Gansera B, Botzenhardt F, Günzinger R, et al. The Mosaic bioprosthesis in the aortic position: seven years' results. *J Heart Valve Dis.* 2003; 12:354–361.
164. Nardi C, Sciotti G, Milano AD, et al. Hemodynamic assessment of the Medtronic Mosaic bioprosthesis in the aortic position. *J Heart Valve Dis.* 2001; 10:100–104.
165. Milano AD, Blanzola C, Mecozzi G, et al. Hemodynamic performance of stented and stentless aortic bioprostheses. *Ann Thorac Surg.* 2001; 72:33–38.
166. Eichinger WB, Botzenhardt F, Keithahn A, et al. Exercise hemodynamics of bovine versus porcine bioprostheses: a prospective randomized comparison of the mosaic and perimount aortic valves. *J Thorac Cardiovasc Surg.* 2005; 129:1056–1063.
167. Habib G, Bénichou M, Bonnet JL, et al. Contribution of Doppler echocardiography to the evaluation and monitoring of normal and pathologic mitral valve prostheses. *Arch Mal Coeur Vaiss.* 1990; 83:469–477.





CHAPTER III

NON-INVASIVE IMAGING *of*  
LEFT-SIDED PROSTHETIC  
HEART VALVE DYSFUNCTION:  
*a* SYSTEMATIC REVIEW *and*  
META-ANALYSIS

J. Habets

W. Tanis

J.B. Reitsma

R.B.A. van den Brink

W.P.Th.M. Mali

S.A.J. Chamuleau

R.P.J. Budde

SUBMITTED

**ABSTRACT**

**PURPOSE** | to determine and compare the diagnostic accuracy of transthoracic echocardiography (TTE), transesophageal echocardiography (TEE), fluoroscopy and multidetector-row computed tomography (MDCT) to (1) detect signs of PHV endocarditis (vegetations, peri-annular complications, PHV dehiscence, PHV endocarditis in general) in patients with suspected PHV endocarditis and (2) to reveal the exact cause of PHV obstruction in patients with suspected PHV obstruction.

**METHODS** | A systematic electronic search was performed in Pubmed and Embase. Full-text publications fulfilling the inclusion criteria were assessed by two reviewers independently. Studies were systematically assessed for methodological quality based on the validated Quality Assessment of Diagnostic Accuracy Studies (QUADAS) II checklist. Primary outcome was the diagnostic accuracy of non-invasive imaging modalities (TTE, TEE, fluoroscopy, and MDCT) for the detection of signs of PHV endocarditis and the exact causes of PHV obstruction. Random effects meta-analysis was performed. Forest plots of sensitivity and specificity with their corresponding 95% confidence intervals (CI) were generated stratified for the different signs of interest and within each forest plot data were grouped by the different index tests (TTE, TEE, fluoroscopy and MDCT).

**RESULTS** | In total, 32 studies were included in this systematic review including 20 on PHV endocarditis and 12 on PHV obstruction. The studies reporting on cause of PHV obstruction did not provide diagnostic accuracy measures for the exact cause of PHV obstruction. Eighteen of 20 endocarditis reported diagnostic accuracy data for the detection of signs of PHV endocarditis. TTE had a pooled sensitivity/specificity for vegetations (29%/100%), peri-annular complications (36%/93%), PHV dehiscence (12%/100%) and PHV endocarditis in general (38%/100%). TEE had a pooled sensitivity/specificity for vegetations (84%/96%), peri-annular complications (89%/98%), PHV dehiscence (85%/96%) and PHV endocarditis in general (82%/97%). TEE is superior to TTE for the detection of signs of PHV endocarditis ( $p$ -value $\leq$ 0.03). Only very limited data was available for fluoroscopy and MDCT.

**CONCLUSION** | The principal findings of this systematic review are: (1) in a mainly surgically explored population, TEE has a good sensitivity for the detection of signs of PHV endocarditis, and is superior to TTE; (2) TEE still misses signs of PHV endocarditis even in this selected population; (3) both TTE and TEE have a good specificity for the detection of signs of PHV endocarditis; and (4) differentiation between pannus and thrombus formation remains difficult or even impossible based echocardiographic evaluation.

Left-sided native heart valve disease often requires prosthetic heart valve (PHV) implantation. In 2003, the total number of patients who required heart valve replacement was approximately 290,000. This annual incidence is increasing mainly due to an aging population and estimated to rise to 850,000 in 2050.<sup>1</sup> PHV dysfunction may develop during clinical follow-up and although occurring infrequently (reported incidence ranging from 0.01% to 6.0% per year) it is a potentially life-threatening disease.<sup>2-6</sup>

In clinical practice, transthoracic echocardiography (TTE), transesophageal echocardiography (TEE) and fluoroscopy are the non-invasive imaging modalities to evaluate PHVs and diagnose PHV dysfunction.<sup>7</sup> PHV dysfunction is a heterogeneous group including PHV obstruction, endocarditis and regurgitation. Diagnostic evaluation with TTE and TEE is very accurate for the detection of pathological PHV regurgitation.<sup>8</sup> In contrast to PHV regurgitation, diagnostic dilemmas may arise in patients with suspected PHV obstruction and endocarditis.<sup>8</sup> TTE is the first line clinical screening tool for the detection of PHV obstruction and endocarditis but often fails to detect the exact cause of PHV dysfunction. TEE can have incremental value to diagnose the exact cause of PHV dysfunction. However, even TEE may also fail to detect this exact cause of PHV dysfunction especially in patients with aortic PHVs.<sup>9</sup> Fluoroscopy can be used for mechanical PHVs to assess leaflet motion which can provide limited additional information to echocardiography. Multidetector-row computed tomography (MDCT) has recently emerged as a promising novel imaging technique to evaluate PHVs and provide information on the exact cause of PHV dysfunction, especially in patients with aortic PHV obstruction and endocarditis.<sup>8,10-12</sup>

Although echocardiography and fluoroscopy are anchored into daily clinical practice for PHV assessment, the diagnostic accuracy of these techniques for diagnosing PHV endocarditis and obstruction has not been systematically reviewed and determined until now. This information is crucial to propose an evidence-based guideline for non-invasive imaging of patients with suspected PHV obstruction and endocarditis. The purpose of this systematic review was to determine and compare the diagnostic accuracy of TTE, TEE, fluoroscopy and MDCT to (1) detect signs of PHV endocarditis (vegetations, peri-annular complications, PHV dehiscence, PHV endocarditis in general) in patients with suspected PHV endocarditis and (2) reveal the exact cause of PHV obstruction in patients with PHV obstruction based on the currently available literature.

## METHODS

### Literature search

A systematic electronic search was performed in the Pubmed and Embase databases for original publications published until July 15<sup>th</sup>, 2011. Language was restricted to English articles and publications before 1985 were excluded. Key search terms included the non-invasive imaging modalities (TTE, TEE, fluoroscopy and MDCT), prosthetic heart valves and corresponding synonyms. The detailed search terms are shown in Appendix I. For all included full-text papers, cross-referencing was performed.

### Selection of publications

After removal of duplicates, the titles and abstracts were independently screened by two reviewers (JH and WT). Articles were included if (1) studies reported on one of the following non-invasive index tests (TTE, TEE, fluoroscopy or MDCT); (2) studies provided data on features of PHV obstruction or PHV endocarditis as the condition of interest; and (3) imaging results were verified against one of the following reference standards (surgical inspection/autopsy or clinical follow-up) which enables

the extraction of 2-by-2 tables. Full-text publications of the included articles were obtained. These full-text publications were assessed by two reviewers (JH and WT) independently. In a consensus meeting, the two reviewers extensively discussed the full-text publications and data extraction.

### Quality assessment

Information on patient population, study enrolment, non-invasive imaging modalities and reference standard was collected. Studies were systematically assessed for quality based on the validated Quality Assessment of Diagnostic Accuracy Studies (QUADAS) II checklist.<sup>13</sup> This checklist assesses the risk of bias and clinical applicability of studies based on different domains: (1) patient selection, (2) index test, (3) reference standard and (4) flow and timing.<sup>13</sup>

### Data analysis

The primary purpose of this review was to determine and compare the diagnostic accuracy of non-invasive imaging modalities for diagnosing the signs of PHV endocarditis and the exact cause of PHV obstruction. In detail, we assessed the diagnostic accuracy of the different imaging modalities to detect the following signs of PHV endocarditis: vegetations, peri-annular complications (abscesses, mycotic aneurysms/pseudoaneurysms), PHV dehiscence and PHV endocarditis in general. These different signs of interest were defined according to echocardiographic criteria: (1) vegetations, defined as irregularly shaped, oscillating masses, adherent to and distinct from the myocardium; (2) abscesses, defined as irregularly shaped, inhomogeneous paravalvular masses within periannular region, myocardium or pericardium; (3) mycotic aneurysms/pseudoaneurysms were defined as echo-free perivalvular cavities with flow communicating with the cardiovascular lumen; and (4) PHV dehiscence as rocking motion of a prosthetic heart valve.<sup>14,15</sup> PHV endocarditis in general included one or more the of above mentioned signs of PHV endocarditis. Forest plots of sensitivity and specificity with their corresponding 95% confidence intervals (CI) were generated, stratified by the different target conditions, and within each forest plot data were grouped by the different index tests (TTE, TEE, fluoroscopy and MDCT).

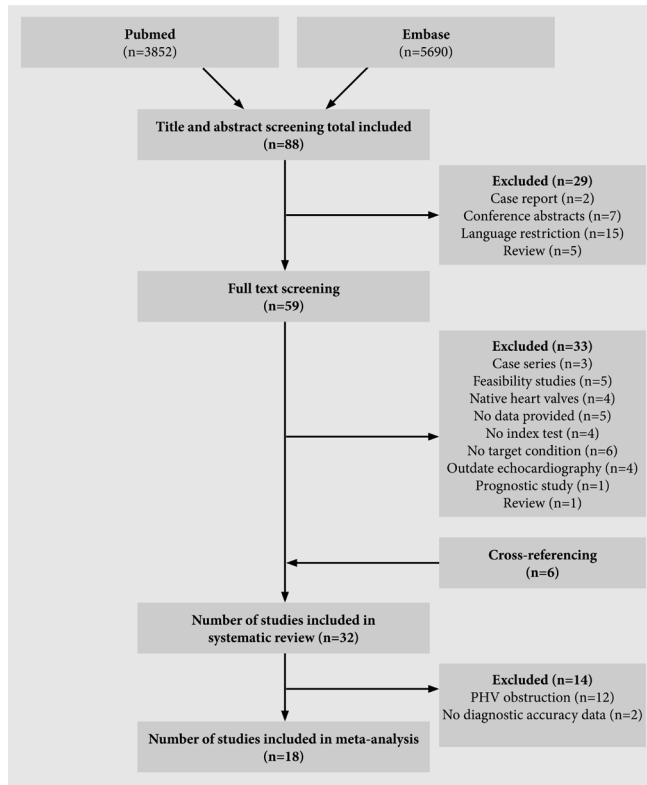
The bivariate random effects model was used to obtain and compare summary estimates of sensitivity and specificity for the different index tests. The bivariate approach simultaneously models pairs of (logit transformed) sensitivity and specificity from studies, thereby incorporating any correlation that might exist between sensitivity and specificity. The model uses a random effects approach for both sensitivity and specificity, allowing for heterogeneity beyond chance due to clinical and methodological differences between studies. In case the results displayed no more variation than expected by chance, models were simplified to fixed effect pooling of sensitivity or specificity or both. To compare index tests, we extended the bivariate model with a covariate indicating the type of index test. Such a model calculates different summary estimates for sensitivity and specificity for each index test and also provides a formal statistical test whether differences are statistically different. The non-linear mixed models procedure (PROC NL MIXED) of SAS 9.2 was used to estimate the parameters of the bivariate models. *P*-values below 0.05 were considered as statistically significant.

## RESULTS

### Search results

The systematic electronic search yielded a total of 88 publications after screening of titles and abstracts. Fifty-nine full-text versions of studies that matched the inclusion criteria were obtained.

Figure 1 Systematic literature search



Thirty-three studies were excluded because of different reasons (Figure 1). Cross-referencing of all included full-text articles resulted in six additional articles. The final selection of articles included 32 studies. In the meta-analyses only studies dealing with PHV endocarditis were included ( $n=18$ ). Two studies were excluded because no diagnostic accuracy data were available. Diagnostic accuracy data of the different index tests on the exact cause of PHV obstruction was so limited that sufficient data for a meta-analysis could not be extracted (Figure 1).

### PHV endocarditis

In Table 1, all included studies ( $n=20$ ) reported on the detection of signs of endocarditis using echocardiography (TTE/TEE) or/and MDCT.<sup>14,16-34</sup> No studies reported on fluoroscopy and only one on MDCT. Diagnostic accuracy measures for the detection of signs of PHV endocarditis could be extracted in eighteen studies ( $n=396$  patients). One study included in the meta-analysis did not report patient numbers. Data were prospectively (dedicated data collection;  $n=9$ ; 45%) and retrospectively (routine care data;  $n=11$ ; 55%) collected. Inclusion period occurred completely or partially  $\leq 1990$  in fifteen (75%) of the studies. The reference standard was surgical inspection or autopsy in 13 (65%) studies. In seven studies (35%), clinical criteria and/or follow-up was mentioned as the reference standard. A minority of the studies ( $n=6$ , 30%) included multiplane TEE assessment. Most studies ( $n=13$ , 65%) did not report on the interval between the index and reference test. Two studies had a long time interval ( $> 2$  weeks) between index test and reference standard.<sup>20,28</sup> The other five studies

Table 1 PHV endocarditis study characteristics

Authors	Journal / Year	Number of patients included (number of PHVs)	Source data	Inclusion period	Study population	Index test	TEE probe	Reference standard
Mugge et al. <sup>28</sup>	JACC 1989	26 (26)	Dedicated data collection	1984-1987	Surgical exploration	TTE/TEE	NR	Surgery/autopsy
Taams et al. <sup>34</sup>	Br Heart J 1990	12 (12)	Dedicated data collection	1984-1988	Suspected for target condition	TTE/TEE	Monoplane	Surgery/clinical follow-up
Daniel et al. <sup>39</sup>	NEJM 1991	34 (34)	Dedicated data collection	1984-1989	Surgical exploration	TTE/TEE	NR	Surgery/autopsy
Khanderia et al. <sup>24</sup>	Circulation 1991	6 (9)	Routine care data	1988-1989	Surgical exploration	TTE/TEE	Monoplane	Surgery/autopsy
Pedersen et al. <sup>29</sup>	Chest 1991	10 (11)	Dedicated data collection	NR	Suspected for target condition	TEE	NR	Surgery/clinical follow-up
Shively et al. <sup>32</sup>	JACC 1991	11 (11)	Dedicated data collection	1988-1989	Suspected for target condition	TTE/TEE	NR	Clinical diagnosis
Birmingham et al. <sup>17</sup>	Am Heart J 1992	2(2)	Routine care data	1988-1990	Suspected for target condition	TEE	NR	Modified Von Reyn criteria
Herrera et al. <sup>21</sup>	Am J Cardiol 1992	9 (9)	Routine care data	NR	Suspected for target condition	TTE/TEE	NR	Surgery/autopsy
Karalis et al. <sup>23</sup>	Circulation 1992	11 (11)	Routine care data	1988-1991	TEE positive for target condition	TTE/TEE	Mono/biplane	Surgery/autopsy
Aguado et al. <sup>16</sup>	Chest 1993	13 (14)	Routine care data	1979-1989	Surgical exploration	TTE	NA	Surgery/autopsy
Daniel et al. <sup>20</sup>	Am J Cardiol 1993	NR (33) <sup>†</sup>	Dedicated data collection	1984-1990	Surgical exploration	TTE/TEE	Monoplane	Surgery/autopsy
Mohr-Kahaly et al. <sup>27</sup>	J Am Soc Echocardiogr. 1993	30 (34)	Dedicated data collection	1987-1991	Surgical exploration	TTE/TEE	Mono/biplane	Surgery/autopsy
Sochowski et al. <sup>33</sup>	JACC 1993	21 (32)	Routine care data	1988-1990	Suspected for target condition	TEE	Monoplane	Clinical follow-up
Leung et al. <sup>25</sup>	Br Heart J 1994	6 (6)	Routine care data	1989-1993	Surgical exploration	TTE/TEE	Mono/bi/multiplane	Surgery/autopsy
Lowry et al. <sup>26</sup>	Am J Cardiol 1994	32 (32)	Routine care data	1989-1992	Suspected for target condition	TEE	Mono/biplane	Surgery/clinical follow-up
Choussat et al. <sup>18</sup>	European Heart Journal 1999	43 (43)	Routine care data	1989-1993	Surgical exploration	TTE/TEE	Mono/bi/multiplane	Surgery/autopsy
San Roman et al. <sup>31</sup>	Am J Cardiol 1999	87 (87)	Routine care data	NR	Surgical exploration	TEE	Bi/multiplane	Surgery/autopsy
Roe et al. <sup>30</sup>	Am Heart J 2000	34 (34)	Routine care data	1988-1995	Suspected for target condition	TEE	Bi/multiplane	Surgery/clinical follow-up
Hill et al. <sup>22</sup>	Am J Cardiol 2007	26 (26)	Dedicated data collection	2000-2005	Surgical exploration	TEE	Multiplane	Surgery/autopsy
Feuchtner et al. <sup>14</sup>	JACC 2009	6 (6)	Dedicated data collection	2006-2007	Surgical exploration	TEE/MDCT	Bi/multiplane	Surgery/autopsy

<sup>†</sup> Not included in meta-analysis because of no available prosthetic heart valve endocarditis data; <sup>‡</sup> episodes

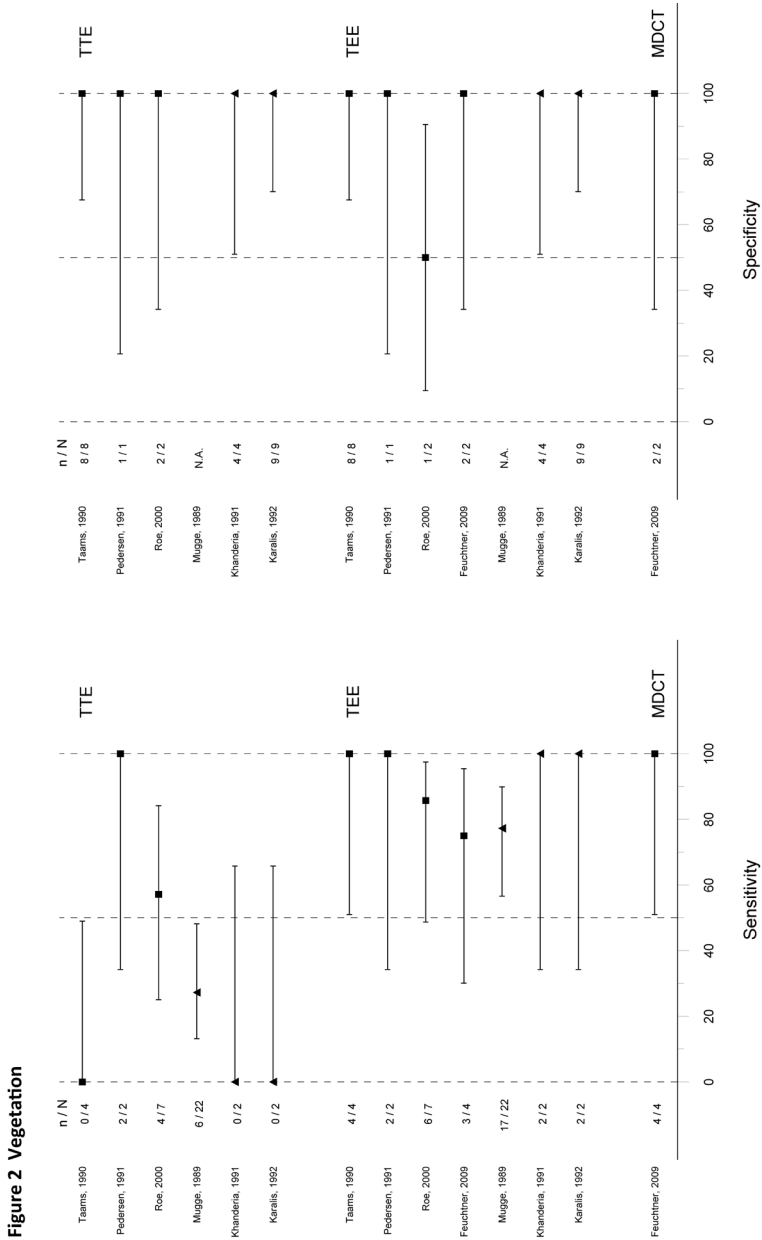
NA = Not Applicable; NR = Not Reported; MDCT = multidetector-row CT; PHV = Prosthetic Heart Valve; TTE = transthoracic echocardiography; TEE = transesophageal echocardiography

Table 1 (Continued) PHV endocarditis study characteristics

Authors	Journal / Year	Assessment of index test without knowledge of reference standard	Interval between reference standard and index test	All patients the same reference standard	All patients included in data analysis
Mugge et al. <sup>28</sup>	JACC 1989	Yes	17±2 days (mean±SD)	Yes	No
Taams et al. <sup>34</sup>	Br Heart J 1990	Yes	1-7 days	No	Yes
Daniel et al. <sup>39</sup>	NEJM 1991	Yes	≤ 7 days	Yes	Yes
Khanderia et al. <sup>24</sup>	Circulation 1991	Yes	NR	Yes	Yes
Pedersen et al. <sup>29</sup>	Chest 1991	Yes	NR	No	No
Shively et al. <sup>32</sup>	JACC 1991	Yes	NR	No	No
Birmingham et al. <sup>17</sup>	Am Heart J 1992	Yes	NR	Yes	Yes
Herrera et al. <sup>21</sup>	Am J Cardiol 1992	Yes	NR	Yes	Yes
Karalis et al. <sup>23</sup>	Circulation 1992	Unclear	NR	No	No
Aguado et al. <sup>16</sup>	Chest 1993	Yes	NR	Yes	Yes
Daniel et al. <sup>20</sup>	Am J Cardiol 1993	Yes	57±16 days (mean±SD)	Yes	Yes
Mohr-Kahaly et al. <sup>27</sup>	J Am Soc Echocardiogr.1993	Unclear	14±3 days (mean±SD)	Yes	Yes
Sochowski et al. <sup>33</sup>	JACC 1993	Unclear	NR	Yes	No
Leung et al. <sup>25</sup>	Br Heart J 1994	No	NR	No	No
Lowry et al. <sup>26</sup>	Am J Cardiol 1994	Unclear	NR	Yes	Yes
Choussat et al. <sup>18</sup>	European Heart Journal 1999	Unclear	Unclear	Yes	Yes
San Roman et al. <sup>31</sup>	Am J Cardiol 1999	Yes	Unclear	Yes	Yes
Roe et al. <sup>30</sup>	Am Heart J 2000	Unclear	NR	No	Unclear
Hill et al. <sup>22</sup>	Am J Cardiol 2007	Yes	≤ 7 days	Yes	No
Feuchtner et al. <sup>14</sup>	JACC 2009	Yes	≤5 days (1 patient 6 weeks)	Yes	No

<sup>†</sup> Not included in meta-analysis because of no available prosthetic heart valve endocarditis data  
NR = Not Reported; PHV = Prosthetic Heart Valve; SD = Standard Deviation

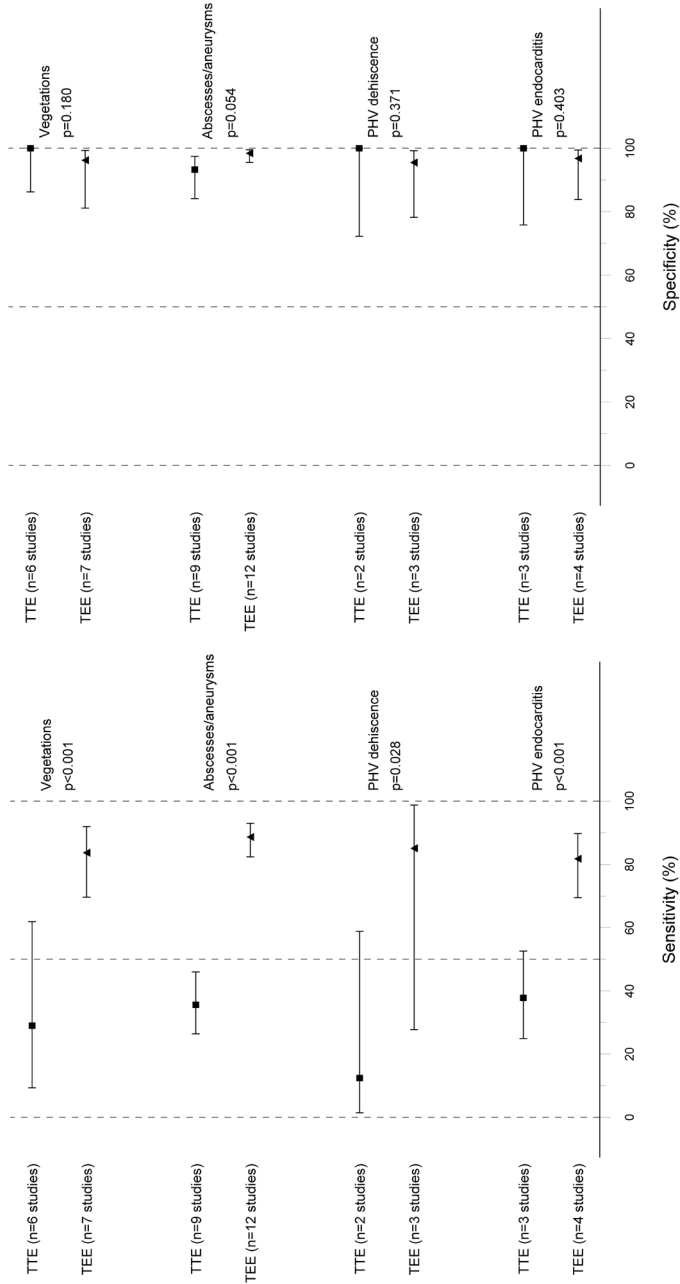




(25%) had an acceptable time interval ( $\leq 2$  weeks).<sup>14,19,22,27,34</sup> Assessment of the index test was blinded (without knowledge of the reference standard) in 13 (65%) studies. In six of the 20 studies (30%), it was unclear if this assessment was blinded. All patients had the same reference standard and were included in the data-analyses in 14 (70%) and 11 (55%) studies, respectively (Table 1).

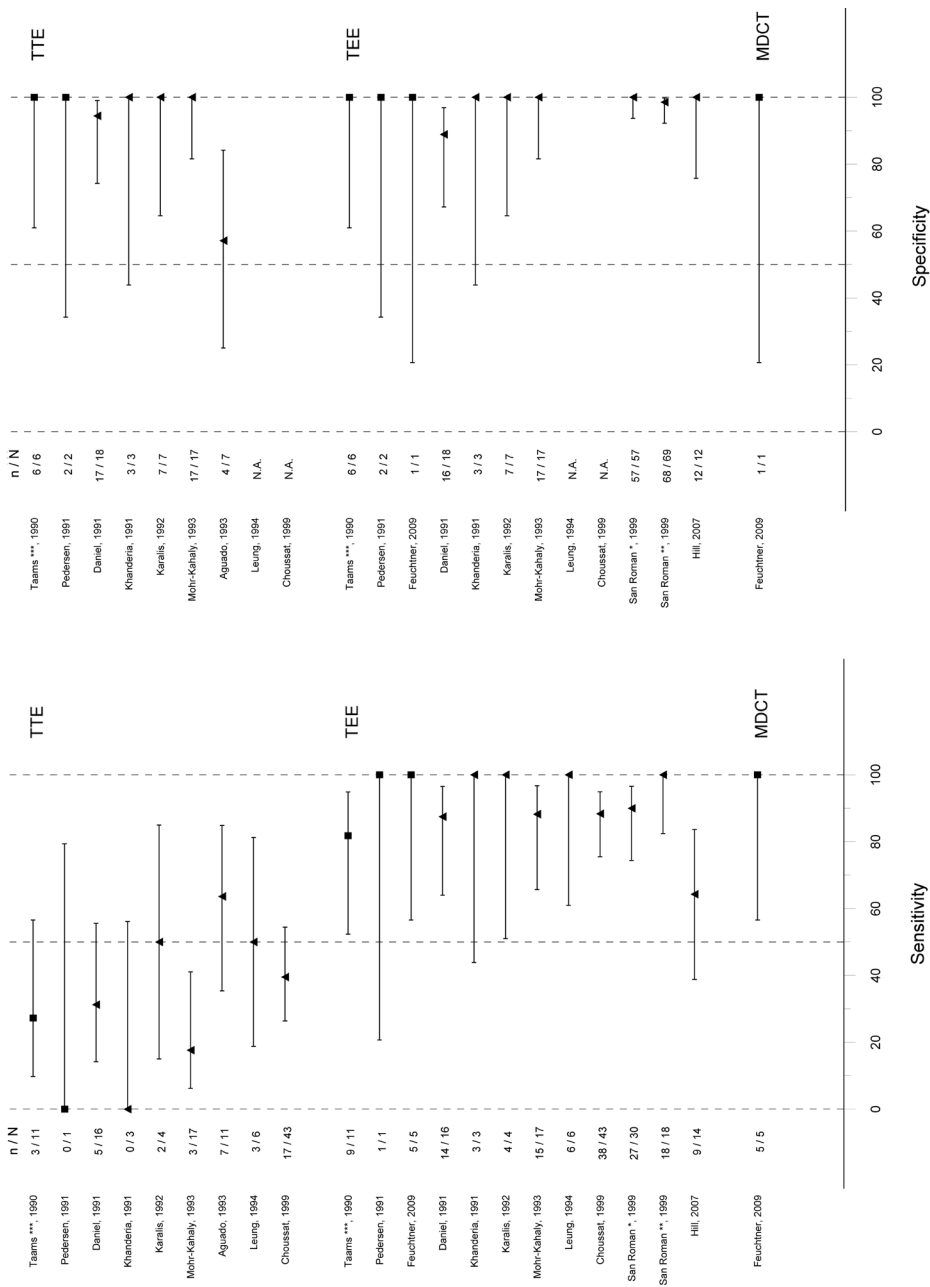
In the data analysis, four different signs were distinguished: (1) vegetations; (2) peri-annular

**Figure 3 Pooled estimates**



complications (abscesses/pseudoaneurysms/mycotic aneurysms); (3) PHV dehiscence and (4) PHV endocarditis in general. Perforations and fistula were not included in the meta-analysis because there was only one study which reported diagnostic accuracy data on these signs of interest.<sup>23,31</sup>

Figure 4 Peri-annular complications



**Vegetations**

In Figure 2, sensitivity and specificity of TTE, TEE and MDCT for the detection of vegetations are presented. The pooled TTE sensitivity and specificity for the detection of vegetations are 29% [95% CI : 9-62%] and 100% [95% CI: 86-100%], respectively. TEE is more sensitive (84% [95% CI: 70%-92%]) than TTE ( $p < 0.001$ ). No significant differences are found in specificity between TTE

Figure 5 PHV dehiscence

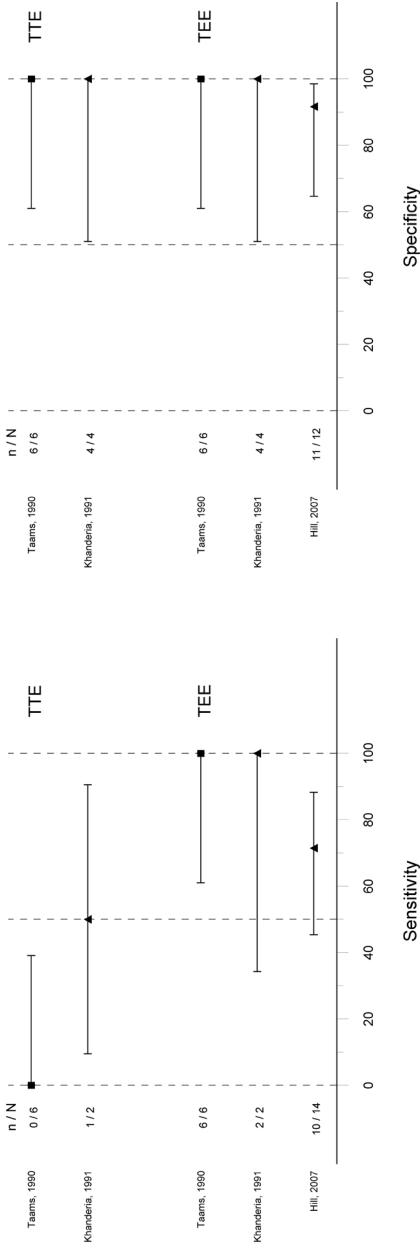
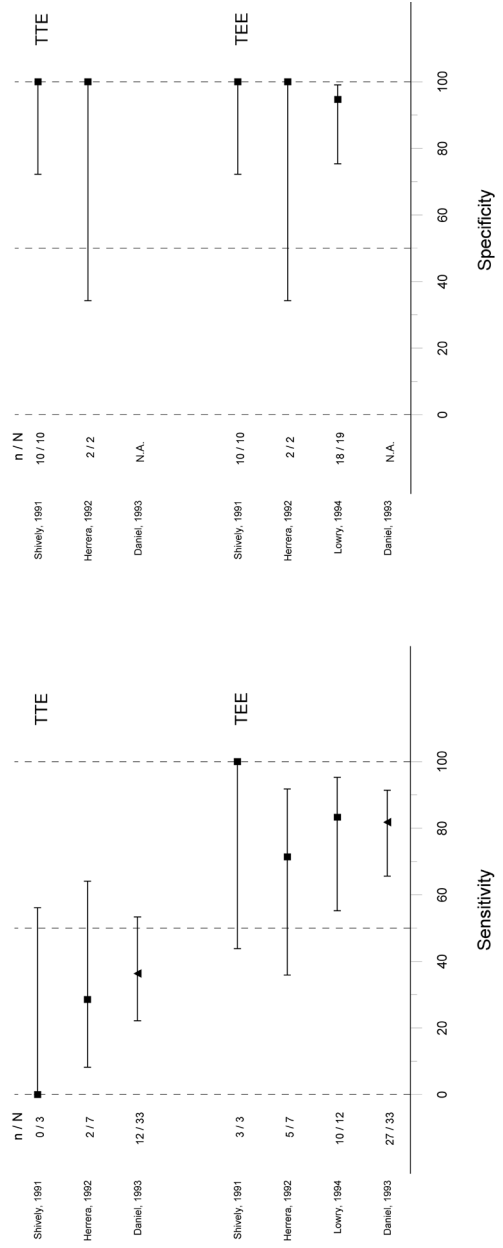


Figure 6 PHV endocarditis



and TEE (96% [95% CI: 81-99%]) ( $p=0.18$ ) (Figure 3). Only one study reported on the diagnostic accuracy of MDCT to detect vegetations in six patients.<sup>14</sup> In this study, patients with suspected PHV endocarditis, underwent both TEE and MDCT to detect signs of PHV endocarditis. TEE and MDCT detected vegetations in three patients which were confirmed by surgical inspection. TEE failed to detect two vegetations in one patient that were detected by MDCT.

Table 2. PHV obstruction study characteristics

Authors	Journal / Year	Number of patients included (number of PHVs)	Source data	Inclusion period	Study population	Index test	TEE probe	Reference standard
Khandaria et al. <sup>24</sup>	Circulation 1991	5 (5)	Routine care data	1988-1989	Surgical exploration	TTE/TEE	Monoplane	Surgery/catheterization
Herrera et al. <sup>21</sup>	Am J Cardiol 1992	5 (5)	Routine care data	NR	Suspected for target condition	TTE/TEE	NR	Surgery/autopsy
Daniel et al. <sup>20</sup>	Am J Cardiol 1993	NR	Dedicated data collection	1984-1990	Surgical exploration	TTE/TEE	Monoplane	Surgery/autopsy
Habib et al. <sup>27</sup>	European Heart Journal 1993	20 (23)	Routine care data	1989-1991	Suspected for target condition	TTE/TEE	Monoplane	Surgery/clinical follow-up
Mohr-Kahaly et al. <sup>27</sup>	J Am Soc Echocardiogr. 1993	30 (34)	Dedicated data collection	1987-1991	Surgical exploration	TTE/TEE	Mono/biplane	Surgery/autopsy
Barbetsis et al. <sup>35</sup>	JACC 1998	23 (24)	Routine care data	NR	Surgical exploration	TEE	Mono/bi/multiplane	Surgery/autopsy
Faletra et al. <sup>36</sup>	Am J Med 2000	NR	Routine care data	1991-1997	Surgical exploration	TTE/TEE	Mono/multiplane	Surgery/autopsy
Lin et al. <sup>38</sup>	Am J Cardiol 2000	53 (53)	Routine care data	1992-1997	Surgical exploration	TEE	Bi/multiplane	Surgery/autopsy
Montorsi et al. <sup>39</sup>	Am J Cardiol 2000	82 (82)	Dedicated data collection	1994-1998	Suspected for target condition	TTE/TEE and fluoroscopy	Multiplane	TEE
Girard et al. <sup>9</sup>	JACC 2001	92 (92)	Routine care data	1989-1998	Surgical exploration	TTE/TEE and fluoroscopy	Mono/bi/multiplane	Surgery/autopsy
Symersky et al. <sup>11</sup>	Am J Cardiol 2009	13 (15)	Routine care data	2005-2008	Suspected for target condition	MDCT	NR	Surgery/autopsy
Tsai et al. <sup>12</sup>	European Radiology 2009	2 (3)	Dedicated data collection	2005-2008	Surgical exploration	MDCT	NA	Surgery/autopsy

NA = not applicable; NR = Not Reported; MDCT = multidetector-row CT; PHV = Prosthetic Heart Valve; TTE = transthoracic echocardiography; TEE = transesophageal echocardiography

Table 2 (Continued) PHV obstruction study characteristics

Authors	Journal / Year	Assessment of index test without knowledge of reference standard	Interval between reference standard and index test	All patients the same reference standard	All patients included in data analysis
Khandaria et al. <sup>24</sup>	Circulation 1991	Yes	NR	No	Yes
Herrera et al. <sup>21</sup>	Am J Cardiol 1992	Yes	NR	Yes	Yes
Daniel et al. <sup>20</sup>	Am J Cardiol 1993	Yes	57±16 days (mean±SD)	Yes	Yes
Habib et al. <sup>27</sup>	European Heart Journal 1993	Unclear	NR	No	Yes
Mohr-Kahaly et al. <sup>27</sup>	J Am Soc Echocardiogr.1993	Unclear	14±3 days (mean±SD)	Yes	Yes
Barbetsis et al. <sup>35</sup>	JACC 1998	Yes	Mean 3.6 days (range 0-25 days)	Yes	Yes
Faletra et al. <sup>36</sup>	Am J Med 2000	Unclear	≤3 weeks	Yes	Yes
Lin et al. <sup>38</sup>	Am J Cardiol 2000	Yes	4±3 days (mean±SD) or intraoperative TEE	Yes	Yes
Montorsi et al. <sup>39</sup>	Am J Cardiol 2000	Yes	Same day	Yes	Yes
Girard et al. <sup>9</sup>	JACC 2001	Yes	Median 10 days (IQR 5-42)	Yes	Yes
Symersky et al. <sup>11</sup>	Am J Cardiol 2009	Yes	NR	No	No
Tsai et al. <sup>12</sup>	European Radiology 2009	Unclear	NR	No	No

IQR = interquartile range; NR = Not Reported; PHV = Prosthetic Heart Valve; SD = Standard Deviation

**Peri-annular complications (Abscesses/pseudoaneurysms/mycotic aneurysms)**

In Figure 4, sensitivity and specificity of TTE, TEE, and MDCT for the detection of peri-annular complications are presented. The pooled TTE sensitivity and specificity for the detection of peri-annular complications are 36% [95% CI : 26-46%] and 93% [95% CI: 84-97%], respectively. One study reported 3 false positive (43%) TTE examinations.<sup>16</sup> TEE is more sensitive (89% [95% CI: 82%-93%]) than TTE (p<0.001). In one study, TEE missed five out of the 14 (36%) peri-annular

complications in patients with aortic PHV endocarditis.<sup>22</sup> No significant differences are found in specificity between TTE and TEE (98% [95% CI: 96-100%]) ( $p=0.05$ ) (Figure 3). Only one study reported on the diagnostic accuracy of MDCT to detect peri-annular complications.<sup>14</sup> TEE and MDCT demonstrated similar results (detected peri-annular complications in five patients and excluded complications in one patient).

### PHV dehiscence

In Figure 5, sensitivity and specificity of TTE, TEE and MDCT for the detection of PHV dehiscence are presented. The pooled TTE sensitivity and specificity for the detection of PHV dehiscence are 12% [95% CI : 1-59%] and 100% [95% CI: 72-100%], respectively. TEE is more sensitive (85% [95% CI: 28%-99%]) than TTE ( $p=0.03$ ). No significant differences are found in specificity between TTE and TEE (96% [95% CI: 78-99%]) ( $p=0.37$ ) (Figure 3). No MDCT studies were available for analysis.

### PHV endocarditis

In Figure 6, sensitivity and specificity of TTE, TEE and MDCT for the detection of PHV endocarditis are presented. The pooled TTE sensitivity and specificity for the detection of PHV endocarditis are 38% [95% CI : 25-53%] and 100% [95% CI : 76-100%], respectively. TEE is more sensitive (82% [95% CI: 70%-90%]) than TTE ( $p<0.001$ ). No significant differences are found in specificity between TTE and TEE (97% [95% CI: 84-99%]) ( $p=0.40$ ) (Figure 3). No MDCT studies were available for analysis.

### PHV obstruction

Table 2 demonstrates all included studies ( $n=12$ ) that reported on diagnosing the exact cause of PHV obstruction based on assessment by TTE, TEE, fluoroscopy and MDCT.<sup>9,11,12,20,21,24,27,35-39</sup> These 12 studies included a total of 325 patients (two studies did not report the patient numbers), who underwent at least one non-invasive examination (TTE/TEE/fluoroscopy or MDCT) for the evaluation of PHV obstruction. Data were prospectively (dedicated data collection;  $n=4$ ; 33%) and retrospectively (routine care data;  $n=8$ ; 67%) collected. The inclusion period occurred completely or partially  $\leq 1990$  in five (42%) of these studies. These studies are relatively old because they are published  $\geq 20$  years ago. The reference standard was surgical inspection or autopsy in 10 (83%) studies. In only one study (8%), clinical follow-up was mentioned as the reference standard. A minority of the studies ( $n=5$ , 42%) included multiplane TEE assessment. Five studies (42%) did not report on the interval between the index test and reference standard. Three studies included patients with a long time interval ( $>2$  weeks) between index test and reference standard.<sup>9,20,36</sup> The other four studies (20%) had an acceptable time interval ( $<2$  weeks).<sup>27,35,38,39</sup> Assessment of the index test was blinded (without knowledge of the reference standard) in eight studies (67%). In four studies (33%), it was unclear if this assessment was blinded. All patients had the same reference standard and were included in the data-analyses in 8 (67%) and 10 (83%) studies, respectively (Table 2). Diagnostic accuracy data of the non-invasive imaging modalities for the detection of the exact cause of PHV obstruction could not be extracted because the included studies did not report these data.

## DISCUSSION

We reviewed all available literature on TTE, TEE, fluoroscopy and MDCT for detection of signs of PHV endocarditis and the exact cause of PHV obstruction. Despite the limited number of studies

reporting on the diagnostic accuracy of these imaging modalities, non-invasive imaging plays a key role in the establishment of the diagnosis PHV endocarditis and obstruction and has important clinical implications for patient management.

### PHV endocarditis

In clinical practice, PHV endocarditis is a difficult diagnosis to establish and is based on the Duke criteria.<sup>40</sup> For the fulfilment of the Duke criteria, a positive echocardiogram is one of the two important major criteria. A positive echocardiogram is defined as the presence of a vegetation, abscess, PHV dehiscence or new (para)valvular regurgitation.<sup>40</sup> However, this systematic review demonstrates that limited data is available for this major criterion in patients with suspected PHV endocarditis.

PHV endocarditis is associated with a high risk of potentially life-threatening complications such as abscess formation and mycotic aneurysms (53-55% of the cases) which are independent predictors for 6-months mortality.<sup>22,31,41</sup> In patients with PHV endocarditis with abscesses 6-months mortality is 30% compared to only 8% in patients with PHV endocarditis without abscesses.<sup>22</sup> Besides the presence of these peri-annular complications, the presence of an AV-block and staphylococcus aureus (13-52%).<sup>18,19,31,41</sup> are independent predictors for 6-months mortality.<sup>18,22</sup> However, negative blood cultures (23%-37%) are not rare in patients with PHV endocarditis and abscesses.<sup>18,19,31</sup> Moreover, the presence of an AV-block on the electrocardiogram is associated (39%) with abscesses in patients with aortic PHVs. In contrast, no AV-block was observed in patients with abscesses in the mitral position.<sup>18</sup>

For the detection of peri-annular complications such as abscess formation, non-invasive imaging is crucial and has important therapeutic implications: ultimately the decision to perform a high-risk re-operation to replace the diseased PHV. In this meta-analysis, TEE proved to have an excellent sensitivity (89%), and was superior to TTE (36%) for the detection of abscesses or mycotic aneurysms because of superior spatial resolution and the close relationship between the TEE probe and the heart. However, the majority of the studies were based on surgical or pathological exploration. This has introduced selection bias because the appropriate population (patients with suspected PHV endocarditis) for our research question was not evaluated. Therefore, these diagnostic accuracy measures possibly can not be fully extrapolated to the clinical practice in which patients present with a suspicion of PHV endocarditis. Therefore, the reported sensitivity in this meta-analysis may be too favourable for a suspected population. Patients with negative imaging findings will often not undergo reoperation and in many studies this specific patient category was not included in the data analyses. Even in this selected population, TEE still misses some life-threatening abscesses and mycotic aneurysms (11%). TEE can miss abscesses and mycotic aneurysms mainly in patients with aortic PHVs and anteriorly located peri-annular complications.<sup>20,22,27,34</sup> This is caused by acoustic shadowing of the PHV in this region. TTE can have additional diagnostic value in the detection of anterior located abscesses because assessment of this region is not hampered by acoustic shadowing.<sup>34</sup> In contrast, TEE almost always detects peri-annular complications in the posterior aortic root and in patients with mitral PHVs.<sup>24,34</sup> Therefore, the combination of TTE and TEE is warranted in these cases.

Many studies did not report on the exact location of the missed abscesses.<sup>18,20,22,26,31</sup> Therefore, meta-regression could not be performed for this covariate. Moreover, TTE and TEE had a very high specificity for detection of peri-annular complications. However, TTE and TEE demonstrated 4/60 (7%) and 3/192 (2%) false positives, respectively. In these patients, these findings may result in unjust exposure to a high-risk reoperation. Therefore, additional confirmation or exclusion of peri-annular complications by additional non-invasive imaging is welcome. MDCT might be a suitable imaging tool to provide this diagnostic information. However, only one study reported on the diagnostic accuracy of MDCT for abscess detection. This study only evaluated six surgical confirmed PHV

endocarditis patients. In this population, both TEE and MDCT detected all abscesses ( $n=5$ ).<sup>14</sup> Thus, one has to be careful to draw conclusions on the value of MDCT given this very limited scientific data.

Besides peri-annular complications, PHV endocarditis can present with vegetations. In our analysis, the sensitivity of TEE (84%) was very good for the detection of vegetations, and superior to TTE (29%) probably because of the superior spatial resolution and its proximity of the probe to the heart.<sup>23,24,28-30</sup> Although the sensitivity of TEE is very good, this diagnostic accuracy measure is also influenced by selection bias as for the detection of peri-annular complications, and possibly too favourable if applied on a suspected population. Even in this selected population, TEE missed vegetations (7/43; 16%) especially in the aortic position because of acoustic shadowing.<sup>23,33</sup> In addition, Sochowski et al.<sup>33</sup> demonstrated that in a selected patient population with negative TEE findings in 2/21 (10%) patients vegetations were missed. In patients with PHV endocarditis, vegetation size is significantly smaller than in patients with native valve endocarditis which also may hamper echocardiographic detection.<sup>28</sup> Fluoroscopy may detect leaflet restriction which may be caused by vegetations in patients with suspected PHV endocarditis. However, no studies reported on the additional diagnostic value of fluoroscopy in this patient population. Additional MDCT imaging may have diagnostic complementary value for the detection of vegetations because of the absence of acoustic shadowing.<sup>14</sup> However, MDCT may miss small vegetations (<3mm) as well due to the inferior spatial resolution compared to TEE.<sup>14</sup> Again the evidence for the value of MDCT is still very scarce.

Some studies also provided diagnostic information on PHV dehiscence and endocarditis in general. These results are similar to the diagnostic accuracy measures of vegetations and peri-annular complications (Figure 5 en 6). However, small patient numbers limit definite conclusions in these subcategories.<sup>20-22,24,26,32,34</sup>

In summary, TEE showed good to excellent sensitivity and specificity for the detection of signs of PHV endocarditis, and was superior to TTE. TTE can have incremental diagnostic value in patients with aortic PHVs and abscesses in the anterior aortic root. Still in a small but substantial part of patients, vegetations and life-threatening peri-annular complications are missed by TEE. Furthermore, it is important to realize that the diagnostic accuracy measures in this meta-analysis could not be fully extrapolated to clinical practice because of several reasons. First, in a substantial part of the included studies, a selection bias has influenced the estimates. Second, only 6 out of 20 studies (30%) accomplished state-of-the-art multiplane TEE examinations. The majority of the studies were performed with monoplane TEE or the specific TEE probe used was not reported. Third, TTE evaluation has improved due to improved TTE probe technology. The relatively old TTE technology could have influenced the reported TTE sensitivity and specificity. Fourth, methodological quality varied from poor to excellent which may have influenced the estimates as well. More prospective diagnostic cross-sectional studies are required to determine the exact value of non-invasive imaging modalities (TTE, TEE and MDCT) in patients with suspected PHV endocarditis.

### **PHV obstruction**

To our knowledge, no studies have been performed to determine the diagnostic accuracy of non-invasive imaging modalities for the exact cause of PHV obstruction. However, many studies with a varying methodological quality reported on non-invasive imaging of patients with PHV obstruction.<sup>9,11,12,20,21,24,27,35-39</sup> PHV obstruction<sup>9</sup> is a pathological entity with different etiologies including pannus formation, thrombus, other subvalvular masses (e.g. subvalvular congenital membrane), and patient-prosthesis mismatch.<sup>8</sup> The differentiation between these pathological entities has important implications for patient management. Pannus formation namely requires surgery



in symptomatic patients, and PHV thrombosis may require thrombolysis according to existing guidelines.<sup>7,42</sup> Two studies have investigated if the differentiation between pannus and thrombus is possible.<sup>35,38</sup> Barbetseas et al.<sup>35</sup> reported on 23 patients with 24 PHVs (10 aortic, 14 mitral PHVs) and proven PHV obstruction caused by either pannus formation or thrombus. This study showed that TTE is not useful for detection of obstructive masses (1/24; 4%). In contrast, TEE was superior for detection of masses (detected 20/24 masses; 83%). For the identification of thrombus formation, this study reported the following: (1) the time from the initial onset of symptoms to reoperation (9 vs. 205 days); (2) time from valve replacement to reoperation (62 months vs. 178 months); and (3) the percentage of patients with adequate anticoagulation (INR $\geq$ 2.5, 21% vs 89%) were significantly lower for patients with PHV thrombosis than in patients with pannus formation. In addition, thrombus formation had a significantly lower video intensity ratio than thrombus (0.46 vs. 0.71). However, this lower video intensity ratio was not confirmed by another group.<sup>38</sup> Although these differences become apparent in this limited number of patients, cut-off points that can be applied to the individual patient are lacking.

Lin et al.<sup>38</sup> evaluated 53 patients with surgically confirmed masses. In this group, TEE identified 42/53 (79%) masses. Lin et al. identified the following predictors for PHV thrombosis: (1) mobile mass, (2) attachment to the occluder, (3) peak aortic prosthetic gradient  $\geq$ 50mm Hg or mean mitral prosthetic gradient  $\geq$ 10mmHg and inadequate anticoagulation (INR $\leq$ 2.5). In contrast to Barbetseas et al.<sup>35</sup>, Lin describes that pannus formation can even occur within 6 months after PHV implantation ( $n=5$ ; 26%).

In contrast to the two previous studies, most studies only describe whether non-invasive imaging modalities can detect masses in patients with PHV obstruction. Girard et al.<sup>9</sup> reported on 34 patients reoperated for aortic PHV obstruction with surgically confirmed pannus formation and thrombus formation. In contrast to the previous studies<sup>35,38</sup>, TTE and TEE detected a mass only in 3/34 (9%) and 7/28 (25%) of the patients. Even in this selected population, this study demonstrated that TEE misses masses in substantial part of patients (75%) with aortic PHV obstruction. Other groups confirmed these findings.<sup>20,21,39</sup> In contrast to patients with aortic PHVs, TEE is often able to detect masses in patients with mitral PHVs. However, exact numbers were not provided.<sup>20,37,39</sup>

This systematic review demonstrates that when TEE is able to detect a mass it is very difficult or even impossible to differentiate between different etiologies of PHV obstruction. Therefore, additional imaging techniques may provide complementary diagnostic information. In two small studies, the potential of MDCT for the detection of the exact cause of PHV obstruction was reported.<sup>11,12</sup> Symersky et al.<sup>11</sup> reported on 13 patients with 15 PHVs with an uncertain cause of PHV obstruction. In this study, five patients with PHV obstruction were reoperated. In these patients, TEE missed in 2 (40%) masses, and MDCT detected all masses ( $n=5$ ; 100%). In the two patients with masses missed by TEE, surgical inspection revealed pannus formation. Moreover, Tsai et al.<sup>12</sup> reported on 2 patients with suspected aortic PHV obstruction who underwent surgical exploration. MDCT revealed pannus formation in both cases. These two studies show the potential of MDCT. However, well-designed large prospective studies are needed to determine the exact complementary value of MDCT.

## CONCLUSIONS

The principal findings of this systematic review are: (1) in a mainly surgically explored population, TEE has a good sensitivity for the detection of signs of PHV endocarditis, and is superior to TTE; (2) TEE still misses signs of PHV endocarditis even in this selected population; (3) both TTE and TEE

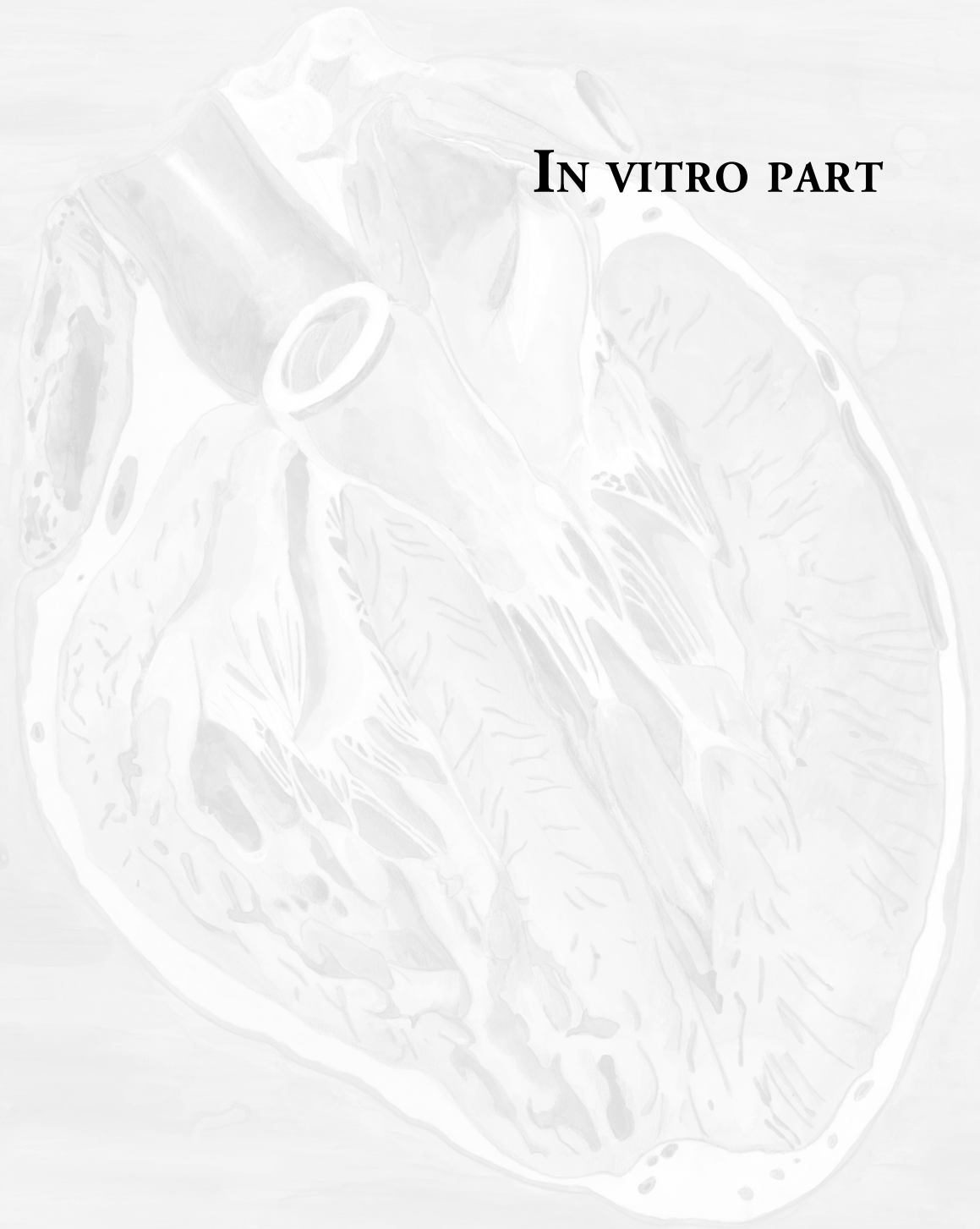
have a good specificity for the detection of signs of PHV endocarditis; and (4) differentiation between pannus and thrombus formation remains difficult or even impossible based echocardiographic evaluation.

## REFERENCES

- 1 Yacoub MH, Takkenberg JJ. Will heart valve tissue engineering change the world? *Nat Clin Pract Cardiovasc Med* 2005; 2:60-61.
- 2 Akins CW, Miller DC, Turina MI, et al. Guidelines for reporting mortality and morbidity after cardiac valve interventions. *J Thorac Cardiovasc Surg* 2008; 135:732-738.
- 3 Cannegieter SC, Rosendaal FR, Briet E. Thromboembolic and bleeding complications in patients with mechanical heart valve prostheses. *Circulation* 1994; 89:635-641.
- 4 Grunkemeier GL, Li HH, Naftel DC, et al. Long-term performance of heart valve prostheses. *Curr Probl Cardiol* 2000; 25:73-154.
- 5 Hammermeister K, Sethi GK, Henderson WG, et al. Outcomes 15 years after valve replacement with a mechanical versus a bioprosthetic valve: final report of the Veterans Affairs randomized trial. *J Am Coll Cardiol* 2000; 36:1152-1158.
- 6 Khan S. Long-term outcomes with mechanical and tissue valves. *J Heart Valve Dis* 2002; 11:S8-14.
- 7 Vahanian A, Baumgartner H, Bax J, et al. Guidelines on the management of valvular heart disease: The Task Force on the Management of Valvular Heart Disease of the European Society of Cardiology. *Eur Heart J* 2007; 28:230-268.
- 8 Habets J, Budde RP, Symersky P, et al. Diagnostic evaluation of left-sided prosthetic heart valve dysfunction. *Nat Rev Cardiol* 2011; 8:466-478.
- 9 Girard SE, Miller FA Jr., Orszulak TA, et al. Reoperation for prosthetic aortic valve obstruction in the era of echocardiography: trends in diagnostic testing and comparison with surgical findings. *J Am Coll Cardiol* 2001; 37:579-584.
- 10 Chenot F, Montant P, Goffinet C, et al. Evaluation of anatomic valve opening and leaflet morphology in aortic valve bioprosthesis by using multidetector CT: comparison with transthoracic echocardiography. *Radiology* 2010; 255:377-385.
- 11 Symersky P, Budde RP, de Mol BA, et al. Comparison of multidetector-row computed tomography to echocardiography and fluoroscopy for evaluation of patients with mechanical prosthetic valve obstruction. *Am J Cardiol* 2009; 104:1128-1134.
- 12 Tsai IC, Lin YK, Chang Y, et al. Correctness of multi-detector-row computed tomography for diagnosing mechanical prosthetic heart valve disorders using operative findings as a gold standard. *Eur Radiol* 2009; 19:857-867.
- 13 Whiting PF, Rutjes AW, Westwood ME, et al. QUADAS-2: a revised tool for the quality assessment of diagnostic accuracy studies. *Ann Intern Med* 2011; 155:529-536.
- 14 Feuchtner GM, Stolzmann P, Dichtl W, et al. Multislice computed tomography in infective endocarditis: comparison with transesophageal echocardiography and intraoperative findings. *J Am Coll Cardiol* 2009; 53:436-444.
- 15 Sachdev M, Peterson GE, Jollis JG. Imaging techniques for diagnosis of infective endocarditis. *Cardiol Clin* 2003; 21:185-195.
- 16 Aguado JM, Gonzalez-Vilchez F, Martin-Duran R, et al. Perivalvular abscesses associated with endocarditis. Clinical features and diagnostic accuracy of two-dimensional echocardiography. *Chest* 1993; 104:88-93.
- 17 Birmingham GD, Rahko PS, Ballantyne F, et al. Improved detection of infective endocarditis with transesophageal echocardiography. *Am Heart J* 1992; 123:774-781.
- 18 Choussat R, Thomas D, Isnard R, et al. Perivalvular abscesses associated with endocarditis; clinical features and prognostic factors of overall survival in a series of 233 cases. Perivalvular Abscesses French Multicentre Study. *Eur Heart J* 1999; 20:232-241.
- 19 Daniel WG, Mugge A, Martin RP, et al. Improvement in the diagnosis of abscesses associated with endocarditis by transesophageal echocardiography. *N Engl J Med* 1991; 324:795-800.
- 20 Daniel WG, Mugge A, Grote J, et al. Comparison of transthoracic and transesophageal echocardiography for detection of abnormalities of prosthetic and bioprosthetic valves in the mitral and aortic positions. *Am J Cardiol* 1993; 71:210-215.
- 21 Herrera CJ, Chaudhry FA, DeFrino PF, et al. Value and limitations of transesophageal echocardiography in evaluating prosthetic or bioprosthetic valve dysfunction. *Am J Cardiol* 1992; 69:697-699.
- 22 Hill EE, Herijgers P, Claus P, et al. Abscess in infective endocarditis: the value of transesophageal echocardiography and outcome: a 5-year study. *Am Heart J* 2007; 154:923-928.
- 23 Karalis DG, Bansal RC, Hauck AJ, et al. Transesophageal echocardiographic recognition of subaortic complications in aortic valve endocarditis. Clinical and surgical implications. *Circulation* 1992; 86:353-362.
- 24 Khandheria BK, Seward JB, Oh JK, et al. Value and limitations of transesophageal echocardiography in assessment of mitral valve prostheses. *Circulation* 1991; 83:1956-1968.
- 25 Leung DY, Cranney GB, Hopkins AP, et al. Role of transoesophageal echocardiography in the diagnosis and management of aortic root abscess. *Br Heart J* 1994; 72:175-181.

- 26 Lowry RW, Zoghbi WA, Baker WB, et al. Clinical impact of transesophageal echocardiography in the diagnosis and management of infective endocarditis. *Am J Cardiol* 1994; 73:1089-1091.
- 27 Mohr-Kahaly S, Kupferwasser I, Erbel R, et al. Value and limitations of transesophageal echocardiography in the evaluation of aortic prostheses. *J Am Soc Echocardiogr.* 1993; 6:12-20.
- 28 Mugge A, Daniel WG, Frank G, et al. Echocardiography in infective endocarditis: reassessment of prognostic implications of vegetation size determined by the transthoracic and the transesophageal approach. *J Am Coll Cardiol* 1989; 14:631-638.
- 29 Pedersen WR, Walker M, Olson JD, et al. Value of transesophageal echocardiography as an adjunct to transthoracic echocardiography in evaluation of native and prosthetic valve endocarditis. *Chest* 1991; 100:351-356.
- 30 Roe MT, Abramson MA, Li J, et al. Clinical information determines the impact of transesophageal echocardiography on the diagnosis of infective endocarditis by the duke criteria. *Am Heart J* 2000; 139:945-951.
- 31 San Roman JA, Vilacosta I, Sarria C, et al. Clinical course, microbiologic profile, and diagnosis of periannular complications in prosthetic valve endocarditis. *Am J Cardiol* 1999; 83:1075-1079.
- 32 Shively BK, Gurule FT, Roldan CA, et al. Diagnostic value of transesophageal compared with transthoracic echocardiography in infective endocarditis. *J Am Coll Cardiol* 1991; 18:391-397.
- 33 Sochowski RA, Chan KL. Implication of negative results on a monoplane transesophageal echocardiographic study in patients with suspected infective endocarditis. *J Am Coll Cardiol* 1993; 21:216-221.
- 34 Taams MA, Gussenhoven EJ, Bos E, et al. Enhanced morphological diagnosis in infective endocarditis by transoesophageal echocardiography. *Br Heart J* 1990; 63:109-113.
- 35 Barbetseas J, Nagueh SF, Pitsavos C, et al. Differentiating thrombus from pannus formation in obstructed mechanical prosthetic valves: an evaluation of clinical, transthoracic and transesophageal echocardiographic parameters. *J Am Coll Cardiol* 1998; 32:1410-1417.
- 36 Faletra F, Constantin C, De Chiara F, et al. Incorrect echocardiographic diagnosis in patients with mechanical prosthetic valve dysfunction: correlation with surgical findings. *Am J Med* 2000; 108:531-537.
- 37 Habib G, Cornen A, Mesana T, et al. Diagnosis of prosthetic heart valve thrombosis. The respective values of transthoracic and transoesophageal Doppler echocardiography. *Eur Heart J* 1993; 14:447-455.
- 38 Lin SS, Tiong IY, Asher CR, et al. Prediction of thrombus-related mechanical prosthetic valve dysfunction using transesophageal echocardiography. *Am J Cardiol* 2000; 86:1097-1101.
- 39 Montorsi P, De Bernardi F, Muratori M, et al. Role of cine-fluoroscopy, transthoracic, and transesophageal echocardiography in patients with suspected prosthetic heart valve thrombosis. *Am J Cardiol* 2000; 85:58-64.
- 40 Durack DT, Lukes AS, Bright DK. New criteria for diagnosis of infective endocarditis: utilization of specific echocardiographic findings. Duke Endocarditis Service. *Am J Med* 1994; 96:200-209.
- 41 Graupner C, Vilacosta I, SanRoman J, et al. Periannular extension of infective endocarditis. *J Am Coll Cardiol* 2002; 39:1204-1211.
- 42 Bonow RO, Carabello BA, Chatterjee K, et al. 2008 focused update incorporated into the ACC/AHA 2006 guidelines for the management of patients with valvular heart disease: a report of the American College of Cardiology/American Heart Association Task Force on Practice Guidelines (Writing Committee to revise the 1998 guidelines for the management of patients with valvular heart disease). Endorsed by the Society of Cardiovascular Anesthesiologists, Society for Cardiovascular Angiography and Interventions, and Society of Thoracic Surgeons. *J Am Coll Cardiol* 2008; 52:e1-142.

# IN VITRO PART







## CHAPTER IV

# A NOVEL ITERATIVE RECONSTRUCTION ALGORITHM ALLOWS REDUCED DOSE MULTIDETECTOR-ROW CT IMAGING *of* MECHANICAL PROSTHETIC HEART VALVES

J. Habets  
P. Symersky  
B.A.J.M. de Mol  
W.P.Th.M. Mali  
T. Leiner  
R.P.J. Budde

**ABSTRACT**

**PURPOSE** | Multidetector-row CT is promising for prosthetic heart valve (PHV) assessment but retrospectively ECG-gated scanning has a considerable radiation dose. Recently introduced iterative reconstruction (IR) algorithms may enable radiation dose reduction with retained image quality. Furthermore, PHV image quality on the CT scan mainly depends on extent of PHV artifacts. IR may decrease streak artifacts. We compared image noise and artifact volumes in scans of mechanical PHVs reconstructed with conventional filtered back projection (FBP) to lower dose scans reconstructed with IR.

**METHODS** | Four different PHV's (St. Jude, Carbomedics, ON-X and Medtronic Hall) were scanned in a pulsatile in vitro model. Ten retrospectively ECG-gated CT scans were performed of each PHV at 120 KV, 600 mAs (high-dose  $CTDI_{vol}$  35.3mGy) and 120 KV, 300 mAs (low-dose  $CTDI_{vol}$  17.7mGy) on a 64 detector-row scanner. Diastolic and systolic images were reconstructed with FBP (high and low-dose) and the IR algorithm (low-dose only). Hypo- and hyperdense artifact volumes were determined using two threshold filters. Image noise was measured.

**RESULTS** | Mean hypo- and hyperdense artifact volumes ( $mm^3$ ) were 1235/5346 (high-dose FBP); 2405/6877 (low-dose FBP) and 1218/5333 (low-dose IR). Low-dose IR reconstructions had similar image noise compared to high-dose FBP ( $16.5 \pm 1.7$  vs.  $16.3 \pm 1.6$ , mean  $\pm$  SD, respectively,  $p=1.0$ ).

**CONCLUSIONS** | Iterative reconstruction allows ECG-gated PHV imaging with similar image noise and PHV artifacts at 50% less dose compared to conventional filtered back projection in an pulsatile in vitro model.



**M**ultidetector-row CT (MDCT) is a promising imaging technique for prosthetic heart valve (PHV) assessment. It provides complementary information to echocardiography and fluoroscopy in patients with suspected PHV dysfunction.<sup>1-5</sup> MDCT scanning of PHVs has been mainly performed with retrospective ECG-gated scan protocols which enable dynamic PHV leaflet assessment and imaging of periprosthetic anatomy in both systole and diastole.<sup>6</sup> In an effort to minimize PHV-related artifacts and to improve image quality, some authors have adjusted exposure parameters by increasing either tube voltage (140kV)<sup>7</sup> or tube current (800-1000 mAs).<sup>3</sup> However, these adjustments cause an increase in radiation exposure, which is already substantial with retrospective ECG-gating (up to 20 mSv).<sup>3,7</sup> For the use of MDCT in clinical practice, it is important to reduce radiation dose while retaining the ability to assess PHV leaflet motion and anatomy in systole and diastole.

Currently, MDCT uses filtered back projection (FBP) for image reconstruction from raw data.<sup>8</sup> Alternative iterative image reconstruction algorithms have been available for a long time and used in positron emission tomography (PET) and single photon emission computed tomography (SPECT).<sup>9,10</sup> Recently, technical developments and increased computational power have allowed the use of novel iterative reconstruction (IR) algorithms for multislice CT image reconstruction.<sup>8,11,12</sup> Theoretically these new reconstruction algorithms allow imaging at reduced dose with retained image quality.<sup>8</sup> Furthermore, these new reconstruction algorithms may reduce PHV artifacts as well. At present, it is unknown whether application of these iterative reconstruction algorithms in MDCT scans of PHVs is beneficial for reduction of radiation dose and PHV induced artifacts.

The purpose of the current study was to assess whether IR allows PHV imaging with reduced radiation dose without increased image noise. In addition, we assessed the effect of using IR on the presence and extent of hypo- and hyperdense PHV artifacts in both systolic and diastolic phases.

## METHODS

### Valves

Four different mechanical PHVs including three bileaflet valves: St Jude (SJ, St Jude Medical Inc., St Paul MN, 27mm), Carbomedics (CM, Carbomedics Inc., Austin, TX, 21mm), ON-X (ON-X, ON-X Life Technologies Inc., Austin, TX, 27mm) and one tilting disc valve: Medtronic Hall (MH, Medtronic Inc., Minneapolis MN, 27mm) were inserted in a pulsatile in vitro model which was described in detail before.<sup>13</sup> In brief, this model consists of a pump-driven mock loop connected to a custom-made polymethyl methacrylate (PMMA) valve chamber via an inlet and outlet portion. The valve chamber used in this study housed a central mounting ring placed under a 45-degree angle to the CT gantry to simulate the normal in vivo aortic position. The different PHVs were inserted in this mounting ring. The valve chamber was placed in a commercially available anthropomorphic thoracic phantom (QRM GmbH, Möhrendorf, Germany) to simulate radiation absorption and scattering from the human thorax. A computer controlled piston-pump produced 60 pulses per minute and emitted an artificial ECG signal, which was read by the CT scanner. Water was used for perfusion in this study. No contrast administration was performed. The valve chamber within the thoracic phantom was positioned in the 64 detector-row CT scanner (Figure 1).

### CT scanner

For each PHV type, twenty scans were performed: ten at 120kV, 600mAs (high dose) and ten at 120kV, 300mAs (low dose). Scanning was performed on a 64 detector-row CT scanner

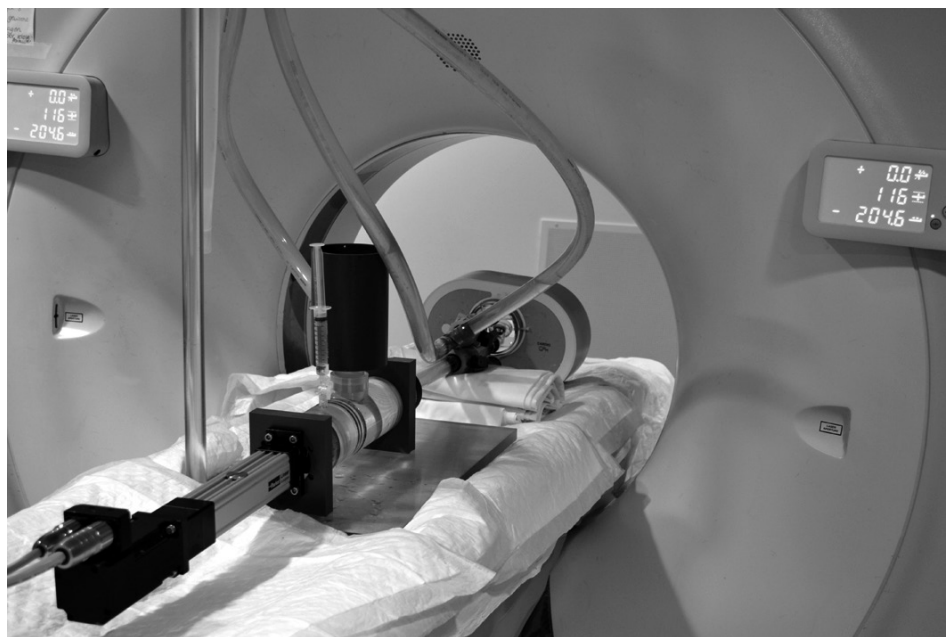


**Figure 1** | Photograph of in vitro pulsatile model in the 64 slice CT-scanner (Brilliance 64, Philips Medical Systems, Cleveland, Ohio)

(Brilliance 64, Philips Medical Systems, Cleveland, Ohio). An additional 15 scans at both scan settings were performed of the St Jude PHV for image noise measurements. Scanning parameters were based on the clinical scanning protocol for retrospectively ECG-gated MDCT coronary angiography: 64x0.625mm collimation, 0.42s rotation time, pitch of 0.2 and a matrix size of 512 x 512 pixels. Scan length was identical for each scan at 100 mm. Total DLP and  $CTDI_{vol}$  for each scan as displayed on the scanner console were recorded.

### Image reconstruction

Images of 0.9 mm thickness with 0.45 mm increment were reconstructed using a cardiac B filter at two phases of the ECG interval corresponding to diastolic (closed valve) and systolic (open valve) phases. For the high-dose scans (120 KV, 600 mAs), raw data were reconstructed using standard FBP. The IR (iDose, Philips Healthcare, Best, the Netherlands) applies a maximum likelihood denoising algorithm based on Poisson statistics on the raw projection data. Subsequently, reconstructed images are compared to optimal anatomical structures in image space, allowing noise reduction without altering the characteristics and overall appearance of the initial image. Besides noise reduction, iDose may decrease streak artifacts. iDose allows reconstruction of images at seven different levels with level one having the least influence on image reconstruction and level seven having most influence.

From the raw data of the low-dose scans performed at 120 KV, 300 mAs two different image sets were reconstructed: one image set using standard FBP and one using level 4 IR. Level 4 IR theoretically leads to image denoising by 29%. A dose reduction from 600 to 300 mAs (factor 2 decrease) would theoretically result in a noise increase by a factor 1.41 ( $\sqrt{2}$ ).<sup>14</sup> Applying level 4 IR would theoretically reduce noise in the low-dose (300 mAs) images to the level of the high-dose scans (noise increase by factor 1.41 due to lower mAs setting, and subsequent reduction by 29% due to IR).

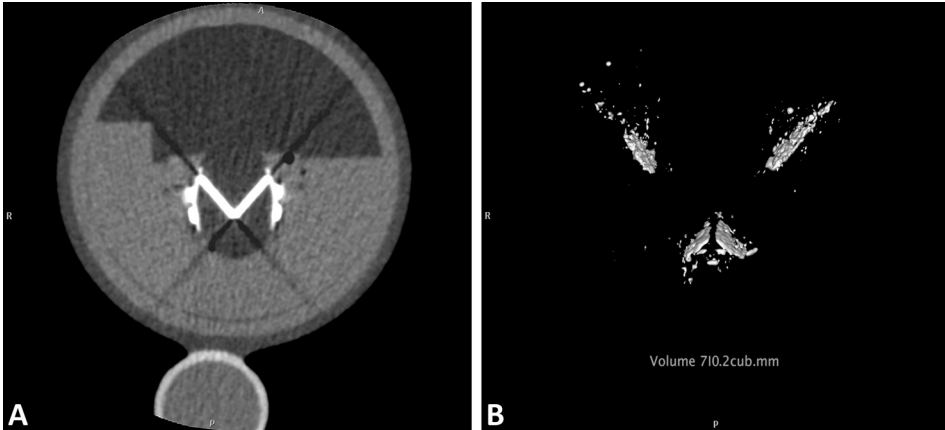


**Figure 2** | MDCT image of ON-X Bileaflet PHV **A** | MDCT image with measured artifacts **B** | Frontal plane with 3D volume PHV hypodense artifacts including PHV artifact measurement.

### Image analysis and artifact measurement

Images were transferred to a dedicated workstation (Extended Brilliance Workstation, Philips Medical Systems, Philips, Best, the Netherlands) for analysis. On the workstation, three-dimensional volume-rendered images were reconstructed from which the thoracic phantom was digitally excised. Subsequently, volumetric threshold filters were used for measurement of hyper- and hypodense artifacts emanating from the PHV (Figure 2). For hypodense artifacts, the upper limit of the threshold value was established by measuring the Hounsfield Unit (HU) values of the least dense periprosthesis structure (water) and subtracting approximately 3 times the standard deviation (SD) of the CT water density. The threshold for hyperdense artifacts was derived from the CT density of the surrounding PMMA structure and adding approximately 3 times the SD of the HU measurement. According to a method described elsewhere<sup>15</sup>, threshold filters were made to include all voxels below the threshold for the hypodense artifacts and above the threshold for the hyperdense artifacts. Thresholds used in this experiment were set at  $\leq -50$  HU and  $\geq 175$  HU for hypo- and hyperdense artifacts, respectively.

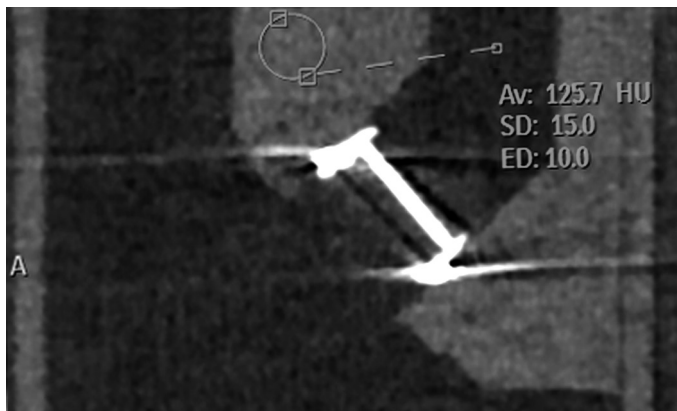


**Figure 3** | MDCT image of St Jude bileaflet PHV. Image noise (SD) is measured with a circular region of interest in a homogenous part of polymethyl methacrylate (PMMA) structure. Av = average image signal; HU = Hounsfield Units; ED = external diameter (mm).

At these settings the  $\leq 50$  HU filter measures the volume of hypodense artifacts, and the  $\geq 175$  HU filter measures the volume of hyperdense artifacts, including the PHV ring and leaflets.

Image noise (SD of the HU measurement) was measured in the 25 scans of the St Jude PHV using a circular region of interest (ROI, diameter 10mm) in a homogenous section of the PMMA structure in the valve chamber on identical locations in the different reconstructions (Figure 3).

### Data analysis

Data were analyzed using SPSS software (SPSS Statistics Version 15.0, SPSS Inc, Chicago, IL) and presented as means  $\pm$ SD. For each PHV type, a two-way repeated measures analysis was performed with reconstruction algorithm (120kV, 600mAs FBP; 120kV, 300mAs FBP and 120kV, 300mAs iDose level 4) and reconstruction phase (systolic or diastolic) defined as within-subject factors. Post-hoc pairwise testing with Bonferroni correction was performed to compare different reconstruction algorithms and reconstruction phases. Mean image noise was compared for the different reconstruction algorithms in a repeated measures analysis. Statistical significance was defined as a  $p$ -value  $< 0.05$ .

## RESULTS

### Dose reduction

For all low-dose scans,  $CTDI_{vol}$  and DLP were equal (17.7mGy and 236.5, respectively). For the high-dose scans,  $CTDI_{vol}$  and DLP were 35.3mGy and 473.4 respectively and equal for all scans. Radiation dose for low-dose scans was 50% of high-dose scans.

### Image noise

Mean image noise in the high-dose (120kV, 600mAs) scans ( $16.3 \pm 1.6$  HU) was 29.7% lower compared to the low-dose (120kV, 300mAs) scans ( $23.2 \pm 2.3$  HU) reconstructed with FBP. This difference was statistically significant ( $p < 0.001$ ). Low-dose scans reconstructed with iDose level 4 demonstrated similar image noise compared to high-dose scans reconstructed with FBP ( $16.5 \pm 1.7$  vs.  $16.3 \pm 1.6$  HU, respectively,  $p = 1.0$ ). Low-dose scans reconstructed with iDose level 4 had lower image noise compared to low-dose scans reconstructed with FBP ( $p < 0.001$ ) (Table 1, Figure 4)

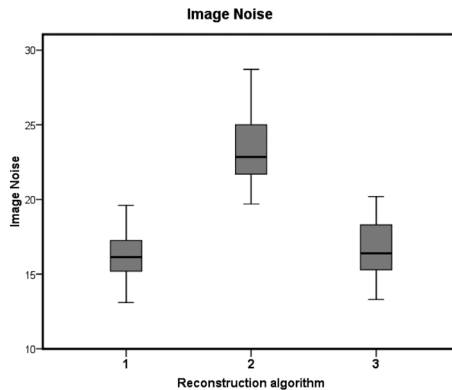


**Figure 4** | Boxplots of image noise for different reconstruction algorithms. (1) 120kV, 600mAs FBP reconstruction; (2) 120kV, 300mAs FBP reconstruction; (3) 120kV, 300mAs iDose level 4

**Table 1** | Mean image noise measured in the plexiglass (PMMA) of the perfusion chamber for different reconstruction algorithms.

Reconstruction algorithm	Image noise PMMA Mean±SD
120 kV 600mAs FBP	16.3±1.6
120 kV 300mAs FBP	23.2±2.3
120kV 300mAs IR level 4	16.5±1.7

FBP = filtered back projection; IR = iterative reconstruction algorithm; SD = standard deviation

**Table 2** | Mean artifact volumes (mm<sup>3</sup>) for hypo- and hyperdense PHV artifacts for different reconstruction algorithms (all PHVs combined diastolic and systolic phases)

Reconstruction algorithm	Hypodense artifacts	Hyperdense artifacts
	Mean±SD	Mean±SD
120 kV 600mAs FBP	1235±731	5346±1677
120 kV 300mAs FBP	2405±1051	6877±1849
120 kV 300mAs (IR level 4)	1218±683	5333±1663

FBP = filtered back projection; IR = iterative reconstruction algorithm

### PHV artifact volumes

Mean hypo- and hyperdense artifact volumes for different reconstruction algorithms are shown in Table 2 and classified per PHV type and reconstruction phase in Table 3. Boxplots of mean hypodense and hyperdense PHV artifact volumes are shown in Figure 5A and B. Repeated measures analyses were performed for each PHV type. For all PHV types, hypo- and hyperdense artifact volumes were significantly higher at low-dose scans compared to high dose scans reconstructed with FBP ( $p<0.001$ ).

For all PHV types, hypodense artifact volumes were similar (ON-X PHVs  $p=0.55$  and other PHVs  $p=1.0$ , respectively) for the high-dose scans reconstructed with FBP when compared to low-dose scans

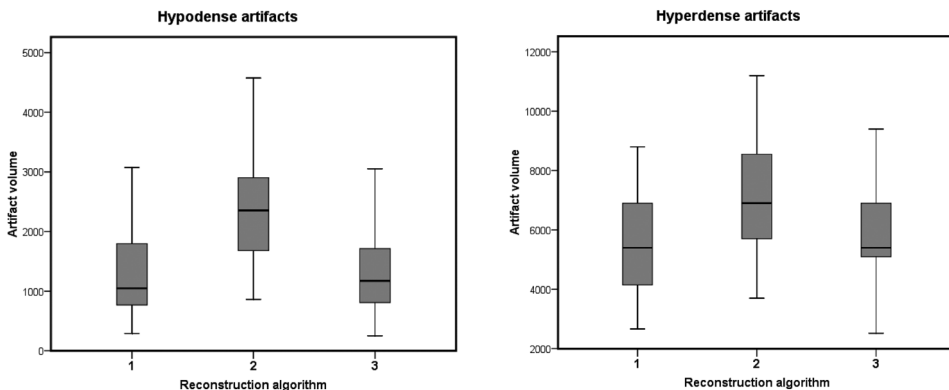


**Figure 5** | Boxplots of hypodense **A** and hyperdense **B** PHV artifacts for different reconstruction algorithms. (1) 120kV, 600mAs FBP reconstruction; (2) 120kV, 300mAs FBP reconstruction; (3) 120kV, 300mAs iDose level 4

**Table 3** | Hypodense and hyperdense artifacts in systolic and diastolic phase for each PHV type and reconstruction algorithm

Reconstruction algorithm	Reconstruction algorithm	Hypodense artifacts Mean±SD		Hypodense artifacts Mean±SD	
		Systolic	Diastolic	Systolic	Diastolic
St Jude Bileaflet PHV	120kV, 600mAs FBP	1829±488	1572±341	7170±352	7180±492
	120kV, 300mAs FBP	2994±275	2436±299	8770±254	8580±355
	120kV, 300mAs IR level 4	1890±208	1484±208	7120±253	6920±294
Carbomedics Bileaflet PHV	120kV, 600mAs FBP	630±137	342±43	3010±175	2836±125
	120kV, 300mAs FBP	1582±232	1062±147	4281±318	3992±153
	120kV, 300mAs IR level 4	683±167	322±56	3051±264	2746±120
ON-X Bileaflet PHV	120kV, 600mAs FBP	1237±216	790±73	5292±178	5052±57
	120kV, 300mAs FBP	2265±267	1637±127	6752±179	6582±107
	120kV, 300mAs IR level 4	1198±138	716±45	5282±171	5032±57
Medtronic Hall tilting disc PHV	120kV, 600mAs FBP	2575±433	905±116	6880±1001	5350±196
	120kV, 300mAs FBP	4534±564	2729±283	8910±928	7150±268
	120kV, 300mAs IR level 4	2385±489	1068±325	7010±936	5500±542

reconstructed with IR. Hypodense artifacts were similar for the high-dose scans reconstructed with FBP when compared to low-dose scans reconstructed with IR (St Jude  $p=0.95$ , all other valves  $p=1.0$ ).

Hypodense artifact volumes were significantly smaller in the diastolic (closed valve) phase compared to the systolic (opened valve) phase for St Jude PHVs ( $p=0.003$ ); Medtronic Hall PHVs ( $p<0.001$ ); Carbomedics PHVs ( $p<0.001$ ) and ON-X PHVs ( $p<0.001$ ) (Table 3). Hypodense artifact volumes were also significant smaller in the diastolic phase as opposed to the systolic phase for Medtronic Hall PHVs ( $p<0.001$ ), Carbomedics PHVs ( $p=0.002$ ), and ON-X PHVs ( $p<0.001$ ). The St Jude PHV demonstrated similar hyperdense artifacts ( $p=0.074$ ).

## DISCUSSION

The principal finding of this study is that iterative reconstruction allows different PHVs in a pulsatile in vitro model to be visualized with similar image noise and artifacts at a considerably reduced radiation dose (50% CTDI<sub>vol</sub> and DLP) compared to conventional acquisitions reconstructed with filtered back projection.

In a recent editorial,<sup>8</sup> Fleischman and Boas provided an insightful summary of the history and principles underlying iterative reconstruction. They explain that reconstruction of raw CT data is currently performed using the filtered back projection algorithm on virtually all commercially available CT systems.<sup>8</sup> The principle of FBP relies on the exact mathematical relationship between the measured X-ray attenuation in the projection data and the pixel values in the corresponding image. FBP assumes exact data. In reality, however, projection data from the CT scanner are noisy. The filter

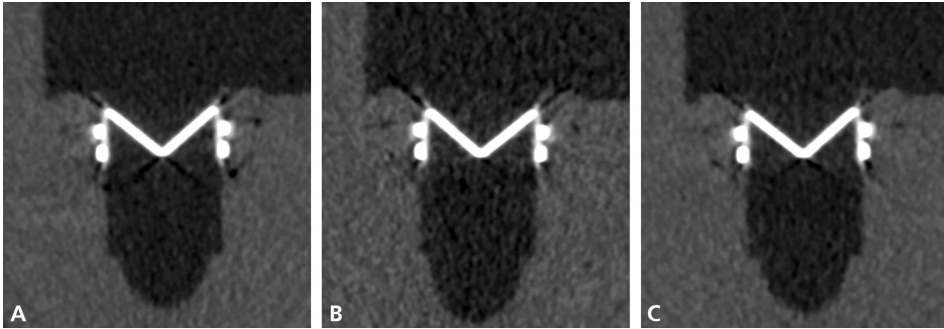


**Figure 6** | MDCT image of ON-X Bileaflet PHV **A** | Frontal plane 120kV, 600mAs reconstructed with FBP **B** | Frontal plane 120kV, 300mAs reconstructed with FBP **C** | Frontal plane 120kV, 300mAs reconstructed with iDose level 4

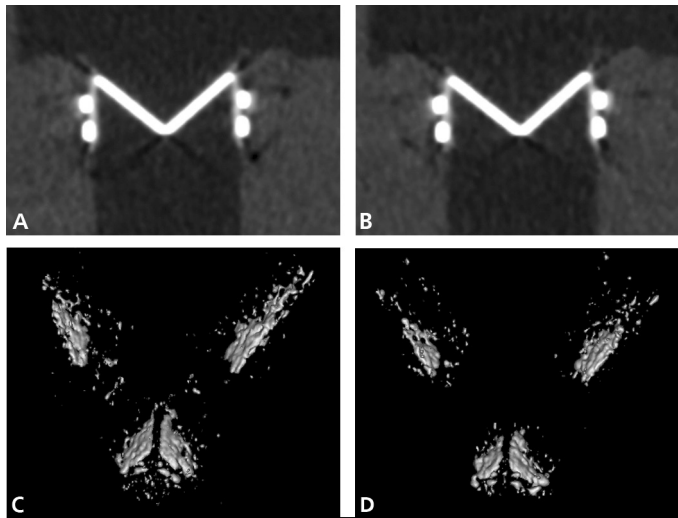


**Figure 7** | MDCT image of ON-X Bileaflet PHV **A** | Frontal plane 120kV, 600mAs reconstructed with FBP **B** | Frontal plane 120 kV, 300mAs reconstructed with iDose level 4 **C** | Frontal plane with 3D volume PHV hypodense artifacts (120kV, 600mAs, FBP) **D** | Frontal plane with 3D volume PHV hypodense artifacts (120 kV, 300mAs, Idose level 4)

used in FBP increases image noise.<sup>8</sup> Iterative reconstruction utilizes statistical models to improve signal to noise with each iteration. The main advantage of iterative reconstruction compared to FBP is the reduced image noise. Furthermore, iterative reconstruction reduces metal streak artifacts.<sup>8,16</sup>

Initial clinical results with iterative reconstruction are encouraging. Iterative reconstruction algorithms have been shown to decrease image noise and improve image quality of coronary segments in patients that underwent cardiac CTA for clinical indications at lower radiation dose.<sup>11,12</sup> Nevertheless, little is known about the application of iterative reconstruction algorithms in MDCT imaging of PHVs. We evaluated the effect of a novel IR algorithm (iDose, Philips Medical Systems, Best, The Netherlands) that performs iterative processing in both the projection and image domains on the image noise at a considerable lower radiation dose. Additionally, the effect of IR on the artifacts typically associated with MDCT imaging of PHV was evaluated.

The amount of noise in CT images depends on several factors: section collimation, acquisition time, and tube current.<sup>14</sup> Theoretically a decrease in tube current by a factor 2 leads to an increase in image noise by the square root of 2 (1.41), given that all other scanning parameters are kept constant.<sup>14</sup> By reconstructing images acquired with half the tube current using IR level 4, we expected, and found, noise to be reduced to the level of the initial tube current setting (Table 1). When low dose scans were reconstructed with IR level 4, mean image noise was again similar to the high-dose scans (Table 1). The 50% radiation dose reduction (CTDI<sub>vol</sub>/DLP 35.3mGy/473.4 vs. 17.7mGy/236.5) is mainly compensated for by the improvement of spatial resolution due to the denoising properties of the iterative reconstruction algorithm (Figure 6). Hypo- and hyperdense artifacts were comparable between high dose scans with FBP and low dose scans reconstructed with iDose level 4 IR (Figure 7). IR performed similar in the systolic and diastolic phase for the reduction of PHV artifacts (Table 3).

### Limitations

This study has limitations. First, the study was performed in an in vitro model. In this model, the normal annular motion present in the human heart, which may induce additional artifacts, is absent. However, strictly standardized conditions are essential for the comparison between different reconstruction algorithms. Second, no contrast medium was administered. The usage of diluted contrast would have represented a more realistic situation. However, in patients contrast timing, amount and enhancement may differ widely between centers. We used water as perfusate to standardize the experimental set-up. Furthermore, we do not expect the artifacts generated by the PHV itself to be influenced by contrast material. Third, no PHV pathology was imaged in this in vitro model. Therefore, diagnostic accuracy could not be verified. Artifacts are the main reasons for non-assessable PHVs. These artifacts were similar for the iterative reconstructions compared to the high-dose scans. Therefore, our assumption is that pathology can be equally well detected. Fourth, because hypodense artifact volumes ( $\leq 50$  HU filter) did not only include hypodense PHV artifacts but also image noise, we cannot rule out an influence on the results. However, the appearance of hypodense artifacts was similar for high dose scans reconstructed with FBP and low dose scans reconstructed with IR (Figure 7). Fifth, we scanned only with one tube voltage setting (120kV). In our institution, 120kV is commonly used for PHV CT imaging. Experiments with different kV settings (100kV, 140kV) would be interesting to optimize PHV CT scan protocols. Sixth, image quality was not assessed. Continuous outcome measures (3D artifact volumes and image noise) were preferred to quantify the effect of iterative reconstruction algorithms on image quality because of the more objective nature of these outcome measures. Further clinical evaluation in patients with PHVs is required to determine if PHV imaging with IR can replace standard FBP at a lower radiation dose. In prospective clinical studies, other patient related factors (e.g. body mass index) which can influence CT image quality have to be taken into account. Besides the novel IR algorithms other dose reducing techniques (e.g. prospective ECG triggering) have to be evaluated for PHV imaging. At present, retrospectively ECG-gated scanning remains essential to obtain dynamic information in both systolic and diastolic phases which is required for adequate leaflet motion assessment. Sixth, only one heart rate (60 bpm) was explored. Higher heart rates and arrhythmia may influence PHV CT image quality. Wide area detector CT scanners (256 slice or higher) enable prospective data acquisition in one or only several heart beats.<sup>17,18</sup> The more efficient radiation use in prospective scanning compared to retrospective scanning and the lower or 0 pitch may influence PHV generated artifacts. On the other hand, this may improve image quality compared to 64 slice CT scanning. High-pitch spiral scanning is an interesting alternative for image acquisition because of the decreased radiation exposure.<sup>19,20</sup> Low heart rates (<60bpm) are required to allow high-pitch spiral scanning. However, most patients



with suspected PHV dysfunction have high heart rates or rhythm disorders and contraindications for  $\beta$ -blockers which preclude high-pitch spiral scanning. In further prospective studies, a multivariate approach including different heart rates and different scanner types would be an interesting research topic. Finally, we investigated just one level of iterative reconstruction. It is possible that lower or higher levels of IR could have led to different results.

## CONCLUSION

In conclusion, MDCT imaging using iterative reconstruction enables in vitro imaging of different PHV types at 50% lower radiation dose with similar image noise and hypo- and hyperdense PHV artifacts.

## REFERENCES

1. Tsai IC, Lin YK, Chang Y, et al. Correctness of multi-detector-row computed tomography for diagnosing mechanical prosthetic heart valve disorders using operative findings as a gold standard. *Eur Radiol.* 2009; 19:857-867.
2. Symersky P, Budde RP, de Mol BA, et al. Comparison of multidetector-row computed tomography to echocardiography and fluoroscopy for evaluation of patients with mechanical prosthetic valve obstruction. *Am J Cardiol.* 2009; 104:1128-1134.
3. Konen E, Goitein O, Feinberg MS, et al. The role of ECG-gated MDCT in the evaluation of aortic and mitral mechanical valves: initial experience. *Am J Roentgenol.* 2008; 191:26-31.
4. Feuchtner GM, Stolzmann P, Dichtl W, et al. Multislice computed tomography in infective endocarditis: comparison with transesophageal echocardiography and intraoperative findings. *J Am Coll Cardiol.* 2009; 53:436-444.
5. Habets J, Budde RP, Symersky P, et al. Diagnostic evaluation of left-sided prosthetic heart valve dysfunction. *Nat Rev Cardiol* 2011; 8:466-478.
6. Habets J, Symersky P, van Herwerden LA, et al. Prosthetic heart valve assessment with multidetector-row CT: imaging characteristics of 91 valves in 83 patients. *Eur Radiol.* 2011; 21:1390-1396.
7. Chenot F, Montant P, Goffinet C, et al. Evaluation of anatomic valve opening and leaflet morphology in aortic valve bioprosthesis by using multidetector CT: comparison with transthoracic echocardiography. *Radiology* 2010; 255:377-385.
8. Fleischmann D, Boas FE. Computed tomography-old ideas and new technology. *Eur Radiol.* 2011; 21:510-517.
9. Lange K, Carson R. EM reconstruction algorithms for emission and transmission tomography. *J Comput Assist Tomogr* 1984; 8:306-316.
10. Shepp LA, Vardi Y. Maximum likelihood reconstruction for emission tomography. *IEEE Trans Med Imaging* 1982; 1:113-122.
11. Leipsic J, LaBounty TM, Heilbron B, et al. Estimated radiation dose reduction using adaptive statistical iterative reconstruction in coronary CT angiography: the ERASIR study. *Am J Roentgenol.* 2010; 195:655-660.
12. Leipsic J, LaBounty TM, Heilbron B, et al. Adaptive statistical iterative reconstruction: assessment of image noise and image quality in coronary CT angiography. *Am J Roentgenol.* 2010; 195:649-654.
13. Symersky P, Budde RPJ, Prokop M, et al. Multidetector-row computed tomography imaging characteristics of mechanical prosthetic valves. *J Heart Valve Dis.* 2011; 20:216-222.
14. Prokop M. Radiation Dose and Image Quality. In: Prokop M, Galanski M (eds): *Spiral and Multislice Computed Tomography of the Body.* Stuttgart, Thieme, 2003.
15. van der Schaaf I, van Leeuwen M, Vlassenbroek A, et al. Minimizing clip artifacts in multi CT angiography of clipped patients. *Am J Neuroradiol* 2006; 27:60-66.
16. Boas FE, Fleischmann D. Evaluation of Two Iterative Techniques for Reducing Metal Artifacts in Computed Tomography. *Radiology* 2011; 259:894-902.
17. Rybicki FJ, Otero HJ, Steigner ML, et al. Initial evaluation of coronary images from 320-detector row computed tomography. *Int J Cardiovasc Imaging* 2008; 24:535-546.
18. Weigold WG, Olaszewski ME, Walker MJ. Low-dose prospectively gated 256-slice coronary computed tomographic angiography. *Int J Cardiovasc Imaging* 2009; 25:217-230.
19. Achenbach S, Marwan M, Ropers D, et al. Coronary computed tomography angiography with a consistent dose below 1 mSv using prospectively electrocardiogram-triggered high-pitch spiral acquisition. *Eur Heart J* 2010; 31:340-346.
20. Achenbach S, Marwan M, Schepis T, et al. High-pitch spiral acquisition: a new scan mode for coronary CT angiography. *J Cardiovasc Comput Tomogr* 2009; 3:117-121.



# CHAPTER V

## ARTIFACT REDUCTION STRATEGIES *for* PROSTHETIC HEART VALVE CT IMAGING

J. Habets  
P. Symersky  
T. Leiner  
B.A.J.M. de Mol  
W.P.Th.M. Mali  
R.P.J. Budde

**ABSTRACT**

**PURPOSE** | Multislice CT evaluation of prosthetic heart valves (PHV) is limited by PHV-related artifacts. We assessed the influence of different kV settings, a metal artifact reduction filter (MARF) and an iterative reconstruction algorithm (IR) on PHV-induced artifacts in an in vitro model.

**METHODS** | A Medtronic-Hall tilting disc and St Jude bileafet PHV were imaged using a 64-slice scanner with 100kV/165mAs, 120kV/100mAs, 140kV/67mAs at an equal  $CTDI_{vol}$ . Images were reconstructed with (1) filtered back projection (FBP), (2) IR, (3) MARF and (4) MARF and IR. Hypo- and hyperdense artifacts volumes (mean  $mm^3 \pm SD$ ) were quantified with 2 thresholds ( $\leq -50$  and  $\geq 175$  Hounsfield Units). Image noise was measured and the presence of secondary artifacts was scored by two observers independently.

**RESULTS** | Mean hypodense artifacts for the Medtronic-Hall/St Jude valve (FBP) were  $966 \pm 23/1738 \pm 21$  at 100kV,  $610 \pm 13/991 \pm 12$  at 120kV, and  $420 \pm 9/634 \pm 9$  at 140kV. Compared to FBP, hypodense artifact reductions for IR were 9/8%, 10/7% and 12/6% respectively, for MARF 92%/84%, 89/81% and 86/77% respectively; for MARF+IR 94/85%, 92/82%, and 90/79% respectively. Mean hyperdense artifacts for the Medtronic Hall/ St Jude valve were  $5530 \pm 48/6940 \pm 70$  at 100kV,  $5120 \pm 42/6250 \pm 53$  at 120kV, and  $5011 \pm 52/6000 \pm 0$  kV at 140kV. Reductions for IR were 2/2%, 2/3% and 3/4% respectively, for MARF were 9/30%, 0/25%, 5/22% respectively, MARF+IR 12/32%, 4/27% and 7/25% respectively. Secondary artifacts were found in all MARF images. Image noise was reduced in the IR images.

**CONCLUSIONS** | In vitro PHV-related artifacts can be reduced by increasing kV despite maintaining identical  $CTDI_{vol}$ . Although MARF is more effective than IR, it induces secondary artifacts.

**P**rosthetic heart valve (PHV) assessment is a promising new application for multidetector-row CT (MDCT).<sup>1-7</sup> Although echocardiography is the mainstay of functional evaluation of prosthetic valves, it is hampered by acoustic shadowing and it may not be able to identify periprosthetic obstructive masses or false aneurysms.<sup>5-7</sup> The visualization of areas considered “off-limits” to echocardiography with MDCT allows detection of obstructive masses and may aid in the management of these patients.<sup>2,5</sup> In addition, MDCT allows the detection of periprosthetic leaks, vegetations and degenerative changes in biological prosthetic valves and allows evaluation of leaflet motion in mechanical valves.<sup>1-7</sup> Despite the excellent spatial and good temporal resolution of current MDCT technology, PHV CT images vary in quality. For mechanical PHV, a variable amount of valve-induced artifacts remains due to the radiopaque and metal components of the PHV.<sup>2,3,8,9</sup> Compounding the problem of artifacts, are the differences in PHV composition. PHV consisting of cobalt chromium components, such as the Björk-Shiley and Sorin tilting disc valves, are associated with severe artifacts that prohibit CT assessment of these valves. In contrast, modern mechanical PHVs that consist of tungsten impregnated carbon leaflets and titanium or nickel alloy rings induce far less artifacts and allow a much more complete visualization of the periprosthetic anatomy.<sup>1,2,4,6</sup> Because the masses interfering with normal PHV function and periprosthetic leaks are directly adjacent to the high attenuation components of the PHV, further reduction of the PHV-related artifacts may further improve the diagnostic yield of MDCT.

The problem of metal artifacts is ubiquitous in CT imaging and many different strategies have been devised to improve the image quality around metal objects. These strategies reflect the multiple mechanisms that cause these artifacts. On the one hand, physics-related interactions such as beam hardening, scatter and photon starvation are important. On the other hand, algorithms used for reconstruction of these faulty raw data may augment artifacts by, for example, creating windmill artifacts and artifacts related to helical interpolation.<sup>9-12</sup> As mentioned above, these interactions are further complicated by the differences in PHV composition which have been related to the severity of artifacts. Hence, a single intervention, such as the increase of beam energy or iterative image reconstruction, may decrease some artifacts but not sufficiently eliminate them.<sup>10,11</sup>

Our goal in this study was to evaluate the effectiveness of three ways to reduce PHV-related artifacts: (1) variation of tube voltage (beam energy), (2) applying a metal artifact reduction filter, and (3) iterative image reconstruction. By comparing these three approaches for the reduction of PHV-related artifacts in an *in vitro* model, we sought to determine the effectiveness of each method for optimizing the MDCT image quality of PHV.

## METHODS

### Valves

The valves were mounted in a previously described<sup>9</sup> polymethyl methacrylate (PMMA) valve chamber, which was placed in a commercially available thoracic phantom (QRM GmbH, Möhrendorf, Germany, Figure 1). The chamber was filled with water and the valve was positioned at a 45 degree angle to the scanner gantry simulating the approximate position of the aortic valve *in vivo*. No valve or leaflet motion was present. Two different PHVs were imaged in a fixed open position: (1) 27mm St Jude masters bileaflet (St Jude Medical Inc., St Paul, MN, USA) and (2) 27mm Medtronic Hall tilting disc (Medtronic Inc., Minneapolis, MN, USA).

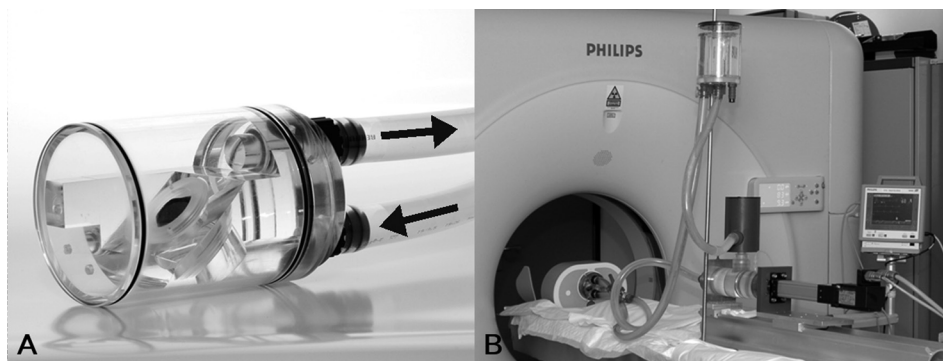


**Figure 1** | Polymethyl methacrylate (PMMA) perfusion chamber **A** | Pulsatile in vitro model in 64 slice CT scanner (Brilliance 64, Philips Medical Systems, Cleveland, Ohio, USA) **B** | (Reprinted with permission<sup>9</sup>, Copyright ICR Publishers)

### Scan protocol

All scans were performed on a 64-slice CT scanner (Brilliance 64, Philips Medical Systems, Cleveland, Ohio, USA). Because the metal artifact reduction filter can not yet be used with ECG-gated scans protocols, we adapted a standard scan protocol for thoracic imaging to have the same imaging parameters as a standard retrospectively gated CT of the heart. This was done by adjusting the following parameters: pitch 0.2, collimation 64x0.625mm, 120 kV, matrix size 512x512, gantry rotation time 420 ms. Because a non-ECG-gated image acquisition results in much lower noise levels, we adjusted the mAs setting to a lower value at which the same level of noise (defined as the standard deviation (SD) of CT attenuation) was present as that found in earlier ECG-gated in vitro experiments<sup>9</sup> using a standard ECG-gated cardiac protocol. Noise was measured using a circular region of interest (diameter 1 cm) in a homogenous part of the PMMA structure of the valve chamber not affected by the PHV-related artifacts. For the adapted thoracic protocol at 120 kV, a mAs setting of 100 resulted in equal image noise.

For the experiment, three different acquisition protocols with different tube voltage settings with identical  $CTDI_{vol}$  and DLP values were used. For this, the adapted thoracic protocol was adjusted to 100 and 140 kV to yield identical  $CTDI_{vol}$  and DLP values obtained for the 120 kV, 100 mAs scan. This resulted in scans performed at 140 kV, 67 mAs and 100 kV with 165mAs. Ten scans of each valve were performed with each kV, mAs setting. A standard reconstruction filter was used because the detailed cardiac filter is not available for non-gated scans. Images were reconstructed at 0.9mm thickness with a 0.45mm increment.

### Image reconstruction:

Images were reconstructed in four different ways: (1) standard filtered back projection (FBP), (2) using iterative image reconstruction (IR, iDose, Philips Healthcare, Best, the Netherlands), (3) FBP combined with a metal artifact reduction filter (MARE, Philips Medical Systems, Best, the Netherlands), and (4) IR combined with MARE. According to the manufacturer the IR used in this study uses several cycles of iterative reconstruction and applies a maximum likelihood denoising algorithm based on Poisson statistics on the raw projection data. Subsequently, the reconstructed images are compared to optimal anatomical structures in image space, allowing noise reduction without altering the characteristics and overall appearance of the initial image. Different levels of IR are possible with increasing influence on image reconstruction. The level used in this study leads to image denoising by 50% according to manufacturer data.

MARF is an image-based algorithm which is based on interpolation of data for the reduction of artifacts. Importantly, the MARF algorithm uses the images provided by the reconstruction of the raw data with either FBP or IR.

### **Image analysis**

All image sets were transferred to a dedicated workstation for analysis (Extended Brilliance Workstation, Philips Medical Systems, Best, the Netherlands). High and low-density artifact volumes were quantified using two thresholds based on the densities of the surrounding structures according to a methodology described previously.<sup>9</sup> We chose threshold values that were approximately 3 SD above the Hounsfield Unit (HU) of PMMA measurement and below the HU of water, respectively. The chosen thresholds were  $\geq 175$  HU for hyperdense artifacts and  $\leq -50$  HU for hypodense artifacts. Because the PHVs are composed of various radiopaque components such as a titanium ring and tungsten impregnated leaflets<sup>9</sup>, the  $\geq 175$  HU threshold included the radiopaque components of the PHV as well. Hence, the percentage change in hyperdense artifacts measured with the  $\geq 175$  HU threshold underestimates the actual change in artifacts because the radiopaque components are included as well. Areas outside the valve chamber and other unrelated sources of artifacts were manually digitally excised in an identical manner for all scans.

In addition to the quantification of artifacts, all images reconstructed with the four different reconstruction algorithms were evaluated for possible induced changes in periprosthetic densities of the water and the PMMA contours. These secondary artifacts were considered induced if: (1) they were localized elsewhere or beyond primary artifact distribution in comparison with the normal FBP reconstruction; and (2) did not follow known contours of water and the PMMA structure. These induced changes were scored (present or absent) by two observers independently (JH and PS).

Image noise (defined as the SD of CT attenuation) was measured in all images using a circular region of interest (diameter 1 cm) that was placed in a homogenous part of the PMMA structure of the valve chamber not affected by the PHV-related artifacts.

### **Data analysis**

Data were analyzed using SPSS software (SPSS Statistics Version 15.0, SPSS Inc, Chicago, IL) and were presented as means  $\pm$  SD. For each PHV type, a two-way repeated measures analysis was performed with reconstruction algorithm (FBP, IR, FBP+MARF, and IR+MARF) as within-subjects factor and tube voltage/scan protocol (100kV, 165mAs; 120kV, 100mAs and 140kV, 67mAs) as between-subjects factor, and hypo- and hyperdense artifacts as dependent variable. Because of a significant interaction between tube voltage and reconstruction algorithm, additional analyses were performed to analyze the main effects of tube voltage (one-way ANOVA) and reconstruction algorithm (repeated measures analysis).

For each PHV, a repeated measures analysis was performed with reconstruction algorithm as within-subjects factor and tube voltage/scan protocol as between-subjects factor and image noise as dependent variable. In case of violation of the sphericity assumption, Greenhouse-Geisser correction was applied. Post-hoc pairwise testing with Bonferroni correction was performed to compare the different levels of the reconstruction algorithms and tube voltages. Statistical significance was defined as a  $p$ -value  $< 0.05$ .

## RESULTS

### Radiation exposure

Scan length was equal for all scans at 109.8 mm. The CTDI<sub>vol</sub>/DLP values were exactly equal for all scans at 5.90 mGy and 960.4 mGy.cm, respectively.

### Artifact volumes

Mean hypo- and hyperdense artifact volumes for different tube voltages are shown in Table 1 and 2. The reductions related to tube voltage and reconstruction algorithm were not proportional to each other e.g. a significant interaction was present for both hypo- and hyperdense artifacts for Medtronic Hall PHV (F-value 2,914,  $p < 0.001$  and 76,  $p < 0.001$ , respectively); and for St Jude bileaflet PHV (F-value 12,502,  $p < 0.001$  and 715,  $p < 0.001$ , respectively). Because of this interaction, the averages could not be compared as a group in the repeated measures analyses, but a  $p$ -value was generated for each of the three kV settings and each reconstruction algorithm.

**Table 1** | The influence of tube voltage and reconstruction algorithm on hypodense PHV artifacts

PHV type	Scan protocol	FBP <sup>a</sup>	IR <sup>a</sup>	FBP+MARF <sup>a</sup>	IR+MARF <sup>a</sup>
Medtronic Hall tilting disc <sup>b</sup>	100kV, 165mAs	966±23	875±20 (-9%)	81±3 (-92%)	56±3 (-94%)
	120kV, 100mAs	610±13	548±13 (-10%)	69±3 (-89%)	48±3 (-92%)
	140 kV, 65mAs	420±9	371±10 (-12%)	57±5 (-86%)	40±2 (-90%)
St Jude Bileaflet <sup>b</sup>	100kV, 165mAs	1,738±21	1,606±20 (-8%)	278±3 (-84%)	257±3 (-85%)
	120kV, 100mAs	991±12	922±8 (-7%)	191±4 (-81%)	175±2 (-82%)
	140 kV, 65mAs	634±9	595±6 (-6%)	146±3 (-77%)	133±2 (-79%)

<sup>a</sup> Different reconstruction algorithms: Filtered Back Projection (FBP), Metal Artifact Reduction Filter (MARF), Iterative Reconstruction (IR)

<sup>b</sup> Manufacturer details: Medtronic Hall tilting disc (Medtronic, Minneapolis, MN, USA) and St Jude bileaflet (St Jude Medical, St Paul, MN, USA)

Between brackets percentage PHV artifact reduction compared to standard FBP

**Table 2** | The influence of tube voltage and reconstruction algorithm on hyperdense PHV artifacts

PHV type	Scan protocol	FBP <sup>a</sup>	IR <sup>a</sup>	FBP+MF <sup>a</sup>	IR+MF <sup>a</sup>
Medtronic Hall tilting disc <sup>b</sup>	100kV, 165mAs	5,530±48	5,420±42 (-2%)	5,009±32 (-9%)	4,850±26 (-12%)
	120kV, 100mAs	5,120±42	4,997±7 (-2%)	5,110±32 (-0%)	4,901±18 (-4%)
	140 kV, 65mAs	5,011±52	4,849±26 (-3%)	4,767±135 (-5%)	4,641±89 (-7%)
St Jude Bileaflet <sup>b</sup>	100kV, 165mAs	6,940±70	6,770±48 (-2%)	4,829±30 (-30%)	4,733±25 (-32%)
	120kV, 100mAs	6,250±53	6,070±48 (-3%)	4,663±19 (-25%)	4,541±19 (-27%)
	140 kV, 65mAs	6,000±0	5,740±52 (-4%)	4,708±14 (-22%)	4,523±14 (-25%)

<sup>a</sup> Different reconstruction algorithms: Filtered Back Projection (FBP), Metal Artifact Reduction Filter (MARF), Iterative Reconstruction (IR)

<sup>b</sup> Manufacturer details: Medtronic Hall tilting disc (Medtronic, Minneapolis, MN, USA) and St Jude bileaflet (St Jude Medical, St Paul, MN, USA)

Between brackets percentage PHV artifact reduction compared to standard FBP



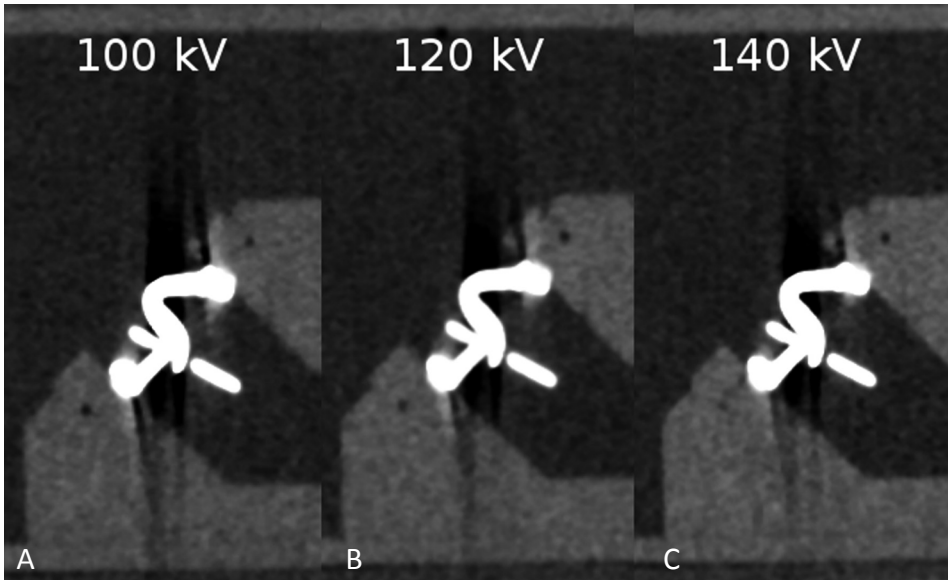


**Figure 2** | CT image reconstructions of Medtronic Hall tilting disc (Medtronic Inc., Minneapolis, MN, USA) reconstructed with filtered back projection and scanned with **A** | 100kV **B** | 120kV and **C** | 140kV Note the moderate reduction of hypodense artifacts and a slight reduction of hyperdense artifacts

#### **Influence of tube voltage on PHV artifact volumes**

For the Medtronic Hall tilting disc PHV, mean hypo- and hyperdense artifacts were significantly lower at 140kV compared to 100 and 120kV for all different reconstruction algorithms (All  $p$ -values  $<0.001$ ) (Table 1 and 2, Figure 2). However for hyperdense artifacts, there was no significant difference between 100 and 120kV when reconstructed with MARF+IR ( $p=0.136$ ).

For St Jude Bileaflet, mean hypo- and hyperdense artifacts were significantly lower in 140kV scans compared to 100 and 120kV scans for all different reconstruction algorithms (All  $p$ -values  $<0.001$ ) (Table 1 and 2). For hyperdense artifacts, there was no significant difference between 120 and 140 kV when reconstructed with MARF+IR ( $p=0.154$ ).

#### **Influence of reconstruction algorithm on PHV artifact volumes**

For Medtronic Hall tilting disc PHV, mean hypo- and hyperdense artifacts were significantly different between the different reconstruction algorithms for each kV setting (All  $p$ -values  $<0.001$ ) (Table 1 and 2). No difference existed for hyperdense artifacts between FBP and MARF at 120kV ( $p=1.0$ ), and between IR and MARF at 140kV ( $p=0.588$ ).

For St Jude bileaflet PHV, mean hypo- and hyperdense artifacts were significantly different between the different reconstruction algorithm at each kV setting (all  $p$ -values  $<0.001$ ) (Table 1 and 2). For both hypodense and hyperdense artifacts, the reduction were more pronounced when with MARF and MARF+IR compared to FBP and IR alone (Table 1 and 2).

#### **Image noise**

For each PHV, mean image noise is presented for different tube voltages and different reconstruction algorithms in Table 3. For both St Jude and Medtronic Hall PHV, mean image noise was not significantly different for different tube voltages ( $p=0.133$  and  $p=0.815$ , respectively). Image noise was significantly lower in scans reconstructed with IR alone and IR+MARF for both PHVs ( $p<0.001$ ).

**Table 3** | Mean image noise ( $\pm$ SD) in different reconstruction algorithms and scan protocols

PHV type	Scan protocol	Image noise (FBP <sup>a</sup> )	Image noise (IR <sup>a</sup> )	Image noise (FBP+MARF <sup>a</sup> )	Image noise (IR+MARF <sup>a</sup> )
Medtronic Hall tilting disc <sup>b</sup>	100kV, 165mAs	13.0 $\pm$ 1.3	10.2 $\pm$ 1.2	12.7 $\pm$ 1.3	10.5 $\pm$ 1.0
	120kV, 100mAs	12.1 $\pm$ 1.3	9.4 $\pm$ 1.2	12.4 $\pm$ 1.1	9.4 $\pm$ 1.2
	140 kV, 65mAs	12.8 $\pm$ 1.4	9.7 $\pm$ 0.7	12.7 $\pm$ 1.1	9.7 $\pm$ 0.9
St Jude Bileaflet <sup>b</sup>	100kV, 165mAs	10.8 $\pm$ 0.5	8.6 $\pm$ 0.5	10.8 $\pm$ 0.6	8.4 $\pm$ 0.6
	120kV, 100mAs	10.7 $\pm$ 1.0	8.7 $\pm$ 1.2	10.8 $\pm$ 1.2	8.3 $\pm$ 1.0
	140 kV, 65mAs	11.1 $\pm$ 0.9	8.6 $\pm$ 0.9	11.0 $\pm$ 1.1	8.7 $\pm$ 1.1

<sup>a</sup> Different reconstruction algorithms: Filtered Back Projection (FBP); Metal Artifact Reduction Filter (MARF); Iterative Reconstruction (IR); SD = standard deviation

<sup>b</sup> Manufacturer details: Medtronic Hall tilting disc (Medtronic, Minneapolis, MN, USA) and St Jude bileaflet (St Jude Medical, St Paul, MN, USA)

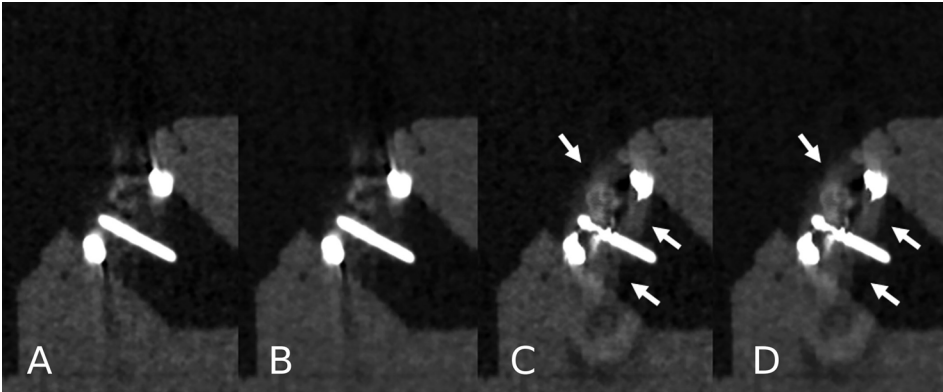


**Figure 3** | CT image reconstructions of Medtronic Hall tilting disc (Medtronic Inc., Minneapolis, MN, USA) with filtered back projection **A** | iterative reconstruction **B** | metal artifact reduction filter and **C** | metal artifact reduction filter and iterative reconstruction **D** | Note the secondary artifacts present in the MARF reconstructions (arrows) (**C** and **D**). These artifacts are not present in the other reconstructions FBP (**A**) and IR (**B**).

**Interpolation artifacts induced by MARF**

For both St Jude bileaflet PHV and Medtronic Hall tilting disc PHV, MARF and MARF+IR caused interpolation artifacts in each of the 10 scans (Figure 3 and 4). In the scans reconstructed with FBP and IR alone no interpolation artifacts were present.

**DISCUSSION**

The principal findings of this study are: (1) increasing tube voltage (kV) while maintaining identical CTDI<sub>vol</sub> reduced mainly hypodense and to a lesser extent hyperdense PHV artifacts; (2) IR reduced PHV artifacts to a lesser extent than an increase in kV but reduced image noise compared to scans reconstructed with FBP; and (3) although MARF is very effective in reducing hypodense artifacts, it induced artifacts and deformed the periprosthetic anatomy.

For MDCT imaging of PHVs using commercially available technology, high energy photons

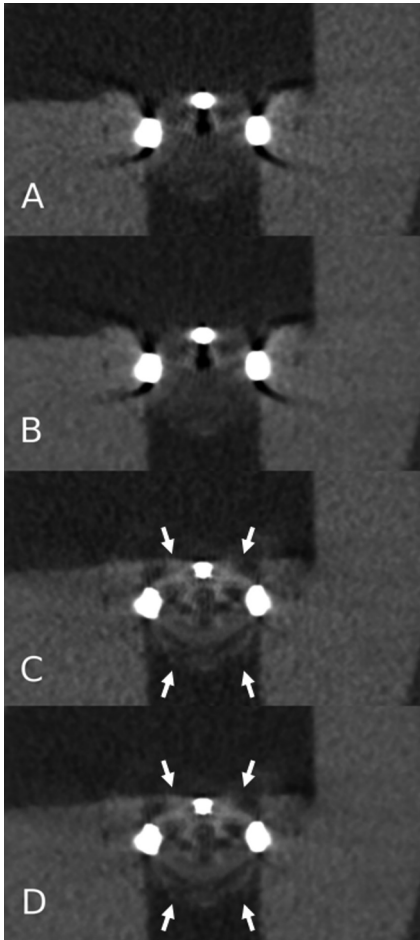


**Figure 4** | CT image reconstructions of Medtronic Hall tilting disc (Medtronic Inc., Minneapolis, MN, USA) with filtered back projection **A** | iterative reconstruction **B** | metal artifact reduction filter **C** | and metal artifact reduction filter and iterative reconstruction **D** |. Note the secondary artifacts present in the MARF reconstructions (arrows) (**C** and **D**).

may be most effective for the reduction of artifacts. Although the effect of iterative reconstruction seems to be little with respect to artifact reduction, it does reduce image noise which may enhance image quality.

Several mechanisms of PHV-related artifacts have been proposed. For one part, the artifacts are related to radiopaque components. All currently implanted mechanical PHVs have tungsten impregnated leaflets and prosthetic rings consisting of metal alloys. These metal alloys vary from titanium, nickel to cobalt-chrome alloys and are associated with various gradations in artifact severity.<sup>1,4,8,9</sup> The artifacts caused by these metal alloys form the rationale for the use of a metal artifact reduction filter. On the other hand, motion of the PHV due to the annular motion in concert with cardiac contractions and leaflet motion are another source of artifacts. For example, the opening and closing motion of leaflets has been associated with increases in hyper- and hypodense artifacts.<sup>8</sup> In clinical acquisitions, annular motion also may increase hypo- and hyperdense PHV artifacts. In this study, we aimed to evaluate different strategies to reduce the artifacts associated with the metal and radiopaque components of PHVs.

Increasing photon energy reduced photon starvation as a cause of PHV-related artifacts. IR demonstrated an additional hypo- and hyperdense artifact reduction depending on tube voltage level (6-12% and 2-4%, respectively). Interestingly, the reduction of tube current did not cause any measurable increase in image noise when measured in the PMMA structure surrounding the PHV.<sup>13</sup> This may have important implications for clinical scanning of PHV: standard coronary protocols should be modified by increasing tube voltage while maintaining equal CTDI<sub>vol</sub> (reducing mAs) to reduce PHV-related artifacts. Although 140 kV has been employed clinically to enhance visibility of bioprostheses, it was done without reduction of tube current and at the expense of an increased radiation exposure.<sup>14</sup> Our results demonstrate that with an equal dose, the increased tube voltage may represent a readily available and reproducible way to enhance PHV image quality because of PHV artifact reduction. Increased tube voltage results in clinically relevant hypodense PHV artifact reductions (Table 1). Although the reductions in hyperdense artifacts are relatively small, the volume of the radiopaque components is included in the  $\geq 175$  HU threshold. When corrected for these components (i.e. tungsten impregnated leaflets and metal alloy prosthetic ring<sup>8</sup>, the artifact reductions amount to 15 and 18% for the Medtronic Hall and St Jude valve, respectively.

Another source of artifacts related to metal objects is scatter and noise.<sup>15</sup> Commercially available iterative reconstruction algorithms are effective in denoising images and improve image quality based on Poisson statistics.<sup>11,15</sup> Our results confirm that IR addresses another mechanism of PHV-related artifacts (it reduces image noise) and has some incremental value to the increase in tube voltage. The decrease in hypodense artifact volume may be attributed to the reduction of image noise compared to the scans reconstructed with FBP. However, a higher tube voltage is more effective for PHV artifact reduction. This approach is similar to the strategy of Boas and Fleischmann<sup>15</sup> who specifically aimed at reducing several mechanisms of metal artifacts. Their findings may not be completely comparable to ours, because of the difference in size and in composition of PHVs. Clinically, IR may be used next to modified exposure parameters to optimize PHV image quality and may possibly reduce radiation dose. Previous *in vitro* work demonstrated that iterative reconstruction enables a 50% dose reduction (120kV, 300mAs) compared to a standard dose (120 kV, 600 mAs) with FBP without an increase in image noise or PHV-related artifacts.<sup>16</sup>

The MARF algorithms have been generally conceived to reduce the artifacts caused by large metallic objects such as hip prostheses.<sup>17</sup> In fact, due to the variation in composition and size of various metal objects, MARF may either be effective in restoring image quality or detrimental by inducing artifacts. Despite advances, a recurrent problem with MARF is the interpolation of detector values considered altered by the metal. Nothing is “recovered” by interpolation but an average value of the surrounding voxels is assumed to be appropriate.<sup>18,19</sup> Hence interpolation artifacts in both PHVs in all scans remain a limitation of this technique as demonstrated by our results (Figure 3 and 4). In clinical practice, these interpolation artifacts are situated on the location where PHV pathology can be expected. These interpolation artifacts may hamper accurate diagnostic assessment of PHV pathology (i.e. pannus or thrombus). Therefore, patients may be denied appropriate (surgical) treatment. Our results are in contrast to the findings of Boas and Fleischmann.<sup>15</sup> As stated above, this may be due to the size and composition of the metal object studied, and, probably, to a different algorithm used in their experiments. However, we preferred commercially available techniques in order to test the effectiveness of readily applicable algorithms for PHV scanning.

Recent *in vitro* work demonstrated that prospectively triggered acquisition on a 256 slice MDCT system generally reduces PHV-related artifacts and image noise substantially compared to retrospectively ECG-gated acquisition at different heart rates.<sup>20</sup> However, further studies are required to evaluate the clinical feasibility of low-dose PHV MDCT protocols that combine prospectively triggered acquisition with iterative reconstruction.

Our study has several limitations. First, we used controlled *in vitro* conditions which precluded any leaflet motion or annular motion. Motion of high density objects is another factor which may considerably increase the PHV-related artifacts.<sup>11</sup> In earlier work, we demonstrated important variation of artifacts due to leaflet motion.<sup>8</sup> Clinical studies must be undertaken to confirm our *in vitro* findings. Second, image acquisition was not done with ECG-gating. Although we approximated the exposure parameters to reflect as accurately as possible a cardiac ECG-gated acquisition, the difference between a standard filter and a detailed cardiac filter may affect the amount of image noise and magnitude of artifacts as well as reproducibility of the results in a clinical setting. However, all scans in the current study used the same reconstruction kernel and thus comparison of the different scan and reconstruction protocols is not likely to be affected. Third, our experiments were performed on a 64 slice MDCT system. Currently available higher end MDCT systems (256 slice or more) allow cardiac MDCT imaging with a faster gantry rotation and a higher temporal resolution. Increased temporal resolution may reduce PHV-related artifacts owing to cardiac and/or annular movement, and therefore may improve MDCT image quality. Additional research has to be conducted to assess the differences in PHV-related artifacts and image quality between 64-slice and higher end MDCT systems. Fourth, we used only two PHVs. We chose the St Jude and Medtronic Hall valves because these valves are the most commonly implanted bileaflet and tilting disc valves respectively. In clinical reports, MDCT has been found of additional value for the detection of the cause of dysfunction for both valves.<sup>1,2,21</sup> Other commonly implanted PHVs are well visualized by MDCT.<sup>4</sup>

In conclusion, our *in vitro* results suggest that optimizing image quality of PHV with respect to the radiopaque components can be achieved at equal dose with higher tube voltage and to lesser extent with iterative reconstruction. MARF in its current form is very effective in reducing artifacts but the induced interpolation artifacts currently limit its use in clinical PHV imaging.

## REFERENCES

1. Tsai IC, Lin YK, Chang Y, et al. Correctness of multi-detector-row computed tomography for diagnosing mechanical prosthetic heart valve disorders using operative findings as a gold standard. *Eur Radiol* 2009; 19:857-867.
2. Symersky P, Budde RP, de Mol BA, et al. Comparison of multidetector-row computed tomography to echocardiography and fluoroscopy for evaluation of patients with mechanical prosthetic valve obstruction. *Am J Cardiol* 2009; 104:1128-1134.
3. Konen E, Goitein O, Feinberg MS, et al. The role of ECG-gated MDCT in the evaluation of aortic and mitral mechanical valves: initial experience. *Am J Roentgenol* 2008; 191:26-31.
4. Habets J, Symersky P, van Herwerden LA, et al. Prosthetic heart valve assessment with multidetector-row CT: imaging characteristics of 91 valves in 83 patients. *Eur Radiol* 2011; 21:1390-1396.
5. Habets J, Budde RP, Symersky P, et al. Diagnostic evaluation of left-sided prosthetic heart valve dysfunction. *Nat Rev Cardiol* 2011; 8:466-478.
6. Girard SE, Miller FA, Jr., Orszulak TA, et al. Reoperation for prosthetic aortic valve obstruction in the era of echocardiography: trends in diagnostic testing and comparison with surgical findings. *J Am Coll Cardiol* 2001; 37:579-584.
7. Feuchtnner GM, Stolzmann P, Dichtl W, et al. Multislice computed tomography in infective endocarditis: comparison with transesophageal echocardiography and intraoperative findings. *J Am Coll Cardiol* 2009; 53:436-444.
8. Symersky P, Budde RP, Westers P, et al. Multidetector CT imaging of mechanical prosthetic heart valves: quantification of artifacts with a pulsatile in vitro model. *Eur Radiol* 2011; 21:2103-2110.
9. Symersky P, Budde RP, Prokop M, et al. Multidetector-row computed tomography imaging characteristics of mechanical prosthetic valves. *J Heart Valve Dis*. 2011; 20:216-222.
10. van der Schaaf I, van Leeuwen M, Vlassenbroek A, et al. Minimizing clip artifacts in multi CT angiography of clipped patients. *Am J Neuroradiol* 2006; 27:60-66.
11. Fleischmann D, Boas FE. Computed tomography-old ideas and new technology. *Eur Radiol*. 2011; 21:510-517.
12. Barrett JF, Keat N. Artifacts in CT: recognition and avoidance. *Radiographics* 2004; 24:1679-1691.
13. Prokop M. Radiation Dose and Image Quality. In: Prokop M, Galanski M (eds). *Spiral and Multislice Computed Tomography of the Body*. Stuttgart, Thieme, 2003.
14. Chenot F, Montant P, Goffinet C, et al. Evaluation of anatomic valve opening and leaflet morphology in aortic valve bioprosthesis by using multidetector CT: comparison with transthoracic echocardiography. *Radiology* 2010; 255:377-385.
15. Boas FE, Fleischmann D. Evaluation of Two Iterative Techniques for Reducing Metal Artifacts in Computed Tomography. *Radiology* 2011; 259:894-902.
16. Habets J, Symersky P, de Mol BA, et al. A novel iterative reconstruction algorithm allows reduced dose multidetector-row CT imaging of mechanical prosthetic heart valves. *Int J Cardiovasc Imaging* 2011; DOI: 10.1007/s10554-011-9954-7.
17. Lee MJ, Kim S, Lee SA, et al. Overcoming artifacts from metallic orthopedic implants at high-field-strength MR imaging and multidetector CT. *Radiographics* 2007; 27:791-803.
18. Bal M, Spies L. Metal artifact reduction in CT using tissue-class modeling and adaptive prefiltering. *Med Phys* 2006; 33:2852-2859.
19. Veldkamp WJ, Joemai RM, van der Molen AJ, et al. Development and validation of segmentation and interpolation techniques in sinograms for metal artifact suppression in CT. *Med Phys* 2010; 37:620-628.
20. Symersky P, Habets J, Westers P, et al. Prospective ECG triggering reduces prosthetic heart valve-induced artifacts compared with retrospective ECG gating on 256-slice CT. *Eur Radiol* 2011; DOI: 10.1007/s00330-011-2358-1.
21. Teshima H, Hayashida N, Fukunaga S, et al. Usefulness of a multidetector-row computed tomography scanner for detecting pannus formation. *Ann Thorac Surg*. 2004; 77:523-526.



## CHAPTER VI

# PROSPECTIVE ECG TRIGGERING REDUCES PROSTHETIC HEART VALVE INDUCED-ARTIFACTS COMPARED *with* RETROSPECTIVE ECG GATING *on* 256-SLICE CT

P. Symersky

J. Habets

P. Westers

B.A.J.M. de Mol

W.P.Th.M. Mali

M. Prokop

R.P.J. Budde

**ABSTRACT**

**OBJECTIVES** | Multidetector computed tomography (MDCT) has diagnostic value for the evaluation of prosthetic heart valve (PHV) dysfunction but it is hampered by artifacts. We hypothesized that image acquisition using prospective triggering instead of retrospective gating would reduce artifacts related to pulsating PHV.

**METHODS** | In a pulsatile in vitro model, a mono- and bileaflet PHV were imaged using 256 MDCT at 60, 75 and 90 beats per minute (BPM) with either retrospective gating (120 kV, 600 mAs, pitch 0.2,  $CTDI_{vol} = 39.8$  mGy) or prospective triggering (120 kV, 200 mAs,  $CTDI_{vol} = 13.3$  mGy). Two thresholds ( $\leq -45$ HU and  $\geq 175$ ), derived from the density of surrounding structures, were used for quantification of hyper- and hypodense artifacts. Image noise and artifacts were compared between protocols.

**RESULTS** | Prospective triggering reduced hyperdense artifacts for both valves at every BPM ( $p=0.001$  all comparisons). Hypodense artifacts were reduced for the monoleaflet valve at 60 ( $p=0.009$ ), 75 ( $p=0.016$ ) and 90 BPM ( $p=0.001$ ), and for the bileaflet valve at 60 ( $p=0.001$ ), 90 ( $p=0.001$ ) but not 75 BPM ( $p=0.6$ ). Prospective triggering reduced image noise at 60 ( $p=0.001$ ) and 75 ( $p<0.03$ ) but not at 90 BPM.

**CONCLUSIONS** | Compared with retrospective gating, prospective triggering reduced most artifacts related to pulsating PHV in vitro.



**E**lectrocardiography (ECG)-gated multislice computed tomography (MDCT) can identify the morphological substrates of prosthetic heart valve (PHV) dysfunction.<sup>1-4</sup> Echocardiography, which is the conventional method of monitoring PHV function, may not always identify the cause of dysfunction because of acoustic shadowing.<sup>4-6</sup> In regions obscured by acoustic shadowing, MDCT has been shown to identify obstructive masses, thrombus, vegetations and degenerated thickened leaflets of biological prostheses.<sup>1-4,7</sup> The identification of these causes of dysfunction may guide clinical management and may even form an indication for the surgical replacement of dysfunctional valves.<sup>1,2,4,8,9</sup>

These imaging results have been achieved mostly with 64-slice systems using retrospectively ECG-gated coronary CT angiography protocols. With retrospectively gated acquisition, the *in vitro* and *in vivo* image quality of modern mechanical PHVs was found to be generally good despite variable amounts of artifacts.<sup>1,10-12</sup> The artifacts seemed to be related to the radiopaque parts of the PHV, such as the metal alloy of the prosthetic ring and the tungsten impregnated carbon leaflets, and consisted of low attenuation (hypodense) and high attenuation (hyperdense) components.<sup>10,12</sup> Because of their resemblance to metal artifacts, probably similar causal mechanisms such as scatter, photon starvation, edge effects, beam hardening and motion may play a role.<sup>13-15</sup> Some of these interactions can be influenced by modifying acquisition parameters, other factors (such as motion) are patient-dependent. A pragmatic approach has been the use of modified coronary protocols with retrospective gating but with an increased tube current and increased tube voltage.<sup>3,7</sup> Although these reports yielded good image quality, it was at the expense of sizable radiation exposure, which may curtail the use of CT for PHV evaluation and withhold the potential advantages of the technique to all but highly selected patients. Other adaptations for enhanced PHV imaging have not been studied and no specific PHV MDCT protocols have been developed to date.

With the introduction of 256- and 320-detector systems, PHV can be imaged within one rotation using prospective ECG-triggering. Experiments with an *in vitro* model of coronary in-stent restenosis suggested that prospective triggering may be associated with improved image quality compared with retrospective gating.<sup>16</sup> In addition, prospective triggering may achieve this with a fraction of the radiation dose compared with modified coronary protocols that have been used for PHV imaging. Because PHV also appear as high density objects on CT, a similar improvement may be possible for prospectively triggered imaging of PHV. In order to test this hypothesis we compared a retrospectively gated and a prospectively triggered protocol using a 256-detector system for imaging the two most common bileaflet and tilting disc mechanical PHVs in a pulsatile *in vitro* model.

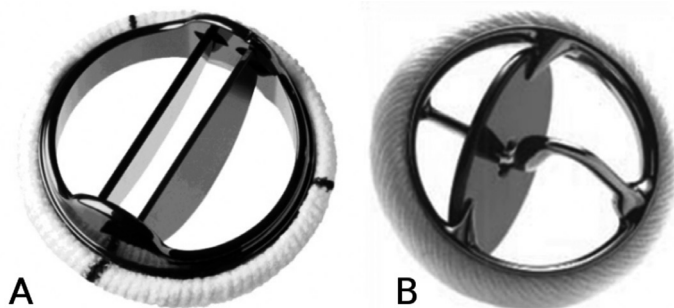


**Figure 1** | Photograph of a St Jude **A** | and Medtronic Hall aortic valve **B** | both pictured from the inflow (ventricular) side. (Images courtesy of St Jude Medical Inc., St Paul, MN, USA, and Medtronic Inc., Minneapolis, MN, USA)

## MATERIALS AND METHODS

Two mechanical PHVs, St Jude bileaflet (SJ, St Jude Medical Inc., St Paul, MN, USA, valve size 27 mm) and Medtronic Hall tilting disc (MH, Medtronic Inc., Minneapolis, MN, USA, valve size 27 mm, Figure 1), were inserted into a pulsatile *in vitro* model, which was described by Symersky et al.<sup>10</sup> In brief, the valves were mounted in a polymethylmethacrylate (PMMA) valve chamber (Figure 2) that was placed in a thoracic phantom (QRM GmbH, Möhrendorf, Germany). The valve chamber was connected to a computer controlled piston pump and to an afterload reservoir. Water was used as a perfusate. The flow pulses were set at a frequency of 60, 75 and 90 beats per minute (BPM) and produced identical pulsation cycles. The valves were opened from 30 to 50% of the artificial ECG interval generated by the computer.

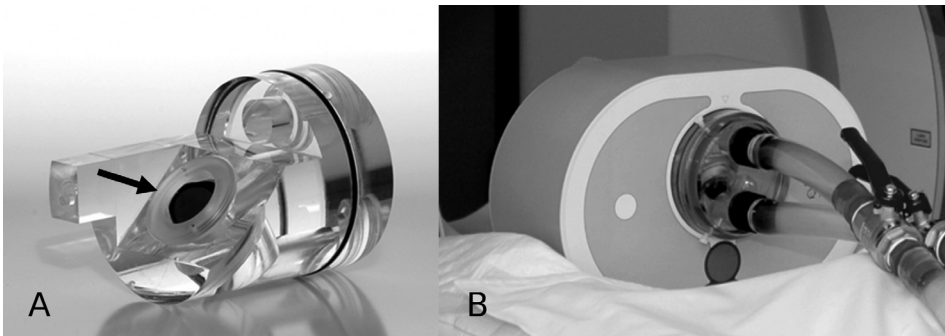


**Figure 2** | The PMMA cylindrical valve chamber in which a mechanical prosthetic valve is tightly mounted (arrow) under a 45° angle to the gantry **A** | Only leaflet motion is possible. The valve chamber is then positioned in a thoracic phantom and **B** | connected to the piston pump for leaflet motion

Imaging was performed using 256 MDCT (iCT, Philips Medical Systems, Best, the Netherlands). Two imaging protocols were used: (1) a standard helical retrospectively ECG-gated protocol based on coronary CT angiography, which has been used for PHV imaging<sup>2,3,7</sup>, and (2) a prospectively ECG-triggered protocol. CT parameters are presented in Table 1. Prospective triggering was performed with 128 x 0.625 mm collimation and axial imaging with no table movement and 8 cm exposed at the centre of the gantry. The maximal range that could be reconstructed from these data was 70 mm. No padding was used. Retrospective gating was also performed with 128 x 0.625 mm collimation at a pitch of 0.2. We chose the smallest possible anatomical range (80.1 mm), which could be covered with the use of this protocol. CT data acquisition only occurred during the 40% ECG interval (opened PHV) with prospective triggering and reconstructed with retrospective gating. Each valve was imaged 8 times using each protocol, yielding a total of 16 acquisitions per valve. Images were reconstructed at 0.9 mm thick slices with 0.45 mm reconstruction increment. These images were used for HU measurements as well as 3D volume rendering. Image acquisition with both protocols was performed at 60, 75 and 90 BPM.

All image sets were transferred to a dedicated workstation for analysis (Extended Brilliance Workstation, Philips Medical Systems, Best, the Netherlands). High- and low-density artifact volumes were quantified in 3D volume rendered images using two thresholds based on the densities of the surrounding structures according to a methodology described elsewhere for neurosurgical

**Table 1** | CT parameters

	Prospective One ECG interval	Retrospective All ECG intervals
Collimation	128 x 0.625 mm	128 x 0.625 mm
Kv	120	120
mAs	200	600
Pitch	0	0.2
Rotation time (ms)	270 ms	270 ms
Filter	Cardiac B	Cardiac B
Anatomical length (mm)	80	80.1
CTDI <sub>vol</sub> (mGy)	13.3	39.8
DLP	106.5	517.8

clips.<sup>13</sup> The PMMA in the valve chamber had a density of  $130 \pm 15$  HU, and water  $1 \pm 16$  HU (mean  $\pm$  standard deviation). We chose threshold values that were approximately 3 standard deviations (SD) above the HU of PMMA measurement and below the HU of water, respectively. The chosen thresholds were  $\geq 175$  HU for hyperdense artifacts and  $\leq -45$  HU for hypodense artifacts. Because the PHVs are composed of various radiopaque components such as a titanium ring and tungsten impregnated leaflets, which have CT densities higher than 800 HU, the  $\geq 175$ -HU threshold included the radiopaque components of the PHV.<sup>12</sup> Hence, the percentage change of the volume measured with the  $\geq 175$ HU threshold underestimates the change in actual artifacts (i.e. the volume measured with the  $\geq 175$ HU threshold without the volume of radiopaque components with densities over 800 HU).<sup>12</sup> Areas outside the valve chamber and other unrelated sources of artifacts were digitally excised in an identical manner for all images.

Image noise (defined as the SD of CT attenuation) was measured in all images using a circular region of interest (diameter 1 cm) that was placed in an identical section of the PMMA structure of the valve chamber.

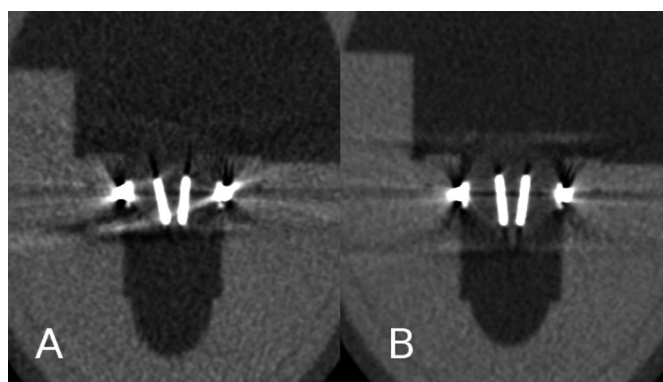


**Figure 3** | Multiplanar reformatted images of the St Jude valve in a view perpendicular to the leaflets acquired with retrospective gating **A** | and prospective triggering **B** | at 60 BPM. Note the increased deformation of the subprosthetic PMMA contours and increased hyper- and hypodense artifacts in **A** |

**Table 2 |** Artifacts measured in opened (systolic) valves

Valve	BPM	Threshold	Median artifact volume (mm <sup>3</sup> ) (interquartile range)	
			Retrospective	Prospective
St Jude	60	≤-45 HU	2056 (1939-2263)	1168 (1146-1201)
		≥175 HU	9000 (8725-10375)	7000 (6925-7150)
	75	≤-45 HU	1609 (1567-1841)	1609 (1558-1641)
		≥175 HU	8400 (7625-8775)	6900 (6700-7275)
	90	≤-45 HU	2742 (1964-2896)	1564 (1527-1589)
		≥175 HU	9700 (9100-10300)	7000 (6800-7450)
Medtronic Hall	60	≤-45 HU	2271 (1873-2630)	1571 (1474-1724)
		≥175 HU	8400 (8300-9225)	6150 (5950-6525)
	75	≤-45 HU	2192 (1788-2522)	1608 (1446-1730)
		≥175 HU	7550 (7400-8075)	5800 (5625-6075)
	90	≤-45 HU	3164 (2547-3770)	1774 (1723-1977)
		≥175 HU	8400 (7575-10000)	5950 (5725-6100)

Artifacts measured in opened (systolic) valves

**Statistical analysis**

Data were analysed using SPSS software (SPSS Statistics Version 16.0, SPSS Inc, Chicago, IL, USA). Non-parametric data were presented as medians with interquartile range (IQR). A Mann–Whitney U test was used for the comparison of artifact volumes and image noise measurements. Statistical significance was defined as  $p < 0.05$ .

**RESULTS**

The median artifact volumes for the two thresholds (≤-45 and ≥175 HU) at different frequencies are summarized in Table 2. For the St Jude valve, prospective triggering reduced hypodense artifacts (all volume ≤-45 HU) at 60 BPM ( $p=0.001$ ), 90 BPM ( $p=0.001$ ) but not 75 BPM ( $p=0.6$ ). Hyperdense artifacts (all volume ≥175 HU) were reduced with prospective triggering at 60 BPM ( $p=0.001$ ), 75 BPM ( $p=0.001$ ) and 90 BPM ( $p=0.001$ , see Figure 3). For the Medtronic Hall valve, hypodense artifacts were reduced with prospective triggering at 60 BPM ( $p=0.009$ ), 75 BPM ( $p=0.016$ ) and 90 BPM ( $p=0.001$ ). Hyperdense artifacts were also reduced at all frequencies ( $p=0.001$  for 60, 75, and 90 BPM, see Figure 4). Volume rendered images illustrate reduction of artifacts emanating from the leaflet and artifacts related to the prosthetic ring (Figure 5).

The image noise measurements are presented in Table 3. Although significant differences were found between retrospective gating and prospective triggering at 60 and 75 BPM, the image noise did not differ at 90 BPM.

**Table 3** | Image noise

Valve	BPM	Retrospective gating	Prospective triggering	
St Jude	60/min	16.0 (14.5-17.0)	11.0 (10.3-12.0)	P=0.001
	75/min	18.0 (17.0-18.8)	13.5 (12.3-14.8)	P=0.001
	90/min	14.0 (12.3-16.0)	13.0 (12.3-13.8)	P=0.198
Medtronic Hall	60/min	16.0 (14.3-17.0)	11.0 (10.3-11.8)	P=0.001
	75/min	17.5 (15.0-19.8)	14.0 (12.5-16.0)	P=0.026
	90/min	15.0 (14.3-15.8)	14.5 (13.0-15.0)	P=0.269

Image noise (median and interquartile range) for retrospective gating and prospective triggering. The *p* values result from Mann-Whitney U test.

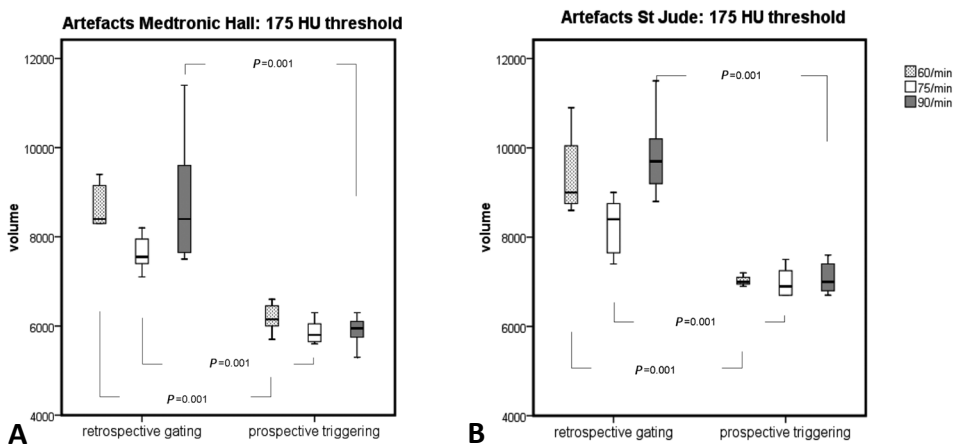


**Figure 4** | Changes in hyperdense artifacts for the Medtronic Hall PHV **A** | and St Jude PHV **B** | PHV = prosthetic heart valve

## DISCUSSION

Our findings demonstrate that axial imaging of PHVs using prospective triggering reduces artifacts with much lower radiation exposure. In our model, prospective triggering reduced artifact volumes for both valves and at all three frequencies with the exception of hypodense artifacts associated with the St Jude valve at 75 BPM.

The imaging of PHV with MDCT is hampered by artifacts that depend on valve material and valve geometry.<sup>1-3,10,12</sup> Because of the radiopaque components, these artifacts have been interpreted as metal-related artifacts and efforts to improve image quality have included the increase in tube voltage and tube current.<sup>3,7</sup> Unfortunately, this approach results in sizable dose exposure (and prohibitive exposure for serial evaluations) and therefore limits the usefulness of CT evaluation of PHV. In addition, retrospectively gated acquisition with reconstruction of 10 intervals (i.e. the full cardiac cycle) has been used to offset the variation of the PHV image quality during the cardiac cycle.<sup>2,3,7</sup> Because of the motion of the radiopaque PHV parts, which occurs due to the leaflet excursions and movement of the valve as a whole, reconstructions at each 10% of the ECG interval may generate

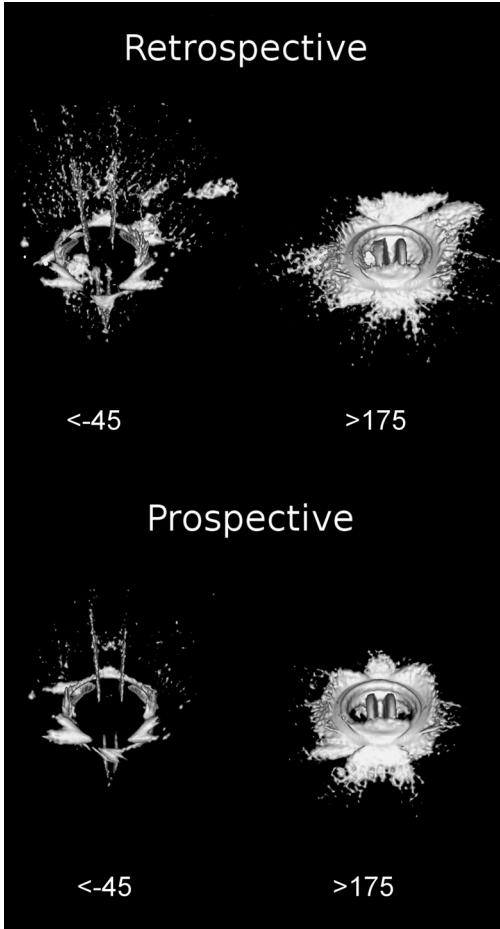


**Figure 5** | Volume rendered images of the 3D volume of a St Jude PHV at 60 BPM measured with the  $\leq -45$ -HU threshold (including all volume less than  $-45$  HU) and with the  $\geq 175$ -HU threshold (including all volume with a density higher than  $175$  HU). The upper panel images demonstrate the artifact configurations with retrospective gating and the lower panel images demonstrate the images with prospective triggering. The  $\geq 175$ -HU threshold volume includes all radiopaque parts of the valve such as the leaflets and the prosthetic ring.

only two or three image sets that are of diagnostic quality.<sup>2,11,12</sup> In vitro, rapid leaflet motion has been shown to increase hyperdense and hypodense artifacts, and rapid motion of the prosthetic ring, which has a higher density than the leaflets, may be expected to further increase artifacts.<sup>12</sup> In this study, we examined how prospective triggering and retrospective gating affected artifact behaviour and noise in PHV imaging.

In our in vitro model, we tested the effect of prospective triggering at different frequencies. Axial acquisition reduced image noise only for 60 and 75 BPM but not for 90 BPM. This may be explained by differences in the efficiency of dose used for image reconstruction. For example, axial acquisition with no padding uses the full dose (200 mAs) for image reconstruction.<sup>17</sup> With equal tube voltage setting, the retrospectively gated protocol at 600 mAs with an R-R interval of 1000 ms (frequency 60/min) and a nominal temporal resolution of 135 ms uses only approximately 80 mAs ( $=600 \text{ mAs} \times 135/1000$ ) for the reconstruction of a single ECG interval. At 75 BPM the dose efficiency increases to approximately 100 mAs. At 90 BPM, 120 mAs is used for the reconstruction of a single ECG interval which results in an image noise level comparable to axial acquisition.

Axial acquisition reduced hyperdense and hypodense artifacts except hypodense artifacts of the St Jude valve at 75 BPM. The mechanisms responsible for this reduction are not yet fully understood.

The important reduction in hyper- and hypodense artifacts for both valves at 60 and 90 BPM are in contrast to the lack of reduction of hypodense artifacts for the St Jude valve at 75 BPM. Possibly, this seems to be related to lower artifact volumes at 75 BPM with retrospective gating. Also, differences between the two valves may play a role. Earlier *in vitro* work showed that the opened tilting disc valve led to a sharper increase in hyper- and hypodense artifacts when compared to the St Jude valve.<sup>12</sup> Furthermore, the St Jude valve is composed of a nickel alloy prosthetic ring in contrast to the titanium alloy used for the Medtronic Hall. How these differences would cause a lack of reduction of hypodense artifacts at 75 BPM is not clear. Based on the differences between the two acquisition techniques one may postulate that factors associated with retrospective gating such as multisegment reconstructions and helical interpolation may play a role.<sup>14-20</sup> Although increased metal artifacts have been associated with increased noise<sup>14,15</sup>, we found a sharp reduction of hyper- and hypodense artifacts at 90 BPM for both valves despite equal image noise. This suggests that reduction of image noise may not be the primary mechanism responsible for the artifacts reduction. However, small variations in leaflet position due to a fluttering motion of the leaflets may cause image discrepancies between consecutive cardiac cycles that increase artifacts with multisegment reconstructions.<sup>17,18</sup> Furthermore, helical interpolation has been suggested as a mechanism for metal artifacts.<sup>16,18-20</sup>

Other experimental work comparing retrospective gating with prospective triggering for metal objects is scarce. Two reports using *in vitro* models of coronary in-stent restenosis found improved image quality and a reduction in artifacts.<sup>16,20</sup> Because of the discrepancy in size and composition of coronary stents, our results are not readily comparable to these reports but similar mechanisms may explain the artifact reduction.

This study has several limitations. Prospectively triggered acquisition allows reconstruction of only one pre-selected cardiac phase, and therefore does not allow dynamic imaging. We used only two mechanical prostheses. Possibly, other prostheses consisting of other metal compounds might yield different results. However, the St Jude prosthesis is the most commonly implanted prosthesis worldwide and is the most likely to be encountered clinically. We used the Medtronic Hall valve because it is the most widely implanted tilting disc valve. Both the Medtronic Hall and St Jude valves have been associated with dysfunction due to tissue ingrowth<sup>2,8,21</sup> and for both prostheses CT imaging has been shown to be of additional value for the diagnosis.<sup>2,4,8</sup> Also, we used a phantom in which the valve was fixed and only the leaflets moved. Movement of the valve as a whole may induce more artifacts. Furthermore, the use of different reconstruction filters may change the amount of PHV-induced artifacts.

Our results suggest a reduction of most PHV-related artifacts at different frequencies that appears independent of the image noise reduction with axial acquisition. Prerequisites, however, are a regular heart rate and the correct timing relative to the cardiac cycle.

## REFERENCES

1. Tsai IC, Lin YK, Chang Y, et al. Correctness of multi-detector-row computed tomography for diagnosing mechanical prosthetic heart valve disorders using operative findings as a gold standard. *Eur Radiol* 2009; 19: 857-867.
2. Symersky P, Budde RP, de Mol BA, et al. Comparison of multidetector-row computed tomography to echocardiography and fluoroscopy for evaluation of patients with mechanical prosthetic valve obstruction. *Am J Cardiol* 2009; 104:1128-1134.
3. Konen E, Goitein O, Feinberg MS, et al. The role of ECG-gated MDCT in the evaluation of aortic and mitral mechanical valves: initial experience. *Am J Roentgenol* 2008; 191:26-31.
4. Habets J, Budde RP, Symersky P, et al. Diagnostic evaluation of left-sided prosthetic heart dysfunction. *Nat Rev Cardiol* 2011; 8:466-478.
5. Girard SE, Miller FA, Orszulak TA, et al. Reoperation for prosthetic aortic valve obstruction in the era of echocardiography: trends in diagnostic testing and comparison with surgical findings. *J Am Coll Cardiol* 2001; 37:579-584.
6. Faletra F, Constantin C, De Chiara F, et al. Incorrect echocardiographic diagnosis in patients with mechanical prosthetic valve dysfunction: correlation with surgical findings. *Am J Med* 2000; 108:531-537.
7. Chenot F, Montant P, Goffinet C, et al. Evaluation of anatomic valve opening and leaflet morphology in aortic valve bioprosthesis by using multidetector CT: comparison with transthoracic echocardiography. *Radiology* 2010; 255:377-385.
8. Teshima H, Hayashida N, Fukunaga S, et al. Usefulness of a multidetector-row computed tomography scanner for detecting pannus formation. *Ann Thorac Surg* 2004; 77:523-526.
9. Toledano D, Acar, C. Usefulness of computed tomography scanning in the diagnosis of aortic prosthetic valve pannus. *J Heart Valve Dis* 2011; 19:665-668.
10. Symersky P, Budde RP, Prokop M, et al. Multidetector-row computed tomography imaging characteristics of mechanical prosthetic valves. *J Heart Valve Dis* 2011; 20:216-222.
11. Habets J, Symersky P, van Herwerden LA, et al. Prosthetic heart valve assessment with multidetector-row CT; imaging characteristics of 91 valves in 83 patients. *Eur Radiol* 2011; 21:1390-1396.
12. Symersky P, Budde RP, Westers P, et al. Multidetector CT imaging of mechanical prosthetic heart valves: quantification of artifacts with a pulsatile in-vitro model. *Eur Radiol* 2011; 21:2103-2110.
13. van der Schaaf I, van Leeuwen M, Vlassenbroek A, et al. Minimizing clip artifacts in multi CT angiography in clipped patients. *Am J Neuroradiol* 2006; 27:60-66.
14. Boas FE, Fleischmann D. Evaluation of two iterative techniques for reducing metal artifacts in computed tomography. *Radiology* 2011; 259:894-902.
15. De Man B, Nuyts J, Dupont P, et al. Metal streak artifacts in x-ray computed tomography: a simulation study. *IEEE Trans Nucl Sci* 1999; 46:691-696.
16. Horiguchi J, Fujioka C, Kiguchi M, et al. Prospective ECG-triggered axial CT at 140-kV tube voltage improves coronary in-stent restenosis at a lower radiation dose compared with conventional retrospective ECG-gated helical CT. *Eur Radiol* 2009; 19:2363-2372.
17. Prokop M. Principles of CT, Spiral CT and Multislice CT. In: Prokop M, Galanski M (eds). *Spiral and Multislice Computed Tomography of the Body*. Stuttgart, Thieme, 2003.
18. Barrett JF, Keat N. Artifacts in CT: recognition and avoidance. *Radiographics* 2004; 24:1679-1691.
19. Wilting JE, Timmer J. Artifacts in spiral-CT images and their relation to pitch and subject morphology. *Eur Radiol* 1999; 9:316-322.
20. Yang WJ, Pan ZL, Zhang H, et al. Evaluation of coronary artery in-stent restenosis with prospectively ECG-triggered axial CT angiography versus retrospective technique: a phantom study. *Radiol Med* 2011; 116:189-196.
21. Cho YH, Jeong DS, Park PW, et al. Serial changes of hemodynamic performance with Medtronic Hall valve in the aortic position. *Ann Thor Surg* 2011; 91:424-431.





CHAPTER VII

LOW-DOSE MULTIDETECTOR-ROW  
CT *of* PROSTHETIC HEART  
VALVES USING PROSPECTIVE  
TRIGGERING *and* ITERATIVE  
RECONSTRUCTION

J.Habets  
P. Symersky  
E.J. Smit  
W.P.Th.M. Mali  
R.P.J. Budde

SUBMITTED

**ABSTRACT**

**PURPOSE** | Multidetector-row computed tomography (MDCT) prosthetic heart valve (PHV) imaging is commonly performed with retrospectively ECG-gated acquisition protocols and associated with a considerable radiation exposure. The purpose of this study was to evaluate image quality of different low-dose axial (i.e. prospectively ECG-triggered MDCT) PHV acquisition protocols compared to a standard helical retrospectively ECG-gated acquisition protocol using a randomized blinded assessment method.

**METHODS** | A mechanical bileaflet PHV was inserted in a pulsatile in-vitro model and imaged on a 256-slice CT system. Eight acquisitions were performed at three different heart rates (60-75-90 beats per minute) using three different acquisition protocols: retrospectively ECG-gated (120kV, 600mAs) and prospectively ECG-triggered (120kV, 210mAs and 120kV, 100mAs) all with filtered back projection reconstruction. The low-dose axial acquisition was also reconstructed with iterative reconstruction. Image quality of systolic imaging phase reconstructions were individually evaluated by two observers using a blinded and randomized forced choice side-by-side comparison method (total 48 combinations per heart rate). Better mean image quality was defined as  $\geq 60\%$  better compared to the paired MDCT acquisition protocol with good ( $\geq 60\%$ ) inter- and intraobserver agreement.

**RESULTS** | For all heart rates, low-dose prospective acquisition with IR had superior image quality to the FBP reconstruction. Prospectively triggered acquisitions had a better image quality (75-100%) compared to retrospectively ECG-gated acquisitions with generally good to excellent inter- and intraobserver agreement at 60 and 75bpm. At 90 bpm, prospectively triggered acquisition had similar image quality as helical acquisition.

**CONCLUSIONS** | Prospectively ECG-triggered acquisition is a promising dose-lowering acquisition technique for PHVs at lower heart rates. At higher heart rates, image quality is similar for axial and helical acquisition.

**M**ultidetector-row CT (MDCT) is a promising imaging technique to evaluate patients with suspected prosthetic heart valve (PHV) dysfunction.<sup>1</sup> MDCT can have complementary diagnostic value to the standard imaging techniques, echocardiography and fluoroscopy, for PHV assessment.<sup>2-6</sup>

MDCT PHV imaging has mainly been performed with helical retrospectively ECG-gated acquisition protocols which allow dynamic PHV leaflet assessment and anatomic assessment in both systole and diastole.<sup>7</sup> Despite the good CT image quality of most PHV types, image interpretation is hampered to some degree by PHV induced artefacts.<sup>7,8</sup> Previous studies showed that CT image quality of PHV may be improved by increasing tube voltage and/or tube current.<sup>2,4</sup> However, these modifications result in an increase in radiation exposure, which is already considerable for retrospectively ECG-gated acquisition (up to 20mSv).<sup>2,4</sup> To decrease the risk of radiation exposure induced malignancies and to enable wider use of MDCT for PHV imaging, radiation reduction strategies are required. Such strategies include prospective ECG-triggered acquisition, dose modulation and the application of novel iterative reconstruction (IR) algorithms. In previous studies exploring prospective acquisitions and IR, only surrogate outcome measures (image noise and PHV-related artifact volumes) were assessed.<sup>9,10</sup>

The purpose of this study was to evaluate image quality of different low-dose MDCT PHV acquisition protocols using prospectively ECG-triggering combined with IR image reconstruction on a 256-slice scanner and compare them to standard helical retrospectively ECG-gated acquisitions using a randomized blinded assessment method.

## METHODS

### Valves

A St Jude (St Jude Medical Inc., St Paul MN, 27mm) mechanical bileaflet PHV was inserted in a pulsatile in vitro model that was described extensively in a previous publication.<sup>11</sup>

In brief, this in vitro model consists of a water filled pump-driven mock loop connected to a custom-made polymethyl methacrylate (PMMA) valve chamber via an inlet and outlet portion. The valve chamber used in this study housed a central mounting ring in which the PHV was placed under a 45-degree angle to the CT gantry to simulate the normal in vivo aortic position. The valve chamber was placed in a commercially available anthropomorphic thoracic phantom (QRM GmbH, Möhrendorf, Germany) to simulate radiation absorption and scattering from the human thorax. A computer controlled piston-pump produced 60, 75 and 90 pulses per minute and emitted an artificial ECG signal, which was used by the MDCT system for ECG-gating.

### MDCT scanner, image acquisition and reconstruction

All acquisitions were performed on a 256-slice CT system (iCT, Philips Medical Systems, Cleveland, Ohio). Four different acquisition protocols were used: (1) normal-dose retrospectively ECG-gated (120kV, 600mAs) reconstructed with filtered back projection (FBP); (2) normal-dose prospectively ECG-triggered (120kV, 210mAs) reconstructed with FBP; and low-dose prospectively ECG-triggered (120kV, 100mAs) reconstructed with (3) filtered back projection (FBP) and (4) iterative reconstruction (IR) level 4 (iDose, Philips Healthcare, Best, the Netherlands)<sup>9</sup> (Table 1). Eight acquisitions were performed for each protocol at 60, 75 and 90 pulsatile cycles per minute (Table 1). Thus, in total four image acquisition / reconstruction protocols were used yielding a total of 32 datasets (4 protocols x 8 acquisitions). The IR algorithm applies a maximum likelihood denoising algorithm based on

**Table 1** | MDCT acquisition parameters for the different acquisition protocols

	Retrospective	Prospective	Prospective low-dose	Prospective low-dose IR
Collimation (mm)	128 x 0.625	128 x 0.625	128 x 0.625	128 x 0.625
kV	120	120	120	120
mAs	600	210	100	100
Pitch	0.16-0.18*	0	0	0
Rotation time (seconds)	0.27-0.33**	0.27	0.27	0.27
Filter	Cardiac B	Cardiac B	Cardiac B	Cardiac B
CTDI <sub>vol</sub> (mGy)	38.5	13.5	6.4	6.4

IR = iterative reconstruction

\* depending on heart rate: 0.18 for heart rate <72 beats per minute (bpm) and 0.16 for >72 bpm.

\*\* = depending on heart rate: 0.33 for heart rates <62 bpm, and 0.27 for >62bpm.

Poisson statistics on the raw projection data. This may allow noise reduction without altering the characteristics and overall appearance of the initial image, and possibly may decrease streak artifacts. Total CTDI<sub>vol</sub> for each scan as displayed on the scanner console was recorded.

### Image quality analysis

Systolic (open valve) imaging phase reconstructions for each of the four different acquisition protocols (retrospective, prospective, low-dose prospective FBP and low-dose prospective IR) at each heart rate (60, 75 and 90 beats per minute) were transferred to a research workstation (iX Viewer, Image Sciences Institute, Utrecht, The Netherlands) that enabled scrolling through the interactive multiplanar reconstructions.<sup>12</sup> Reconstructions were manually aligned perpendicular to the PHV leaflets for image quality assessment. For each heart rate, we compared the images of the four different acquisition protocols in a blinded and randomized fashion. All different protocols were compared with each other in pairs (6 combinations x 8 acquisitions = 48 comparisons) for each of the three different heart rates separately. Image quality was individually assessed by two experienced observers (JH and PS). To determine, intraobserver variability, the total dataset was presented to both observers twice (after a new randomization procedure). PHV MDCT image quality scoring was based on previous described criteria and regions.<sup>7</sup> For each pair, observers were forced to determine the image with the best PHV image quality.

### Statistical analysis:

Statistical analyses were performed in Excel software (Excel 2003 SP3, Microsoft). Observer scores from the visual evaluation were expressed as mean percentage of cases in which one acquisition protocol was better or worse compared to the other PHV acquisition protocol. Better mean image quality was defined as >60% better compared to the paired MDCT acquisition protocol with good (≥60%) inter- and intraobserver agreement. Data was stratified for the three different heart rates. Inter- and intraobserver variability were determined using inter- and intraobserver agreement. Agreement was defined as poor (≤40%), moderate (40-60%), good (60-80%) and excellent (≥80%).

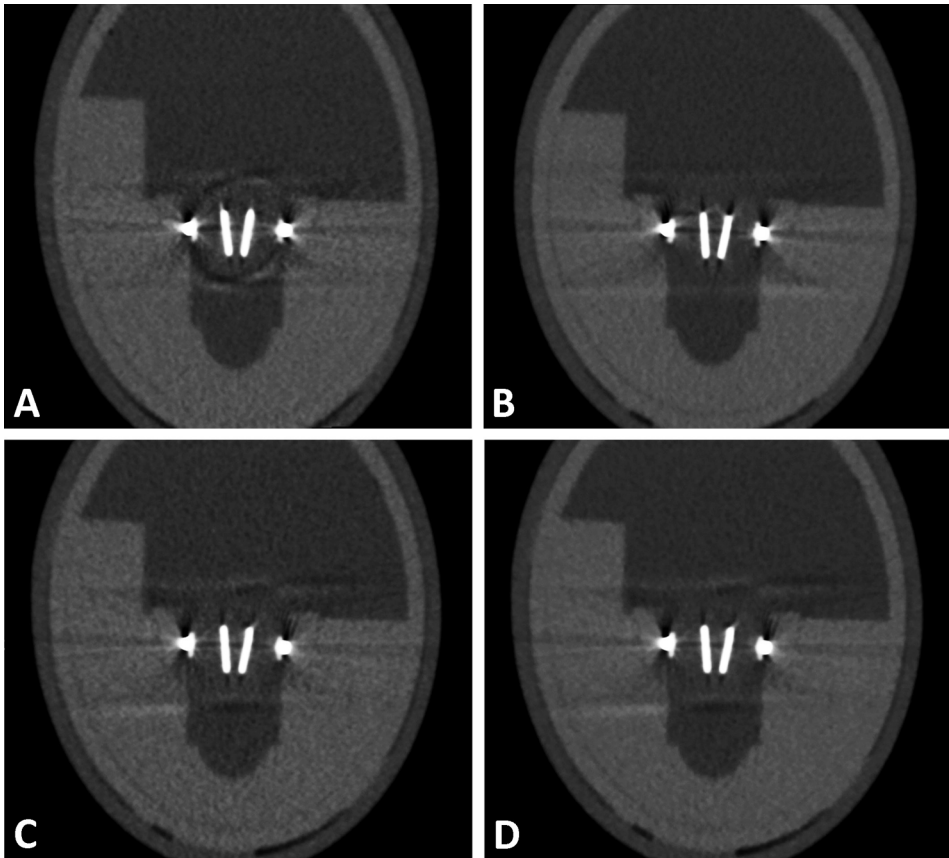


**Figure 1** | MDCT reconstruction of a St Jude PHV imaged with different acquisition/reconstruction protocols at 60bpm. **A** | retrospectively ECG-gated (120kV, 600mAs) **B** | prospectively triggered acquisition (120kV, 210mAs) **C** | low-dose prospectively triggered acquisition (120kV, 100mAs) reconstructed with FBP and **D** | low-dose prospectively triggered acquisition (120kV, 100mAs) reconstructed with IR. FBP = filtered back projection; IR = iterative reconstruction; PHV = prosthetic heart valve

## RESULTS

### Radiation dose

CTDI<sub>vol</sub> values for the different acquisition/reconstruction protocols are given in Table 1. CTDI<sub>vol</sub> values were substantially lower (65%-83%) for the axial acquisition protocols compared to the helical acquisition protocol.

### Image quality assessment

The paired comparisons of the different MDCT acquisition protocols are presented in Tables 2-4, and Figures 1-3. For all heart rates, the low-dose prospective acquisition with IR had superior image quality to low-dose prospective acquisition with FBP reconstruction.

At 60 bpm, both normal- and low-dose prospectively triggered acquisitions had a better image quality compared to retrospectively ECG-gated acquisitions with good to excellent inter- and intraobserver agreement except for the prospectively triggered low-dose acquisition which had a better

**Table 2 |** Best image quality score for the paired MDCT acquisitions protocol at 60 beats per minute

	Retrospective	Prospective	Prospective Low-dose	Prospective Low-dose IR
Retrospective better	X	22% (81%/69%)	22% (69%/56%)	16% (81%/69%)
Prospective better	78% (81%/69%)	X	63% (75%/25%)	25% (63%/50%)
Prospective low-dose better	78% (69%/56%)	37% (75%/25%)	X	12% (88%/75%)
Prospective low-dose IR better	84% (81%/69%)	75% (63%/50%)	88% (88%/75%)	X

Mean percentage better compared to paired MDCT acquisition protocol.  
 Between brackets (mean intraobserver agreement/mean interobserver agreement)  
 IR = iterative reconstruction; MDCT = multidetector-row computed tomography

**Table 3 |** Best image quality score for the paired MDCT acquisitions protocol at 75 beats per minute

	Retrospective	Prospective	Prospective Low-dose	Prospective Low-dose IR
Retrospective better	X	0% (100%/100%)	25% (75%/56%)	13% (100%/75%)
Prospective better	100% (100%/100%)	X	91% (81%/81%)	62% (63%/56%)
Prospective low-dose better	75% (75%/56%)	9% (81%/81%)	X	9% (81%/81%)
Prospective low-dose IR better	87% (100%/75%)	38% (63%/56%)	91% (81%/81%)	X

Mean percentage better compared to paired MDCT acquisition protocol.  
 Between brackets (mean intraobserver agreement/mean interobserver agreement)  
 IR = iterative reconstruction; MDCT = multidetector-row computed tomography

**Table 4 |** Best image quality score for the paired MDCT acquisitions protocol at 90 beats per minute

	Retrospective	Prospective	Prospective Low-dose	Prospective Low-dose IR
Retrospective better	X	53% (56%/56%)	53% (56%/38%)	44% (63%/56%)
Prospective better	47% (56%/56%)	X	50% (88%/63%)	41% (56%/63%)
Prospective low-dose better	47% (56%/38%)	50% (88%/63%)	X	12% (88%/75%)
Prospective low-dose IR better	56% (63%/56%)	59% (56%/63%)	88% (88%/75%)	X

Mean percentage better compared to paired MDCT acquisition protocol.  
 Between brackets (mean intraobserver agreement/mean interobserver agreement)  
 IR = iterative reconstruction; MDCT = multidetector-row computed tomography

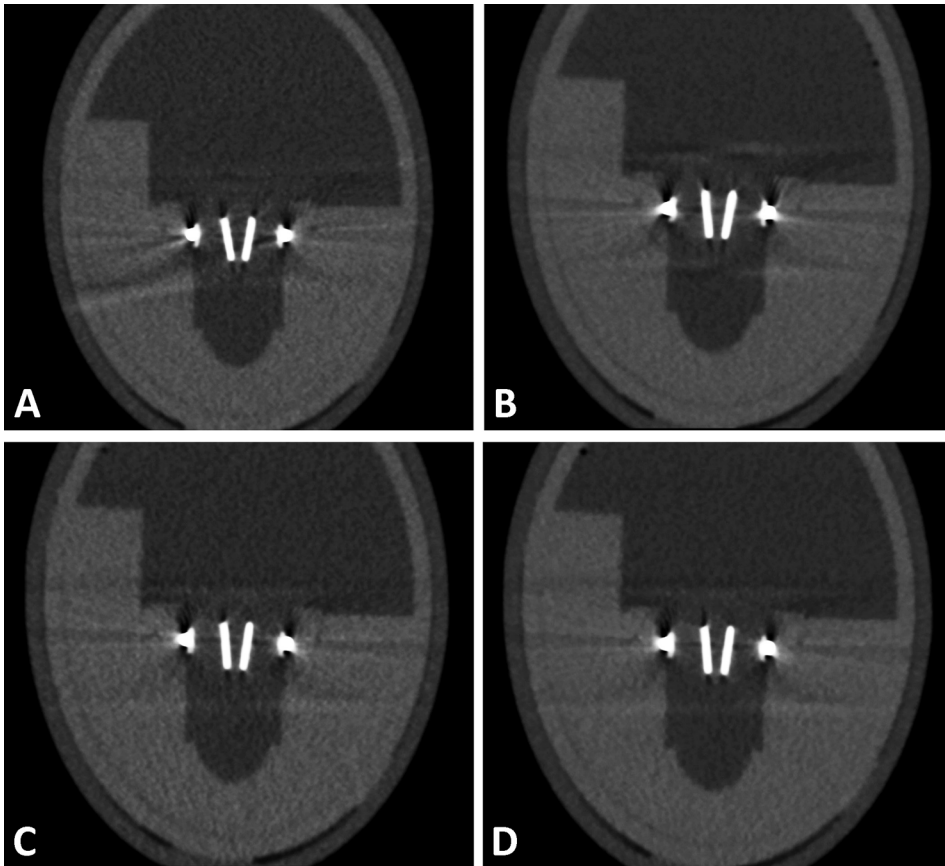


**Figure 2** | MDCT reconstruction of a St Jude PHV imaged with different acquisition/reconstruction protocols at 75bpm **A** | retroactively ECG-gated (120kV, 600mAs) **B** | prospectively triggered acquisition (120kV, 210mAs) **C** | low-dose prospectively triggered acquisition (120kV, 100mAs) reconstructed with FBP and **D** | low-dose prospectively triggered acquisition (120kV, 100mAs) reconstructed with IR.  
 FBP = filtered back projection; IR = iterative reconstruction; PHV = prosthetic heart valve

mean image quality (78%) compared to retroactively ECG-gated acquisition with good intra-observer agreement but moderate inter-observer agreement (Table 2). At 60 bpm, the normal dose prospectively triggered acquisition was better than the low-dose prospectively triggered acquisition with good intraobserver agreement but poor interobserver agreement. Overall, at 60 bpm low-dose prospectively triggered acquisition reconstructed with IR had the best image quality.

At 75 bpm, prospectively triggered acquisitions had a better image quality compared to retroactively ECG-gated acquisitions with good to excellent inter- and intraobserver agreement except for moderate interobserver agreement (low-dose prospectively triggered reconstructed with FBP vs. retroactively ECG-gated). Overall, at 75 bpm normal-dose prospectively triggered acquisition (120kV, 210mAs) had the best image image quality.

At 90 bpm, prospectively triggered and retroactively ECG-gated acquisitions had a similar image quality (44-56%) with moderate inter- and intraobserver agreement.

Within the prospectively triggered acquisition group, normal-dose prospectively triggered acquisition had a similar image quality (41-59%) compared with low-dose prospectively triggered acquisition (both with FBP and IR ) with moderate to excellent inter- and intraobserver agreement.

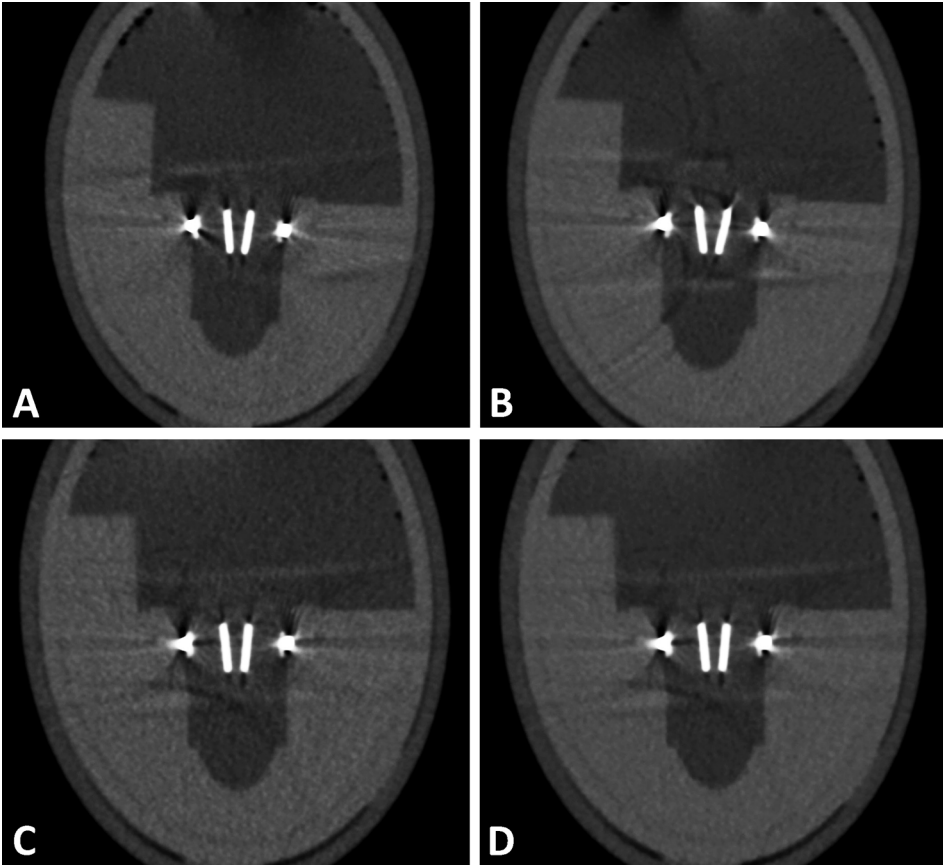


**Figure 3** | MDCT reconstruction of a St Jude PHV imaged with different acquisition/reconstruction protocols at 90bpm. **A** | retrospectively ECG-gated (120kV, 600mAs) **B** | prospectively triggered acquisition (120kV, 210mAs) **C** | low-dose prospectively triggered acquisition (120kV, 100mAs) reconstructed with FBP and **D** | low-dose prospectively triggered acquisition (120kV, 100mAs) reconstructed with IR.

FBP = filtered back projection; IR = iterative reconstruction; PHV = prosthetic heart valves

## DISCUSSION

The principal findings of this study are: (1) axial imaging of PHVs using prospectively triggered acquisition had a better image quality than retrospectively ECG-gated helical acquisitions at both 60 and 75 bpm using a randomized blinded assessment method; (2) at a higher heart rate of 90 BPM, image quality was similar for prospectively triggered and retrospectively ECG-gated acquisition protocols; and (3) low-dose prospectively ECG-triggered acquisition with IR reconstruction was superior to FBP image reconstruction at all heart rates.

Previous work demonstrated that prospective triggering and iterative reconstruction may be useful for radiation dose reduction in PHV imaging.<sup>9,10</sup> In an *in vitro* set-up, prospectively triggered acquisition allows for PHV imaging with reduced PHV-related artifact volumes and image noise levels at different heart rates.<sup>10</sup> However, this study did not show an image noise reduction at 90 beats per minute. This may be explained by multisegment reconstruction and helical interpolation used in retrospectively ECG-gated image acquisition.<sup>13</sup> Iterative reconstruction enables PHV imaging with a



50% dose reduction (120kV, 300mAs) compared to a standard dose (120 kV, 600 mAs) reconstructed with standard FBP without an increase in image noise or PHV-related artifacts.<sup>9</sup> An important limitation of these studies is that they only evaluated PHV-related artifacts and image noise levels but image quality was not assessed.

This study demonstrated that prospectively triggered acquisition resulted in superior image quality compared to retrospectively ECG-gated helical acquisitions at 60 and 75 BPM. As discussed in previous work<sup>10</sup>, dose efficiency may play a role. At 60 and 75 BPM, a retrospectively ECG-gated acquisition protocol (120kV, 600mAs) with an R-R-interval of 810 ms at 75bpm and 1000ms at 60bpm and a nominal temporal resolution of 135ms uses only approximately 80mAs at 60 bpm and 100mAs at 75 bpm (= 600mAs x 135/1000ms or 810ms) for reconstruction of a single ECG interval.<sup>10</sup> This dose is substantially lower than 210mAs which is used during the prospectively acquisition (120kV, 210mAs) for reconstruction of a single ECG interval (no padding was used in this study). This difference in dose efficiency may explain the superior image quality of prospectively triggered acquisitions at these heart frequencies. However, low-dose prospectively triggered acquisition (120kV, 100mAs) has the same effective dose at 75 bpm as retrospectively ECG-gated acquisition but still demonstrated a substantial better image quality than the retrospectively ECG-gated acquisition (Table 2). Therefore, other mechanisms that influence MDCT image quality of PHVs are likely to play a role (e.g. helical interpolation and multisegment reconstruction). Further prospective studies are required to unravel the individual effect of these parameters on MDCT image quality of PHVs. Another interesting finding is that low-dose prospectively triggered acquisition (120kV, 100mAs) reconstructed with IR had best image quality at 60bpm. The iterative reconstruction reduces image noise by way of the denoising algorithm which may explain the better MDCT image quality than the low-dose prospectively triggered acquisition reconstructed with standard FBP at the different heart rates (60-75-90bpm).

Image quality was similar for the different acquisition protocols at 90 beats per minute. At 90 beats per minute (RR interval 675ms), approximately 120mAs was used for the image reconstruction of one ECG-interval in helical acquisitions (120kV, 600mAs) and the image quality for these acquisitions is comparable to prospectively acquisitions with 120kV 210mAs and 120kV 100mAs. This finding implies that other factors than effective dose influences MDCT image quality at these higher heart rates.

Our findings provide an experimental basis for the development of clinical low-dose acquisition protocols for PHV evaluation. However, we did find that a low heart rate was imperative for low-dose prospectively triggered acquisition. At higher heart rates, image quality of prospectively triggered acquisition was similar to retrospectively ECG-gated acquisitions. In patients without contraindications,  $\beta$ -blocker administration to reduce the heart rate will allow for prospectively triggered axial PHV imaging with a substantial radiation dose reduction to the standard helical acquisitions. Further clinical studies to validate these low-dose MDCT acquisitions protocols are needed.

### Limitations

This study has several limitations. First, dynamic PHV imaging using prospectively triggered acquisition is not possible because it only allows imaging at one predefined cardiac reconstruction phase with minimal padding (5%) on the scanner used in this study. Other wide detector scanners that allow zero pitch prospectively ECG-triggered axial imaging with wider padding may allow systolic and diastolic phase MDCT imaging acquisition during one contrast administration. Second, we imaged only one mechanical PHV. The St Jude PHV was chosen because it is the most commonly implanted

mechanical PHV worldwide. Whether the findings of the current study can be extrapolated to other PHV types remains to be established. However, an earlier study found reduction of PHV-related artifacts for both a tilting disc valve and a bileaflet valve.<sup>10</sup> Third, in this in vitro setup only leaflet motion was possible. The absent cardiac and annular movement may influence MDCT image quality in patients. However, the different acquisition protocols were compared in a randomized blinded fashion and the influence of cardiac and annular movement may influence all MDCT acquisition protocols in a similar way. Fourth, we only imaged three regular heart frequencies. In patients with rhythm disturbances, errors in ECG-gating or triggering may result in decreased MDCT image quality, and may not be suitable for prospectively triggered image acquisition.

## CONCLUSION

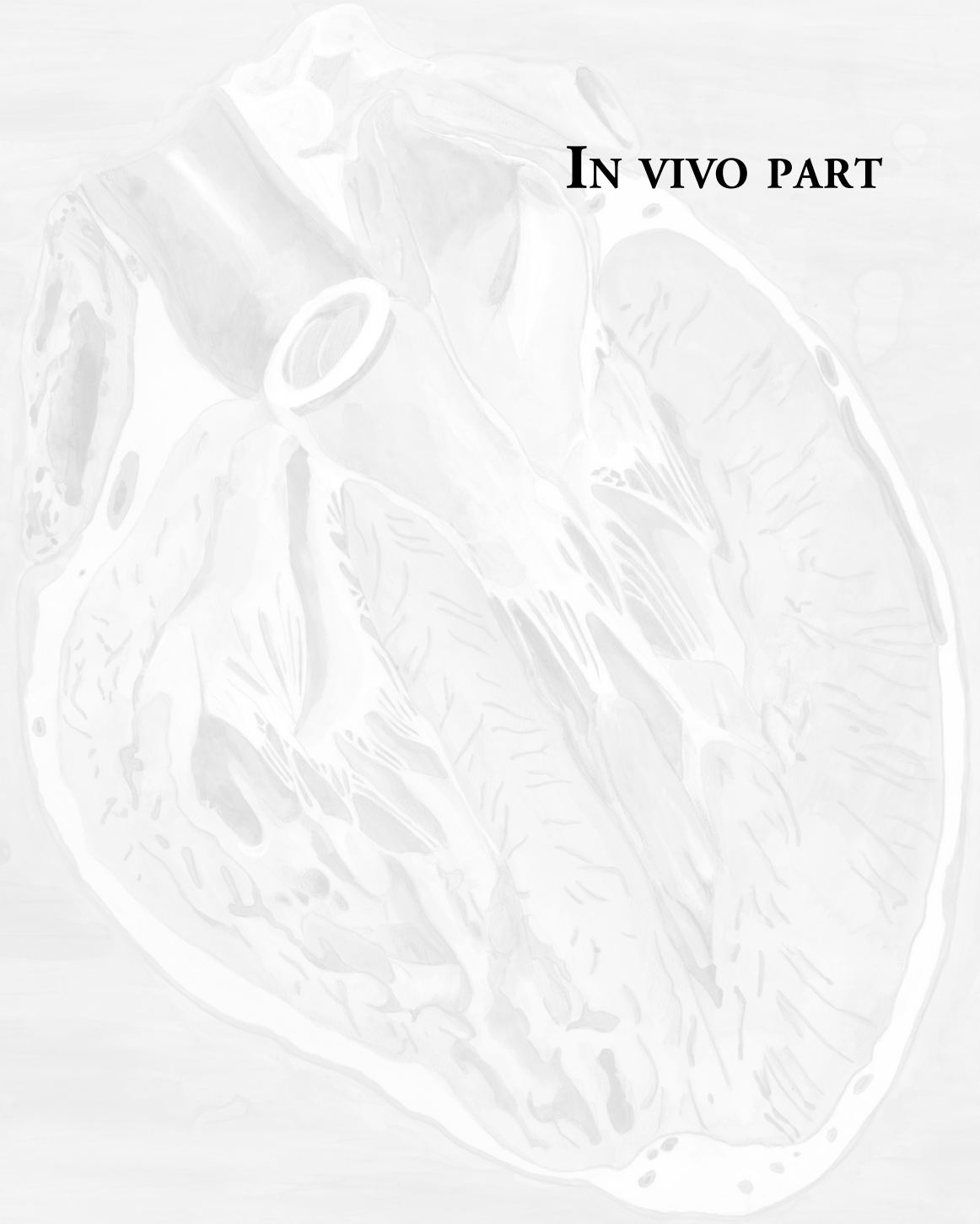
Axial PHV imaging using prospectively ECG-triggered acquisition provided better image quality than retrospectively ECG-gated helical acquisition at lower heart rates ( $\leq 75$  bpm). At higher heart rates (90 bpm), prospectively triggered acquisition had a similar image quality to retrospectively ECG-gated acquisition but at a lower radiation dose. Using IR reconstruction techniques was beneficial at all heart rates. Heart rate lowering strategies and IR reconstruction techniques are recommended to enable low-dose prospectively triggered acquisition for CT imaging of PHV with superior image quality.

## REFERENCES

1. Habets J, Budde RP, Symersky P, et al. Diagnostic evaluation of left-sided prosthetic heart valve dysfunction. *Nat Rev Cardiol* 2011; 8:466-478.
2. Chenot F, Montant P, Goffinet C, et al. Evaluation of anatomic valve opening and leaflet morphology in aortic valve bioprosthesis by using multidetector CT: comparison with transthoracic echocardiography. *Radiology* 2010; 255:377-385.
3. Feuchtner GM, Stolzmann P, Dichtl W, et al. Multislice computed tomography in infective endocarditis: comparison with transesophageal echocardiography and intraoperative findings. *J Am Coll Cardiol* 2009; 53:436-444.
4. Konen E, Goitein O, Feinberg MS, et al. The role of ECG-gated MDCT in the evaluation of aortic and mitral mechanical valves: initial experience. *Am J Roentgenol* 2008; 191:26-31.
5. Symersky P, Budde RP, de Mol BA, et al. Comparison of multidetector-row computed tomography to echocardiography and fluoroscopy for evaluation of patients with mechanical prosthetic valve obstruction. *Am J Cardiol* 2009; 104:1128-1134.
6. Tsai IC, Lin YK, Chang Y, et al. Correctness of multi-detector-row computed tomography for diagnosing mechanical prosthetic heart valve disorders using operative findings as a gold standard. *Eur Radiol* 2009; 19:857-867.
7. Habets J, Symersky P, van Herwerden LA, et al. Prosthetic heart valve assessment with multidetector-row CT: imaging characteristics of 91 valves in 83 patients. *Eur Radiol*. 2011; 21:1390-1396.
8. Symersky P, Budde RP, Westers P, et al. Multidetector CT imaging of mechanical prosthetic heart valves: quantification of artifacts with a pulsatile in-vitro model. *Eur Radiol* 2011; 21:2103-2110.
9. Habets J, Symersky P, de Mol BA, et al. A novel iterative reconstruction algorithm allows reduced dose multidetector-row CT imaging of mechanical prosthetic heart valves. *Int J Cardiovasc Imaging* 2011; DOI: 10.1007/s10554-011-9954-7.
10. Symersky P, Habets J, Westers P, et al. Prospective ECG triggering reduces prosthetic heart valve-induced artefacts compared with retrospective ECG gating on 256-slice CT. *Eur Radiol* 2011; DOI: 10.1007/s00330-011-2358-1.
11. Symersky P, Budde RPJ, Prokop M, et al. Multidetector-row computed tomography imaging characteristics of mechanical prosthetic valves. *J Heart Valve Dis*. 2011; 20:216-222.
12. Smit EJ, Vonken EJ, van der Schaaf IC, et al. Timing-Invariant Reconstruction for Deriving High-Quality CT Angiographic Data from Cerebral CT Perfusion Data. *Radiology* 2012; 263:216-225.
13. Prokop M. Radiation Dose and Image Quality. In: Prokop M, Galanski M (eds). *Spiral and Multislice Computed Tomography of the Body*. Stuttgart, Thieme, 2003.



**IN VIVO PART**







CHAPTER VIII

MULTISLICE CT ANGIOGRAPHY  
*of* PROSTHETIC HEART VALVES:  
NORMAL *and* DYSFUNCTIONAL  
PROSTHETIC HEART VALVE  
IMAGING CHARACTERISTICS

J.Habets  
W.P.Th.M. Mali  
R.P.J. Budde

**ABSTRACT**

In daily clinical routine, echocardiography and fluoroscopy are the imaging modalities for the diagnostic evaluation of patients with suspected prosthetic heart valves (PHV) dysfunction. These imaging modalities may fail to detect the exact cause of PHV dysfunction. Multislice CT angiography is a promising additional imaging technique to evaluate PHV dysfunction and has complementary diagnostic value in patients with suspected PHV obstruction and endocarditis. Furthermore, retrospectively ECG-gated CT angiography can have additional value for preoperative surgical planning: simultaneous assessment of coronary arteries and bypass grafts, right ventricle-sternum relationship and proximal aortic dimensions. Contrary to echocardiography, multislice CT angiography is associated with radiation exposure and the administration of potential nephrotoxic iodinated contrast agent. In this paper, we will discuss practical aspects of multislice CT angiography of prosthetic heart valves including setting the correct indication for CT imaging, considerations for optimal image acquisition, image reconstruction and interpretation, structured reporting and communication of findings with the cardiologists and cardiothoracic surgeons.



Prosthetic heart valves are commonly implanted to replace diseased native valves. In 2003, 290,000 patients underwent prosthetic heart valve (PHV) implantation worldwide.<sup>1</sup> During surgery, the diseased native valve is excised and replaced by a PHV. There are two main groups of PHVs: biological and mechanical PHVs. Biological PHVs consist of bovine or pericardial tissue often supported by a frame. Mechanical PHVs consist of metal alloy and/or carbon components. Biological PHVs require no anticoagulation but are prone to wear whereas mechanical PHVs are designed to last decades but require lifelong anticoagulation. In contrast to mechanical PHVs, biological PHVs degenerate within 10-20 years due to degeneration of the valve leaflets.<sup>2</sup> To detect this degeneration, routine transthoracic echocardiography 5 years after implantation is recommended according to the American Heart Association and European Society of Cardiology guidelines.<sup>3,4</sup> The PHV type that is implanted depends on patient characteristics and surgeon preferences.

Mechanical PHV dysfunction is a rare but potentially life-threatening disease with a wide reported incidence between 0.01-6.0%.<sup>5-9</sup> Patients with suspected PHV dysfunction normally present on the outpatient clinic or emergency room. The cardiologist starts with transthoracic echocardiography (TTE) as the first line screening tool for PHV dysfunction. Although TTE is a widely available, non-invasive and fast screening tool for PHV dysfunction, it often detects the effects of PHV dysfunction (i.e. increased pressure gradient over the PHV in patients with suspected PHV obstruction) but often fails to determine its exact cause and more imaging is required. In daily clinical practice, TTE is therefore often followed by transesophageal echocardiography (TEE) and fluoroscopy (in patients with mechanical PHVs). TEE can have additional diagnostic value compared to TTE especially in patients with mitral PHVs. Fluoroscopy provides information on the opening and closing angles of mechanical PHV leaflets only. Even with the findings of TTE, TEE and fluoroscopy combined, the diagnostic workup can be inconclusive and diagnostic dilemmas may arise.

ECG-gated or triggered multislice CT angiography can have additional diagnostic value to the clinical routine workup in the evaluation of patients with suspected PHV dysfunction, especially in patients with PHV obstruction and/or PHV endocarditis.<sup>2</sup> Besides this diagnostic information, CT angiography can also provide relevant preoperative anatomical information such as the presence of coronary artery disease, the patency of bypass grafts, and the right ventricle-sternum distance. In this paper, we will discuss practical aspects of multislice CT angiography imaging of PHVs including setting the correct indication for CT imaging, considerations for optimal image acquisition, image reconstruction and interpretation, structured reporting as well as communication of imaging findings with the cardiologists and cardiothoracic surgeons.

## PATIENT SELECTION AND TECHNICAL ASPECTS

### *Surgical technique*

In patients selected for PHV implantation, the diseased valve is excised after exposition, and the annular tissue is carefully decalcified. After selection of the appropriate PHV size, the PHV is fixated in place by passing approximately 12-20 sutures through the suture ring of the PHV and the annulus (Figure 1). Polytetrafluorethylene (PTFE) pledgets attached to the sutures are commonly used to disperse the pressure of the sutures on the annulus and present as hyperdense structures on CT images (Figure 1).<sup>10</sup>

### *PHV types*

The two main PHV types are mechanical and biological PHVs. In the mechanical PHV group, two

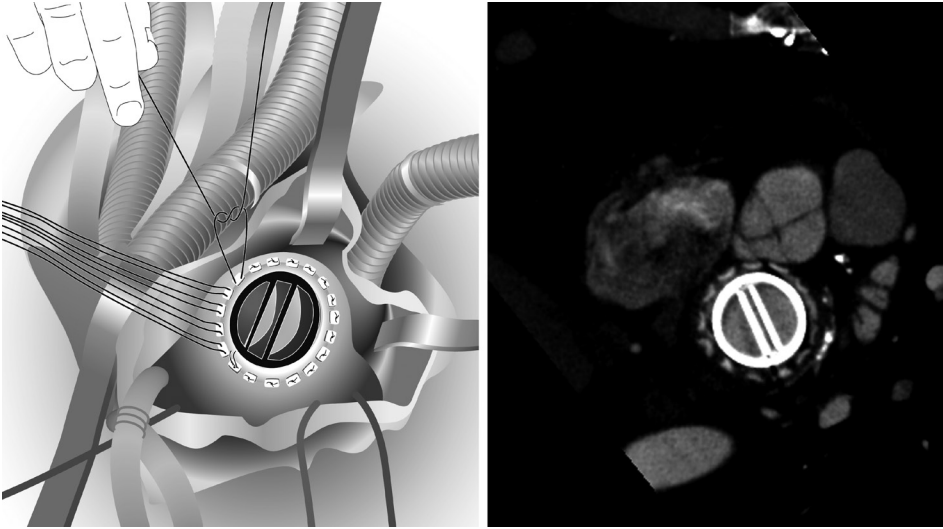


**Figure 1** | The left image panel illustrates the implantation of a mitral prosthetic heart valve (PHV) with PTFE pledgets sutures. Each knot of a single suture is tied individually. The pledgets are visible as hyperdense structures on CT images (right image panel).

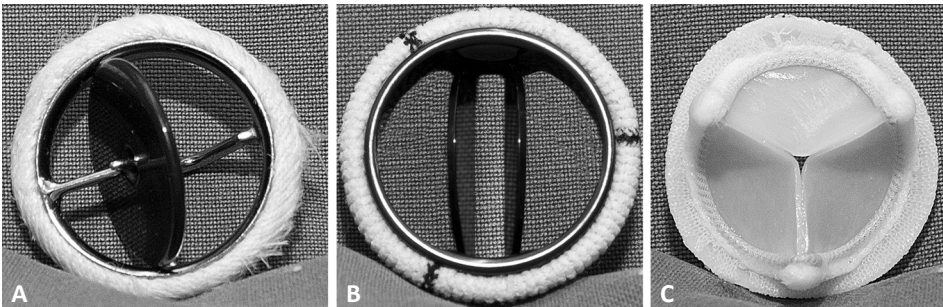


**Figure 2** | Photographs of different prosthetic heart valves: **A** | Medtronic Hall tilting disc with one leaflet **B** | St Jude bileaflet with two leaflets **C** | Perimount biological valve with three leaflets.

different types are distinguished: bileaflet and tilting-disc PHVs (Figure 2). The PHV composition is different for each PHV type and has important implications for CT image quality.<sup>11-13</sup> The mechanical valve leaflets have specific opening and closing angles which are unique for each PHV type. PHV are available in different sizes (e.g. size 19, size 21, size 23 etc.), and the implanted size depends on the annular size. The size is not equal to the diameter in millimeters. Characteristics of different PHVs including PHV type, PHV composition, CT visibility, and normal opening and closing angles are presented in Table 1.

### ***Patient selection***

Patients with suspected PHV dysfunction present on the outpatient clinic, emergency room or ward. Patients can present with widely varying complaints such as complaints of heart failure (dyspnea, edema), fever, new murmur, dizziness during exercise, angina pectoris or aspecific complaints (e.g. palsy in patient with stroke and a cardiac embolus). Important echocardiographic parameters are:

**Table 1** | Different PHV types and CT friendliness (modified from Habets et al.<sup>2</sup>)

PHV manufacturer	Type	PHV metal contents	Opening angles (degrees)	Closing angles (degrees)	CT visibility
ATS Open Pivot® (Medtronic ATS Medical, Minneapolis, MN, USA)	Mechanical Bileaflet	Titanium alloy ring	AVR: 85	AVR: 25	Unknown
Carbomedics® (Sorin Group USA Inc., Arvada, CO, USA)	Mechanical Bileaflet	Titanium alloy ring	AVR/MVR: 78	AVR/MVR: 25	++
Duromedics (Baxter Healthcare Corp, Santa Ana, CA, USA)	Mechanical Bileaflet	Cobalt-chrome alloy ring	AVR: 78 MVR: 73	AVR: 20 MVR: 20	-
St Jude Medical (St Jude Medical, St Paul, MN, USA)	Mechanical Bileaflet	Nickel alloy ring	AVR/MVR: 85	AVR/ MVR: 30 (19-25mm) 25 (27-31mm)	+
ON-X® (ON-X Life Technologies Inc., Austin, TX, USA)	Mechanical Bileaflet	Titanium Alloy ring	AVR/MVR: 90	AVR/MVR: 40	++
Sorin® Bicarbon (Sorin Biomedica Cardio, Milan, Italy)	Mechanical Bileaflet	Titanium alloy ring	AVR/MVR: 80	AVR/MVR: 20	++
Björk-Shiley (Shiley Inc, Irvine, CA, USA)	Mechanical Tilting disc	Cobalt-chrome Alloy	AVR/MVR: 60-70*	AVR/MVR: 0	-
Medtronic® Hall (Medtronic, Minneapolis, MN, USA)	Mechanical Tilting disc	Titanium Alloy ring	AVR/MVR: 75	AVR/MVR: 0	++
Omniscience (Medical Inc, St Paul, MN, USA)	Mechanical Tilting disc	Titanium alloy ring	AVR: 60	AVR: 0	Unknown
Sorin® Allcarbon (Sorin Biomedica Cardio, Milan, Italy)	Mechanical Tilting disc	Cobalt-chrome Alloy	AVR/MVR: 60	AVR/MVR: 0	-
Biocor® stentless (St Jude Medical, St Paul, MN, USA)	Biological	-	NA	NA	Unknown
Extended Biocor® (St Jude Medical, St Paul, MN, USA)	Biological	Stainless steel wire	NA	NA	Unknown
Bioflow pericardial (Biomedical, Glasgow, UK)	Biological	Unknown	NA	NA	Unknown
Carpentier Edwards® bovine (Edwards Lifesciences, Irvine, CA, USA)	Biological	Elgiloy	NA	NA	++
Carpentier-Edwards® pericardial (Edwards Lifesciences, Irvine, CA, USA)	Biological	Elgiloy	NA	NA	++
Hancock® I (Medtronic, Minneapolis, MN, USA)	Biological	Stellite band around the polypropylene stent	NA	NA	Unknown
Hancock® II (Medtronic, Minneapolis, MN, USA)	Biological	Small Haynes alloy rings in each stent post tip	NA	NA	Unknown
Ionescu-Shiley (Shiley inc, Irvine, CA, USA)	Biological	Titanium frame covered with Dacron	NA	NA	Unknown
Medtronic® Freestyle (Medtronic, Minneapolis, MN, USA)	Biological	-	NA	NA	++
Medtronic® Intact (Medtronic, Minneapolis, MN, USA)	Biological	-	NA	NA	++
Medtronic® Mosaic (Medtronic, Minneapolis, MN, USA)	Biological	Small Haynes alloy rings in each stent post tip and Haynes alloy band around the outside of the stent	NA	NA	++
Mitroflow® (Mitroflow, Sorin Group, Canada, Burnaby, Canada)	Biological	-	NA	NA	++

\* 60 degrees manufactured before 1981 and after 1981 70 degrees.  
AVR = Aortic valve replacement; MVR = Mitral valve replacement; NA = not applicable

**Table 2** | CT acquisition parameters for PHV imaging

CT acquisition parameters	Non-contrast enhanced CT	Retrospectively ECG-gated CTA 64 slice	Retrospectively ECG-gated CTA 256 slice
Slice thickness	0.9	0.9	0.9
Increment	0.45	0.45	0.45
kV	120	120	120
mAs	30	500-700*	600-700**
Collimation	128x0.625	64x0.625	128x0.625
Pitch	-	0.20	0.16-0.18***
Rotation time	0.27	0.42	0.27-0.33****
FOV	250	250	250
Filter	Cardiac B	Cardiac B	Cardiac B
Matrix	512x512	512x512	512x512
Reconstruction algorithm	FBP	FBP	FBP
Reconstruction phases	75%	10 phases (equally spaced)	10 phases (equally spaced)

\* <60kg = 500mAs, 65-80kg = 600mAs, >80kg = 700mAs

\*\* 65-80kg = 600mAs, >80kg = 700mAs

\*\*\* Heart rate < 72 beats per minute = 0.18, heart rate >72 beats per minute = 0.16

\*\*\*\* Heart rate <62 beats per minute = 0.33, heart rate > 62 beats per minute = 0.27

the mean and peak pressure gradients over the PHV, prosthetic orifice area, and the evaluation of regurgitation pattern. A detailed description of the echocardiographic assessment of PHVs is beyond the scope of this article. For the interested reader, Zoghbi et al. provide an excellent overview on PHV assessment by echocardiography.<sup>14</sup> PHV obstruction presents with an increased pressure gradient and decreased prosthetic orifice area. Fluoroscopy can demonstrate leaflet restriction in patients with PHV obstruction. All mechanical PHVs have a physiological regurgitant jet that is necessary to close the valve. After routine evaluation with echocardiography and fluoroscopy, cardiologists and cardiothoracic surgeons may request for additional CT evaluation. In the appropriate selection of patients for multislice CT angiography PHV imaging, several factors are important. First, of course the usual contraindications for multislice CT angiography (i.e. contrast allergy, renal failure and pregnancy) apply. However, these contraindications are not absolute and CT can be reconsidered if it is likely that CT will provide crucial information that can not be obtained otherwise and/or is likely to change patient management significantly. Second, it is important to check which PHV type is implanted as PHV composition influences the CT image quality. The CT visibility of different PHV types is presented in Table 1. Most PHVs have a good image CT quality but PHVs containing cobalt-chrome alloy rings (Björk-Shiley and Sorin tilting disc PHVs) cause severe PHV-related

artifacts which prohibit diagnostic assessment. These cobalt-chrome PHVs are not suitable for CT evaluation.<sup>11,15</sup> Third, pacemaker leads may interfere with diagnostic assessment of PHVs and also hamper assessment of other cardiac structures especially coronary arteries. However, in most patients with cardiac pacemakers diagnostic assessment of PHVs is possible.

Besides these practical issues, it is important to know the indications for CT assessment. In patients with suspected PHV obstruction and endocarditis, multislice CT angiography can have additional diagnostic value by determining the exact cause of PHV dysfunction and/or visualizing the exact extent of the disease. In patients with primarily regurgitation, multislice CT angiography may have little additional value besides assessing the location of the leak in selected patients because of the lack of functional information. However, in patients with suspected PHV endocarditis and regurgitation due to (suspected) mycotic aneurysms CT definitely has additional value by depicting 3D anatomy. Furthermore, multislice CT angiography may depict the regurgitation area that can be valuable information for surgical planning.

### ***Image acquisition***

In general, patients with PHV dysfunction are different from patients who undergo CT angiography for coronary assessment. They often have impaired left and/or right ventricular function, arrhythmia and altered thoracic anatomy (previous sternotomy, adhesions). For coronary CT angiography, prospectively triggered volume scanning is preferred to reduce radiation dose and one diagnostic diastolic imaging phase is often enough for adequate coronary assessment. In patients with suspected PHV dysfunction, information on the anatomy of the valve and the periprosthetic region has to be obtained both in the systolic and diastolic phase. Furthermore, dynamic information on the opening and closing of the valve leaflets is required, especially in mechanical PHVs. Therefore, retrospectively ECG-gated image acquisition is preferred. Retrospectively ECG-gated image acquisition is associated with a higher radiation dose than prospectively triggered scanning. However, the risk of reoperation to replace a dysfunctional PHV is high and overall mortality after aortic PHV reoperation varies between 3.8-15.3% depending on the cause of PHV dysfunction.<sup>16,17</sup> Patients with congenital valve abnormalities are a relatively young patient group. Especially in this group, dose reduction methods such as dose modulation, prospective triggering and iterative reconstruction are evaluated to reduce radiation dose.<sup>18,19</sup>

A  $\geq 64$ -slice CT system is required for optimal imaging. Our 64- and 256-slice MDCT scan protocol is based on retrospectively gated coronary CT angiography protocols (Table 2), and imaging volume is planned on a standard survey (80kV, 20mAs). The PHV may be difficult to detect on the survey images. Using previous chest X-rays may help to identify the PHV using its relationship with the sternal wires as a reference. For PHV imaging, it is important to evaluate the complete heart including the ascending aorta. A non-contrast enhanced scan of the PHV only can be added to help differentiate PTFE pledgets (suture material commonly used during PHV implantation) from paravalvular leakage, and assess calcifications (Table 2). For the contrast-enhanced scan, we plan the scan from 2cm above the carina (including ascending aorta) to the bottom of the heart to obtain complete imaging of the heart. The scan range can be reduced in the cranio-caudal direction to reduce radiation exposure if desired.

In cardiac CT angiography imaging, a low heart frequency is preferable because of better image quality. Unfortunately, patients with PHV dysfunction may have contraindications for  $\beta$ -blockers (rhythm disorders in the postoperative phase, or impaired left ventricular (LV) function). It is advisable to consult the cardiologist before  $\beta$ -blockers are administered. In our institution, 5-20mg metoprolol is administered intravenously with a target heart rate of 60 beats per minute in the absence of contraindications for  $\beta$ -blockers. When the referring clinician also requests diagnostic information



**Figure 3** | CT reconstruction of prosthetic heart valves: **A** | in plane; **B** | parallel to valve leaflets; and perpendicular to valve leaflets **C** |

on the coronary arteries, it is advisable to administer nitroglycerin (in absence of contraindications such as aortic valve stenosis and impaired LV function) to dilate the coronary arteries for optimal image quality.

We use a triphasic contrast administration protocols to reach optimal contrast enhancement in the left ventricle and atrium. In our institution, a locator is placed in the descending aorta. When the threshold of 100 HU is reached, scan acquisition starts after an added post-threshold delay of 8 seconds. A triphasic contrast administration (300mg jopromide/ml) is performed with a mean flow rate of 5.0-6.0cc/sec. Contrast volume is dependent on patient body weight (BW), scan duration and the added delay. Iodine flow varies between 1.6 (BW<70kg), 1.8 (BW 70-85kg) and 2.0 gram (BW>85kg) iodine/sec. In the first phase, only contrast medium is injected. Secondly, a mixture of 30% contrast medium and 70% saline is administered followed by a saline flush. These contrast protocols are performed for left-sided PHV evaluation. Right-sided contrast-enhanced PHV evaluation is more complex because it is difficult to obtain good right contrast enhancement and should be tailored to the individual patient.

#### ***Image reconstruction***

Raw data is reconstructed into 10 equally spaced datasets within the R-R interval of the cardiac cycle, and sent to dedicated workstations. All reconstructed datasets are loaded simultaneously in the dedicated cardiac analysis software. The imaging planes are aligned parallel and perpendicular to the valve leaflets as well as in plane with the valve in three perpendicular imaging planes (Figure 3). For dynamic evaluation, a cine movie in the plane perpendicular to the valve leaflets is recorded after appropriate alignment and windowing. For anatomical assessment, the best systolic and diastolic reconstruction phase is selected. From these phases, batches in the same three perpendicular imaging planes are saved. Additional reconstructions in echocardiographic views and coronary multiplanar reconstructions can be performed on indication. Finally, these reconstructions are sent to PACS for archiving and assessed together with the standard axial images.

#### ***Image interpretation:***

PHV assessment starts with the evaluation of the cine movie which provides information on the dynamic behaviour of the PHV (opening/closing). For mechanical PHV leaflets, closing and opening angles can be measured and compared to PHV and size specific reference values (Table 1, Figure 4). After the dynamic assessment, anatomical assessment is performed in both systole and diastole. The reconstructed batches in three perpendicular directions are evaluated for abnormalities. The specific pathology will be discussed in the different sections on PHV obstruction,

PHV regurgitation and PHV endocarditis. In patients considered for reoperation, it is important that the radiologist reports additional relevant preoperative information. First, it is important to be informed on the presence of coronary artery disease and/or the patency of bypass grafts. In most patients that can be simultaneously assessed.<sup>20</sup> Coronary artery assessment is especially important in patients with suspected PHV endocarditis. In these patients, vegetations may embolize into the coronary arteries due to catheter manipulation during conventional coronary angiography which is therefore best avoided. Second, before aortic PHV reoperations it is important to inform the cardiologist and cardiothoracic surgeon on the aortic dimensions to make an appropriate decision on aortic root and/or arch surgery. Third, it is important to inform the cardiothoracic surgeon on the sternum-right ventricle distance for the optimal planning of re-sternotomy. Relevant extracardiac findings need to be assessed and reported as well.

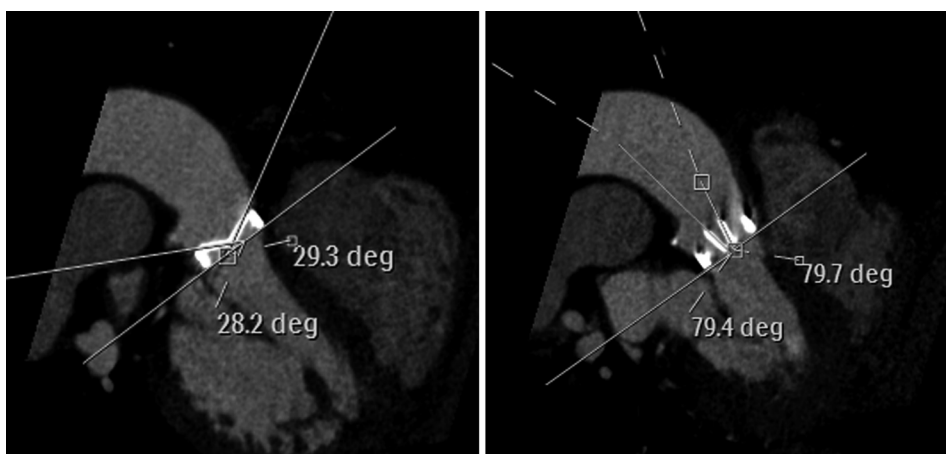


**Figure 4** | Closing **A** | and opening **B** | angle measurements for mechanical prosthetic heart valves. A reference line parallel to the valve leaflets is used for the angle measurement.

**Reporting of imaging findings:**

Essential for excellent diagnostic care in patients with PHV dysfunction is a well functioning multidisciplinary cooperation between the departments of Cardiology, Cardiothoracic Surgery and Radiology. Diagnostic PHV evaluation is a multifactorial process including clinical history, physical examination and imaging techniques (TTE, TEE, fluoroscopy and multislice CTA). For the optimal complementary value of multislice CTA, it is important for the radiologist to be informed on the details of PHV implantation (operation report), previous clinical and imaging findings (post-operative TTE images) as well as have a solid understanding of the procedures used by the surgeon. An appropriate CTA request including relevant clinical and imaging information increases the CTA value. It is best to discuss the case directly with the cardiologist and cardiothoracic surgeon before the scan. A proposed standardized report is shown in Figure 5. In addition to the standardized report, we feel it is important that imaging findings are discussed in a multidisciplinary meeting with the cardiologists and cardiothoracic surgeons for appropriate diagnosis and treatment decisions.

**Imaging characteristics of normal PHVs**

Previous papers demonstrated that most commonly implanted PHVs can be well visualized by multislice CT angiography.<sup>11-13,21</sup> The CTA image quality of PHVs largely depends on the PHV

**Figure 5** | Proposed standardized report for CT angiography of prosthetic heart valves

1. Patient data (Name, birth date, Hospital number)
2. Scan indication and request
3. Scan parameters
  - drug administration ( $\beta$ -blockers/nitroglycerin, dose (mg), oral/sublingual/intravenously)
  - heart rate during scan
  - scanner type
  - scan protocol including radiation dose
  - contrast protocol (tri/biphasic, total amount of contrast)
4. PHV type and position
5. Dynamic PHV assessment
  - normal opening/closing of PHV, presence of rocking motion
  - measurement of opening and closing angles and comparison with reference values
6. Anatomical assessment of the PHV in three perpendicular axes
  - presence of thrombus (yes/no. If yes describe the location)
  - presence of pannus (yes/no. If yes describe the location)
  - PHV angulation (normal/abnormal. If abnormal describe the abnormal angulation)
  - signs of PHV endocarditis (vegetations, paravalvular leakage, mycotic aneurysm)
  - presence of paravalvular leakage (yes/no. If yes describe the location)
  - the presence of Left Outflow Tract (LVOT) narrowing (yes/no. If yes specify the cause and provide systolic and diastolic LVOT surface area measurements)
  - provide systolic valve leaflet opening orifice area (biological PHVs only)
  - presence of PHV degeneration (biological PHVs only)
7. Cardiac assessment and dimensions
  - coronary artery and coronary bypass grafts assessment
  - distance between sternum and right ventricle
  - ventricle and atrial dimensions
  - proximal aortic dimensions
  - cardiac contraction (especially left ventricle)
8. Other structures (in particular evaluation in lung/bone/mediastinal windows)
9. Conclusion

composition.<sup>11,13,22</sup> PHVs which contain nickel or titanium alloy rings are well visualized by multislice CT (Table 1). CT imaging characteristics of two commonly implanted normal bileaflet PHVs, Carbomedics and St Jude, are shown in Figures 6 and 7. Dynamic assessment of valve leaflets is possible on the cine-images. A Medtronic Hall Tilting disc PHV, composed of titanium, is shown in Figure 8. Björk-Shiley and Sorin tilting disc PHVs and Duromedics bileaflet PHVs contain a cobalt-chrome alloy which induces severe PHV artifacts precluding PHV assessment (Figure 9). Most biological PHVs are well visualized by multislice CT<sup>11,23</sup> (Figure 10). The valve leaflets may have moderate image quality.<sup>11</sup> Chenot et al. demonstrated that a higher tube voltage (140kV) for the reduction of blooming metal artifacts may improve leaflet visualization of biological PHVs.<sup>23</sup>

### ***Imaging characteristics of dysfunctional PHVs***

Mechanical PHV dysfunction is a heterogeneous disease with three main categories: PHV obstruction, PHV regurgitation and PHV endocarditis that are discussed below.



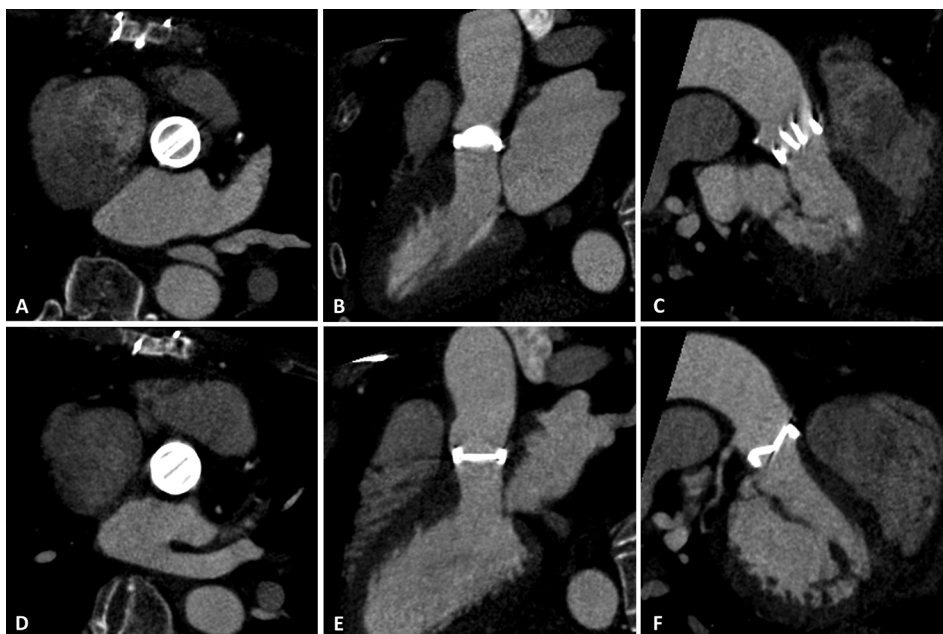


**Figure 6** | A Carbomedics bileaflet prosthetic heart valve in the aortic position: systolic in plane **A** | systolic parallel **B** | systolic perpendicular **C** | diastolic in plane **D** | diastolic parallel **E** | and diastolic perpendicular **F** | reconstructions

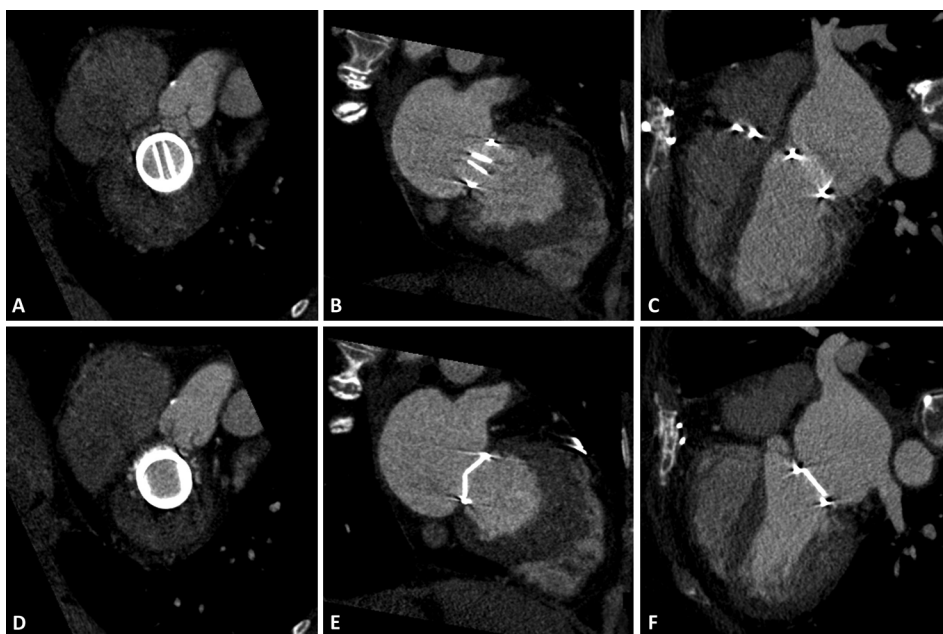


**Figure 7** | A St. Jude bileaflet prosthetic heart valve in the mitral position: diastolic in plane **A** | diastolic perpendicular **B** | diastolic parallel **C** | systolic in plane **D** | systolic perpendicular **E** | and systolic parallel **F** | reconstructions

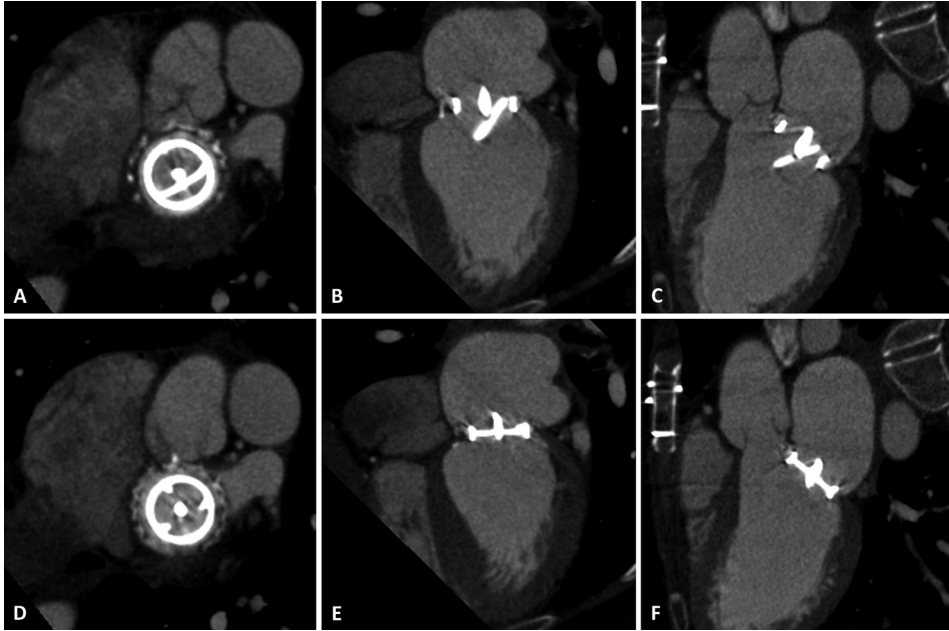


**Figure 8** | A Medtronic Hall tilting disc prosthetic heart valve in the mitral position: diastolic in plane **A** | diastolic parallel **B** | diastolic perpendicular **C** | systolic in plane **D** | systolic parallel **E** and systolic perpendicular **F** | reconstructions. Note that the perpendicular reconstructions are not completely perpendicular.

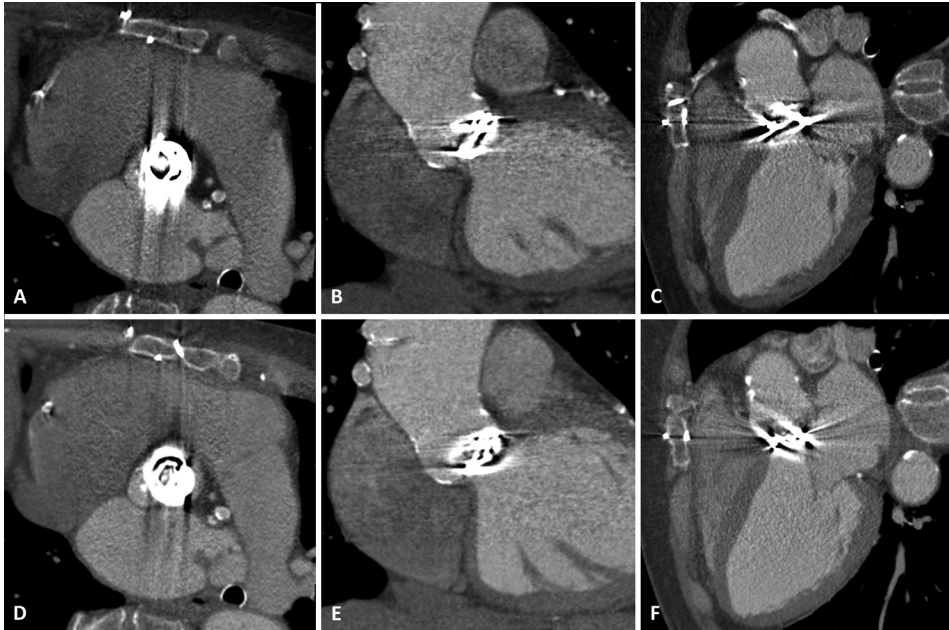


**Figure 9** | A Björk-Shiley tilting disc prosthetic heart valve in the aortic position: systolic in plane **A** | systolic perpendicular **B** | systolic parallel **C** | diastolic in plane **D** | diastolic perpendicular **E** and diastolic parallel **F** | reconstructions. Note the severe PHV-related artifacts that preclude diagnostic assessment.

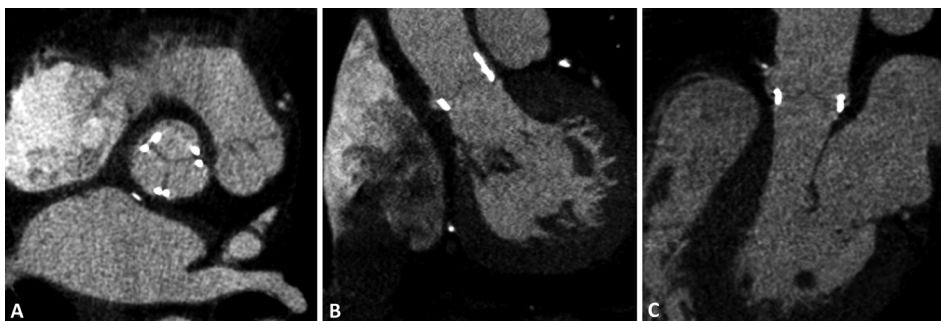


**Figure 10** | A Perimount biological prosthetic heart valve in the aortic position: diastolic in plane **A** | diastolic perpendicular **B** | and diastolic parallel **C** | reconstructions

### PHV obstruction

PHV obstruction can have several causes: thrombosis, pannus formation (fibrotic tissue), vegetations (in patients with PHV endocarditis), patient-prosthesis mismatch (PPM) and PHV angulation. PHV obstruction has to be differentiated from subvalvular obstruction such as systolic anterior motion of the anterior mitral valve leaflet or a subvalvular membrane.

In daily clinical practice, it is important to diagnose the exact cause of PHV obstruction because treatment differs substantially for different etiologies. Thrombosis treatment consists of drug administration, thrombolysis or reoperation. Pannus formation, PPM and extreme PHV angulation may require reoperation in symptomatic patients. Vegetations that cause PHV obstruction are treated with antibiotics or reoperation. Aortic PHV pannus formation with an incidence of 0.2-4.5% per year, is tissue originating from the left ventricular septum which contains myofibroblasts and extracellular matrix.<sup>2,12,24,25</sup> Pannus formation is very difficult to differentiate from thrombus with echocardiography and fluoroscopy.<sup>26-28</sup> Multislice CT angiography may offer additional diagnostic value in the visualization of pannus tissue. Pannus presents as soft tissue density rims underneath the PHV usually in a (semi) circular pattern (Figure 11).

PHV thrombosis has an incidence of 0.1-0.4% per year depending on PHV type, PHV position and adequacy of anticoagulation therapy.<sup>6,9</sup> PHV thrombosis occurs more often on the atrial side in the mitral position and on the aortic side in the aortic position. In contrast, pannus formation, occurs more often on the ventricular side in both the aortic and mitral position.<sup>2</sup> Thrombosis also results more often in leaflet restriction than pannus formation.<sup>29</sup> In our experience, thrombosis presents

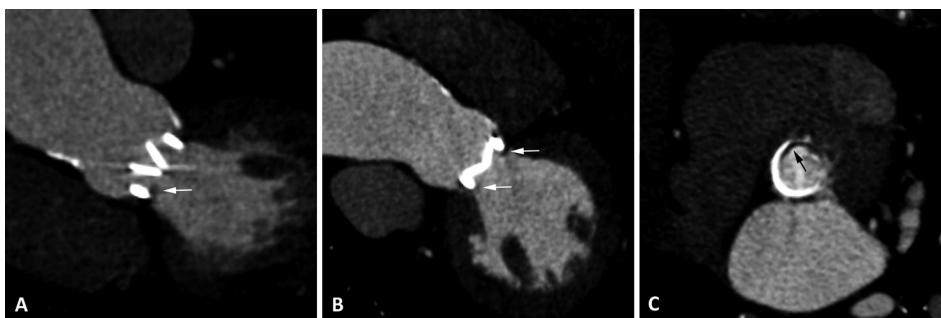


**Figure 11** | A Carbomedics bileaflet prosthetic heart valve in the aortic position with pannus formation: systolic perpendicular **A** | diastolic perpendicular **B** | and diastolic in plane **C** |. Notice the hypodense subvalvular abnormality (arrows) which is originating from the interventricular septum and is present in a circular pattern **C** |

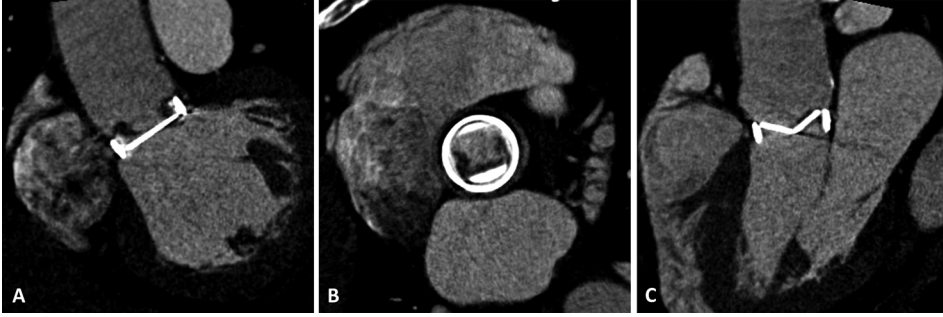


**Figure 12** | A bileaflet Carbomedics prosthetic heart valve in the aortic position with thrombus formation: perpendicular **A** | in plane **B** | and parallel **C** | reconstructions. Notice the hypodense abnormalities around the valve leaflets on the aortic side of the prosthesis.

more irregularly shaped compared to the (semi)circular shape of pannus. However, patients may present with combined pathology (pannus and thrombus). A CT example of a patient with PHV thrombosis and leaflet restriction is shown in Figure 12.

Pannus and thrombus formation are two of the most common causes of PHV obstruction. During CT interpretation, it is important to also consider more rare causes of PHV obstruction such as abnormal PHV angulation. When the PHV is positioned in an inappropriate angle in the annulus with regard to the LVOT and aortic root, it can result in obstruction. There are no definite angles that serve as a cutoff between normal and abnormal. It is important to assess the PHV angulation in multiple views. Figure 13 demonstrates a CT example of PHV angulation. The above mentioned causes of PHV obstruction also apply to biological PHVs. In addition, degeneration of biological PHVs can cause biological PHV dysfunction. Degeneration of biological PHVs presents as leaflet thickening, leaflet calcifications and diminished prosthetic orifice area which in turn result in obstruction of the valve.

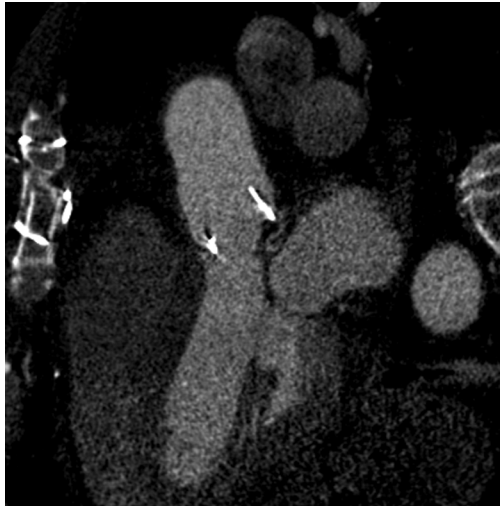


**Figure 13** | Biological CE Perimount prosthetic heart valve in the aortic position. The valve is angulated in the LVOT resulting in LVOT narrowing.

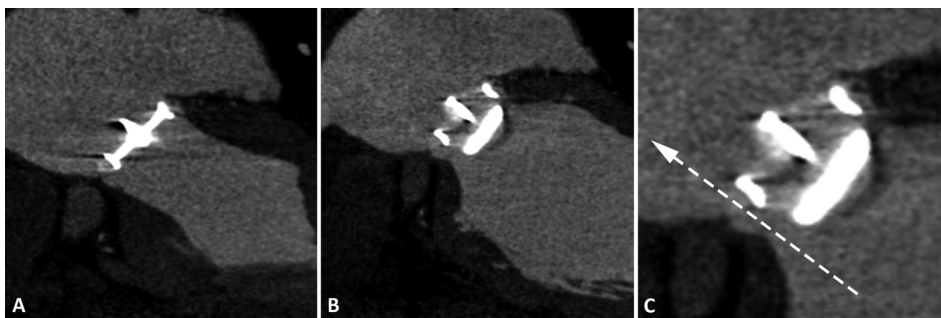


**Figure 14** | Medtronic Hall tilting disc in the mitral position with a paravalvular leak. Systolic **A** | Diastolic **B** | and detailed diastolic **C** | reconstructions. Notice the continuum of contrast material passing outside the PHV connecting the left ventricle and left atrium. The flow will be mainly directed from the high pressure left ventricle to the low pressure left atrium (dotted arrow)

### PHV regurgitation

All mechanical PHVs have a normal small volume of regurgitation. In clinical practice, it is important to differentiate between normal and pathological regurgitation. The presence and severity of regurgitation is routinely assessed with echocardiography. Regurgitation has to be differentiated in valvular and paravalvular regurgitation. Valvular regurgitation is caused by pathological entities

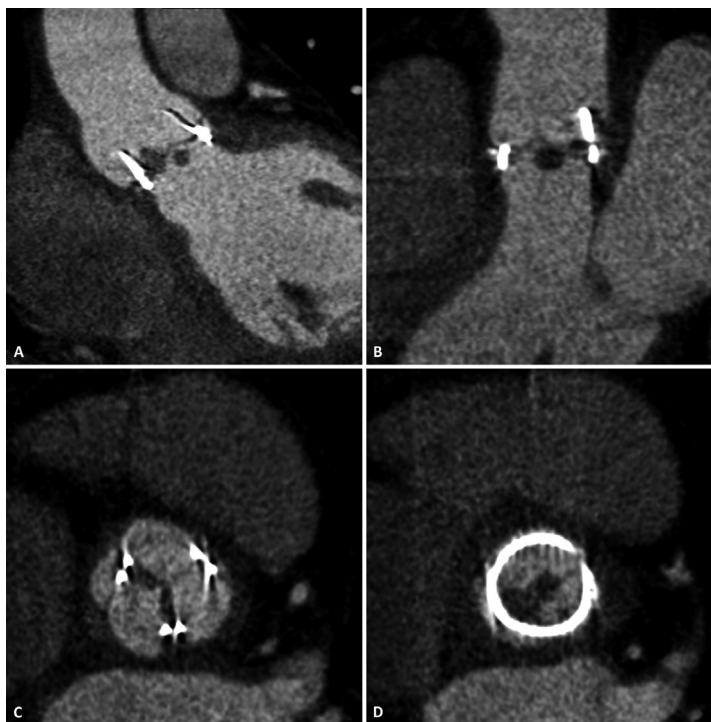


**Figure 15** | Biological CE Perimount prosthetic heart valve in the aortic position with vegetations. Diastolic perpendicular **A** | diastolic parallel **B** | diastolic in plane **C** | and diastolic in plane at the level of the vegetations **D** | reconstructions. Notice the thickened valve leaflets that are typical for both vegetations and leaflet degeneration. However, the spherical shaped hypodense abnormalities are typical for vegetations.

(vegetations, pannus, thrombus, trapped suture) which interfere with leaflet closing. Paravalvular leakage is caused by suture loosening or PHV endocarditis. Multislice CT angiography is an anatomic imaging modality and is inferior in the visualization of PHV regurgitation compared with echocardiography. However, in some cases CT may visualize the exact cause and location of the PHV regurgitation (e.g. pannus/thrombus/vegetation/mycotic aneurysm). Figure 14 demonstrates an CT example of PHV regurgitation with a paravalvular origin.

### PHV endocarditis

PHV endocarditis is most commonly seen in the first years after PHV implantation and has an incidence of 1.4-5.7%.<sup>30</sup> In the evaluation of patients with suspected PHV endocarditis, it is important to assess the CT images for the presence of vegetations, paravalvular leakage and mycotic aneurysms/abscesses. Multislice CT is comparable to TEE for the detection of vegetations (Figure 15) and mycotic aneurysms/abscesses (Figure 16). However, small vegetations can be missed on CT images.<sup>31</sup> Vegetations may be difficult to differentiate from biological PHV degeneration because both pathological entities can present as diffuse thickened valve leaflets (Figure 16). Multislice CT may have additional value for the evaluation of the extent of the PHV endocarditis: the extent of the mycotic aneurysms/abscesses and the relation with the coronary arteries. This additional anatomical information may guide and/or change surgical strategies.

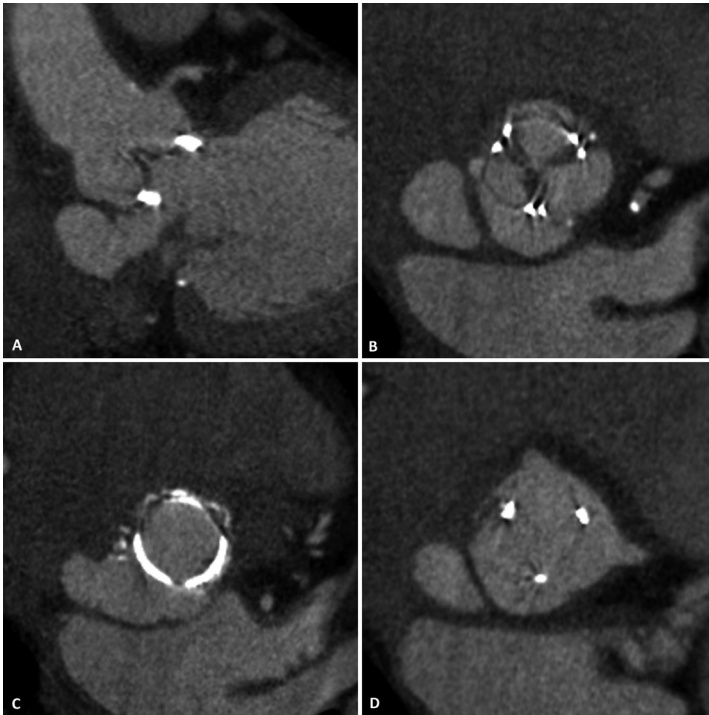


**Figure 16** | Biological CE perimount prosthetic heart valve in the aortic position with PHV endocarditis: perpendicular **A** | and three in plane reconstructions on different levels (**B-D**). Notice the mycotic aortic aneurysm with connection to the left ventricle **A** | The mycotic aortic aneurysm is located on the former non-coronary cusp. Besides the mycotic aortic aneurysm, the valve leaflets are diffusely thickened.

## CONCLUSION

Prosthetic heart valve assessment by CT angiography is a promising new cardiac CT application that can provide complementary diagnostic value to the clinical routine image techniques, echocardiography and fluoroscopy, and can provide additional relevant anatomical information that can change or guide surgical treatment. The radiologist as part of a multidisciplinary team (also including cardiologists and cardiothoracic surgeons) can contribute to the complex diagnostic process of patients with suspected PHV dysfunction.

## REFERENCES

1. Yacoub MH, Takkenberg JJ. Will heart valve tissue engineering change the world? *Nat Clin Pract Cardiovasc Med* 2005; 2:60-61.
2. Habets J, Budde RP, Symersky P, et al. Diagnostic evaluation of left-sided prosthetic heart valve dysfunction. *Nat Rev Cardiol* 2011; 8:466-478.
3. Bonow RO, Carabello BA, Chatterjee K, et al. 2008 focused update incorporated into the ACC/AHA 2006 guidelines for the management of patients with valvular heart disease: a report of the American College of Cardiology/American Heart Association Task Force on Practice Guidelines (Writing Committee to revise the 1998 guidelines for the management of patients with valvular heart disease). Endorsed by the Society of Cardiovascular Anesthesiologists, Society for Cardiovascular Angiography and Interventions, and Society of Thoracic Surgeons. *J Am Coll Cardiol* 2008; 52:e1-142.
4. Vahanian A, Baumgartner H, Bax J, et al. Guidelines on the management of valvular heart disease: The Task Force on the Management of Valvular Heart Disease of the European Society of Cardiology. *Eur Heart J* 2007; 28:230-268.
5. Akins CW, Miller DC, Turina MI, et al. Guidelines for reporting mortality and morbidity after cardiac valve interventions. *J Thorac Cardiovasc Surg* 2008; 135:732-738.
6. Cannegieter SC, Rosendaal FR, Briet E. Thromboembolic and bleeding complications in patients with mechanical heart valve prostheses. *Circulation* 1994; 89:635-641.
7. Grunkemeier GL, Li HH, Naftel DC, et al. Long-term performance of heart valve prostheses. *Curr Probl Cardiol* 2000; 25:73-154.
8. Hammermeister K, Sethi GK, Henderson WG, et al. Outcomes 15 years after valve replacement with a mechanical versus a bioprosthetic valve: final report of the Veterans Affairs randomized trial. *J Am Coll Cardiol* 2000; 36:1152-1158.
9. Khan S. Long-term outcomes with mechanical and tissue valves. *J Heart Valve Dis* 2002; 11:S8-14.
10. Habets J, Meijer TS, Meijer RCA, et al. Computed tomography attenuation measurements are valuable to discriminate pledgets used in prosthetic heart valve implantation from paravalvular leakage. *Br J Radiol*. 2012 (In Press).
11. Habets J, Symersky P, van Herwerden LA, et al. Prosthetic heart valve assessment with multidetector-row CT: imaging characteristics of 91 valves in 83 patients. *Eur Radiol*. 2011; 21:1390-1396.
12. Konen E, Goitein O, Feinberg MS, et al. The role of ECG-gated MDCT in the evaluation of aortic and mitral mechanical valves: initial experience. *Am J Roentgenol* 2008; 191:26-31.
13. Symersky P, Budde RP, Prokop M, et al. Multidetector-row computed tomography imaging characteristics of mechanical prosthetic valves. *J Heart Valve Dis* 2011; 20:216-222.
14. Zoghbi WA, Chambers JB, Dumesnil JG, et al. Recommendations for evaluation of prosthetic valves with echocardiography and doppler ultrasound: a report From the American Society of Echocardiography's Guidelines and Standards Committee and the Task Force on Prosthetic Valves, developed in conjunction with the American College of Cardiology Cardiovascular Imaging Committee, Cardiac Imaging Committee of the American Heart Association, the European Association of Echocardiography, a registered branch of the European Society of Cardiology, the Japanese Society of Echocardiography and the Canadian Society of Echocardiography, endorsed by the American College of Cardiology Foundation, American Heart Association, European Association of Echocardiography, a registered branch of the European Society of Cardiology, the Japanese Society of Echocardiography, and Canadian Society of Echocardiography. *J Am Soc Echocardiogr* 2009; 22:975-1014.
15. Tsai IC, Lin YK, Chang Y, et al. Correctness of multi-detector-row computed tomography for diagnosing mechanical prosthetic heart valve disorders using operative findings as a gold standard. *Eur Radiol* 2009; 19:857-867.
16. Jaussaud N, Gariboldi V, Giorgi R, et al. Risk of reoperation for aortic bioprosthesis dysfunction. *J Heart Valve Dis* 2009; 18:256-261.
17. Leontyev S, Borge MA, Modi P, et al. Redo aortic valve surgery: Influence of prosthetic valve endocarditis on outcomes. *J Thorac Cardiovasc Surg* 2011; 142:99-105.
18. Habets J, Symersky P, de Mol BA, et al. A novel iterative reconstruction algorithm allows reduced dose multidetector-row CT imaging of mechanical prosthetic heart valves. *Int J Cardiovasc Imaging* 2011; DOI: 10.1007/s10554-011-9954-7.
19. Symersky P, Habets J, Westers P, et al. Prospective ECG triggering reduces prosthetic heart valve-induced artifacts compared with retrospective ECG gating on 256-slice CT. *Eur Radiol*. 2011; DOI: 10.1007/s10554-011-9954-7.
20. Habets J, Van den Brink RB, Uijlings R, et al. Coronary artery assessment by multidetector computed tomography in patients with prosthetic heart valves. *Eur Radiol*. 2011; DOI: 10.1007/s00330-011-2360-7.
21. LaBounty TM, Agarwal PP, Chughtai A, et al. Evaluation of mechanical heart valve size and function with ECG-gated 64-MDCT. *Am J Roentgenol* 2009; 193:W389-W396.



22. Symersky P, Budde RP, Westers P, et al. Multidetector CT imaging of mechanical prosthetic heart valves: quantification of artifacts with a pulsatile in-vitro model. *Eur Radiol* 2011; 21:2103-2110.
23. Chenot F, Montant P, Goffinet C, et al. Evaluation of anatomic valve opening and leaflet morphology in aortic valve bioprosthesis by using multidetector CT: comparison with transthoracic echocardiography. *Radiology* 2010; 255:377-385.
24. Deviri E, Sareli P, Wisenbaugh T, et al. Obstruction of mechanical heart valve prostheses: clinical aspects and surgical management. *J Am Coll Cardiol* 1991; 17:646-650.
25. Teshima H, Hayashida N, Yano H, et al. Obstruction of St Jude Medical valves in the aortic position: histology and immunohistochemistry of pannus. *J Thorac Cardiovasc Surg.* 2003; 126:401-407
26. Girard SE, Miller FA, Jr., Orszulak TA, et al. Reoperation for prosthetic aortic valve obstruction in the era of echocardiography: trends in diagnostic testing and comparison with surgical findings. *J Am Coll Cardiol* 2001; 37:579-584.
27. Lin SS, Tiong IY, Asher CR, et al. Prediction of thrombus-related mechanical prosthetic valve dysfunction using transesophageal echocardiography. *Am J Cardiol* 2000; 86:1097-1101.
28. Barbetseas J, Nagueh SF, Pitsavos C, et al. Differentiating thrombus from pannus formation in obstructed mechanical prosthetic valves: an evaluation of clinical, transthoracic and transesophageal echocardiographic parameters. *J Am Coll Cardiol* 1998; 32:1410-1417.
29. Licata A, Matthai WH Jr. Evaluating the etiology of mechanical valve obstruction: use of clinical parameters, fluoroscopy, and echocardiography. *Catheter Cardiovasc Interv* 2002; 55:495-500.
30. Bashore TM, Cabell C, Fowler V Jr. Update on infective endocarditis. *Curr Probl Cardiol* 2006; 31:274-352.
31. Feuchtner GM, Stolzmann P, Dichtl W, et al. Multislice computed tomography in infective endocarditis: comparison with transesophageal echocardiography and intraoperative findings. *J Am Coll Cardiol* 2009; 53:436-444.





## CHAPTER IX

# IMAGING *of* PROSTHETIC HEART VALVE DYSFUNCTION: COMPLEMENTARY DIAGNOSTIC VALUE *of* TRANSESOPHAGEAL ECHOCARDIOGRAPHY *and* MULTIDETECTOR COMPUTED TOMOGRAPHY

J. Habets

W. Tanis

W.P.Th.M. Mali

S.A.J. Chamuleau

R.P.J. Budde

**P**rothetic heart valves are increasingly implanted worldwide to replace diseased native valves. Prosthetic heart valve (PHV) dysfunction is rare but potentially life-threatening. In clinical practice, transthoracic (TTE) and transesophageal echocardiography (TEE), and fluoroscopy for mechanical valves, are the routine imaging modalities to evaluate suspected PHV dysfunction.<sup>1</sup> Establishing the exact cause of PHV dysfunction is important to determine the appropriate treatment strategy but can be difficult. Multidetector computed tomography (MDCT) may have complementary diagnostic value to the routine imaging modalities in these patients.<sup>1</sup> In this imaging vignette, we present the spectrum of findings with echocardiography, fluoroscopy and computed tomography for a variety of PHV dysfunction etiologies that includes endocarditis, thrombus and pannus formation.

**Abbreviations**

Ao = Aorta

AMVL = Anterior Mitral Valve Leaflet

IVS = Interventricular Septum

LA = Left Atrium

LAA = Left Atrial Appendage

LM = Left Main

LV = Left Ventricle

MDCT = Multidetector Computed Tomography

PHV = Prosthetic Heart Valve

RV = Right Ventricle

RVOT = Right Ventricular Outflow Tract

TTE = Transthoracic Echocardiography

TEE = Transesophageal Echocardiography

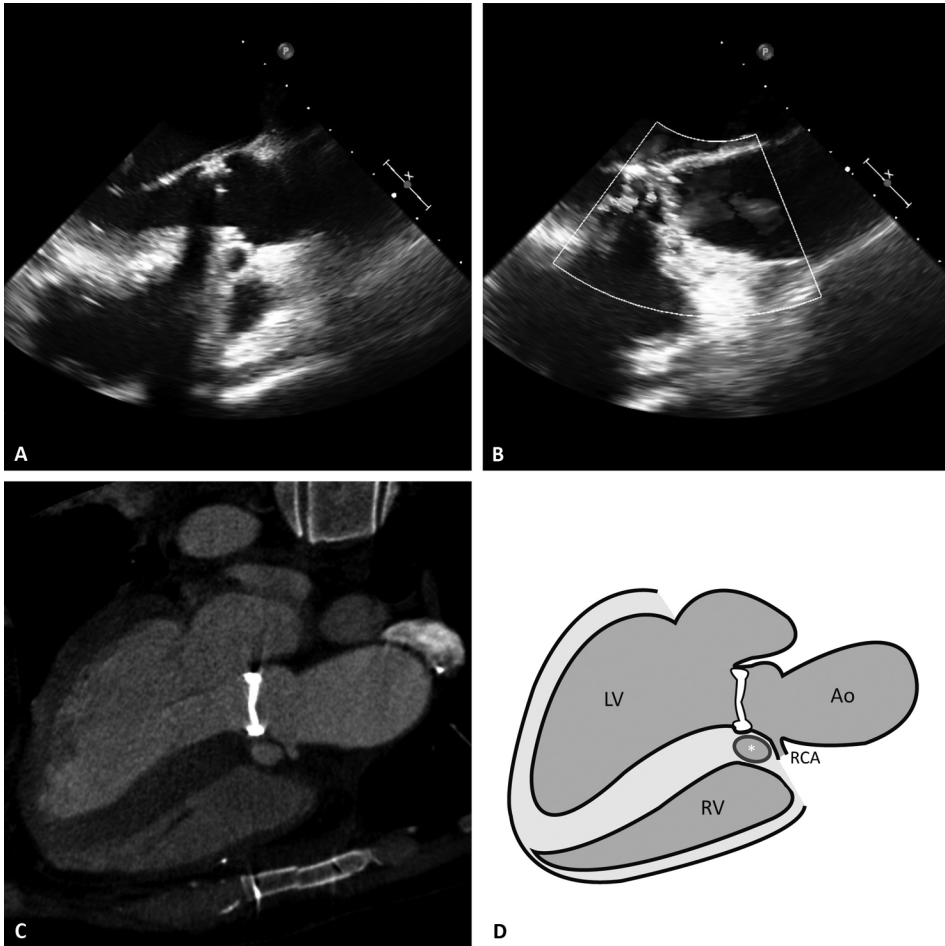


**Figure 1** | PHV endocarditis: 120 degree TEE view and matching MDCT reconstruction

Definite or possible diagnosis of PHV endocarditis is based on the modified Duke criteria in which non-invasive imaging plays a key role.<sup>2</sup> A low threshold for performing TEE after TTE is advisable because of the low sensitivity of TTE for the detection of signs of PHV endocarditis. In this patient with a Carbomedics bileaflet PHV in the aortic position, TTE demonstrated severe aortic regurgitation. In addition, TEE and MDCT revealed a mycotic aortic root aneurysm directly underneath the right coronary artery origin (RCA) (A, C) with diastolic paravalvular leakage as seen on color Doppler imaging (B). Acoustic shadowing on the TEE images (A) hampers complete and accurate assessment of the PHV, but MDCT did not show any vegetations (C). MDCT nicely demonstrated the close relationship of the mycotic aneurysm and the RCA (C, D). The location of the mycotic aneurysm is indicated by an asterisk on the schematic drawing (D). MDCT images can be reconstructed in any desired imaging plane after acquisition and allow for a one on one comparison with every echocardiographic view.

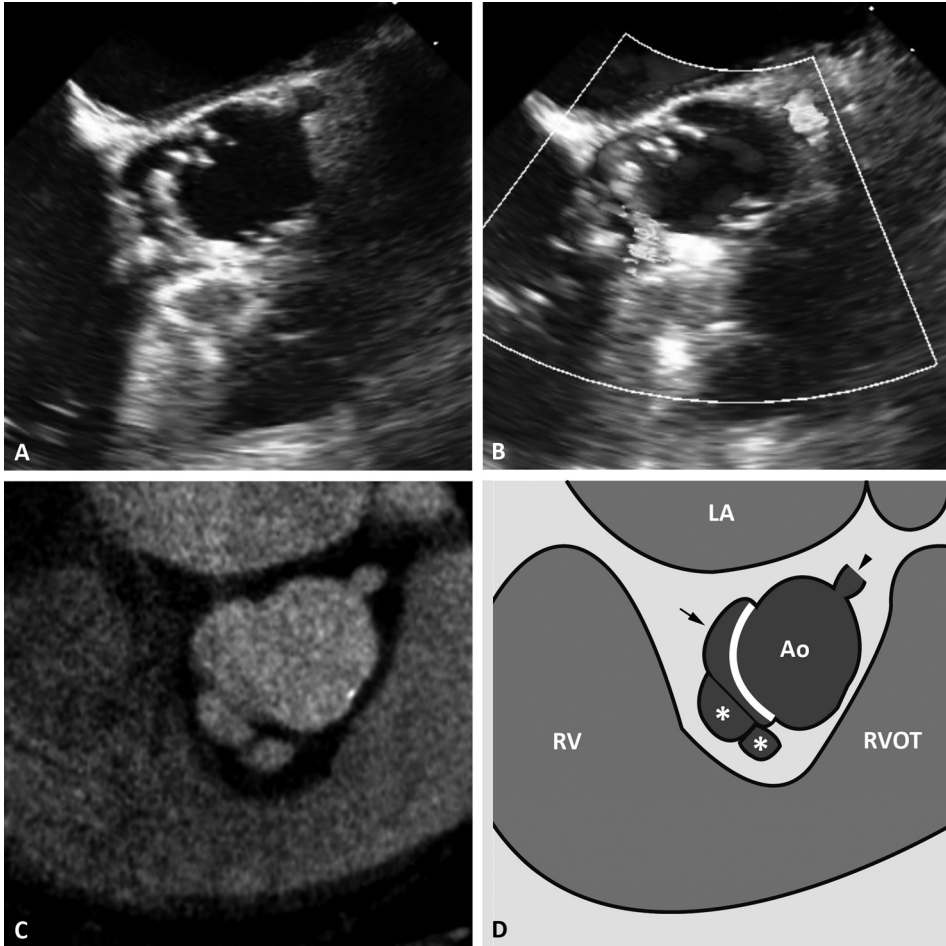


**Figure 2** | PHV endocarditis: short axis TEE view and matching MDCT reconstruction

In the same patient as presented in Figure 1, short axis TEE images demonstrated the mycotic aneurysm (A) and the diastolic paravalvular leakage on color Doppler (B). MDCT also demonstrated the mycotic aneurysm and allowed for detailed delineation of its contours (C) due to lack of acoustic shadowing present on TEE images (A). However, TEE provides additional hemodynamic information by color Doppler flow demonstrating the diastolic flow paravalvular leakage (B). Although MDCT confirms the paravalvular route by showing contrast outside the valve it can not determine the diastolic and systolic flow direction. The illustration (D) illustrates the partition of the mycotic aneurysm on MDCT images (D; \*) and the close relationship of the aneurysm with the right sinus of Valsalva (arrow). The arrowhead (D) indicates the orifice of the left main branch.

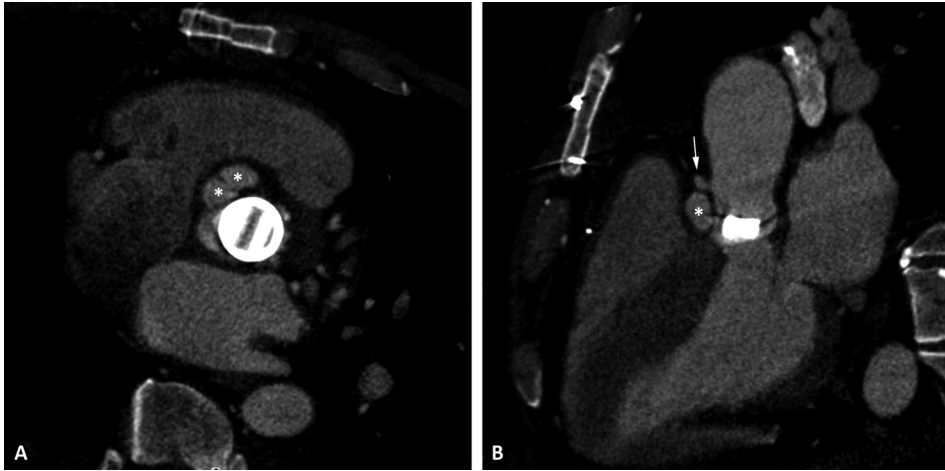


**Figure 3** | PHV endocarditis: MDCT short axis and parallel view

In the same patient as Figures 1 and 2, MDCT images demonstrated the extent of the mycotic aneurysm (A/B; \*) and the close relationship with the right coronary artery (RCA) (B; arrow). This anatomical information is of high clinical importance for the preoperative surgical guidance in case of re-operation (prosthetic heart valve replacement with/without pericardial patch or homograft implantation with coronary re-implantation). In this case, the extent of the mycotic aneurysm and the close relationship with the RCA resulted in a successful homograft implantation with re-implantation of the coronary arteries.

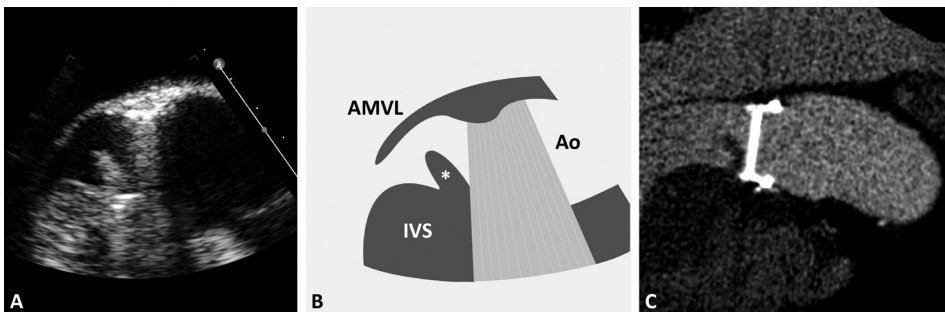


**Figure 4** | PHV endocarditis: 120 degree TEE view and corresponding MDCT reconstruction

This patient with a St Jude bileaflet PHV in the aortic position presented with suspected PHV endocarditis (fever and multiple positive blood cultures with streptococcus). Both TTE and TEE (A) revealed a large (11x14mm) mobile echodense mass indicating the presence of a vegetation. The potential presence of an abscess or mycotic aneurysm on the septal side of the PHV was difficult to assess due to acoustic shadowing (A/B). The illustration demonstrates the relation of the vegetation (\*) with the interventricular septum (IVS) and the anterior mitral valve leaflet (AMVL). MDCT confirmed the presence of the vegetation underneath the PHV (C) and definitely excluded the presence of an abscess or mycotic aneurysm.



**Figure 5 |** PHV endocarditis: simultaneous coronary and aortic dimension assessment by MDCT

The presence of a large vegetation is an indication for urgent reoperation. For appropriate preoperative assessment, the cardiothoracic surgeon needs to be informed on the presence of coronary artery disease (CAD). Invasive coronary angiography is the gold standard for coronary assessment. However, the presence of a large vegetation is associated with an increased risk of distal embolization by catheter manipulation. Therefore, non-invasive evaluation of the coronary arteries is preferred. Figure 5A demonstrates the ability of MDCT to evaluate coronary arteries (i.e. RCA) simultaneously with PHV assessment. MDCT excluded coronary artery disease and given the high negative predictive value of MDCT for these presence of coronary artery disease, invasive coronary angiography was omitted (same patient as Figure 4). Although MDCT is a suitable technique to exclude coronary artery disease, it is difficult to identify significant coronary stenosis in patients with severe coronary calcifications.

Proximal aortic assessment is important because of possible therapeutic consequences (aortic root and/or arch replacement). In this case, MDCT (Figure 5B) revealed an aneurysm of the ascending aorta (diameter 50mm) which was not visualized with TEE because of focusing on PHV assessment. Although TEE is able to detect aneurysms of the ascending aorta, it is inferior to MDCT for diameter measurements. The presence of a large vegetation and the dilated ascending aorta resulted in the choice for replacement of both the PHV and ascending aorta (Bentall procedure). Surgical inspection confirmed the presence of a large vegetation and the absence of a mycotic aneurysm in the aortic root. Surgery also confirmed the dilated ascending aorta.



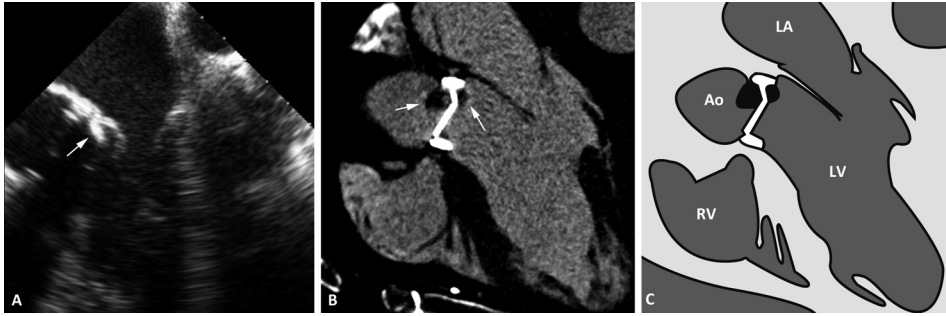


**Figure 6** | PHV thrombosis: 0 degree TEE view and corresponding MDCT reconstruction

Patients with PHV obstruction present with an increased pressure gradient and/or decreased prosthetic orifice area on TTE. The exact cause of PHV obstruction is often not detected with TTE. In this patient with a Carbomedics bileaflet PHV in the aortic position, additional TEE, fluoroscopy and MDCT was performed. TEE demonstrates a subvalvular echodense mass located between the septal side of the PHV and the anterior mitral valve leaflet (A, arrow). MDCT confirmed the presence of this mass on the ventricular side of the PHV. Moreover, an additional hypodense mass was seen on the aortic side of the PHV (B, arrows). The irregular shape and the location on both the aortic and ventricular side of the PHV (C) favours the diagnosis of PHV thrombosis over pannus formation.

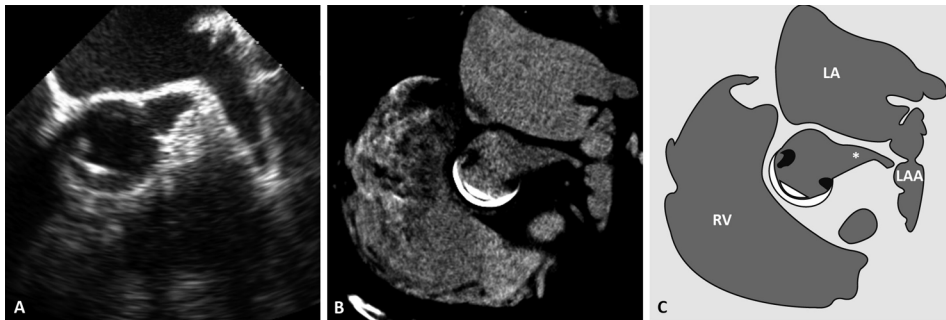


**Figure 7** | PHV thrombosis: short axis TEE view and corresponding MDCT reconstruction

In the same patient as Figure 6, diastolic TEE short axis images demonstrate two possible echodense masses on the aortic side at the level of the origin of the aneurysmatic left coronary artery (A). These possible lesions were missed at the initial TEE interpretation. MDCT was performed for determination of the exact cause of the PHV obstruction, and nicely delineated two hypodense irregular shaped lesions on the aortic side of the PHV which are compatible with PHV thrombosis (B). After this observation, two possible echodense masses were identified on TEE images. The illustration (C) demonstrates the two irregular shaped lesions (black) and their relationship with the PHV and aneurysmatic left main branch (\*).

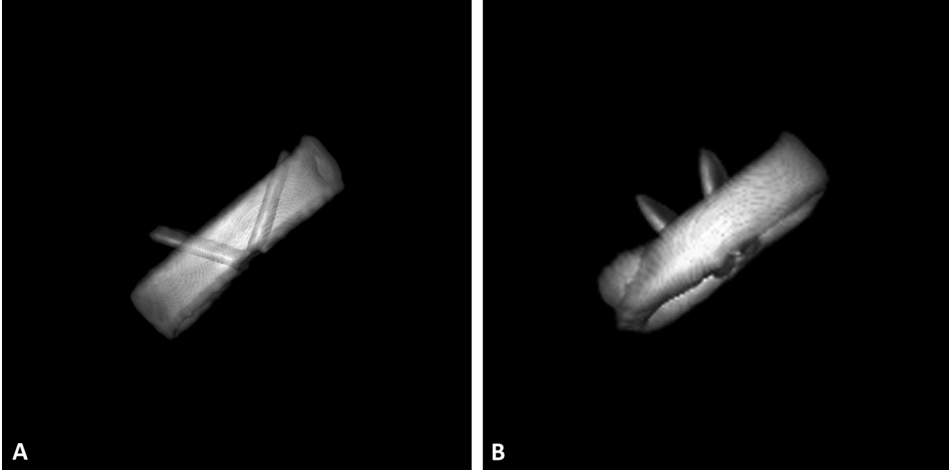


**Figure 8** | PHV thrombosis: 3D volume rendered MDCT images

In the same patient as Figure 7, both fluoroscopy and MDCT (A) demonstrated restricted leaflet opening, more pronounced on one side but also present on the other side. Asymmetric leaflet restriction is often present in PHV thrombosis, and not very common in patients with pannus formation. Comprehensive imaging evaluation resulted in the diagnosis of PHV thrombosis which was treated with additional anticoagulation therapy (warfarin plus low-molecular weight heparins) and antiplatelet therapy (aspirin). After two months, TTE showed normalization of maximum pressure gradient over the aortic PHV. MDCT confirmed this by showing normal leaflet opening of both leaflets (B), and the hypodense irregular shaped mass disappeared confirmed the successful diagnosis and treatment of PHV thrombosis.



**Figure 9** | PHV pannus formation: 120 degree TEE view and corresponding MDCT reconstruction

This patient presented with a gradual increase of maximum pressure gradient over the aortic PHV (Carbomedics Tophat bileaflet) and complaints of dyspnea (NYHA class II). TTE did show an

increased pressure gradient but could not determine its exact cause. The assessment of the PHV especially the subvalvular area on TEE images was hampered by acoustic shadowing. No echodense masses were seen on the subvalvular side, but a possible supra-annular echodense mass (') was identified. This contour is however typical for this specific PHV type that is implanted in supra-annular position. MDCT did not show any supra-annular mass. However, MDCT identified a semicircular hypodense mass on the ventricular side of the PHV ring (arrows) which is compatible with pannus formation. Pannus formation is a known cause for PHV obstruction leading to a gradual increase of the pressure gradient over the PHV.

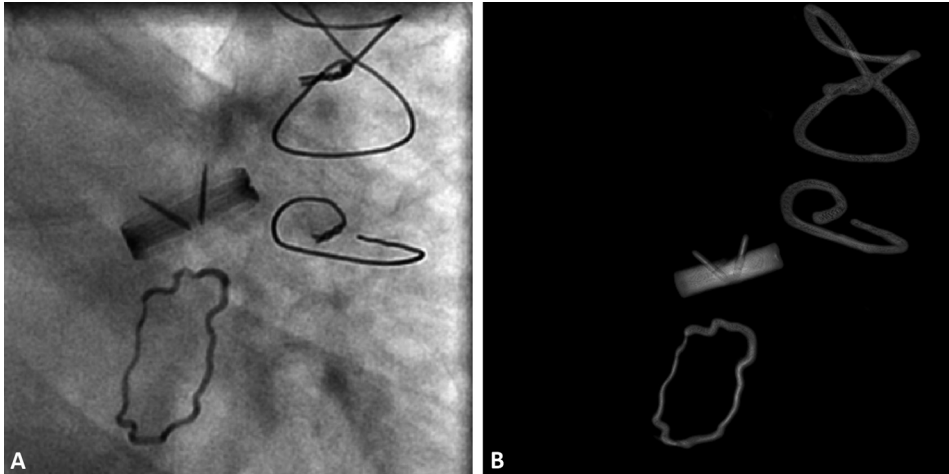


**Figure 10** | PHV pannus formation: Fluoroscopy and MDCT fluoroscopy

PHV leaflet assessment was hampered by acoustic shadowing on TEE. Fluoroscopy was performed to assess leaflet motion. Normal manufacturer leaflet opening angles of this PHV are 78 degrees. Fluoroscopy (A) revealed decreased leaflet opening of both leaflets (49 degrees at posterior side and 54 degrees at septal side, respectively). MDCT confirmed this leaflet restriction (B). Furthermore, notice the presence of a mitral annuloplasty ring. Leaflet restriction is more suggestive for PHV thrombosis than pannus formation.

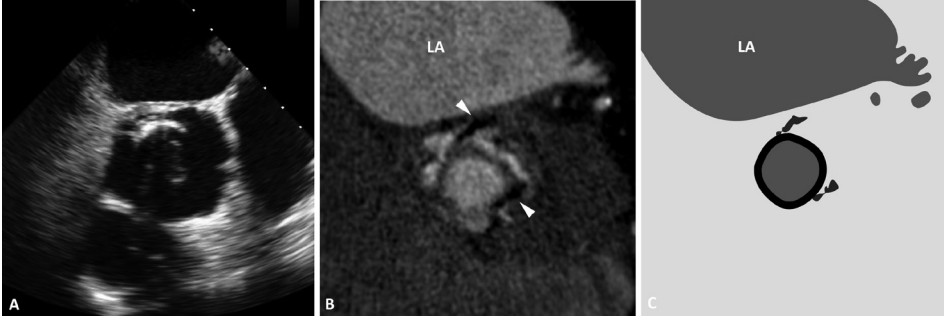


**Figure 11** | PHV pannus formation: short axis TEE and MDCT view

TEE images did not show a subvalvular mass (A). However, MDCT demonstrated a circular hypodense mass in the subvalvular region (B). Hypodense PHV-related artifacts are indicated with arrowheads. The illustration (C) emphasizes the circular pattern and the PHV-related artifacts (black). This circular hypodense mass is more suggestive for pannus formation. Therefore, thrombolysis was not considered and the patient was referred for surgery. Surgical inspection confirmed pannus formation as the case of PHV dysfunction.

## REFERENCES

1. Habets J, Budde RP, Symersky P et al. Diagnostic evaluation of left-sided prosthetic heart valve dysfunction. *Nat Rev Cardiol* 2011; 8:466-78.
2. Durack DT, Lukes AS, Bright DK. New criteria for diagnosis of infective endocarditis: utilization of specific echocardiographic findings. Duke Endocarditis Service. *Am J Med* 1994; 96:200-209.





CHAPTER X

PROSTHETIC HEART VALVE  
ASSESSMENT *with*  
MULTIDETECTOR-ROW CT:  
IMAGING CHARACTERISTICS *of*  
91 VALVES *in* 83 PATIENTS

J. Habets  
P. Symersky  
L.A. van Herwerden  
B.A.J.M. de Mol  
A.M. Spijkerboer  
W.P.Th.M. Mali  
R.P.J. Budde

**ABSTRACT**

**PURPOSE** | Multidetector CT (MDCT) has shown potential for prosthetic heart valve (PHV) assessment. We assessed the image quality of different PHV types to determine which valves are suitable for MDCT evaluation.

**METHODS** | All ECG-gated CTs performed in our institutions since 2003 were reviewed for the presence of PHVs. After reconstruction in three specific PHV planes, image quality of the supra-avalvular, perivalvular, subvalvular and valvular regions was scored on a four-point scale (1=non-diagnostic, 2=moderate, 3=good and 4=excellent) by two independent observers.

**RESULTS** | Eighty-four CT examinations (66 cardiac, 18 limited-dose aortic protocols) of 83 patients with a total of 91 PHVs in the aortic ( $n=71$ ), mitral ( $n=17$ ), pulmonary ( $n=1$ ) and tricuspid ( $n=2$ ) position were included. CT was performed on a 16-slice ( $n=4$ ), 64-slice ( $n=28$ ) or 256-slice ( $n=52$ ) MDCT system. Median image quality scores for the supra-, peri- and subvalvular regions and valvular detail were (3.5, 3.3, 3.5 and 3.5, respectively) for bileaflet PHVs; (3.0, 3.0, 3.5 and 3.0, respectively) for Medtronic Hall PHVs; (1.0, 1.0, 1.0 and 1.0, respectively) for Björk-Shiley and Sorin monoleaflet PHVs and (3.5, 3.5, 4.0 and 2.0 respectively) for biological PHVs.

**CONCLUSION** | Currently implanted PHVs have good image quality on MDCT and are suitable for MDCT evaluation.



**P**rothetic heart valve (PHV) dysfunction is an uncommon complication after PHV implantation with potential life-threatening consequences. In daily clinical practice, (suspected) PHV dysfunction is evaluated by the following non-invasive imaging techniques: transthoracic echocardiography (TTE), transesophageal echocardiography (TEE) and fluoroscopy<sup>1</sup> These imaging techniques can detect PHV dysfunction accurately. However, echocardiography and fluoroscopy may fail to detect the anatomical substrate which causes PHV dysfunction.<sup>2</sup> Causes of PHV dysfunction include: pannus formation (subprosthetic tissue proliferation), thrombus formation, patient prosthesis mismatch (PPM, a too small valve for the patient's body size), pathologic (para)valvular leakage and endocarditis.<sup>1</sup>

Recently, multidetector computed tomography (MDCT) has shown potential for non-invasive evaluation of PHV (dys)function. In small studies, MDCT demonstrated additional diagnostic value to echocardiography and fluoroscopy for the evaluation of PHV dysfunction, especially in detecting pannus tissue.<sup>3-6</sup> It is important to know which PHV types have a CT appearance that allows detection of PHV problems. However, little is currently known about the MDCT appearance of different valve types.<sup>3</sup> In our article titled "Multidetector-row computed tomography imaging characteristics of mechanical prosthetic valves" accepted for publication in *Journal of Heart Valve Disease*, we recently reported on imaging characteristics of five different PHV types in a controlled in-vitro model. The purpose of the current study was to assess the CT image quality of different PHV types in patients to determine which valves are suitable for CT evaluation.

## MATERIALS AND METHODS

### CT selection

We reviewed all ECG-gated CT(A)s performed in the University Medical Centre Utrecht (UMCU) and Academic Medical Centre Amsterdam (AMC) between 2003 and April 2010 for the presence of PHVs based on the presence of a PHV and / or steel wires through the sternum (indicating an previous median sternotomy) on the surview images. If one or both criteria were met the CT images were reviewed for the presence and type of PHV. Patients with only a mitral or tricuspid annuloplasty ring or a stented valvegraft as used in percutaneous valve replacement were excluded. All other PHV types were included. CT data, as well as the reason for requesting the CT examination, were retrieved from the PACS archive of the Radiology department. CT data was sent to a workstation for image analysis.

Heart rate during the examination was obtained from the CT data. Patient data on specific valve type and size were obtained from the patient medical files. The study was performed under a waiver from the local ethics committee.

### Image analysis

Assessment of the CT examinations was performed on a dedicated workstation (Extended Brilliance Workstation, Philips Medical Systems, Philips, Best, the Netherlands). Three sets of images were reconstructed in three perpendicular imaging planes of each PHV: one set in plane with the valve, one set parallel and one set perpendicular to the valve leaflet(s). Reconstructions were made in both the diastolic and systolic phase of the cardiac cycle, if both phases were available.

For each PHV, image quality of the supralvalvular, perivalvular, subvalvular and valvular region was scored on a four-point scale: 1 = non-diagnostic, 2 = moderate visualization, 3 = good visualization and 4 = excellent visualization. The different regions are illustrated in Figure 1.

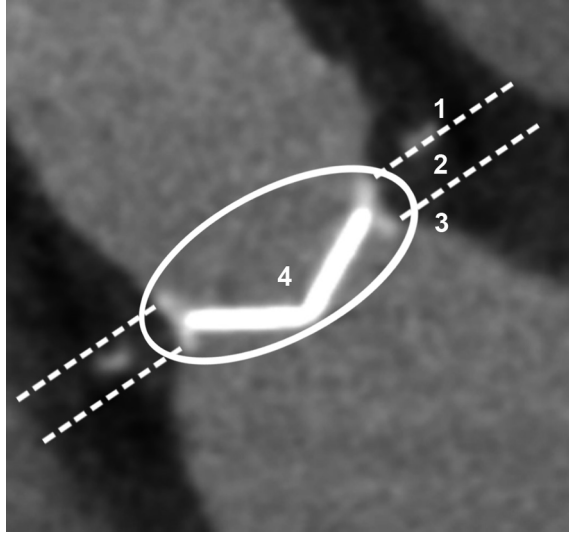


**Figure 1** | Different valvular regions for MDCT assessment (1 = supra- valvular, 2 = perivalvular, 3= subvalvular, 4 = valvular detail)

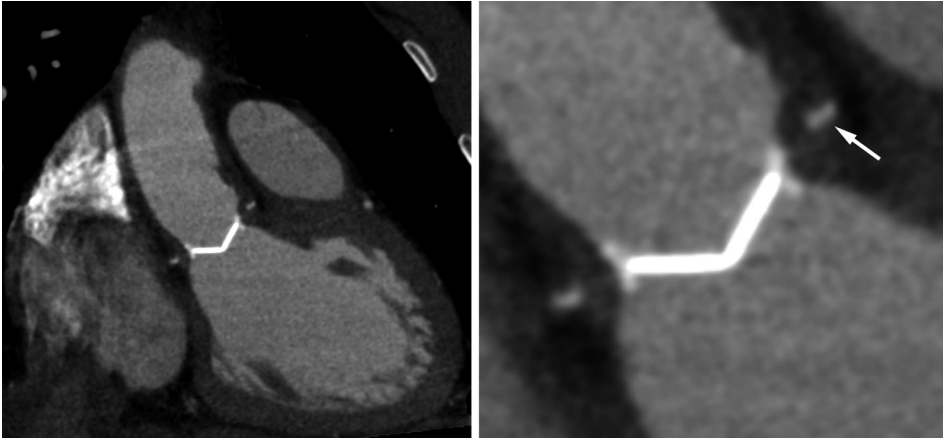


**Figure 2** | St. Jude PHV in aortic position. The left image plane shows the excellent PHV visualization. The arrow head in the detailed right image plane indicates a PTFE pledget (component of the suture material) commonly used in PHV implantation.

The criteria for the different scores per region were formulated as follows: for the supra-, sub- and perivalvular region: 1: no discernible supra-, sub-, or perivalvular detail widely beyond prosthesis; 2: no or limited details within 5 mm of prosthesis; 3: adequate details within 5 mm of prosthesis; 4: perfect details. For valvular detail: 1: no discernible leaflet; 2: leaflet discernible but no angle measurements possible; 3: leaflet angle measurement possible and 4: excellent leaflet detail. For the general score the image quality scores for all the regions were taken into account.

Scoring was performed by two observers (PS and JH) independent of each other. The observers had three and one year experience with cardiac CT, respectively.

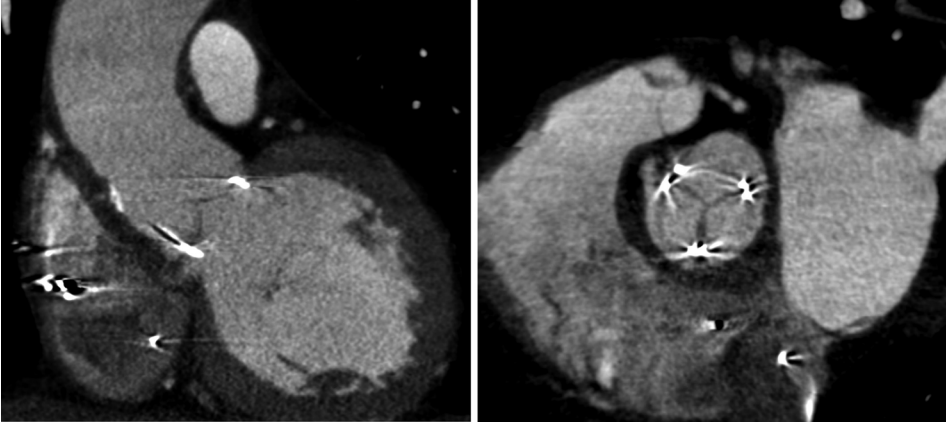


**Figure 3** | C-E Perimount PHV in aortic position. In the left image panel (long axis view), the artifacts caused by the metallic components of the struts are visualized. In particular in the supra-avalvular region. In the right image panel (the short axis view), the valve leaflets are well visualized.

### Data analysis

Data were analyzed using SPSS software (SPSS Statistics Version 15.0, SPSS Inc, Chicago, IL). The scores of the image quality scores per region of both observers was calculated and used for analysis. Data were presented as medians with minimum and maximum values because of a non-parametric data distribution. Image quality scores for different PHV types (bileaflet, tilting-disc and biological PHVs) and different manufacturers were compared with the Kruskal-Wallis test. If the Kruskal-Wallis test showed a significant result, the post-hoc Mann-Whitney U test was performed with Bonferroni correction. Interobserver variability was analyzed by weighted kappa statistics based on Cohen. Correlations between image quality scores and heart rate, were analyzed using the Spearman correlation. The influence of the CT protocol (aortic CTA/dedicated cardiac CTA) or CT system (16/64/256 slice) on the image quality scores were analyzed using the Fisher's Exact Test. Statistical significance was defined as a *p*-value <0.05.

## RESULTS

### Patient characteristics

A total of 84 ECG-gated examinations of 83 patients (Age  $56.3 \pm 14.8$  years (mean  $\pm$  SD), 47 men) with 91 PHVs were available. Seventy mechanical PHVs and 21 biological PHVs were evaluated. One patient, who underwent two CTs, was included twice. This patient underwent a reoperation in which different PHVs were implanted between both CTs.

PHVs were positioned in the aortic ( $n=71$ ), mitral ( $n=17$ ), pulmonary ( $n=1$ ) and tricuspid position ( $n=2$ ). Seventy mechanical PHVs of 8 different manufacturers including 50 bileaflet PHVs (20 Carbomedics, 14 St Jude and 16 other PHVs) and 20 tilting disc valves (13 Medtronic Hall valves, 5 Björk-Shiley valves and 2 Sorin monoleaflet valves) were assessed. Twenty-one biological PHVs, thirteen Perimount valves and eight other valves, were evaluated.

### CT parameters

All patients underwent a retrospectively ECG-gated CT on a 16-slice ( $n=4$ ), 64-slice ( $n=28$ ) or

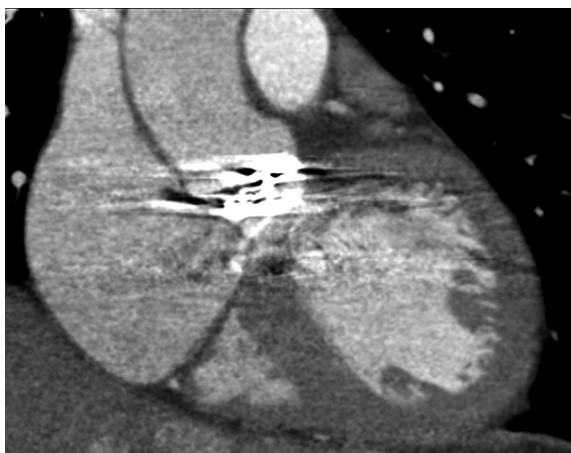


**Figure 4** | Björk-Shiley tilting disc in aortic position. This PHV type and the periprosthetic anatomy are not suitable for MDCT diagnostic assessment due to severe artifacts.

256-slice ( $n=52$ ) MDCT system (Brilliance 16, Brilliance 64 and iCT, Philips Medical Systems, Cleveland, Ohio). The indications for the CT examinations were PHV or surrounding anatomy assessment ( $n=42$ ), evaluation of aortic aneurysms or dissection ( $n=22$ ) and other cardiac and pulmonary indications ( $n=20$ ). In 38/84 (45%) of the patients the delay between surgery and CT could be inferred from the medical records. The median interval between surgery and the CT examination was 31 months (range: 0-175). Mean heart rate during CT was  $58\pm 31$  bpm (range 48-139). In thirteen of the 83 patients (16%) the mean heart rate during CT was unknown. Sixty-six out of eighty-four (79%) examinations were performed as a dedicated cardiac CT ( $\geq 600$ mAs) and 18/84 (21%) as an ECG-gated CT of the aorta (200-400mAs). Forty-two of the 66 (64%) dedicated cardiac CT examinations were performed assessed for diagnostic PHV purposes Contrast agents (Ultravist<sup>®</sup> - 300 mg jopromide/ml, Bayer Schering Pharma AG, Berlin, Germany or Imeron<sup>®</sup> - 400 mg iodine/ml, Bracco UK Limited, London, United Kingdom) were administered in all patients except in one patient with a Björk-Shiley PHV.

### Image quality scores

The median image quality scores per PHV manufacturer type and PHV design type are shown in Tables 1 and 2. MDCT characteristics of different PHVs are illustrated in Figures 2 to 6.

Comparing bileaflet PHVs with tilting disc PHVs demonstrated significant higher image quality scores for the bileaflet valves for all regions ( $p<0.001$ ). Nevertheless, the Medtronic Hall tilting disc demonstrated no significant differences in image quality scores for all regions compared with the bileaflet PHVs. The comparison of bileaflet PHVs versus biological PHVs resulted in no significant differences in image quality per region, except for the valvular detail which was significantly higher image for bileaflet valves ( $p<0.001$ ). The comparison of tilting disc PHVs versus biological PHVs resulted in significant ( $p<0.001$ ) higher image quality scores for the biological PHVs except for the valvular detail which did not differ significantly. In the tilting disc group, the image quality scores for all regions of the Medtronic Hall PHVs were significantly higher than for the Björk-Shiley PHVs and the Sorin monoleaflet PHVs ( $p=0.001$ ). In the biological and the bileaflet group, no significant differences in image quality scores were present for the different PHV manufacturers. No significant correlation between heart rate and the general image quality score was found ( $p=0.635$ ).

**Table 1** | Image quality (IQ) score specified per PHV manufacturer type

Type	Type	Manufacturer	N	Supravalvular	Perivalvular	Median IQ score (minimum-maximum)	Subvalvular	Valvular	General IQ score	
Mechanical (n = 70)	Bileaflet (n = 50)	Carbomedics	20	3.8 (2.5-4.0)	3.5 (2.0-4.0)	3.5 (2.5-4.0)	3.5 (2.5-4.0)	3.5 (2.0-4.0)	3.5 (1.5-4.0)	
		St. Jude	14	3.0 (2.0-4.0)	3.0 (2.0-4.0)	3.0 (2.0-4.0)	3.0 (2.0-4.0)	3.0 (1.5-4.0)	3.0 (2.5-4.0)	
	ON-X	Sorin	8	3.5 (2.5-4.0)	3.5 (2.5-4.0)	3.5 (2.5-4.0)	3.5 (2.5-4.0)	4.0 (2.5-4.0)	3.5 (3.0-4.0)	
		ON-X	7	3.5 (3.5-4.0)	3.5 (3.5-4.0)	3.5 (3.5-4.0)	4.0 (3.0-4.0)	4.0 (3.5-4.0)	4.0 (3.5-4.0)	
		Duromedics	1	3.0 (3.0-3.0)	2.0 (2.0-2.0)	2.5 (2.5-2.5)	3.0 (3.0-3.0)	3.0 (3.0-3.0)	2.5 (2.5-2.5)	
	Tilting disc (n = 20)	Medtronic Hall	13	3.0 (2.5-4.0)	3.0 (2.0-4.0)	3.5 (2.5-4.0)	3.0 (2.0-4.0)	3.0 (2.0-4.0)	3.0 (2.0-4.0)	
		Björk-Shiley	5	1.0 (1.0-1.0)	1.0 (1.0-1.0)	1.0 (1.0-1.0)	1.0 (1.0-1.0)	1.0 (1.0-1.0)	1.0 (1.0-1.0)	
		Sorin monoleaflet		2	1.0 (1.0-1.0)	1.0 (1.0-1.0)	1.0 (1.0-1.0)	1.0 (1.0-1.0)	1.0 (1.0-1.0)	1.0 (1.0-1.0)
			Perimount	13	3.5 (3.0-4.0)	3.5 (3.0-4.0)	4.0 (3.0-4.0)	4.0 (3.0-4.0)	2.0 (1.5-4.0)	3.0 (3.0-4.0)
		Medtronic intact	2	3.5 (3.0-4.0)	3.3 (3.0-3.5)	3.3 (2.5-4.0)	3.3 (2.5-4.0)	1.5 (1.0-2.0)	3.0 (2.5-3.5)	
Biological (n = 21)	Medtronic mosaic		2	4.0 (4.0-4.0)	3.8 (3.5-4.0)	3.8 (3.5-4.0)	3.8 (3.5-4.0)	2.5 (2.0-3.0)	3.8 (3.4-4.0)	
		Mitroflow	2	3.3 (3.0-3.5)	2.0 (2.0-2.0)	3.5 (3.0-4.0)	3.5 (3.0-4.0)	1.8 (1.5-2.0)	2.5 (2.0-3.0)	
	St. Jude Epic	1	3.5 (3.5-3.5)	3.5 (3.5-3.5)	3.5 (3.5-3.5)	3.5 (3.5-3.5)	1.5 (1.5-1.5)	3.0 (3.0-3.0)		
	Freestyle	1	4.0 (4.0-4.0)	4.0 (4.0-4.0)	4.0 (4.0-4.0)	4.0 (4.0-4.0)	2.0 (2.0-2.0)	4.0 (4.0-4.0)		

**Table 2** | Image quality (IQ) score specified per PHV design type

Type	N	Median IQ score (minimum-maximum)				General IQ score
		Supravalvular	Perivalvular	Subvalvular	Valvular	
Bileaflet	50	3.5 (2.0-4.0)	3.3 (2.0-4.0)	3.5 (2.0-4.0)	3.5 (1.5-4.0)	3.5 (2.5-4.0)
Tilting disc	20	3.0 (1.0-4.0)	2.5 (1.0-4.0)	2.8 (1.0-4.0)	2.5 (1.0-4.0)	2.8 (1.0-4.0)
Biological	21	3.5 (3.0-4.0)	3.5 (2.0-4.0)	4.0 (2.5-4.0)	2.0 (1.0-4.0)	3.0 (2.0-4.0)

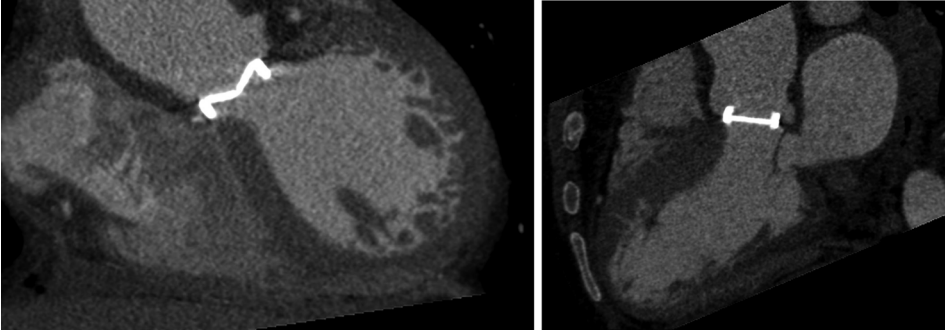


**Figure 5** | Carbomedics mechanical PHV in aortic position



**Figure 6** | Medtronic Hall mechanical PHV in mitral position

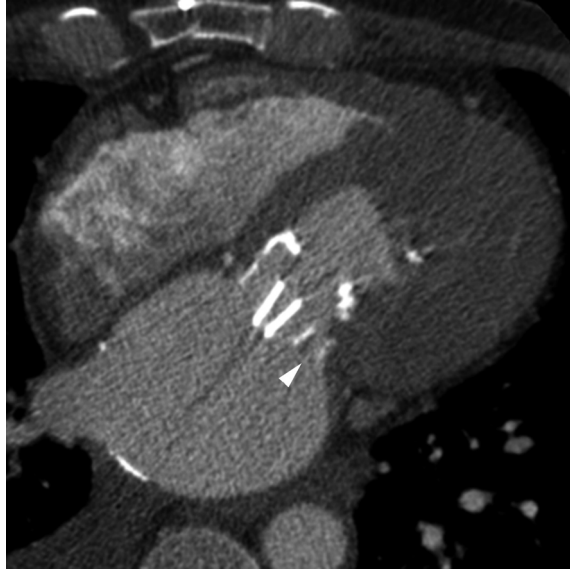


**Figure 7** | PHV dysfunction on MDCT. A St Jude PHV in the mitral position with a paravalvular leakage (arrowhead).

Furthermore, the use of different CT systems showed no significant differences for general image quality scores ( $p=0.889$ , 64 vs. 256-slice, 16-slice CT systems excluded from calculation because only 4 CT examinations available). Different CT protocols (aortic CTA vs dedicated cardiac CTA) demonstrated no significant difference in general image quality score ( $p=0.629$ ).

### **Interobserver variability**

The weighted kappa value for the image quality scores of both observers was 0.79 with a standard error of 0.10. This indicates a good interobserver agreement.

## **DISCUSSION**

The principal results of this study are: (1) currently implanted PHVs and the periprosthetic region can be visualized with at least a good image quality by MDCT; (2) Björk-Shiley and Sorin monoleaflet tilting disc valves have significantly lower image quality than other PHV and demonstrate severe artifacts which preclude diagnostic assessment.

TTE, TEE and fluoroscopy are the primary non or limited-invasive imaging modalities used for PHV assessment.<sup>1</sup> Echocardiography provides both anatomical and functional information. Fluoroscopy provides information on the leaflet motion in patients with a mechanical PHV only. These imaging techniques are suitable to detect PHV dysfunction, but may fail to detect the pathologic anatomical substrate, especially if this is pannus tissue.<sup>2</sup> Girard et al.<sup>2</sup> evaluated a total of 92 patients that underwent reoperation for prosthetic aortic valve obstruction: 49 mechanical and 43 biological PHVs. In the mechanical PHV group, the mechanism of obstruction (pannus, thrombosis and PPM) was correctly identified by TTE and TEE in 5/49 (10%) and 17/35 (49%) of cases, respectively. In the biological PHV group, the mechanism of aortic valve obstruction was correctly diagnosed in 27/43 63% (TTE) and 21/26 81% (TEE) of the cases, respectively. These

findings illustrate that a conventional work-up of PHV dysfunction with echocardiography fails to detect the cause of dysfunction in up to 51% of mechanical PHVs.

MDCT is emerging as a new diagnostic modality to evaluate PHV dysfunction. Figure 7 illustrates the potential diagnostic potential of MDCT in visualizing PHV dysfunction.

We previously reported our findings in 13 patients with 15 mechanical heart valves. MDCT imaging provided additional diagnostic findings to echocardiography and fluoroscopy in 9 of 13 patients (69%).<sup>4</sup> MDCT is especially suitable to visualize pannus formation.<sup>5</sup> Our findings are supported by other groups. Tsai et al.<sup>6</sup> reported on 25 patients with 31 PHVs evaluated by TTE and MDCT. In 6 patients who underwent reoperation, MDCT findings were confirmed by intraoperative surgical findings. The image quality of PHVs was good, except for one Björk-Shiley tilting disc valve. In this prospective study diagnostic evaluation with TEE and fluoroscopy were lacking. Because some PHV types present with severe artifacts on CT, it is important to determine which PHV types are suitable for CT assessment. Data concerning the CT compatibility of PHV are scarce. Konen et al.<sup>3</sup> assessed leaflet motion in 20 patients with 23 PHVs using a 40- or 64-MDCT. This study included 18 bileaflet and 5 tilting disc valves. The image quality of the bileaflet mechanical valves was good to excellent whereas the image quality of the tilting disc valves (Björk-Shiley and Sorin monoleaflet PHVs) was significantly lower. In only two out of the five tilting disc valves the opening and closing angles could be measured. Tsai et al.<sup>6</sup> evaluated two tilting disc valves (Medtronic Hall and Björk-Shiley tilting disc) and found severe artifacts in the Björk-Shiley valve precluding diagnostic assessment. In our article titled "Multidetector-row computed tomography imaging characteristics of mechanical prosthetic valves" accepted for publication in the *Journal of Heart Valve Disease*, we examined the CT imaging characteristics of 5 different PHV types in a strictly controlled in vitro test set-up with valve leaflet motion but no annular motion. In this study modern PHVs manufactured of carbon and titanium (St Jude, ON-X, Medtronic Hall, Carbomedics) showed a good image quality. The Björk-Shiley valve, made of a cobalt chrome alloy, exhibited severe artifacts. Within the carbon titanium group, the Carbomedics and ON-X valve scored better than the St Jude and Medtronic Hall valves. These differences were attributed to valve design. Although this study demonstrated the suitability of CT for the assessment of PHV, the clinical application of CT could well be compromised by motion artifacts and rhythm irregularities. The current study was undertaken to systematically examine the clinical performance of CT, and, to our knowledge, is the largest series of PHVs assessed by CT described to date.

In addition to the 5 PHVs tested in vitro, we currently evaluated 9 additional PHV types covering a whole range of mechanical and biological PHVs. For the mechanical PHVs, our findings reflected the in vitro experience: we found that the Medtronic Hall valve had a significantly better image quality than Björk-Shiley and Sorin tilting disc valves. Furthermore, the Carbomedics and ON-X valves had a better image quality than the St Jude and Medtronic Hall valves (Table 1). However, this finding was not significant. This discrepancy in image quality can be related to the differences in PHV design. The assessment of the Björk-Shiley and the Sorin monoleaflet tilting disc valves resulted in non-diagnostic image quality of all scoring regions due to severe artifacts. These artifacts are the result of the presence of cobalt in the valve housing and strut mechanism. In clinical practice, these cobalt containing PHVs are not suitable for evaluation with MDCT.<sup>3,4,6</sup> All currently implanted mechanical PHVs can be assessed by MDCT because they are all manufactured of titanium and carbon.

The biological PHVs show a good image quality except for valvular detail. We scored diastolic images and found that the leaflets of several bioprostheses could not be identified properly. We postulate that the limitations in spatial and temporal resolution of the CT may preclude good



image quality in bioprostheses with thin leaflets (porcine aortic valve leaflets). Our results were less promising than a recent report from Chenot et al.<sup>7</sup> that demonstrated the feasibility of planimetric measurement of the orifice area of biological prostheses. The primary cause for this disparity may well be that our series was purely retrospective and that not all scans were specifically made for imaging of the bioprosthesis. Six of the 21 (29%) biological PHVs were examined using a CT protocol for aortic imaging that uses a lower mAs setting which may have hampered the visualization of the valve leaflets. The differences in contrast and imaging protocols may have resulted in a superior image quality in Chenot's series. Furthermore, Chenot et al.<sup>7</sup> identified several modes of biological PHV dysfunction such as leaflet thickening, calcification and possible thrombus. Leaflet thickening is likely to make the leaflets more easily discernable on CT. However, the retrospectively ECG-gated scans that allow for dynamic assessment of PHV are associated with a relative high radiation dose. Lower dose PHV CT protocols are currently being explored.<sup>8</sup>

Continued efforts for large scale prospective studies are required to further determine (1) normal MDCT characteristics of commonly implanted PHV types, (2) the exact additional diagnostic value of MDCT in evaluation of PHV dysfunction, (3) and the best imaging protocols for PHV with special attention to dose reduction.

### **Limitations**

The study has a retrospective study design. In addition to dedicated cardiac CT, 18 ECG-gated aortic CT studies with a lower mAs setting were included. The lower mAs setting may have negatively influenced image quality. However, the aortic scan protocol was not associated with a significant lower image quality score. Some PHVs were present in small numbers. However, MDCT scans of the currently most commonly implanted PHVs (Carbomedics, St Jude, ON-X, Sorin and Perimount) were available for at least 7 valves each. Despite a mean heart rate of 58 bpm during scanning there was a relatively wide range (48-139) of heart rates. Although heart rates were not significantly correlated with a lesser CT image quality in our series, motion artifacts at higher heart rates may decrease image quality. In addition, aggressive heart rate lowering using  $\beta$ -blockers during scanning is contraindicated in some PHV patients as they may have poor left ventricular function and conduction abnormalities.

Although no correlation between image quality and heart rate, type of CT system and CT protocol were found, it should be noted that this retrospective study was not specifically designed for this.

## **CONCLUSION**

MDCT is a promising imaging technique to evaluate PHV dysfunction. Currently implanted PHVs generate only limited artifacts and are suitable for evaluation with MDCT. CT assessment of Björk-Shiley and Sorin monoleaflet tilting disc PHVs is hampered by severe artifacts.

## REFERENCES

1. Zoghbi WA, Chambers JB, Dumesnil JG, et al. Recommendations for evaluation of prosthetic valves with echocardiography and doppler ultrasound: a report From the American Society of Echocardiography's Guidelines and Standards Committee and the Task Force on Prosthetic Valves, developed in conjunction with the American College of Cardiology Cardiovascular Imaging Committee, Cardiac Imaging Committee of the American Heart Association, the European Association of Echocardiography, a registered branch of the European Society of Cardiology, the Japanese Society of Echocardiography and the Canadian Society of Echocardiography, endorsed by the American College of Cardiology Foundation, American Heart Association, European Association of Echocardiography, a registered branch of the European Society of Cardiology, the Japanese Society of Echocardiography, and Canadian Society of Echocardiography. *J Am Soc Echocardiogr.* 2009; 22:975-1014.
2. Girard SE, Miller FA, Jr., Orszulak TA, et al. Reoperation for prosthetic aortic valve obstruction in the era of echocardiography: trends in diagnostic testing and comparison with surgical findings. *J Am Coll Cardiol.* 2001; 37:579-584.
3. Konen E, Goitein O, Feinberg MS, et al. The role of ECG-gated MDCT in the evaluation of aortic and mitral mechanical valves: initial experience. *Am J Roentgenol* 2008; 191:26-31.
4. Symersky P, Budde RP, de Mol BA, et al. Comparison of multidetector-row computed tomography to echocardiography and fluoroscopy for evaluation of patients with mechanical prosthetic valve obstruction. *Am J Cardiol* 2009; 104:1128-1134.
5. Teshima H, Hayashida N, Fukunaga S, et al. Usefulness of a multidetector-row computed tomography scanner for detecting pannus formation. *Ann Thorac Surg.* 2004; 77:523-526.
6. Tsai IC, Lin YK, Chang Y, et al. Correctness of multi-detector-row computed tomography for diagnosing mechanical prosthetic heart valve disorders using operative findings as a gold standard. *Eur Radiol* 2009; 19:857-867.
7. Chenot F, Montant P, Goffinet C, et al. Evaluation of anatomic valve opening and leaflet morphology in aortic valve bioprosthesis by using multidetector CT: comparison with transthoracic echocardiography. *Radiology* 2010; 255:377-385.
8. Symersky P, Budde RP, Prokop M, et al. Abstract 541: Prosthetic Valve Evaluation Using Prospective Triggering With 256-Detector Row Computed Tomography Reduces Radiation Dose. *Circulation* 2009; 120:S355.



# CHAPTER XI

## CT ATTENUATION MEASUREMENTS *are* VALUABLE *to* DISCRIMINATE PTFE FELT PLEDGES *used in* PROSTHETIC HEART VALVE IMPLANTATION *from* PARAVALVULAR LEAKAGE

J. Habets  
T.S. Meijer  
R.C.A. Meijer  
W.P.Th.M. Mali  
E.P.A. Vonken  
R.P.J. Budde

**ABSTRACT**

**OBJECTIVES** | Sutures with polytetrafluorethylene (PTFE) felt pledgets are commonly used in prosthetic heart valve (PHV) implantation. Paravalvular leakage can be difficult to distinguish from PTFE felt pledgets on multislice CT because both present as hyperdense structures. We assessed if pledgets can be discriminated from contrast-enhanced solutions (blood/saline) on CT images based on attenuation difference in an ex-vivo experiment and under in vivo conditions.

**METHODS** | PTFE felt pledgets were sutured to the suture ring of a mechanical PHV and porcine aortic annulus and immersed and scanned in four different contrast-enhanced (Ultravist<sup>®</sup> - 300mg jopromide/ml) saline concentrations (10.0,12.0,13.6 and 15.0 mg/ml). Scanning was performed on a 256-slice scanner with eight different scan protocols with various kV (100,120) and mAs (400,600,800,1000) settings. Attenuation of the pledgets and surrounding contrast-enhanced saline were measured. Additionally, the attenuation of pledgets and contrast-enhanced blood was measured on ECG-gated CTA scans of 19 patients with 22 PHVs.

**RESULTS** | Ex-vivo CT attenuation differences between the pledgets and contrast-enhanced solutions were larger by using higher tube voltages. CT attenuation values of the pledgets were higher than contrast-enhanced blood in patients:  $420 \pm 26$  Hounsfield units (mean $\pm$ SD, range 383–494) and  $288 \pm 41$  Hounsfield units (range 202–367), respectively.

**CONCLUSIONS** | PTFE felt pledgets have consistently higher attenuation than surrounding contrast-enhanced blood. This may help to clinically differentiate pledgets from paravalvular leakage.

**ADVANCES IN KNOWLEDGE** | CT attenuation measurements may help to detect paravalvular leakage in patients with suspected PHV dysfunction

In 2003, approximately 290,000 patients underwent prosthetic heart valve (PHV) implantation worldwide.<sup>1</sup> During PHV implantation, the affected native valve is excised and replaced by a mechanical or biological PHV. The PHV is fixated by sutures that are placed through the suture ring of the PHV and the aortic or mitral annulus. To prevent the suture from being pulled through the annular tissue, polytetrafluoroethylene (PTFE) pledged sutures are commonly used. These sutures have a PTFE absorbent pad, attached to the suture which disperses the pressure of the single suture on the annulus.<sup>2,3</sup>

Paravalvular leakage, defined as blood flow outside the suture ring through the annulus, is a relatively common echocardiographic finding after PHV implantation.<sup>4</sup> Paravalvular leakage is reported in up to 15% of patients after mitral valve replacement (MVR) and in up to 10% of patients after aortic valve replacement (AVR).<sup>5-7</sup> Paravalvular leakage is mainly caused by (1) incomplete apposition of the PHV suture ring to the native annular tissue, (2) suture dehiscence or rupture, or (3) infective PHV endocarditis.<sup>8</sup> Paravalvular leakage is one of the most common causes for reoperation after PHV implantation.

In daily clinical routine, suspected PHV dysfunction is evaluated by transthoracic and transesophageal echocardiography (TTE and TEE). TTE is the first line imaging method to detect paravalvular leakage. In patients with acoustic shadowing caused by the PHV material, TEE can be of additional diagnostic value especially for valves in the mitral position.

Multidetector-row computed tomography (MDCT) has recently been shown to have complementary value to echocardiography to evaluate PHV dysfunction.<sup>9,10</sup> Paravalvular leakage is visualized on MDCT as contrast-enhanced blood next to the valve prosthesis at the level of the annulus. In our experience, it can be difficult to differentiate paravalvular leakage from the PTFE felt pledgets on CTA scans, because of the similar location and hyperdense appearance. Thus diagnostic dilemmas may arise. Additional non-contrast enhanced scans may help to differentiate paravalvular leakage from pledgets, but has the disadvantage of additional radiation exposure.

Currently no data are available on the normal MDCT imaging characteristics of PTFE felt pledgets. The purpose of this study was (1) to determine normal MDCT imaging characteristics of PTFE felt pledgets both ex-vivo and in vivo and (2) to examine the possibility to distinguish PTFE felt pledgets from contrast-enhanced blood (paravalvular leakage) based on the level of Hounsfield units (HU).

## MATERIALS AND METHODS

To determine the CT attenuation level of the contrast required for the conduction of the ex-vivo experiment, the CT attenuation value of contrast-enhanced blood was measured in routine cardiac ECG-gated CT angiography (CTA) scans of 50 patients including both coronary CTAs and CTAs for aortic aneurysm assessment. CT attenuation of contrast-enhanced blood was measured in the left atrium, left ventricle and proximal ascending aorta. For each patient, the mean of these three measurements was calculated.

### **Ex-vivo imaging**

A cardiothoracic surgeon (RM) implanted an ON-X (MRCI, Austin, TX, USA) mechanical prosthetic valve in the aortic position in an ex-vivo porcine heart. The porcine cardiac tissue was acquired from the butcher. No permission by the animal ethical committee was required. The native valve leaflets were excised. The annulus was encircled with multiple interrupted pledged mattress



**Figure 1** | Image of an ON-X valve (ON-X Life Technologies Inc., Austin, TX, USA), implanted in a porcine heart with PTFE felt pledgets at the ventricular side of the suture ring.

sutures (2-0 Ticron 8x30" 75-cm Y-31 tapercutting, double armed with 7x3x1.5-mm PTFE pledget, Synature™ Covedien, Mansfield, MA). Pledgets were positioned at the ventricular side of the porcine annulus. Most of the adjacent cardiac tissue was excised leaving the aortic root and periannular myocardial tissue (Figure 1). The implanted valve was suspended in a paper cup containing contrast-enhanced saline solutions (10.0, 12.0, 13.6 and 15.0 mg/ml iodine) and scanned. Several supporting sutures prevented contact between the cardiac tissue and the bottom of the cup. CT attenuation of the pledgets was measured at five separate points in various pledgets. The attenuation of contrast-enhanced saline was measured at five separate points in the surroundings of the pledgets. The location of these five separate points was selected by the single observer (TSM).

### MDCT scanner parameters

Ex-vivo imaging was performed on a 256-slice CT scanner (Brilliance iCT, Philips Healthcare, Best, the Netherlands). Various scan parameters were used; two tube voltage settings (100 and 120 kV) and four tube current settings (400, 600, 800 and 1000 mAs) resulting in a total of eight combinations of kV and mAs. Scanning was based on a retrospectively ECG-gated acquisition. Other scan settings were: slice collimation 128x0.625mm; gantry rotation time 0.33s; matrix size of 512 x 512 pixels and pitch 0.18. An ECG-signal was continuously simulated with a frequency of 60 beats per minute to enable ECG-gated scanning (Medi Cal Instruments Inc., Model 430B, 12 Lead ECG Simulator, Lewis Center, OH).

### In vivo imaging

All ECG-gated MDCT scans of patients who had underwent PHV implantation with pledgets were selected from the PHV ECG-gated CTA database in our hospital. These scans were performed with a dedicated cardiac CT protocol; 120kV, 400-600mAs, pitch 0.16-0.18, slice thickness 0.9mm, collimation 64-128x0.625, gantry rotation 0.27-0.40 and matrix 512x512 or aortic CT angiography protocol; 120kV, 200-250mAs, pitch 0.25-0.30, collimation 64-128x0.625, gantry rotation 0.27-0.40 and matrix 512x512 on a 256 slice or 64 slice CT scanner.

Intravenous contrast (Ultravist® - 300mg jopromide/ml, Bayer Schering Pharma AG, Berlin, Germany) was administered. A three phase contrast injection protocol was used for the dedicated

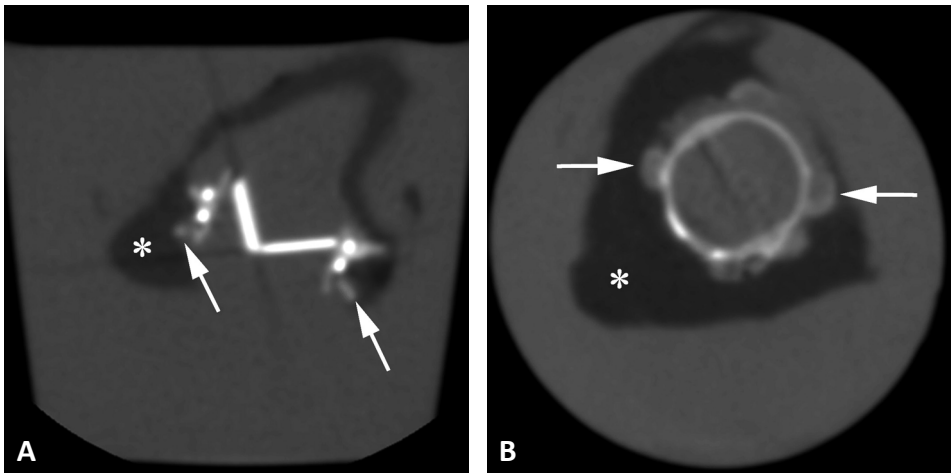


**Figure 2** | **A** | CT image reconstruction of the valve implanted in the aortic porcine annulus perpendicular to the valve leaflets. **B** | CT image reconstruction of the valve in plane with valve leaflets. Note the pledgets are visualized as hyperdense structures (arrows), with at one side the hypodense myocardial tissue (\*), and at the other side the more hyperdense ring of the ON-X valve.

cardiac scans. The protocol started with 100% contrast injection (phase 1), followed by a 30%/70% contrast/saline mixture and finally a saline flush. The volumes were adjusted for the patients body weight with an iodine flow of 1.6 gram/sec for patients <70kg, 1.8gram/sec for patients 70-85kg and 2.0gram/sec for patients >85kg. For the aortic CTAs, a fixed bolus of 100cc contrast followed by a 50ml saline flush was administered. In general, injection flow rates were set at 5-6ml/sec. A trigger was placed in the aorta which monitored until the HU level reached the predefined 100 HU threshold. After reaching the threshold, the scan was started automatically. Patient and specific valve data were collected from the medical files. Heart rate during the CT scan was recorded from the CT data. The study was performed under a waiver from the institutional reviewing board.

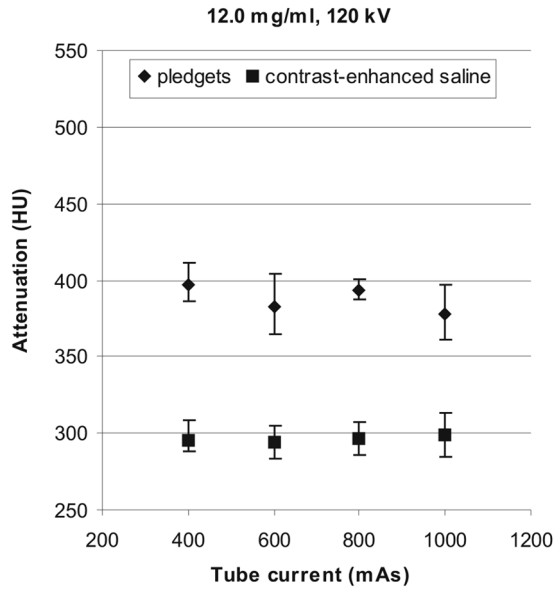
### Image Analysis

Image analysis was performed on a dedicated workstation (Philips Extended Brilliance Workspace, Philips Healthcare, Best, the Netherlands). CT attenuation values were determined using the cursor available in the analysis software. All measurements in the ex-vivo experiment were done by a single

**Table 1** | Mean CT attenuation differences (in HU) measured in the pledgets and the surrounding contrast-enhanced fluid. For the ex-vivo experiment, attenuation differences were calculated for the four contrast-enhanced saline solutions at 120 kV and 100 kV. Since tube current did not significantly affect the attenuation level, the means for the various currents were pooled. In vivo CT attenuation measurements were done in CT scans performed with 120kV

	Tube voltage (kV)	10.0mg/ml	12.0mg/ml	13.6mg/ml	15.0mg/ml
Ex-vivo experiment*	120	112	92	79	73
	100	87	55	42	29
In vivo measurements	120	132			

\* Prosthetic heart valve in porcine aortic annulus



**Figure 3** | Box plot with range bars. This figure shows the mean attenuation of PTFE felt pledgets and contrast-enhanced saline surrounding the pledgets in the ex-vivo experiment (PHV with pledgets surrounded by porcine cardiac tissue). Attenuation values measured in solution 12.0mg/ml, scanned at 120 kV. Note, there is no overlap between the ranges of the mean attenuation value of the pledgets and the surrounding fluid.

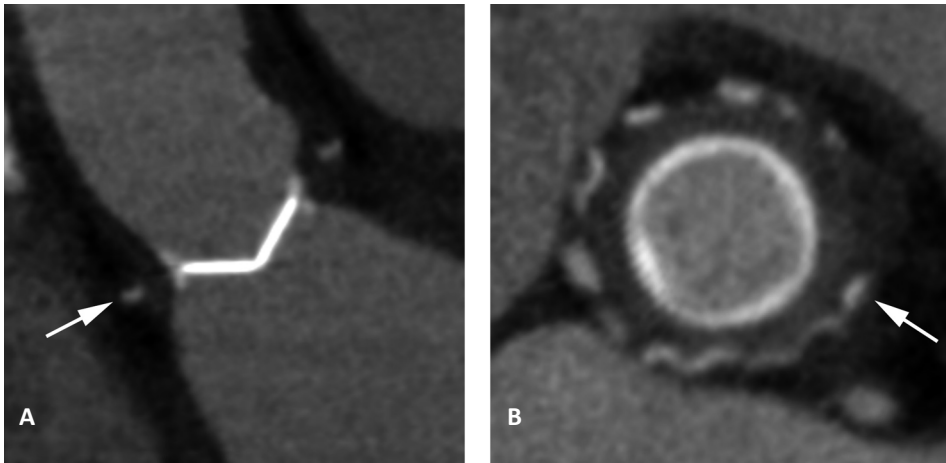


**Figure 4** | In vivo images of a St. Jude mechanical bileaflet PHV (St. Jude Medical Inc., St. Paul, MN, USA), implanted in the aortic position with PTFE felt pledgets (arrows). **A** | CT image reconstruction of the valve perpendicular to the valve leaflets. **B** | CT image reconstruction of the valve in plane (short axis view).

observer (TSM). Center- and window level settings were visually adjusted before each measurement to optimally visualize and measure the attenuation of the pledget. In the in vivo scans, CT attenuation of pledgets and contrast-enhanced blood surrounding the pledgets were measured for each PHV at five different points (in different pledgets) by a single observer (JH). The five different pledgets were randomly selected by the single observer (JH).



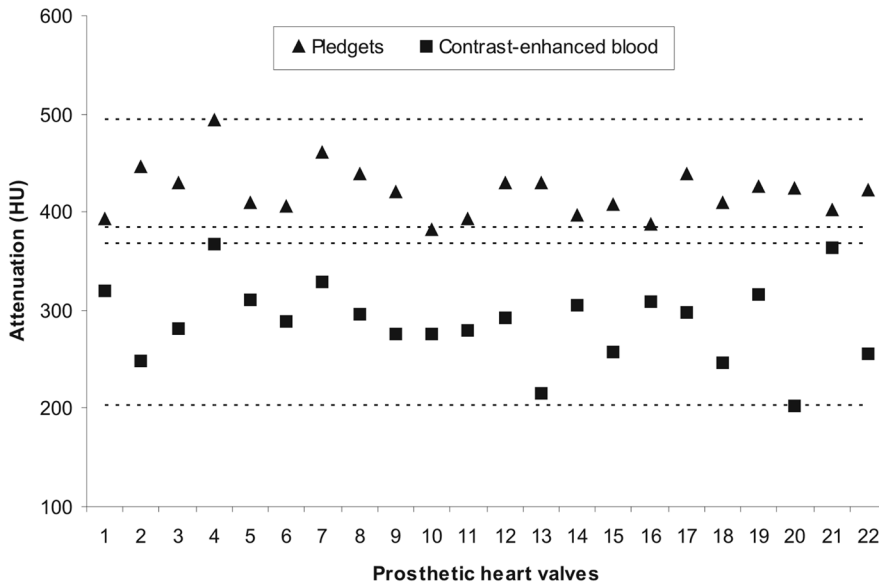


**Figure 5** | CT attenuation of PTFE felt pledgets and contrast-enhanced blood in patients who underwent PHV implantation. The two dotted lines show the range for the pledgets and the contrast-enhanced blood that was determined for all valves as a group. The attenuation of pledgets and contrast-enhanced blood for all PHVs, was  $420 \pm 26$  HU (range 383–494), and  $288 \pm 41$  HU (range 202–367), respectively. Note that the ranges show no overlap.

### Statistical analysis

Statistical analyses were performed using SPSS software (SPSS Statistics version 15.0, SPSS Inc, Chicago, IL). CT attenuation values were expressed as mean  $\pm$  SD with a range (minimal and maximal value). To compare in vivo CT attenuation of the pledgets and the contrast-enhanced blood a paired student T test was performed. A *p*-value of  $< 0.05$  was considered statistically significant.

## RESULTS

Fifty ECG-gated CTA scans with different tube voltages (100kV  $n=23$ ; 120kV  $n=27$ ) were analyzed. Mean attenuation values for contrast-enhanced blood in the scans performed with 100 kV and 120 kV, were  $434 \pm 69$  HU and  $306 \pm 43$  HU, respectively.

### Ex-vivo imaging

No substantial artifacts were generated by the PHV. Pledgets presented as hyperdense structures (Figure 2). In all scan settings, the attenuation of the pledgets was consistently higher than the attenuation of the surrounding contrast-saline solution (Table 1).

In the 12.0 mg/ml contrast-enhanced saline solution, scanned with 120 kV, the mean attenuation was  $296 \pm 2$  HU (range 294–296) for the contrast-enhanced solution, and  $388 \pm 9$  HU (377–397) for the pledgets (Figure 3). This attenuation value for the contrast-enhanced solution approximates the attenuation of contrast-enhanced blood measured in the cardiac CTA scans, performed with 120 kV, the most. At 100kV, the mean attenuation was  $431 \pm 3$  HU (range 429–435) for the 15.0mg/ml contrast-enhanced saline solution, and  $460 \pm 4$  HU (455–464) for the pledgets.

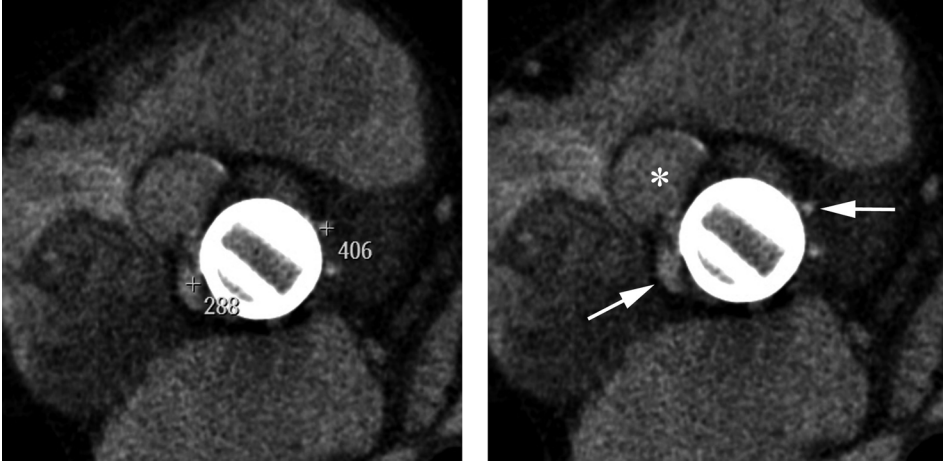


**Figure 6** | In vivo images of a Carbomedics bileaflet mechanical prosthetic heart valve (Carbomedics Inc, Austin, TX) implanted in the aortic position with PTFE felt pledgets (right panel; right arrow) and paravalvular leakage (right panel; \* and left arrow). The paravalvular leak was proven echocardiographically. Left panel) CT attenuation measurement of both the pledget (406 HU) and the paravalvular leakage (288 HU) indicating the difference in Hounsfield units. Right panel) CT image reconstruction of the valve in plane (short axis view)

### In vivo imaging

Nineteen patients with 22 PHVs (seventeen mechanical PHVs and five biological PHVs) were available for analysis. The mechanical PHV group included 15 bileaflet PHVs (including six Carbomedics PHVs, four St Jude PHVs, three Sorin PHVs and two ON-X PHVs) and two Medtronic Hall tilting disc PHVs. The PHVs were located in the aortic ( $n=13$ ), mitral ( $n=7$ ), pulmonary ( $n=1$ ) and the tricuspid ( $n=1$ ) position. MDCT scans were performed on a 256 slice ( $n=15$ ) or 64 slice scanner ( $n=2$ ) with a dedicated cardiac CT protocol ( $n=15$ ) or aortic CTA protocol ( $n=4$ ). Mean heart rate during the CT scan was  $72 \pm 18$  beats per minute (mean  $\pm$  SD). The pledgets presented as hyperdense structures in all patients (Figure 4). The mean attenuation values of pledgets and contrast-enhanced blood that we measured in 22 PHVs, were  $420 \pm 26$  HU (range 383–494) and  $288 \pm 41$  HU (range 202–367), respectively (Figure 5 and 6). CT attenuation of pledgets was significantly higher (mean difference of  $132 \pm 51$  HU,  $p < 0.001$ ) than the contrast-enhanced blood without an overlap in attenuation values.

## DISCUSSION

The principal finding of the study is that PTFE felt pledgets have a consistently higher CT attenuation than contrast-enhanced blood in patients after PHV implantation. In our study, the ex-vivo experiments demonstrated the same findings.

Although echocardiography is the gold standard for the evaluation of PHV dysfunction including paravalvular leakage, MDCT evaluation of patients with suspected PHV dysfunction has complementary diagnostic value.<sup>9,10</sup> Furthermore, MDCT offers anatomic information valuable for the surgical planning, e.g. the presence of coronary artery disease and volume rendered three-dimensional images of the affected cardiac region in case of reoperation. The clinical value of MDCT for the detection of paravalvular leakage remains unclear. This study demonstrates that the differentiation between contrast-enhanced blood (appearance of paravalvular leakage on MDCT)

and PTFE pledgets may be possible based on CT attenuation measurements (Figures 5 and 6). This contributes to making the correct diagnosis of paravalvular leakage on MDCT scans.

In both the *ex vivo* experiment and *in vivo* measurements, the pledgets were visualized as hyperdense structures. The mean attenuation value of the pledgets was consistently higher than the mean attenuation value of the contrast-enhanced fluid/blood surrounding the pledgets. Moreover, the ranges of the attenuation of the pledgets and the contrast-enhanced fluid showed no overlap (Figures 3 and 5). With a difference of approximately 130 HU, pledgets were generally well differentiated from the contrast-enhanced blood in patients who underwent mechanical PHV implantation and scanned with 120 kV.

Our *in vivo* results suggest that CT attenuation measurements with a value above 380 HU excludes the presence of paravalvular leakage in patients scanned with a tube voltage of 120kV. This attenuation difference between contrast-enhanced blood and the pledget is important because of the potential ability to distinguish paravalvular leakage from PTFE pledgets based on straightforward HU measurements. However, these HU values are only applicable for the specific CTA protocol applied in our patients. In clinical practice, the attenuation value for PTFE felt pledgets and contrast-enhanced blood depends on the contrast protocol which is applied.

### **Limitations**

This study has several limitations. First, in this study the *ex vivo* experiment was conducted under static conditions. The possible effects of annular and valvular motion on the assessment of CT attenuation of the pledgets were not taken into account. However, attenuation measurements were performed in patients scanned under dynamic conditions. The reconstruction phase with the least amount of motion artifacts was selected to perform CT attenuation measurements. In this selected imaging phase, attenuation measurements were easy to perform.

Another limitation of this study is the use of only one mechanical PHV type in the *ex vivo* experiment. The ON-X valve causes less artifacts than other valve types resulting in a better periprosthetic image quality. However, measurements in patients were done in CT images of nine different PHV types. Most PHV types did not generate extensive artifacts which are likely to affect pledget attenuation measurements except for the Björk-Shiley tilting disc valve. This valve type prohibits assessment of the periprosthetic anatomy due to severe artifacts.<sup>11</sup> Björk-Shiley tilting disc valves were not included in the *in vivo* measurements. A previous study demonstrated that the periprosthetic image quality of most commonly implanted PHVs is good which enables clinical application of the attenuation measurements.<sup>11</sup> To determine the diagnostic value of MDCT in the detection of paravalvular leakages, prospective studies should be performed comparing MDCT with echocardiography.

## **CONCLUSION**

PTFE felt pledgets present with a consistently higher CT attenuation values than contrast-enhanced blood using our specific CT scan protocol. In clinical practice, this attenuation difference can help to distinguish paravalvular leakage from PTFE felt pledgets on CT scans.

## REFERENCES

1. Yacoub MH, Takkenberg JJ. Will heart valve tissue engineering change the world? *Nat Clin Pract Cardiovasc Med* 2005; 2:60-61.
2. Newton JR Jr., Glower DD, et al. Evaluation of suture techniques for mitral valve replacement. *J Thorac Cardiovasc Surg* 1984; 88:248-252.
3. Gago O, Kirsh MM. A new technique for cardiac valve replacement. *Chest* 1972; 61:674-675.
4. Rallidis LS, Moyssakis IE, Ikonomidis I, et al. Natural history of early aortic paraprosthesis regurgitation: a five-year follow-up. *Am Heart J* 1999; 138:351-357.
5. Piechaud JF. Percutaneous closure of mitral paravalvular leak. *J Interv Cardiol* 2003; 16:153-155.
6. Ionescu A, Fraser AG, Butchart EG. Prevalence and clinical significance of incidental paraprosthesis valvar regurgitation: a prospective study using transoesophageal echocardiography. *Heart* 2003; 89:1316-1321.
7. Genoni M, Franzen D, Vogt P, et al. Paravalvular leakage after mitral valve replacement: improved long-term survival with aggressive surgery? *Eur J Cardiothorac Surg* 2000; 17:14-19.
8. Piechaud JF. Percutaneous closure of mitral paravalvular leak. *J Interv Cardiol* 2003; 16:153-155.
9. Habets J, Budde RP, Symersky P, et al. Diagnostic evaluation of left-sided prosthetic heart valve dysfunction. *Nat Rev Cardiol* 2011; 8:466-478.
10. Tsai IC, Lin YK, Chang Y, et al. Correctness of multi-detector-row computed tomography for diagnosing mechanical prosthetic heart valve disorders using operative findings as a gold standard. *Eur Radiol* 2009; 19: 857-867.
11. Habets J, Symersky P, van Herwerden LA, et al. Prosthetic heart valve assessment with multidetector-row CT: imaging characteristics of 91 valves in 83 patients. *Eur Radiol* 2011; 21:1390-1396.



CHAPTER XII

CORONARY ARTERY  
ASSESSMENT *with*  
MULTIDETECTOR COMPUTED  
TOMOGRAPHY *in* PATIENTS *with*  
PROSTHETIC HEART VALVES

J. Habets  
R.B.A. van den Brink  
R. Uijlings  
A.M. Spijkerboer  
W.P.Th.M. Mali  
S.A.J. Chamuleau  
R.P.J. Budde

**ABSTRACT**

**OBJECTIVES** | Patients with prosthetic heart valves may require assessment for coronary artery disease. We assessed whether valve artifacts hamper coronary artery assessment by multidetector CT.

**METHODS** | ECG-gated or -triggered CT angiograms were selected from our PACS archive based on the presence of prosthetic heart valves. The best systolic and diastolic axial reconstructions were selected for coronary assessment. Each present coronary segment was scored for the presence of valve-related artifacts prohibiting coronary artery assessment. Scoring was performed in consensus by two observers.

**RESULTS** | Eighty-two CT angiograms were performed on a 64-slice ( $n=27$ ) or 256-slice ( $n=55$ ) multidetector CT. Eighty-nine valves and five annuloplasty rings were present. Forty-three out of 1160 (3.7%) present coronary artery segments were non-diagnostic due to valve artifacts (14/82 patients). Valve artifacts were located in right coronary artery (15/43; 35%), left anterior descending artery (2/43; 5%), circumflex artery (14/43; 32%) and marginal obtuse (12/43; 28%) segments. All cobalt-chrome containing valves caused artifacts prohibiting coronary assessment. Biological and titanium-containing valves did not cause artifacts except for three specific valve types.

**CONCLUSIONS** | Most commonly implanted prosthetic heart valves do not hamper coronary assessment on multidetector CT. Cobalt-chrome containing prosthetic heart valves preclude complete coronary artery assessment because of severe valve artifacts.

**Keypoints**

- Most commonly implanted prosthetic heart valves do not hamper coronary artery assessment
- Prosthetic heart valve composition determines the occurrence of prosthetic heart valve-related artifacts
- Björk–Shiley and Sorin tilting disc valves preclude diagnostic coronary artery segment assessment

The introduction of ECG-gated and triggered multidetector computed tomography (MDCT) technology has resulted in new diagnostic cardiac applications, most noticeably coronary artery assessment.<sup>1</sup> Recently, MDCT has also shown potential for the evaluation of prosthetic heart valve (PHV) (dys)function by providing complementary diagnostic information to echocardiography and fluoroscopy, especially in patients with suspected PHV obstruction and PHV endocarditis.<sup>2-6</sup>

Besides evaluation of the exact cause of PHV dysfunction, MDCT may have complementary clinical value for the surgical planning in patients considered for reoperation after previous PHV implantation. MDCT can be used to evaluate the presence of coronary artery disease (CAD) and the patency of present bypass grafts to serve as an alternative for classical coronary angiography, and the distance between the sternum and the right ventricle can be measured.<sup>7</sup> Patients with a normal functioning PHV may also be candidates for CT assessment of the coronary arteries in newly developed angina.

Each PHV type has its own specific imaging characteristics on CT.<sup>8,9</sup> Most PHVs have limited artifacts but at present little is known about which PHV types and positions induce artifacts to such an extent that they prohibit coronary assessment on MDCT. Knowledge of which PHV types and positions prohibit coronary assessment is clinically important to determine whether adequate CT assessment of coronary segments is to be expected or that the patient should be referred for conventional coronary angiography straight away. The purpose of this study was to determine which PHV types induce artifacts that hamper coronary artery segment assessment on MDCT in a cohort of patients with a PHV in whom an ECG-gated or -triggered PHV had been performed.

## MATERIALS AND METHODS

### CT angiogram selection

We reviewed all ECG-gated or prospectively triggered PHV CT angiograms (CTAs) performed in the University Medical Center Utrecht and Academic Medical Center Amsterdam between 2003 and September 2011 for the presence of PHVs that were imaged in both systolic and diastolic phase. We excluded CTAs that included only systolic or diastolic imaging, were performed on 16-slice MDCT, non-contrast enhanced imaging as well as CTAs in patients enrolled in an ongoing prospective diagnostic cross-sectional study on CT PHV assessment. Furthermore, patients with multiple CTA examinations were included only once. Patients with a concomitant mitral or tricuspid annuloplasty ring were included.

CTAs were performed on 64 or 256 slice MDCT systems (Brilliance 64 and iCT, Philips Medical Systems, Cleveland, Ohio). Contrast agents [Ultravist (iopromide) - 300mg I/mL, Bayer Schering Pharma AG, Berlin, Germany or Iomeron (iomeprol) - 400mg I/mL, Bracco UK Limited, London, United Kingdom] were administered in all patients. Cardiac CTAs were performed with a triphasic or dual phasic contrast injection protocol. The triphasic protocol started with a 100% contrast injection (phase 1) followed by a 30%/70% contrast/saline mixture (phase 2), and concluded with a saline flush (phase 3). Contrast volumes were adjusted for the patients body weight with an iodine flow of 1.6gram/second for patients <70 kilogram (kg), 1.8gram/second for patients 70-85kg and 2.0gram/second for patients >85kg. The dual phase contrast protocol consisted of a contrast injection of 100 millilitre (mL) followed by a saline flush. For aortic CTAs, a fixed bolus of 100ml was followed by a saline flush of 50ml. In general, injection flow was set to 5-6ml/sec. The CTA selection resulted in the inclusion of eighty-two patients (48 males, 34 females) with 94 PHVs and annuloplasty rings.

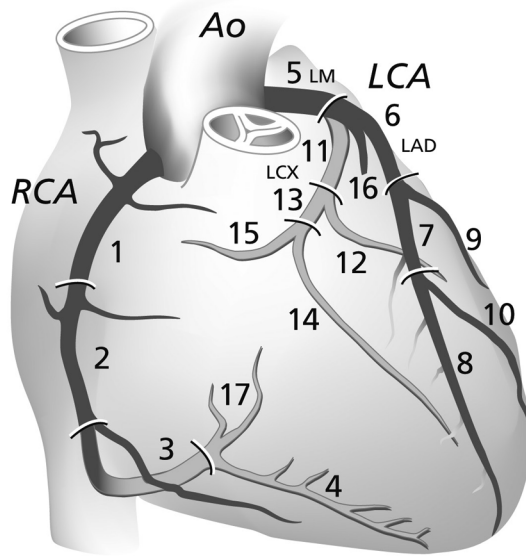


**Figure 1** | Coronary artery segments according to the American Heart Association classification.<sup>10</sup> Ao = Aorta; RCA = Right Coronary Artery; LCA = Left Coronary Artery; LM = Left Main branch; LAD = Left Anterior Descending Coronary Artery; LCX = Left Circumflex Coronary Artery

The mean age of our study population was  $58 \pm 14$  years (mean  $\pm$  SD). All 82 patients underwent CTA examinations on 64-slice ( $n=27$ ) or 256-slice ( $n=55$ ) MDCT systems. The indications for CTA examinations were: PHV dysfunction ( $n=47$ ), aortic aneurysm evaluation ( $n=17$ ), aortic dissection ( $n=8$ ), coronary assessment ( $n=3$ ), cardiac other ( $n=5$ ) and other ( $n=2$ ). In four of 82 patients (5%)  $\beta$ -blockers were administered to lower the heart rate. Nitroglycerin was not routinely administered in our patients.

CT data were retrieved from the PACS archive of the Radiology department and sent to a dedicated workstation for image analysis. Heart rate during imaging was obtained from the CT data. DLP values were obtained if dose information was available. DLP values were converted to radiation exposure (mSv) by using 0.017 for cardiac CTAs, and 0.016 (mean of 0.017 for the chest and 0.015 for the abdomen) for thoraco-abdominal aortic CTAs as conversion factor. Patient and PHV data were obtained from the patient's medical files. The study was performed under a waiver from the institutional reviewing board. Data on the image quality of the PHV itself in a number of these patients have been previously published.<sup>9</sup>

### Image analysis

Assessment of the MDCT was performed on a dedicated workstation (Extended Brilliance Workstation, Philips Healthcare, Best, the Netherlands). The best systolic and diastolic image phase in the retrospectively gated or prospectively triggered CT dataset for coronary assessment was selected. Coronary arteries were assessed according to the 17-segment modified American Heart Association classification<sup>10</sup> on the axial images (Figure 1).

First, each coronary segment was scored as present or absent. Absent was defined as no visible segment, but sufficient high image quality to exclude non-visibility of other causes or a segment not included in the imaging range. For present segments, the image quality was scored on a three-point scale (1= non-diagnostic, 2 = acceptable, 3 = good). The criteria for the different scores were



formulated as follows: (1) non-diagnostic: segment details not sufficient visualized to perform diagnostic assessment; (2) acceptable: adequate segment details with limited artifacts; and (3) good: perfect segment details without artifacts. Reasons for non-diagnostic segments were classified as: valve- or ring annuloplasty-related artifacts, or other (e.g. motion, small vessel size, low contrast enhancement and pacemaker lead artifacts). Scoring was performed in consensus by two observers (JH and RB) with 2 years and 5 years experience in CT coronary assessment, respectively.

### Data analysis

Data analysis was restricted to descriptive statistics. Data were presented as means  $\pm$  standard deviation (SD) for continuous data with a parametric data distribution. Categorical data were presented in total numbers or percentages. The presence of PHV-related artifacts precluding coronary artery segment assessment was determined for the different PHV types and PHV positions. These PHV-related artifacts are presented per coronary artery segment.

**Table 1** | Presence of valve-related artifacts classified per prosthetic heart valve (PHV) manufacturer and position

Manufacturer	Type	PHV* type	Number per valve position*				Total
			Aortic	Mitral	Pulmonary	Tricuspid	
Carbomedics	Mechanical	Bileaflet	21 (0)	3 (1)	0 (0)	0 (0)	24 (1)
St Jude	Mechanical		8 (2)	4 (3)	0 (0)	0 (0)	12 (5)
ON-X	Mechanical		5 (0)	0 (0)	0 (0)	1 (0)	6 (0)
Sorin bileaflet	Mechanical		5 (3)	1 (0)	1 (1)	0 (0)	7 (4)
Duromedics	Mechanical		0 (0)	1 (1)	0 (0)	0 (0)	1 (1)
Medtronic Hall	Mechanical	Tilting disc	9 (0)	3 (0)	0 (0)	0 (0)	12 (0)
Sorin monoleaflet	Mechanical		1 (1)	1 (1)	0 (0)	0 (0)	2 (2)
Björk–Shiley	Mechanical		3 (3)	1 (1)	0 (0)	0 (0)	4 (4)
CE	Annuloplasty ring		0 (0)	4 (0)	0 (0)	1 (0)	5 (0)
Perimount	Biological		15 (0)	0 (0)	0 (0)	0 (0)	15 (0)
Mitroflow	Biological		1 (0)	0 (0)	0 (0)	0 (0)	1 (0)
Medtronic mosaic	Biological		2 (0)	0 (0)	0 (0)	0 (0)	2 (0)
Freestyle	Biological		1 (0)	0 (0)	0 (0)	0 (0)	1 (0)
Epic St Jude	Biological		2 (0)	0 (0)	0 (0)	0 (0)	2 (0)
<b>Total</b>			<b>73 (9)</b>	<b>18 (7)</b>	<b>1 (1)</b>	<b>2 (0)</b>	<b>94 (17)</b>

\* The number of PHVs causing artifacts prohibiting assessment of at least one coronary artery segment are presented in parentheses.

**Table 2** | Coronary artery segments and valve-related artifacts specified per prosthetic heart valve (PHV) manufacturer type in aortic position

PHV position	PHV manufacturer	PHV type	Present segments*/ non-assessable due to PHV artifacts	Non-diagnostic coronary segments due to PHV artifacts
Aortic	Carbomedics	Bileaflet	307/0	None
	St Jude		117/2	2x RCA segment 1
	Sorin		77/3	2x RCA segment 1 1x LCX segment 11
	ON-X		69/0	None
	Medtronic Hall	Tilting disc	127/0	None
	Björk–Shiley		34/11	3x RCA segment 1 3x RCA segment 2 1x LCX segment 11 1x MO segment 12 2x LCX segment 13 1 x MO segment 14
	Sorin		16/2	1 x RCA segment 1 1 x RCA segment 2
	CE Perimount	Biological	218/0	None
	Medtronic Mosaic		31/0	None
	Freestyle		15/0	None
Mitroflow		16/0	None	
Epic St Jude		27/0	None	

\*Total number of present segments in Tables 1-3 is higher than 1160 owing to multiple assessment of coronary segments in patients with multiple PHVs as the segments are presented for each PHV separately.

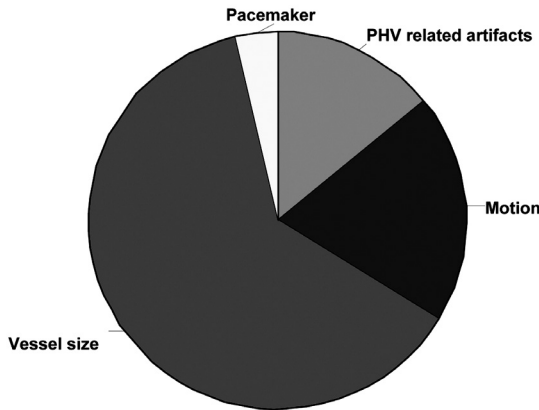


**Figure 2** | Distribution of non-diagnostic coronary segments in patients with prosthetic heart valves.



**Figure 3** | **A** | Sorin tilting disc Prosthetic Heart Valve (PHV) in the aortic position, which causes PHV-related artifacts in RCA segment 1 **B** | ON-X bileaflet Prosthetic Heart Valve (PHV) in the aortic position, which causes no PHV-related artifacts in RCA segment 1

## RESULTS

Mean heart rate during the 82 CTA examinations was  $73 \pm 18$  beats per minute (bpm). In 15 of the 82 patients (18%), the heart rate during CT data acquisition was missing. Mean heart rates were  $73 \pm 18$  bpm and  $72 \pm 19$  bpm for the mechanical PHV group and biological PHV group, respectively. Sixty of 82 (73%) CT acquisitions were performed as a dedicated cardiac CTA including 51 retrospectively ECG-gated CTAs (120kV,  $\geq 600$  mAs) and nine prospectively triggered CTAs (120kV, 200-250 mAs); and 22/82 (27%) CTAs as a retrospectively ECG-gated CTA of the thoraco-(abdominal) aorta with a lower tube current (200-400 mAs). Radiation dose information was available for 42/82 patients (51%). Mean radiation dose for retrospectively ECG-gated cardiac CTAs was  $15.6 \pm 5.5$  mSv, and for thoraco-abdominal aortic CTAs  $17.6 \pm 4.2$  mSv. Ninety-four PHVs and annuloplasty rings of 14 different PHV and annuloplasty ring types were present: 68 mechanical PHVs (72%), 21 biological PHVs (22%), and 5 annuloplasty rings (5%) (mitral  $n=4$  and tricuspid  $n=1$ ). PHVs and annuloplasty rings were positioned in the aortic ( $n=73$ ; 78%), mitral ( $n=18$ ; 19%), pulmonary ( $n=1$ ; 1%) and tricuspid ( $n=2$ ; 2%) positions (Table 1).

### PHV-related artifacts interfering with coronary artery assessment on MDCT

In total 17/94 (18%) PHVs and annuloplasty rings induced artifacts prohibiting assessment of at least one coronary segment (Table 1). Valve-related artifacts per coronary segment are shown in Tables 2 and 3.

A theoretical total of 1394 coronary segments (82 patients  $\times$  17 segments) were available for analysis. Two hundred and thirty-four of the 1394 segments (17%) were scored absent. In total 1160 coronary segments were present for assessment. Three-hundred and six of 1160 coronary segments (26%) demonstrated a non-diagnostic image quality, 538/1160 (46%) had acceptable image quality;

**Table 3** | Coronary artery segments and valve-related artifacts specified per PHV manufacturer type in other positions

PHV position	PHV manufacturer	PHV type	Present segments*/non-assessable due to PHV artifacts	Non-diagnostic coronary segments due to PHV artifacts
Mitral	Carbomedics	Bileaflet	46/1	1 x LCX segment 13
			51/8	1 x LCX segment 11 1 x MO segment 12 3 x LCX segment 13 3x MO segment 14
	Duromedics		11/4	1 x LCX segment 11 1 x MO segment 12 1 x LCX segment 13 1 x MO segment 14
	Sorin		15/0	None
	CE Mitral ring	Annuplasty ring	62/0	None
	Medtronic Hall	Tilting disc	46/0	None
	Björk–Shiley		14/6	1 x RCA segment 2 1 x RCA segment 3 1 x LAD segment 8 1 x MO segment 12 1 x LCX segment 13 1 x MO segment 14
	Sorin		16/5	1 x LAD segment 8 1 x LCX segment 11 1 x MO segment 12 1 x LCX segment 13 1 x MO segment 14
	Pulmonary	Sorin	Bileaflet	15/1
Tricuspid	ON-X	Bileaflet	15/0	None
	CE Tricuspid ring	Annuplasty ring	15/0	None

\* Total number of present segments in Tables 1-3 is higher than 1160 owing to multiple assessment of coronary segments in patients with multiple PHVs as the segments are presented for each PHV separately.

and in 316/1160 (27%) image quality was good. The reasons for non-diagnostic image quality were PHV-related artifacts ( $n=43$ ; 14%), motion ( $n=60$  segments; 20%), vessel size ( $n=192$ ; 63%), and pacemaker artifacts ( $n=11$ ; 4%) (Figure 2). In patients with more than one PHV implanted, no coronary segments were non-assessable owing to artifacts originating from both valves.

None of the biological PHVs (0/21; 0%) and annuloplasty rings (0/5; 0%), and none of the ON-X (0/6; 0%) and Medtronic Hall (0/12; 0%) mechanical PHVs caused artifacts prohibiting coronary assessment.

In the aortic position, St Jude (2/8; 25%) and Sorin (3/5; 60%) bileaflet PHVs caused artifacts prohibiting coronary assessment, mainly of the proximal right coronary artery (RCA). The Björk–Shiley ( $n=3$ ; 100%) and Sorin tilting disc PHVs ( $n=1$ ; 100%) caused severe artifacts in RCA segments.

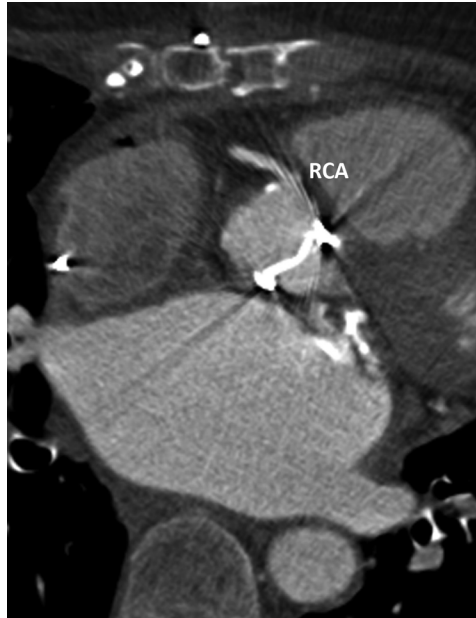


**Figure 4** | St Jude bileaflet Prosthetic Heart Valve (PHV) in the aortic position, which causes PHV-related artifacts in RCA segment 1.

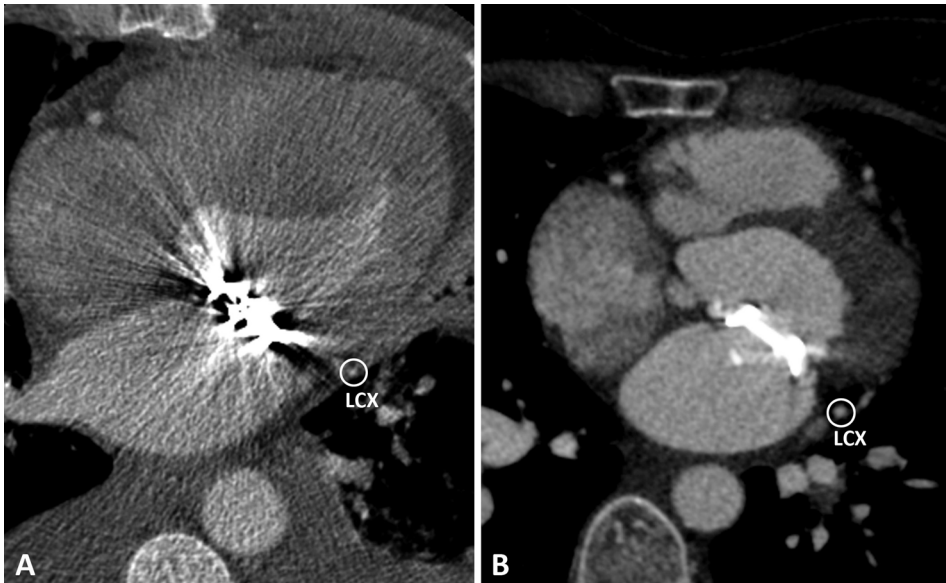


**Figure 5** | **A** | Björk-Shiley tilting disc Prosthetic Heart Valve (PHV) in the mitral position, which causes PHV-related artifacts in LCX **B** | Medtronic Hall tilting disc PHV in the mitral position, which causes no PHV-related artifacts in LCX

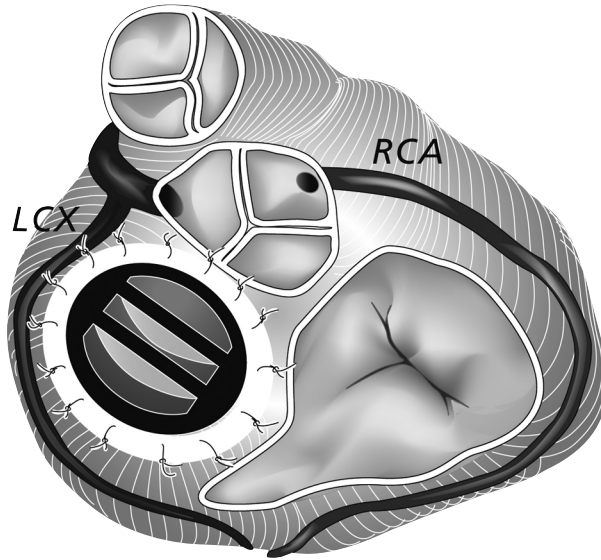


**Figure 6** | Cardiac valvular anatomy with a St Jude Prosthetic Heart Valve (PHV) in the mitral position. The illustration demonstrates the close relationship between the LCX and the mitral PHV.

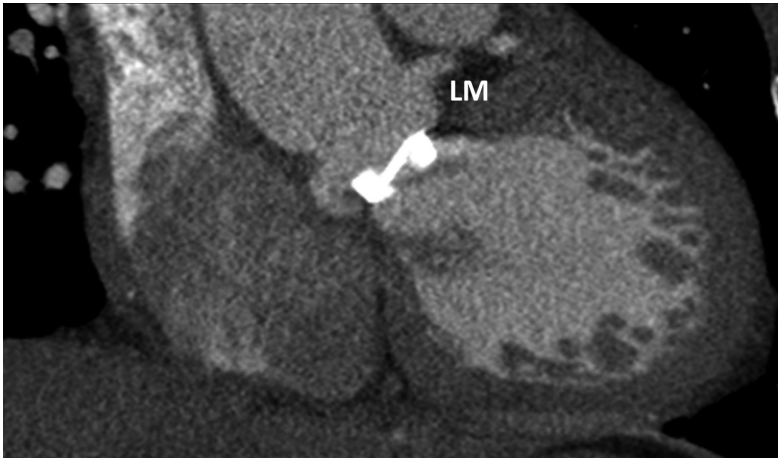


**Figure 7** | Carbomedics bileaflet Prosthetic Heart Valve (PHV) in the aortic position, which causes no PHV-related artifacts in the LM branch. LM = left main

Moreover, the Björk–Shiley tilting disc also caused artifacts in the left circumflex (LCX) and obtuse marginal (MO) branches (Table 2). The commonly implanted PHVs (Carbomedics bileaflet ( $n=21$ ; 0%) and Medtronic Hall tilting disc ( $n=9$ ; 0%) demonstrated no PHV-related artifacts in the aortic position (Tables 1 and 2). Figure 3 and 4 illustrate aortic PHVs with and without PHV-related artifacts in the RCA.

In the mitral position, Carbomedics (1/3; 33%), St Jude (3/4; 75%) and the Duromedics (1/1; 100%) bileaflet PHVs caused artifacts prohibiting assessment of at least one coronary segment in the LCX and MO branches. Both Björk–Shiley and the Sorin tilting disc PHVs caused severe artifacts in

LCX and MO segments. The Björk–Shiley tilting disc also caused severe artifacts in RCA segments. Affected segments are detailed in Table 3. Figure 5 illustrates mitral PHVs with and without artifacts in the LCX. In the pulmonary position, the Sorin bileaflet PHV ( $n=1$ ; 100%) demonstrated PHV-related artifacts in RCA segment 2. In the tricuspid position, ON-X bileaflet PHV ( $n=1$ ) and tricuspid annuloplasty ring ( $n=1$ ) showed no PHV-related artifacts (Table 3).

#### PHV-related artifacts in different imaging phases:

In all patients, coronary artery segments were assessed in the best systolic and diastolic imaging phase. In the aortic position, four patients (5%) demonstrated PHV-related artifacts precluding diagnostic coronary assessment of RCA segment 1 only in diastolic ( $n=2$ ; 50%) or systolic ( $n=2$ ; 50%) phase. In the mitral position, one patient (6%) had only PHV-related artifacts in the diastolic phase in the LCX and MO branches.

In summary, PHV-related artifacts were present in RCA segments (1, 2 and 3), left anterior descending artery (LAD) segment 8, LCX segments (11 and 13), and MO branches (12 and 14). The close relationship between RCA and aortic PHV, and LCX and mitral PHV is illustrated in Figure 6. The assessment of the remaining coronary segments (including the left main branch, Figure 7) was not disturbed by PHV-related artifacts (Figure 1, Table 2 and 3).

**Table 4** | Metallic properties of different prosthetic heart valves (PHV)

PHV Manufacturer	PHV design	Metallic contents*
Carbomedics	Mechanical bileaflet	Titanium alloy
St Jude	Mechanical bileaflet	Nickel alloy
ON-X	Mechanical bileaflet	Titanium alloy
Sorin bileaflet	Mechanical bileaflet	Titanium alloy
Duromedics	Mechanical bileaflet	Cobalt-chrome alloy
Medtronic Hall	Mechanical tilting disc	Titanium alloy
Sorin monoleaflet	Mechanical tilting disc	Cobalt-chrome alloy
Björk–Shiley	Mechanical tilting disc	Cobalt-chrome alloy
CE	Annuloplasty ring	Elgiloy
CE Perimount	Biological	Elgiloy
Sorin Mitroflow	Biological	-
Medtronic Mosaic	Biological	Haynes® alloy (stent post markers)
Medtronic Freestyle	Biological	-
St Jude Epic Stented	Biological	Stainless steel wire in sewing cuff

\* Manufacturer data

## DISCUSSION

The principle findings of our study are: (1) the diagnostic assessment of most coronary artery segments in patients with PHVs was not hampered by PHV-related artifacts, (2) Björk–Shiley tilting disc PHVs, Sorin tilting disc PHVs and Duromedics bileaflet PHVs precluded complete diagnostic assessment of coronary artery segments; and (3) ON-X and Medtronic Hall PHVs, biological PHVs and annuloplasty rings never hampered coronary artery assessment by MDCT.

The PHV-related artifacts on MDCT images seem to be more dependent on PHV composition than on the PHV design (bileaflet, tilting disc and biological valves) (Table 4).<sup>8,9</sup> As far as the material of the PHV is concerned our study showed notable differences.

Björk–Shiley and Sorin tilting disc PHVs as well as Duromedics bileaflet PHVs demonstrated severe artifacts which precluded diagnostic coronary assessment of RCA, LCX and the distal segment of the LAD, dependent on the PHV position. This finding is supported by previous studies that described that these PHV types are associated with valve-related artifacts that also prohibit the evaluation of the PHV itself on MDCT.<sup>8,9,11,12</sup> The severe artifacts of the Björk–Shiley, Sorin tilting disc and Duromedics bileaflet PHVs were caused by the cobalt-chrome alloy that is present in these valves. Therefore, MDCT is not suitable for the assessment of the coronary arteries in patients who have one of these PHVs implanted. The Saint Jude PHV, consisting of a nickel alloy, produced fewer artifacts but still enough to preclude assessment of a limited number of coronary artery segments in the right coronary artery and circumflex territory (segments 1, 13 and 14). The other segments did not suffer from artifacts that precluded assessment. The Saint Jude PHV is one of the most commonly implanted PHV types worldwide and therefore one of the most likely PHVs to be encountered. The possibility of the non-diagnostic image quality of the above-mentioned segments should be kept in mind when performing cardiac CT in these patients.

In general, Carbomedics, ON-X and Medtronic Hall mechanical PHVs caused no PHV-related artifacts hampering coronary artery assessment. These PHVs are mainly composed of titanium alloys that are associated with only limited artifacts on MDCT.<sup>8</sup>

The biological PHVs and annuloplasty rings produced fewer PHV artifacts than mechanical PHVs on MDCT. Some biological PHVs have a radiopaque frame that supports the valve leaflets, but this does not generally induce many artifacts.<sup>2,9</sup> In our study, no PHV-related artifacts that interfered with diagnostic coronary assessment were found in biological PHVs or annuloplasty rings.

Prosthetic heart valves in the aortic position may show mainly artifacts in the proximal RCA (segments 1 and 2) because of the close relationship between the aortic PHV and the proximal RCA. Interestingly, the left main branch, which also has a close relationship with the aortic PHV, did not show any PHV-related artifacts. The reason for the absence of PHV-related artifacts in this segment may be the angulation of the PHV with respect to the X-ray beam of the gantry.

In the mitral position, PHV-related artifacts occurred in the LCX and MO branches. The close relationship between these segments and the mitral PHV position is a likely explanation for the presence of the PHV-related artifacts in these specific segments.

### Limitations

Our study contains many different PHV types. A few PHV types are only represented in small numbers. However the most commonly implanted PHVs (Carbomedics, St Jude, Medtronic Hall and the Perimount biological PHVs) are present in considerable numbers. The mean heart rate of 73±18 bpm is relatively high for CT coronary assessment because 79 of 82 CTAs (96%) were performed for other clinical indications without a specific heart rate reduction. High heart rates



may cause considerable motion artifacts that influence diagnostic CAD assessment. However, the specific interest of this study was to address the question: do PHV-related artifacts disturb coronary assessment? Other reports emphasized the importance of an optimal heart rate and the restricted diagnostic value of MDCT in the detection of CAD in distal coronary segments.<sup>13</sup> To optimize coronary image quality, beta-blockers and nitroglycerin should be routinely administered in patients without contraindications for these drugs. In this study, CT coronary angiography was not compared with conventional coronary angiography. Further prospective studies are required to determine the diagnostic accuracy of CT coronary angiography in patients after PHV implantation. However, as most commonly implanted PHV types generate only limited artifacts, we would expect the diagnostic accuracy to be close to published results in patients who have not yet undergone PHV implantation.<sup>13</sup> Consensus reading was performed. Interobserver variability has to be investigated in further studies to validate the PHV-related artifacts scoring system. Axial CT images only were assessed for the presence of PHV-related artifacts. Multiplanar reconstructions were not separately assessed because PHV-related artifacts were present in both axial and multiplanar reconstructions.

In conclusion, the most commonly implanted PHVs do not cause artifacts that prohibit coronary artery assessment of at least one coronary segment by MDCT. Carbomedics, Medtronic Hall and ON-X mechanical PHVs, bioprosthesis, and annuloplasty rings virtually never hamper coronary artery assessment by MDCT. However, in patients with a Björk–Shiley or Sorin tilting PHVs, coronary artery assessment by MDCT is virtually always hampered by PHV induced artifacts.

## REFERENCES

1. Meijboom WB, Meijs MF, Schuijf JD, et al. Diagnostic accuracy of 64-slice computed tomography coronary angiography: a prospective, multicenter, multivendor study. *J Am Coll Cardiol* 2008; 52:2135-2144.
2. Chenot F, Montant P, Goffinet C, et al. Evaluation of anatomic valve opening and leaflet morphology in aortic valve bioprosthesis by using multidetector CT: comparison with transthoracic echocardiography. *Radiology* 2010; 255:377-385.
3. Feuchtner GM, Stolzmann P, Dichtl W, et al. Multislice computed tomography in infective endocarditis: comparison with transesophageal echocardiography and intraoperative findings. *J Am Coll Cardiol* 2009; 53:436-444.
4. Habets J, Budde RP, Symersky P, et al. Diagnostic evaluation of left-sided prosthetic heart valve dysfunction. *Nat Rev Cardiol* 2011; 8:466-78.
5. Symersky P, Budde RP, de Mol BA, et al. Comparison of multidetector-row computed tomography to echocardiography and fluoroscopy for evaluation of patients with mechanical prosthetic valve obstruction. *Am J Cardiol* 2009; 104:1128-1134.
6. Tsai IC, Lin YK, Chang Y, et al. Correctness of multi-detector-row computed tomography for diagnosing mechanical prosthetic heart valve disorders using operative findings as a gold standard. *Eur Radiol* 2009; 19:857-867.
7. Bonow RO, Carabello BA, Chatterjee K, et al. 2008 focused update incorporated into the ACC/AHA 2006 guidelines for the management of patients with valvular heart disease: a report of the American College of Cardiology/American Heart Association Task Force on Practice Guidelines (Writing Committee to revise the 1998 guidelines for the management of patients with valvular heart disease). Endorsed by the Society of Cardiovascular Anesthesiologists, Society for Cardiovascular Angiography and Interventions, and Society of Thoracic Surgeons. *J Am Coll Cardiol*. 2008; 52:e1-142.
8. Symersky P, Budde RP, Prokop M, et al. Multidetector-row computed tomography imaging characteristics of mechanical prosthetic valves. *J Heart Valve Dis*. 2011; 20:216-222.
9. Habets J, Symersky P, van Herwerden LA, et al. Prosthetic heart valve assessment with multidetector-row CT: imaging characteristics of 91 valves in 83 patients. *Eur Radiol*. 2011; 21:1390-1396.
10. Austen WG, Edwards JE, Frye RL, et al. A reporting system on patients evaluated for coronary artery disease. Report of the Ad Hoc Committee for Grading of Coronary Artery Disease, Council on Cardiovascular Surgery, American Heart Association. *Circulation* 1975; 51:5-40.
11. LaBounty TM, Agarwal PP, Chughtai A, et al. Evaluation of mechanical heart valve size and function with ECG-gated 64-MDCT. *Am J Roentgenol*. 2009; 193:389-396.
12. Konen E, Goitein O, Feinberg MS, et al. The role of ECG-gated MDCT in the evaluation of aortic and mitral mechanical valves: initial experience. *Am J Roentgenol*. 2008; 191:26-31.
13. Meijboom WB, Mollet NR, Van Mieghem CA, et al. Pre-operative computed tomography coronary angiography to detect significant coronary artery disease in patients referred for cardiac valve surgery. *J Am Coll Cardiol*. 2006; 48:1658-1665.



CHAPTER XIII

OPTIMAL SYSTOLIC *and*  
DIASTOLIC RECONSTRUCTION  
PHASE *for* AORTIC PROSTHETIC  
HEART VALVE IMAGING *with*  
ECG-GATED  
MULTIDETECTOR-ROW CT

J. Habets  
P. Symersky  
E.J. Smit  
B.A.J.M. de Mol  
L.A. van Herwerden  
W.P.Th.M. Mali  
R.P.J. Budde

SUBMITTED

**ABSTRACT**

**PURPOSE** | Multidetector-row computed tomography (MDCT) can provide complementary diagnostic information to echocardiography in case of suspected prosthetic heart valve (PHV) dysfunction. Mainly retrospectively ECG-gated MDCT image acquisition is used for CT evaluation of PHV dysfunction as it allows PHV assessment in open and closed condition. Such a scan protocol is however associated with relatively large radiation exposure. Knowledge of the optimal imaging reconstruction phases for PHV MDCT imaging would allow optimization of lower-dose scan protocols. The objectives of this study were: (1) to determine the best systolic and diastolic CT imaging reconstruction phase for mechanical and biological PHVs, and (2) to identify imaging phases with low image quality which can be omitted in case of axial prospectively triggered acquisition or are suitable for the application of dose modulation.

**METHODS** | Patients with aortic mechanical and biological PHVs that underwent retrospectively ECG-gated cardiac CTAs were included. Images were reconstructed for 11 different ECG-gated (every 10% of the cardiac cycle plus phase 75%) phases. These eleven imaging phases were compared to each other and scored for the best image quality by 2 experienced observers, individually, using a blinded and randomized forced choice side-by-side comparison method. In total, 55 pairwise comparisons were available per patient. An imaging phase was considered superior to another phase if rated with better image quality in more than 60% of cases and with good inter- and intra-observer agreement ( $\kappa \geq 0.6$ ).

**RESULTS** | In total 43 scans of 42 patients with 43 aortic PHVs (one patient was imaged twice with different aortic PHVs) were evaluated. Mean heart rate was  $71 \pm 18$  beats per minute. Overall inter- and intraobserver agreement was good ( $\geq 0.6$ ) in 41/55 (75%) of all comparisons. Overall intra- and interobserver agreement was  $\geq 0.6$  in 51/55 (93%) and 41/55 (75%) of the paired comparisons, respectively. The best systolic imaging phases for mechanical and biological PHVs were 30% and 40%, respectively. For mechanical PHVs, 75-80% were the best diastolic imaging phases and 70% for biological PHVs. Low image quality imaging phases were 10%, 20%, 50% and 60% for both mechanical and biological PHVs.

**CONCLUSIONS** | The optimal systolic and diastolic MCDT reconstruction phases for PHV imaging are 30-40% and 70-75-80%. Scan protocols for PHV imaging using prospectively triggered acquisition or dose modulation should be tailored to include these phases. Other phases could be omitted or imaged using dose-modulation.

**P**rothetic heart valve (PHV) dysfunction is an infrequent but potentially severe event. In clinical practice, transthoracic and transoesophageal echocardiography, and fluoroscopy are the routine imaging techniques to evaluate suspected PHV dysfunction. These imaging techniques may fail to determine the exact cause of PHV dysfunction. Therefore, diagnostic dilemmas may arise.<sup>1,2</sup>

Multidetector-row computed tomography (MDCT) has shown promising results in the evaluation of PHV dysfunction, especially in patients with PHV obstruction and endocarditis.<sup>1,3-5</sup> Recent publications have increased the knowledge on the normal CT imaging characteristics of PHVs.<sup>6-8</sup> Image quality of aortic PHVs on MDCT images is a result of many different factors including aortic annular motion, PHV leaflet motion, PHV composition, CT acquisition protocol, heart rate during acquisition and PHV-related artifacts.<sup>6,9</sup>

MDCT PHV imaging is generally performed with retrospectively ECG-gated acquisitions, because multiple imaging phases are required for dynamic assessment. Images are reconstructed at every 5-10% of the ECG interval resulting in 10-20 image datasets. Contrary to coronary imaging, it is important to have both systolic and diastolic images for PHV assessment because leaflets need to be assessed in both phases. Currently, little is known on which are the best systolic and diastolic imaging phases to assess PHVs on MDCT images. Identification of these phases is important because it may help to construct lower dose acquisition protocols that image only these two phases opposed to higher dose retrospectively ECG-gated image acquisition. Previous studies which addressed general CT image quality of PHVs used the subjective Likert method to assess the image quality.<sup>6,7</sup> Recently a novel method for image quality comparison was developed that uses a randomized blinded paired forced choice approach.<sup>10</sup> It is better suited to compare different imaging reconstruction phases than traditional Likert scale scoring methods.

The objectives of this study were: (1) to determine the best systolic and diastolic ECG-gated MDCT imaging reconstruction phase using a randomized blinded image quality assessment method and (2) to identify possible imaging phases with inferior image quality which are suitable for the application of dose modulation or can be skipped in case of axial prospectively triggered acquisition.

## MATERIALS AND METHODS

### Scan selection

We reviewed all ECG-gated cardiac CT angiograms (CTA) performed in the University Medical Center Utrecht for (1) a radiopaque biological or mechanical PHV in the aortic position; (2) retrospectively-ECG gated image reconstructions at each 10% of the ECG interval in addition to the 75% interval and (3) heart rate registration. Patient data were obtained from the electronic patient medical records. Some patients were participating in an ongoing study which was approved by our local institutional reviewing board (number 10/008). For the remaining patients, the study was performed under a waiver of the local institutional reviewing board (number 11-514/C).

### CT acquisition parameters

Retrospectively ECG-gated cardiac CTAs were performed on a 64-slice or 256-slice MDCT systems (Brilliance 64 and iCT, Philips Medical Systems, Cleveland, Ohio, USA). The following acquisition parameters were used on the 64-slice MDCT system: tube voltage 120kV; tube current 600-1000 mAs; collimation 64x0.625; pitch 0.2; gantry rotation time 0.40 seconds and matrix size 512x512. Acquisition parameters on the 256-slice MDCT system were: tube voltage 120kV; tube current 600-700 mAs; collimation 128x0.625; pitch 0.16-0.18; gantry rotation time 0.27-0.33 seconds; and matrix size 512x512.

Contrast agent (Ultravist® (iopromide) - 300mg I/ml, Bayer Schering Pharma AG, Berlin, Germany) was administered at a mean flow rate of 5-6ml/second and a triphasic contrast injection protocol was used. This protocol started with 100% contrast injection (phase 1), followed by 30%/70% contrast/saline mixture (phase 2) and finally a saline flush (phase 3). The iodine flow was adjusted for patient body weight with an iodine flow of 1.6 grams/sec for patients <70kg, 1.8 gram/sec for patients 70-85kg and 2.0 gram/sec for patients >85kg. Heart rate was noted from the scan data. Radiation exposure was calculated by multiplying the total DLP value (including scout view and tracker) by a conversion factor of 0.017.

### **Image analysis**

Raw data were reconstructed for every 10% of the ECG-interval as well as the 75% phase resulting in 11 datasets. These datasets were evaluated on a research workstation (iX Viewer, Image Sciences Institute, Utrecht, The Netherlands) that enables scrolling through the interactive multiplanar reconstructions (arbitrary planes and slice thickness).<sup>10</sup> Switching between coronal, sagittal and axial imaging planes was possible. The reconstruction was manually aligned to the PHV leaflets for the image quality assessment.

### **Comparison of different ECG-gated reconstructions**

We compared 11 different ECG-gated reconstructions (0%, 10%, 20%, 30%, 40%, 50%, 60%, 70%, 75%, 80%, 90%). These reconstructions were randomized and blinded by the software package.<sup>10</sup> All different phases were compared with each other in pairs (55 combinations x 43 CTAs = 2365 comparisons). For visual evaluation, two observers (JH and PS) with at least two years of experience in the evaluation of PHV MDCT examinations evaluated the complete dataset individually. Patients were individually presented in randomized and blinded pairs for the different ECG-gated imaging phases. To determine, intraobserver variability, the total dataset was presented to both observers twice (after a new randomization procedure). The time interval between both randomizations was four weeks for both observers. The primary outcome measure was the systolic and diastolic imaging phase with the best image quality compared to the other series of that patient. Both observers evaluated MDCT PHV image quality based on previous described regions and criteria.<sup>6</sup> Supra-, sub- and perivalvular regions were assessed for adequately visible details and presence of artifacts prohibiting diagnostic assessment. The valvular leaflets were assessed for visible detail and the possibility of leaflet measurements.<sup>6</sup> For each pair, observers were forced to choose the image with the best image quality.

### **Statistical analysis**

Statistical analyses were performed in SPSS (SPSS statistics Version 15.0, SPSS Inc, Chicago, IL) and Excel software (Excel 2003 SP3, Microsoft). Data with a parametric distribution were presented as means with standard deviation (SD), and data with a non-parametric distribution presented as medians and an interquartile range (IQR). Parametric distribution was assessed with QQ-plots and the Kolgomorov-Smirnov test.

Observer scores from the visual evaluation were expressed as mean percentage of cases in which one PHV imaging phase was better or worse compared to the other PHV imaging phase. Better imaging phase was defined as a mean image quality score  $\geq 60\%$  and inter- and intraobserver kappa  $\geq 0.6$ . Data was stratified for PHV type (biological and mechanical PHVs). Inter- and intraobserver variability were determined using  $\kappa$  statistics with correction for equal probability. Intraobserver  $\kappa$  values were calculated for each observer individually (two  $\kappa$  values) and interobserver  $\kappa$  values for each observer pair (four  $\kappa$  values). Inter- and intraobserver  $\kappa$  values were expressed as mean  $\kappa$  values with

**Table 1** | Patient characteristics

Gender (Male) (%)	31 (74%)
Age (years)*	61±14
Number of mechanical PHVs (%)	27 (63%)
Heart rate (beats per minute)*	71±18
Radiation exposure (mSv)**	13.1 (12.5-14.2)
Interval between PHV implantation and CTA (months)**	1.0 (1.0-37.0)
CTAs on MDCT system 256-slice (%)	40 (93%)
64-slice (%)	3 (7%)

\*Mean±standard deviation

\*\*Median (interquartile range)

CTA = Computer tomography angiography; IQR = Interquartile range; MDCT = Multidetector-row computed tomography; PHV = Prosthetic heart valve

range. A  $\kappa$  value of 0.81-1.00 indicated very good agreement, 0.61-0.80 good agreement; 0.41-0.60 moderate agreement; 0.21-0.40 fair agreement and  $\leq 0.20$  poor agreement.<sup>11</sup>

## RESULTS

### Patient and scan characteristics

In total, 42 patients with 43 aortic PHVs underwent 43 ECG-gated cardiac CTAs. One patient was imaged twice with different aortic PHVs. Patient characteristics are shown in Table 1. In total, 27 mechanical PHVs of five different manufacturers and 16 biological PHVs of three different PHV manufacturers were evaluated. The mean heart rate was 71±18 beats per minute for the total group of patients, 71±19 beats per minute for patients with a mechanical PHV and 72±16 beats per minute for patients with a biological PHV. Retrospectively ECG-gated cardiac CTAs were performed on 64-slice ( $n=3$ ) or 256-slice ( $n=40$ ) MDCT systems.

### Image quality assessment

The overall image quality scores, inter-observer and intra-observer agreement for each comparison are presented in the data supplement (Appendix I, II and III). Table 2 summarizes the image quality scores for the best systolic and diastolic imaging phases. In systole and diastole 30-40% and 75-80% were the best imaging phases, respectively (Table 2, Figure 1). The overall best imaging phases (not discriminating a systolic and diastolic group) were 75-80% (Table 3). Overall for each scan inter- and intraobserver agreement was  $\geq 0.6$  in 41/55 (75%) of the paired comparisons. Overall interobserver agreement was  $\geq 0.6$  in 51/55 (93%) and 41/55 (75%) of the paired comparisons, respectively. For the mechanical and biological PHV group, inter- and intraobserver kappas were  $\geq 0.6$  42/55 (76%) and 35/55 (64%), respectively.

### Systolic optimal imaging phase

The complete image quality scores stratified for mechanical and biological PHVs are presented in

**Table 2 |** Overall image quality scores for systolic and diastolic MDCT imaging

Better	Systolic				Better	Diastolic				
	10%	20%	30%	40%		70%	75%	80%	90%	
<b>10%</b>	X	32.0* (23.3-37.2)	16.3* (11.6-18.6)	16.9* (14.0-23.3)	<b>70%</b>	X	34.9 (27.9-41.9)	44.2* (39.5-51.2)	53.5* (51.2-58.1)	0%
<b>20%</b>	68.0* (62.8-76.7)	X	29.7 (23.3-32.6)	30.8* (23.3-34.9)	<b>75%</b>	<b>65.1</b> <b>(58.1-72.1)</b>	X	<b>51.2</b> <b>(44.2-60.5)</b>	<b>58.7</b> <b>(53.5-65.1)</b>	<b>70.3*</b> <b>(69.8-72.1)</b>
<b>30%</b>	<b>83.7*</b> <b>(81.4-88.4)</b>	<b>70.3</b> <b>(67.4-76.7)</b>	X	<b>54.1*</b> <b>(44.2-60.5)</b>	<b>80%</b>	<b>55.8*</b> <b>(48.8-60.5)</b>	<b>48.8</b> <b>(39.5-55.8)</b>	X	<b>64.5*</b> <b>(60.5-69.8)</b>	<b>66.9*</b> <b>(65.1-69.8)</b>
<b>40%</b>	<b>83.1*</b> <b>(76.7-86.0)</b>	<b>69.2*</b> <b>(65.1-69.8)</b>	<b>45.9*</b> <b>(39.5-55.8)</b>	X	<b>90%</b>	46.5* (41.9-48.8)	41.3* (34.9-46.5)	35.5* (30.2-39.5)	X	52.9 (39.5-62.8)
					<b>0%</b>	37.8* (37.2-39.5)	29.7* (27.9-30.2)	33.1* (30.2-34.9)	47.1 (37.2-60.5)	X

This table shows the mean image quality percentage better compared with other reconstruction phases. For example in 32% of all the comparisons the 10% image phase is better than the 20% image phase. The best systolic and diastolic imaging phases are printed in bold. \* Inter- and intraobserver kappas ≥0.6.



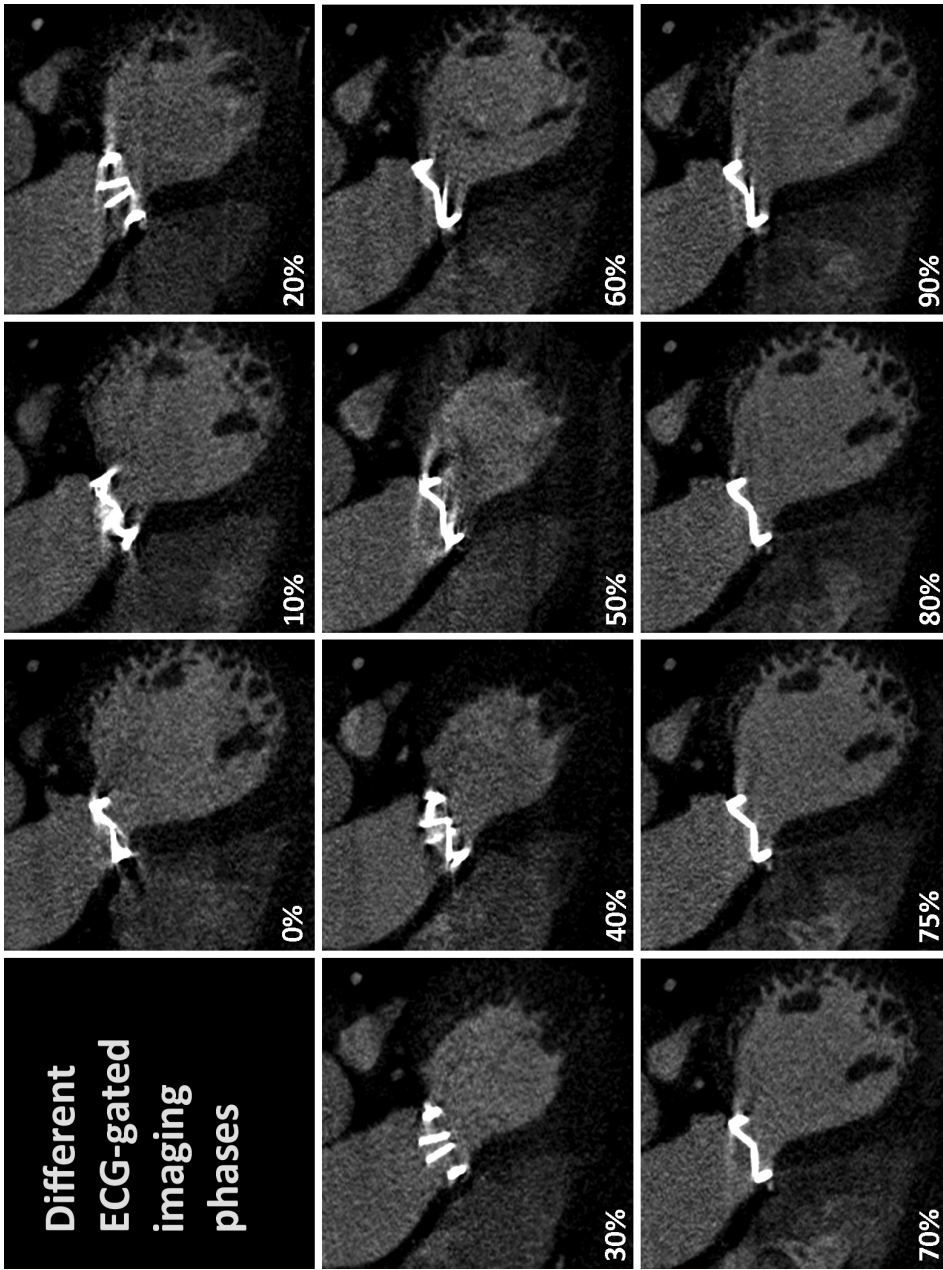


**Figure 1** | Patient with an aortic bileaflet CarboMedics PHVs. The 11 different imaging reconstruction phases are shown. Note the considerable difference in image quality between the different imaging reconstruction phases.

**Table 3 | Overall image quality scores for the best MDCT imaging phase**

Better	The best overall imaging phase			
	30%	40%	75%	80%
<b>30%</b>	X	54.1* (44.2-60.5)	27.9* (23.3-32.6)	27.9* (16.3-34.9)
<b>40%</b>	45.9* (39.5-55.8)	X	29.7* (20.9-37.2)	28.5* (11.6-41.9)
<b>75%</b>	<b>72.1*</b> <b>(67.4-76.7)</b>	<b>70.3*</b> <b>(62.8-79.1)</b>	X	<b>51.2</b> <b>(44.2-60.5)</b>
<b>80%</b>	<b>72.1*</b> <b>(65.1-83.7)</b>	<b>71.5*</b> <b>(65.1-88.4)</b>	<b>48.8</b> <b>(39.5-55.8)</b>	X

This table shows the mean image quality percentage better compared with other reconstruction phases. For example in 54% of all the comparisons the 30% image phase is better than the 40% image phase. The best imaging phases 75% and 80% are printed in bold. \* Inter- and intraobserver kappas  $\geq 0.6$ .

the data supplement (Appendix IV and V). For mechanical and biological PHVs, the summarized paired comparisons of the systolic imaging phases (10-20-30-40%) are presented in Table 4. The inter- and intraobserver kappas were  $\geq 0.6$  in 5/6 (83%) and 4/6 (67%) for mechanical and biological PHVs, respectively. In the mechanical PHV group, one pairwise comparison had an interobserver and intraobserver  $\kappa$  value  $\leq 0.6$ : (20% vs. 30%: best image quality for the 30% phase, inter- and intraobserver  $\kappa$  0.5 and 0.6, respectively). In the biological group, two pairwise comparisons had lower inter- and intraobserver  $\kappa$ 's than 0.6. The paired comparison 10% vs. 30% resulted in better image quality in favor of the 30% phase ( $\kappa$  0.6 and 0.5, respectively). Moreover, the paired comparison 20% vs. 30% demonstrated a better image quality for the 30% (inter- and intraobserver  $\kappa$  0.4 and 0.5, respectively).

For both PHV types, the systolic imaging phases 30% and 40% demonstrated a better image quality than the 10% and 20% imaging phases. For mechanical PHVs, 30% was the best systolic imaging phase. For biological PHVs, 40% was the best systolic imaging phase.

**Diastolic optimal imaging phase**

For mechanical and biological PHVs, the paired comparisons of the diastolic imaging phases (70%-75%-80%-90%-0%) are presented in Table 5. The inter- and intraobserver kappas were  $\geq 0.6$  in 7/10 (70%) and 6/10 (60%) for mechanical and biological PHVs, respectively.

In the mechanical PHV group, three pairwise comparisons had an inter- and intraobserver  $\kappa$  value  $\leq 0.6$ : 70-75% ( $\kappa$  0.4 and 0.5, respectively); 75%-80% ( $\kappa$  0.4 and 0.4, respectively); and 90%-0% ( $\kappa$  0.5 and 0.8, respectively). In the biological PHV group, four pairwise comparisons had an inter- and intraobserver  $\kappa$  value  $\leq 0.6$ : 70-75% ( $\kappa$  0.1 and 0.4, respectively); 75-80% ( $\kappa$  0.3 and 0.6, respectively); 80-90% ( $\kappa$  0.3 and 0.7, respectively); and 80%-0% ( $\kappa$  0.5 and 0.7, respectively).

For mechanical PHVs, the best diastolic imaging phases were 75% and 80%. In the biological PHV group, the 70% imaging phase was the best diastolic imaging phase.

**Table 4** | Best systolic MDCT imaging phase for mechanical and biological PHVs

Better	Systolic								
	Mechanical prostheses				Biological prostheses				
	10%	20%	30%	40%	Better	10%	20%	30%	40%
<b>10%</b>	X	30.6 <sup>*</sup> (18.5-37.0)	13.0 <sup>*</sup> (11.1-14.8)	20.4 <sup>*</sup> (18.5-25.9)	<b>10%</b>	X	34.4 <sup>*</sup> (31.3-37.5)	21.9 (12.5-31.3)	10.9 <sup>*</sup> (6.3-18.8)
<b>20%</b>	69.4 <sup>*</sup> (63.0-81.5)	X	28.7 (22.2-33.3)	37.0 <sup>*</sup> (25.9-48.1)	<b>20%</b>	65.6 <sup>*</sup> (62.5-68.8)	X	31.2 (25.0-37.5)	20.3 <sup>*</sup> (12.5-25.0)
<b>30%</b>	<b>87.0<sup>*</sup></b> <b>(85.2-88.9)</b>	<b>71.3</b> <b>(66.7-77.8)</b>	<b>X</b>	<b>64.8<sup>*</sup></b> <b>(55.6-70.4)</b>	<b>30%</b>	78.1 (68.8-81.3)	68.8 (62.5-75.0)	X	35.9 <sup>*</sup> (25.0-43.8)
<b>40%</b>	79.6 <sup>*</sup> (74.1-81.5)	63.0 <sup>*</sup> (51.9-74.1)	35.2 <sup>*</sup> (29.6-44.4)	X	<b>40%</b>	<b>89.1<sup>*</sup></b> <b>(81.3-93.8)</b>	<b>79.7<sup>*</sup></b> <b>(75.0-87.5)</b>	<b>64.1<sup>*</sup></b> <b>(56.3-75.0)</b>	<b>X</b>

This table shows the mean image quality percentage better compared with other reconstruction phases. For example in 31% of all the comparisons the 10% image phase is better than the 20% image phase (Mechanical prostheses). The best systolic imaging phases for biological and mechanical PHVs are printed in bold. \* Inter- and intraobserver kappas ≥0.6.

**Table 5 |** Best diastolic MDCT imaging phase for mechanical and biological PHVs

		Diastolic										
		Mechanical prostheses					Biological prostheses					
Better		70%	75%	80%	90%	0%	Better	70%	75%	80%	90%	0%
70%		X	25.9 (22.2-29.6)	35.2* (29.6-40.7)	56.5* (48.1-63.0)	63.0* (59.3-66.7)	70%	X	50.0 (25.0-68.8)	59.4* (50.0-68.8)	48.4* (37.5-62.5)	60.9* (56.3-62.5)
75%		74.1 (70.4-77.8)	X	49.1 (44.4-51.9)	66.7* (59.3-70.4)	72.2* (70.4-74.1)	75%	50.0 (31.3-75.0)	X	54.7 (31.3-75.0)	45.3* (37.5-56.3)	67.2* (62.5-75.0)
80%		64.8* (59.3-70.4)	50.9 (48.1-55.6)	X	68.5* (63.0-81.5)	74.1* (70.4-77.8)	80%	40.6* (31.3-50.0)	45.3 (25.0-68.8)	X	57.8 (50.0-68.8)	54.7 (43.8-68.8)
90%		43.5* (37.0-51.9)	33.3* (29.6-40.7)	31.5* (18.5-37.0)	X	57.4 (44.4-70.4)	90%	51.6* (37.5-62.5)	54.7* (43.8-62.5)	42.2 (31.3-50.0)	X	45.3* (31.3-62.5)
0%		37.0* (33.3-40.7)	27.8* (22.2-29.6)	25.9* (22.2-29.6)	42.6 (29.6-55.6)	X	0%	39.1* (37.5-43.8)	32.8* (25.0-37.5)	45.3 (31.3-56.3)	54.7* (37.5-68.8)	X

This table shows the mean image quality percentage better compared with other reconstruction phases. For example: In the mechanical PHV group, 70% is in 26% of all the comparisons better than the 75% reconstruction phase. The best diastolic imaging phases for biological and mechanical PHVs are printed in bold. \* Inter- and intraobserver kappas ≥0.6.

## DISCUSSION

The principle findings of this study are: (1) the diastolic ECG-gated imaging phases (75% and 80%) are the overall best imaging phases for MDCT PHV evaluation based on a randomized blinded image quality assessment method; (2) the best systolic imaging phases are 30% for mechanical PHVs and 40% for biological PHVs; and (3) the best diastolic imaging phases are 75%/80% for mechanical PHVs and 70% for biological PHVs. Previous studies demonstrated that most PHVs are visualized with at least good image quality. However, these studies are based on Likert image quality scoring assessment.<sup>6,7,12</sup> In this study, two observers assessed MDCT PHV image quality with a blinded randomized method individually. This assessment method was previously described in detail by Smit et al.<sup>10</sup>, and provides the possibility to assess image quality in a randomized blinded fashion. In this study, the inter- and intraobserver agreement was good ( $\geq 0.6$ ; 93% and 75%, respectively).

In the overall image quality assessment, 75% and 80% image phases were the best imaging phases for MDCT PHV imaging. Our results suggests that these imaging phases has to be selected for MDCT PHV imaging. Other diastolic phases (70%/90%/0%) were also acceptable for diastolic PHV assessment. For systolic assessment, 30% and 40% imaging phases were the best imaging phases. For systolic imaging, 30% or 40% has to be selected. Several imaging reconstruction phases can be omitted or imaged with dose modulation because of inferior image quality (10%-20%-50%-60%).

Knowledge on the optimal imaging phases for MDCT PHV evaluation has important clinical consequences. For diagnostic assessment of PHVs, it is crucial to have a diagnostic systolic and diastolic imaging reconstruction phase to accurately detect PHV pathology.<sup>1</sup> Previous studies with patients with PHV dysfunction were imaged with retrospectively ECG-gating acquisition protocols allowing for dynamic (systolic/diastolic) PHV assessment.<sup>3-5,12</sup> However, retrospectively ECG-gated PHV CT imaging has a considerable radiation exposure for the patient. To reduce this radiation exposure, several methods are available including dose modulation, prospective triggering and iterative reconstruction.<sup>13,14</sup> This study demonstrated that several imaging phases result in suboptimal quality (10%/20%/50%/60%). Therefore, dose modulation applied in these phases may be an effective method to reduce radiation exposure without loss of diagnostic information.

Prospective triggering is an acquisition method that is commonly used in the clinical setting for coronary CT angiography imaging.<sup>15</sup> Prospective triggered acquisition protocols may also be of value for MDCT PHV imaging as they are associated with lower radiation exposure. Furthermore, a previous *in vitro* study showed that prospective triggering also resulted in lower image noise levels and PHV-related artifacts than retrospectively ECG-gated helical acquisitions at different heart rates.<sup>14</sup> Prospectively triggered acquisitions require setting the desired cardiac phase to be imaged before image acquisition. Therefore, it is essential to know the optimal systolic and diastolic imaging phase beforehand. This study demonstrated that 30-40% (systolic) or 75-80% (diastolic) has to be selected for the development of prospectively triggered acquisition protocols. When a MDCT system with a wide detector coverage is available, prospectively triggered acquisition of both systolic and diastolic imaging phases may be possible with one contrast administration. In contrast, MDCT systems without wide detector coverage require a separate contrast administration for both systolic and diastolic prospectively triggered MDCT acquisition. Furthermore, optimal imaging phases can vary between individuals. To solve this problem of individual variation, a low-dose non-contrast enhanced retrospectively ECG-gated helical acquisition can be performed to determine the optimal opening and closing phase of the valve leaflets. This method is only helpful for patients with mechanical PHVs, because the valve leaflets of biological PHVs are radiolucent and not visible on unenhanced MDCT images. Instead of prospective triggering, low-dose helical acquisitions may be an alternative

for MDCT imaging of biological PHVs. Besides dose modulation, iterative reconstruction may result in decrease radiation exposure in this retrospectively ECG-gated helical acquisitions. Recently published in vitro results demonstrated that radiation exposure can be reduced with 50% (120kV, 600mAs to 120kV, 300mAs) with similar image noise levels and PHV-related artifacts for mechanical PHVs.<sup>13</sup> Further prospective clinical studies are needed to evaluate new low-dose MDCT acquisition protocols for mechanical and biological PHV imaging.

## CONCLUSIONS

The optimal systolic imaging phases for mechanical and biological PHV MDCT imaging are 30% and 40%. Optimal diastolic phases for mechanical and biological CT imaging are 75%/80% and 70%, respectively. The imaging phases with inferior image quality (10%/20%/50%/60%) can be omitted or imaged with dose modulation which will result in a considerable reduction in radiation exposure. The findings of this study will help to devise prospectively ECG-triggered low-dose PHV MDCT acquisition protocols.

## REFERENCES

1. Habets J, Budde RP, Symersky P, et al. Diagnostic evaluation of left-sided prosthetic heart valve dysfunction. *Nat Rev Cardiol* 2011; 8:466-478.
2. Girard SE, Miller FA, Jr., Orszulak TA, et al. Reoperation for prosthetic aortic valve obstruction in the era of echocardiography: trends in diagnostic testing and comparison with surgical findings. *J Am Coll Cardiol* 2001; 37:579-584.
3. Feuchtner GM, Stolzmann P, Dichtl W, et al. Multislice computed tomography in infective endocarditis: comparison with transesophageal echocardiography and intraoperative findings. *J Am Coll Cardiol* 2009; 53:436-444.
4. Symersky P, Budde RP, de Mol BA, et al. Comparison of multidetector-row computed tomography to echocardiography and fluoroscopy for evaluation of patients with mechanical prosthetic valve obstruction. *Am J Cardiol* 2009; 104:1128-1134.
5. Tsai IC, Lin YK, Chang Y, et al. Correctness of multi-detector-row computed tomography for diagnosing mechanical prosthetic heart valve disorders using operative findings as a gold standard. *Eur Radiol* 2009; 19:857-867.
6. Habets J, Symersky P, van Herwerden LA, et al. Prosthetic heart valve assessment with multidetector-row CT: imaging characteristics of 91 valves in 83 patients. *Eur Radiol*. 2011; 21:1390-1396.
7. Konen E, Goitein O, Feinberg MS, et al. The role of ECG-gated MDCT in the evaluation of aortic and mitral mechanical valves: initial experience. *Am J Roentgenol*. 2008; 191:26-31.
8. Symersky P, Budde RP, Prokop M, et al. Multidetector-row computed tomography imaging characteristics of mechanical prosthetic valves. *J Heart Valve Dis*. 2011; 20:216-222.
9. Symersky P, Budde RP, Westers P, et al. Multidetector CT imaging of mechanical prosthetic heart valves: quantification of artifacts with a pulsatile in-vitro model. *Eur Radiol*. 2011; 21:2103-2210.
10. Smit EJ, Vonken EJ, van der Schaaf IC, et al. Timing-Invariant Reconstruction for Deriving High-Quality CT Angiographic Data from Cerebral CT Perfusion Data. *Radiology* 2012; 263:216-225.
11. Altman DG. *Practical statistics for medical research*. Chapman & Hall/CRC, 1990.
12. Chenot F, Montant P, Goffinet C, et al. Evaluation of anatomic valve opening and leaflet morphology in aortic valve bioprosthesis by using multidetector CT: comparison with transthoracic echocardiography. *Radiology* 2010; 255:377-385.
13. Habets J, Symersky P, de Mol BA, et al. A novel iterative reconstruction algorithm allows reduced dose multidetector-row CT imaging of mechanical prosthetic heart valves. *Int J Cardiovasc Imaging* 2011; DOI: 10.1007/s10554-011-9954-7.
14. Symersky P, Habets J, Westers P, et al. Prospective ECG triggering reduces prosthetic heart valve-induced artefacts compared with retrospective ECG gating on 256-slice CT. *Eur Radiol* 2011; DOI: 10.1007/s00330-011-2358-1.
15. Sun Z, Ng KH. Diagnostic value of coronary CT angiography with prospective ECG-gating in the diagnosis of coronary artery disease: a systematic review and meta-analysis. *Int J Cardiovasc Imaging* 2012; DOI: 10.1007/s10554-011-0006-0.







CHAPTER XIV

AORTIC PROSTHETIC HEART  
VALVE MOTION DURING *the*  
CARDIAC CYCLE: IMPLICATIONS  
*for* CT IMAGING

P. Symersky  
J. Habets  
B.A.J.M de Mol  
R.P.J. Budde  
M. Prokop

SUBMITTED

**ABSTRACT**

**BACKGROUND** | CT is a promising technique for prosthetic heart valve (PHV) assessment. We previously described the image quality of PHVs on CT imaging during different phases of the cardiac cycle. We currently examined the relation of three-dimensional cardiac motion to image quality of PHV during the various phases of the cardiac cycle at different heart rates.

**METHODS** | This retrospective observational study was approved by the institutional review board. In forty-two patients with an aortic PHV that underwent 43 retrospectively ECG-gated CT studies, the PHV position during the cardiac cycle was measured in three orthogonal planes in each of the 11 reconstruction phases. PHV velocity was calculated by determining 3D displacement and the duration of the reconstruction interval. Image quality was quantified with a two-alternative forced choice test. PHV velocity was related to PHV image quality for all patients and for three heart rate groups <60/min ( $n=11$ ), 60-90/min ( $n=25$ ) and >90/min ( $n=7$ ).

**RESULTS** | During systole the PHV moved more in the direction of the mitral valve (median 6.2 mm IQR 5.2-7.3) than towards the left ventricle (4.1 mm IQR 2.7-6.2,  $p<0.001$ ). Systolic and diastolic image quality was best at 30-40% and 75-80% of the ECG interval which coincided with end-systolic and mid-diastolic velocity troughs. Systolic velocity was increased at 90/min when compared with 60-90/min ( $p=0.015$ ) and <60/min ( $p=0.035$ ). Diastolic velocity was increased at 60-90/min ( $p=0.024$ ) and >90/min ( $p=0.033$ ) when compared to <60/min. Although mid-diastolic image quality decreased at higher heart rates, it remained superior to end-systolic image quality.

**CONCLUSION** | Cardiac phases with the lowest PHV velocity displayed the best CT image quality. At higher heart rates, the mid-diastolic velocity increased and was superior to systolic velocity. Although the diastolic image quality decreased at higher heart rates, it remained superior to systolic image quality. The use of  $\beta$ -blockers is warranted for optimized CT image quality of PHVs.

**E**CG-gated CT imaging of prosthetic heart valves (PHV) is a promising new technique for the evaluation of PHV.<sup>1-4</sup> However, CT evaluation is hampered by two main difficulties: PHV appear as hyperdense objects on CT images due to radiopaque (i.e. metal) components and PHV move in concert with cardiac contractions. As a result, PHV emanate variable amounts of artifacts that may obscure the periprosthetic anatomy.<sup>1-3</sup> Because the lesions of interest such as obstructive masses and other morphological correlates of PHV dysfunction are located directly adjacent to the valves<sup>2,3,5,6</sup> further improvement of the diagnostic yield CT could be achieved by a reduction of artifacts and an improved image quality.

Strategies for the reduction of artifacts have primarily focused on the interaction of photons with the radiopaque components. In analogy to metal artifacts related to other objects (i.e. neurosurgical clips), artifacts can be reduced by increasing photon energy (kV) and increasing tube current (mAs).<sup>3,7-10</sup> In an *in vitro* model devoid of valve motion, good to excellent periprosthetic image quality was found for commonly used PHV.<sup>11</sup> Hence, in absence of motion the image quality was surprisingly good when compared to *in vivo* images. This suggests that choosing the cardiac phase with the least motion may be at least as important as modifying CT acquisition parameters in order to achieve the best image quality for PHV imaging.

Selection of the optimal cardiac phase has been extensively studied in order to improve image quality of coronary CT angiography.<sup>12-15</sup> In fact, it has been established that at higher heart rates end-systolic image quality may be superior to mid-diastolic phases.<sup>12-16</sup> Husmann et al.<sup>12</sup> found that increased coronary velocities at higher heart rates due to a non-proportional shortening of the diastole caused a decrease in diastolic image quality.

Due to the radiopaque and metal components of PHV, motion may have a considerable impact on PHV-related artifacts and CT image quality. PHV inevitably display two forms of motion: (1) motion of the valve as a whole (e.g. annular motion) and (2) the motion of the leaflets. *In vitro* studies found that rapid leaflet motion increased artifacts in a pulsatile model.<sup>17</sup> Clinical experience with the use of retrospective ECG-gating found important variation of image quality between reconstruction phases but no formal investigations have assessed CT image quality of PHV in different cardiac phases.

We undertook this study to evaluate the effect of PHV motion during the cardiac cycle on image quality and to assess the effect of higher heart rate on systolic and diastolic image quality.

## METHODS

### Patient selection

The study protocol was evaluated by the local institutional review board and a waiver for the study was obtained (number 11-514/C). In 42 patients with an aortic PHV that underwent 43 retrospectively ECG-gated cardiac CTAs with image reconstruction at each 10% of the ECG interval in addition to the 75% interval image quality was scored as previously described [Habets et al., Chapter XIII]. One patient was imaged twice with different aortic PHVs. In total, 27 mechanical PHVs and 16 biological PHVs were evaluated. Mean heart rate was  $71 \pm 18$  beats per minute. Seven patients had a heart rate higher than 90/min, 25 patient had a heart rate between 60 and 90/min and 11 patients had a heart rate less than 60/min.

### CT parameters

Retrospectively ECG-gated cardiac CTAs were performed on 64-slice ( $n=2$ ) or 256-slice ( $n=41$ )

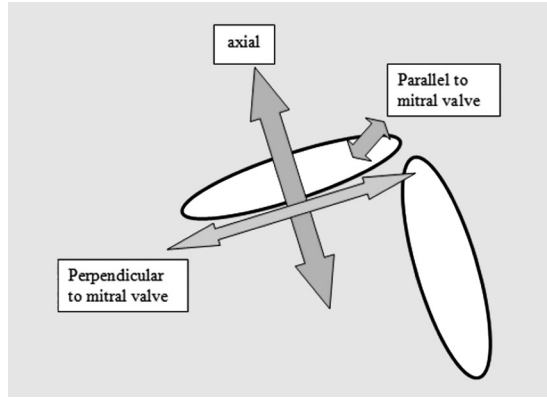


Figure 1 |

MDCT systems (Brilliance 64 and iCT, Philips Medical Systems, Cleveland, Ohio, USA). Image acquisition and contrast administration protocols were described in detail earlier [Habets et al., Chapter XIII]. No beta-blockers had been administered prior to the image acquisition.

**Measurement of PHV displacement and velocity**

For measurement of PHV displacement, image sets of all 11 ECG intervals were transferred to a dedicated workstation for analysis (Extended Brilliance Workstation, Philips Medical Systems, Philips, Best, the Netherlands). In the multiplanar viewer application, three orthogonal planes were adjusted in order to achieve a short axis view perfectly in plane to the prosthesis and the other planes perfectly perpendicular and parallel to the base of the mitral valve (see Figure 1). Displacement of the PHV was measured along three orthogonal planes: (1) axial plane, motion directed towards the ventricular outflow tract measured in a long axis view, (2) in plane perpendicular to the mitral valve, motion directed towards the mitral valve, and (3) in-plane parallel to the mitral valve, motion directed to the left coronary ostium both measured in a short axis view. For each plane separately, the cardiac phase with the most displacement towards the left ventricular outflow tract (axial plane), towards the mitral valve (in-plane perpendicular to the mitral valve) and towards the left coronary ostium (in-plane parallel to the mitral valve) was used as a reference point with a value of 0. Measurements were done independently by two observers for 10 patients and after finding good concordance the rest of the measurements were performed by one observer (PS).

Velocity was calculated by measuring displacement between two ECG intervals and by determining the absolute time delay between two intervals according to the method used for coronary arteries by Vembar et al.<sup>18</sup> and Husmann et al.<sup>12</sup> In short, the 3D displacement was calculated from the change in position in the three orthogonal planes between two consecutive ECG intervals (see equation 1, where x, y and z represent three orthogonal planes, p the position of the valve in each of the planes in each planes and p(n) and p(n-1) stand for an ECG interval and the previous ECG interval).

$$\text{displacement}(3D) = \sqrt{[x(p_{p(n)}) - x(p_{p(n-1)})]^2 + [y(p_{p(n)}) - y(p_{p(n-1)})]^2 + [z(p_{p(n)}) - z(p_{p(n-1)})]^2}$$

For the absolute time location in the cardiac cycle, delay was calculated using the adaptive timing algorithm described by Vembar et al.<sup>18</sup> This adaptive timing algorithm adjusts for the fixed length of the systole and the non-proportional shortening of the diastole at higher heart rates. For each patient,

the absolute time delays between two ECG intervals were calculated. The velocity was subsequently calculated by dividing the 3D displacement by the time delay.

### Visual assessment

Data evaluation was performed on a 4D research workstation (iX Viewer, Images Sciences Institute, Utrecht, the Netherlands) that allowed for scrolling through the data sets using interactive multiplanar reformatting. A two-alternative forced choice method was used as described by Smit et al.<sup>19</sup> in a manner described previously. In short, two observers (PS, JH) were each presented separately with all possible randomized and blinded pair-wise comparisons of the 11 ECG intervals. Images were judged on the prosthetic and periprosthetic detail and artifacts as described before.<sup>20</sup>

From the visual assessment, an image quality score was derived that represented the average percentage that the particular ECG interval was superior to other intervals. Image quality scores were then determined for the three heart rate groups.

### Statistical analysis

Data were analyzed using SPSS software (SPSS Statistics Version 16.0, SPSS Inc, Chicago, IL). Parametric data are presented as means  $\pm$  SD and non-parametric data as medians with interquartile range (IQR). A Kruskal Wallis test was used to detect differences in grouped non-parametric data (e.g. total displacement in a single motion plane, PHV velocity) and a Mann Whitney U test with Bonferroni correction was used to detect the differences between the specific subgroups. Statistical significance was defined as  $p < 0.05$ . PHV velocities at particular intervals were compared for three frequency ranges using a Kruskal Wallis and a posthoc Mann Whitney U test.

For the visual assessment, the superiority of image quality of one ECG interval over other ECG intervals was expressed as a percentage in cross tables (as reported in Habets et al, Chapter XIII). Inter- and intra-observer agreement was determined using kappa ( $\kappa$ ) statistics with correction for equal probability. Inter- and intra-observer agreement were expressed as mean  $\kappa$  value with standard error (SE) between observers for each scoring round and for individual observers. A  $\kappa$  value of 0.81-1.00 indicated very good agreement; 0.61—0.80, good agreement; 0.41-0.60, moderate agreement; 0.21-0.40, fair agreement; and 0.20 or lower, poor agreement.<sup>21</sup>

## RESULTS

The position of the PHV in the 3 orthogonal planes relative to the cardiac phases (Figure 2) followed a similar pattern in the axial and the plane perpendicular to the mitral valve. During systole, the displacement was directed towards the left ventricle and in the direction of the mitral valve until 40% of the ECG interval at which the nadir was reached (Figure 2). After 40% of the ECG interval, the displacement reversed and the PHV moved away from the left ventricle and away from the mitral valve. In the plane parallel to the mitral valve little change of position was measured and there appeared no relation to the cardiac cycle. During the cardiac cycle, the largest displacement was found in the plane perpendicular to the mitral valve (median 6.2 mm; IQR 5.2-7.3), followed by the axial plane (4.1 mm; IQR 2.7-6.2) and the least for the plane parallel to the mitral valve (2.3 mm; IQR 1.9-3.1, all differences  $p < 0.001$ ).

Median velocity per cardiac phase demonstrated a systolic and diastolic velocity trough: at 30 to 40% and at 75 to 80% respectively (Figure 3). Velocities varied widely and for every ECG interval maximal velocities in particular cases exceeded 40mm/sec (Table 1). The highest median velocity for

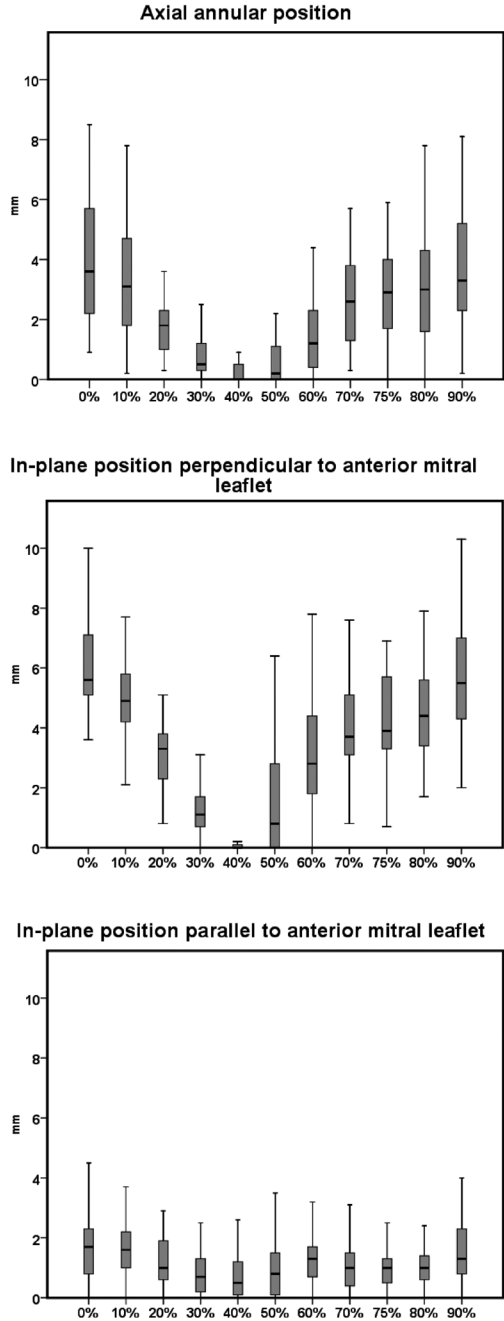


**Figure 2** | Aortic annular position during the cardiac cycle in the three planes of motion axial (top panel), perpendicular to the mitral valve (middle panel) and parallel to the mitral valve (lower panel). A reference plane for axial displacement (with a value of 0 mm) was aligned to the PHV position in the cardiac phase in which the PHV was most displaced in the direction of the left ventricular outflow tract. For displacement perpendicular and parallel to the mitral valve similar reference planes were established in the phases that the PHV was most displaced in the direction of the mitral valve and the left coronary artery respectively.

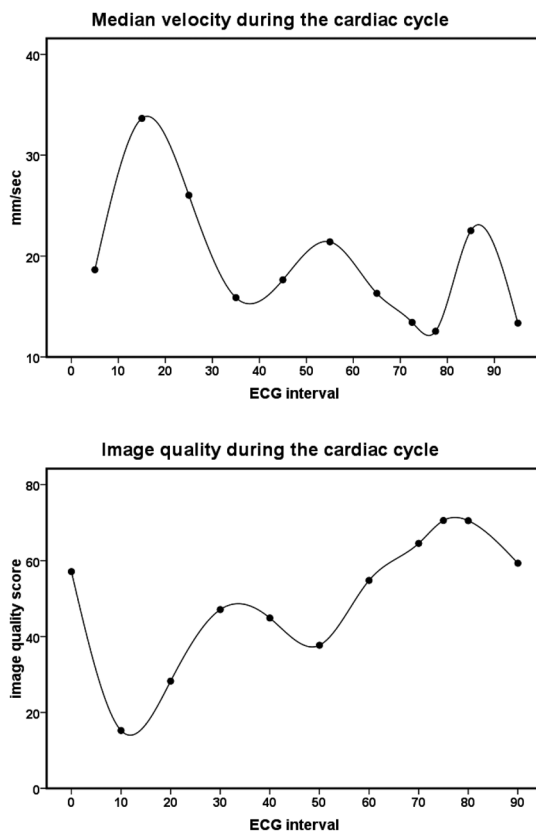


**Figure 3** | The average image quality determined with visual assessment (lower panel) and the median velocity of the PHV during the cardiac cycle (upper panel) of all patients ( $n=43$ ).

the entire group of patients was present at 0 to 20% of the ECG interval and other velocity peaks occurred at 50 to 60% and 80 to 90% of the ECG interval (Figure 3).

Image quality score was best in diastole at 75 and 80% and in systole at 30% followed by 40% (Figure 3). The cross tables on which these average percentages are presented in the data supplement (Appendix I). The associated intra- and interobserver kappa values are presented in the data supplement (Appendix II/III). For all 55 side by side comparisons intraobserver kappa was less than 0.6 in only four, and interobserver kappas were less than 0.6 in 14 comparisons.

When divided in three heart rate groups: (1)  $<60/\text{min}$  ( $n=11$ ), (2)  $60\text{-}90/\text{min}$  ( $n=25$ ) and (3)  $>90/\text{min}$  ( $n=7$ ), differences emerge in velocities at both the systolic trough (30 to 40%) and the diastolic trough (75-80%, see Table 1, Figure 4). Significant differences existed in the velocities at 30 to 40% and at 75 to 80% for the three frequency ranges when tested as a group ( $p=0.04$  and  $p=0.023$ , respectively). Post-hoc testing for the end systolic phase (30 to 40%) demonstrated a significantly higher velocity for  $>90/\text{min}$  difference in velocities between  $>90/\text{min}$  and  $60\text{-}90/\text{min}$  ( $p=0.015$ ), and  $>90/\text{min}$  and  $<60/\text{min}$  ( $p=0.035$ ). No significant difference was found between  $<60/\text{min}$  and  $60\text{-}90/\text{min}$  ( $p=0.85$ ). For the diastolic phase (75 to 80%), significant differences were found for velocities between  $<60/\text{min}$  and  $60\text{-}90/\text{min}$  ( $p=0.024$ ), and between  $<60/\text{min}$  and  $>90/\text{min}$  ( $p=0.033$ ). No significant difference was found between  $>90/\text{min}$  and  $60\text{-}90/\text{min}$  ( $p=0.164$ , Figure 4).

**Table 1 |**

Cardiac phase	Velocity (median, IQR) mm/sec	Heartrate <60/min (n=11)	Heartrate 60-90/min (n=25)	Heartrate >90/min (n=7)	Maximum velocity
0 to 10%	18.9 (12.6-28.2)	17.7 (11.4-19.8)	19.1 (10.9-31.8)	17.5 (14.7-27.1)	68.8
10 to 20%	32.8 (26.3-47.7)	31.5 (17.8-44.1)	39.8 (28.9-52.1)	32.7 (27.2-49.6)	91.7
20 to 30%	26.0 (20.1-38.5)	24.2 (19.6-27.1)	28.0 (20.7-40.1)	26.7 (22.0-31.6)	62.1
30 to 40%	<b>15.0 (10.8-24.5)</b>	<b>16.7 (10.5-24.2)</b>	<b>13.8 (11.1-20.6)</b>	<b>28.7 (24.5-43.4)</b>	45.4
40 to 50%	20.1 (9.5-35.4)	24.0 (9.2-45.9)	20.6 (9.1-35.2)	12.2 (6.2-13.5)	69.6
50 to 60%	21.1 (15.0-31.0)	20.7 (15.0-23.1)	21.1 (16.3-32.8)	31.0 (16.8-55.6)	61.1
60 to 70%	15.4 (9.4-36.1)	9.8 (5.5-11.9)	16.3 (10.5-32.4)	52.6 (38.1-54.4)	92.0
70 to 75%	13.0 (8.0-28.9)	8.8 (6.0-12.6)	14.2 (8.4-30.1)	37.7 (21.0-86.0)	137.9
75 to 80%	<b>12.6 (6.9-26.2)</b>	<b>6.9 (5.6-11.7)</b>	<b>12.9 (7.9-28.4)</b>	<b>50.1 (12.2-64.0)</b>	71.2
80 to 90%	22.5 (10.6-35.9)	10.6 (6.7-24.1)	24.5 (17.9-38.6)	25.8 (14.6-56.6)	67.4
90 to 0%	12.6 (6.9-18.9)	10.7 (6.1-16.9)	12.6 (7.2-19.4)	18.9 (9.9-21.9)	48.1

Velocity expressed as medians with interquartile range (IQR).

**Table 2 |** Average visual assessment scores (average percentage in which one interval was found to have better image quality than the other ECG interval). For complete data see data supplement as reported previously (Habets et al, Chapter XIII)

Cardiac phase	Image score all patients	Image score <60/min (n=11)	Image score 60-90/min (n=25)	Image score >90/min (n=7)
0 %	57	45	61	56
10 %	15	11	14	26
20 %	28	26	27	34
30 %	47	<b>49</b>	<b>46</b>	<b>48</b>
40 %	45	38	46	52
50 %	38	41	36	40
60 %	55	48	57	56
70 %	65	71	65	54
75 %	71	<b>79</b>	<b>70</b>	<b>59</b>
80 %	71	75	71	60
90 %	59	63	57	62



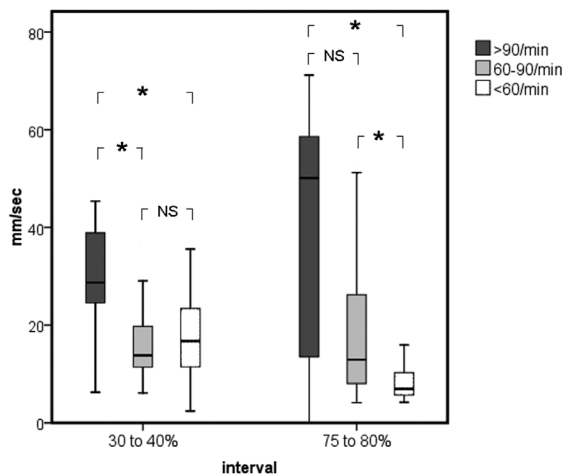


**Figure 4** | Differences between PHV velocities expressed with boxplots. Asterisks indicate  $p < 0.05$ .

**Median velocity during the cardiac cycle for 3 frequency ranges**

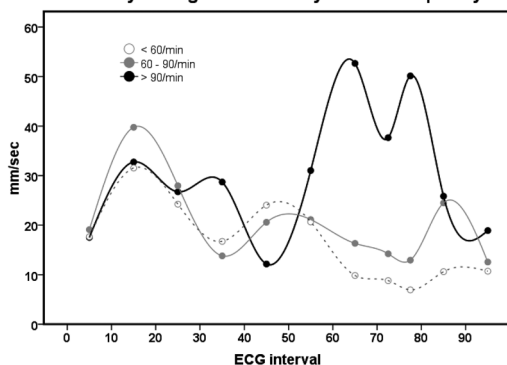


**Image quality for three frequency ranges**

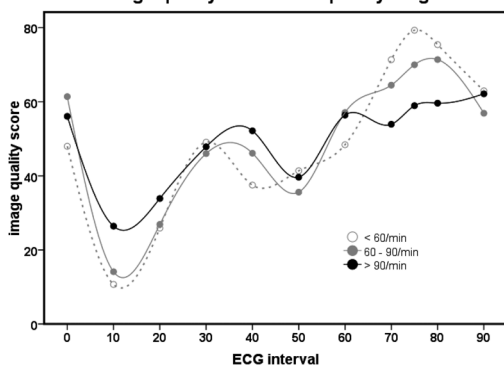


**Figure 5** | Image quality for each frequency range determined with visual assessment (lower panel) and median velocity of PHV during the cardiac cycle for three frequency ranges (upper panel). Despite a decrease in diastolic image quality at higher frequencies, end-systolic image quality remains inferior to diastolic image quality. Disparities in velocity appear in the systolic (30 to 40%) and diastolic (75 to 80%) velocity troughs.

The image quality scores for each interval are presented for the three frequency ranges in Table 2 and Figure 5. The mid-diastolic image quality scores decreased at higher frequencies but the end-systolic image quality did not vary with the frequency. Furthermore, the end-systolic image quality was not superior to mid-diastolic image quality in any frequency range, despite a small difference at  $>90/\text{min}$ . The image quality scores for each cardiac interval relative to the other is presented in the cross tables in the appendix (Appendix VI-VIII).

## DISCUSSION

In this study we found that PHV velocity during the cardiac cycle was least during end-systole (30 to 40% of the ECG interval) and mid-diastole (75 to 80% of the ECG interval) which corresponded to the best systolic and diastolic image quality. Furthermore, with an increased heart rate mid-diastolic velocity increased and despite mid-diastolic velocities superior to end-systolic velocities at  $>90/\text{min}$ , the mid-diastolic image quality remained superior to systolic phases. For CT image acquisition of PHV the use of heart rate lowering drugs such as  $\beta$ -blockers is warranted as best imaging results are expected in mid-diastolic phases at low heart rates.

The velocities of PHV in the aortic position during the cardiac cycle are important for two reasons: (1) velocities may exceed the temporal resolution of the CT system which may cause double contours and a non-diagnostic image, and (2) motion is known to augment metal-related artifacts which are commonly encountered with CT imaging of mechanical and many biological PHVs. In earlier *in vitro* simulations where only leaflet motion was possible, rapid opening and closing motion increased PHV-related artifacts.<sup>17</sup> Hence, the motion of the prosthesis as a whole may also increase PHV-related artifacts and affect image quality.

Although the motion of the aortic root has been studied in patients with native aortic valves, no studies have been performed on the three-dimensional motion of implanted aortic prostheses. Motion quantified as the total displacement of the aortic root measured with aortograms<sup>22-24</sup> was found to change after aortic valve replacement.<sup>23</sup> However, the quantification using aortograms quantified only two-dimensional motion and did not take into consideration anatomical variation and differences in orientation of the aortic root. More detailed studies of the native aortic root motion with magnetic resonance imaging demonstrated axial and in-plane aortic movement with a wide range of velocities which commonly exceeded 50 mm/sec in early systole and early diastole.<sup>25</sup> Motion was primarily in the axial plane. In our study where the motion was quantified relative to the anatomical structures of the root, we found more in-plane displacement towards the mitral valve than in the axial direction. A possible explanation may be the postoperative adhesions that fix the aortic root and proximal ascending aorta to its surroundings and limit axial motion.

The motion of the coronary arteries and the effect of motion on image quality has been studied by Husmann et al.<sup>12</sup> Image quality quantified with Likert scores was best in the cardiac phases with the lowest systolic and diastolic velocity, and a correlation between coronary velocity and image quality was found. With increased heart rates and the non-proportional shortening of the diastole, the velocities in diastole exceeded systolic velocities and the diastolic image quality deteriorated and was inferior to end-systolic image quality. For PHV in the aortic position, the cardiac phases with the lowest systolic and diastolic velocity were associated with the best image quality in a pattern corresponding to the pattern found with coronary arteries by Husmann et al.<sup>12</sup> Contrary to their findings, however, we did not find a superior end-systolic image quality at higher heart rates when compared to the diastolic image quality. Although we found higher diastolic velocities when compared to the systolic phases

at heart rates >90/min, this did not translate in an inferior image quality. Three factors may explain this discrepancy. First, CT imaging of coronary arteries and PHV is not comparable due to lower average velocities of the PHV and the variable metal-related artifacts associated with PHV imaging. We did not include stentless bioprostheses or homografts in our series and therefore all the PHV in this study had some radiopaque components. Because motion exacerbates metal-related artifacts, the image quality may not be determined by motion only but may also depend on the amount of artifacts generated by the PHV<sup>9,10</sup> and other interactions.<sup>26,27</sup> Second, we used a two-alternative forced choice test instead of a Likert scale for the comparison of image quality between the cardiac phases. This method has been extensively used to assess lossless compression of digital image data<sup>27</sup> and is easily applicable to the comparison of image quality between cardiac phases which resulted in robust inter- and intraobserver kappa values. However, it may generate different data than Likert scale image grading. A third factor may involve the earlier *in vitro* observation that closed PHV emanate the least artifacts.<sup>17</sup> This may contribute to the better diastolic image quality at higher frequencies despite a higher velocity.

Our study has several limitations. First, the distribution of patients among the three heart rate groups was unequal with only seven patients in the >90/min group. Second, the timing algorithms may differ between vendors. Although the majority of vendors use algorithms that correct for the non-proportional shortening of the diastole at higher heart rates, small differences between the specific algorithms may result in different velocities. Third, due to the radiolucency of the leaflets of certain (biological) PHV, the exact cardiac phase could not be checked by assessing the full opening during systole. We could, however, assess complete closure of the leaflets at the onset of diastole. In addition, we found a uniform change in PHV position corresponding to the cardiac cycle in the axial plane and in the plane perpendicular to the mitral valve.

In conclusion, PHV velocity during the cardiac cycle exhibited an end-systolic and mid-diastolic trough which corresponded to the best systolic and diastolic image quality relative to the other phases. At higher heart rates, image quality during diastole decreased but remained superior to the systolic image quality. For CT imaging of PHV, our results support the use of  $\beta$ -blockers and dose reduction strategies for early systolic and early diastolic phases.

## REFERENCES

1. Tsai IC, Lin YK, Chang Y, et al. Correctness of multi-detector-row computed tomography for diagnosing mechanical prosthetic heart valve disorders using operative findings as a gold standard. *Eur Radiol* 2009; 19: 857-867.
2. Symersky P, Budde RP, de Mol BA, et al. Comparison of multidetector-row computed tomography to echocardiography and fluoroscopy for evaluation of patients with mechanical prosthetic valve obstruction. *Am J Cardiol*. 2009; 104:1128-1134.
3. Konen E, Goitein O, Feinberg MS, et al. The role of ECG-gated MDCT in the evaluation of aortic and mitral mechanical valves: initial experience. *Am J Roentgenol*. 2008; 191:26-31.
4. Habets J, Budde RP, Symersky P, et al. Diagnostic evaluation of left-sided prosthetic heart dysfunction. *Nat Rev Cardiol* 2011; 8:466-478.
5. Teshima H, Hayashida N, Fukunaga S, et al. Usefulness of a multidetector-row computed tomography scanner for detecting pannus formation. *Ann Thorac Surg*. 2004; 77:523-526.
6. Toledano D, Acar, C. Usefulness of computed tomography scanning in the diagnosis of aortic prosthetic valve pannus. *J Heart Valve Dis*. 2010; 19:665-668.
7. van der Schaaf I, van Leeuwen M, Vlassenbroek A, et al. Minimizing clip artifacts in multi CT angiography in clipped patients. *Am J Neuroradiol* 2006; 27:60-66.
8. Chenot F, Montant P, Goffinet C, et al. Evaluation of anatomic valve opening and leaflet morphology in aortic valve bioprosthesis by using multidetector CT: comparison with transthoracic echocardiography. *Radiology* 2010; 255:377-385.
9. De Man B, Nuyts J, Dupont P, et al. Metal streak artifacts in x-ray computed tomography: a simulation study. *IEEE Trans Nucl Sci* 1999; 46:691-696.
10. Boas FE, Fleischmann D. Evaluation of two iterative techniques for reducing metal artifacts in computed tomography. *Radiology* 2011; 259:894-902.
11. Symersky P, Budde RPJ, Prokop M, et al. Multidetector-row computed tomography imaging characteristics of mechanical prosthetic valves. *J Heart Valve Dis*. 2011; 20:216-222.
12. Husmann L, Leschka S, Desbiolles L, et al. Coronary artery motion and cardiac phases: dependency on heart rate – implications for CT image reconstruction. *Radiology* 2007; 245:567-576.
13. Wintersperger BJ, Nikolaou K, von Ziegler F, et al. Image quality, motion artifacts, and reconstruction timing of 64-slice coronary computed tomography angiography with 0.33-second rotation speed. *Invest Radiol* 2006; 41:436-442.
14. Seifarth H, Wienbeck S, Pusken M, et al. Optimal systolic and diastolic reconstruction windows for coronary CT angiography using dual source CT. *Am J Roentgenol*. 2007; 189:1317-1323.
15. Weustink AC, Mollet NR, Pugliese F, et al. Optimal electrocardiographic pulsing windows and heart rate: effect on image quality and radiation exposure at dual-source coronary CT angiography. *Radiology* 2008; 248:792-798.
16. Araoz PA, Kirsch J, Primak AN, et al. Optimal image reconstruction phase at low and high heart rates in dual-source CT coronary angiography. *Int J Cardiovasc Imaging* 2009; 25:837-845.
17. Symersky P, Budde RP, Westers P, et al. Multidetector CT imaging of mechanical prosthetic heart valves: quantification of artifacts with a pulsatile in-vitro model. *Eur Radiol* 2011; 21:2103-2110.
18. Vembar M, Garcia MJ, Heuscher DJ, et al. A dynamic approach to identifying desired physiological phases for cardiac imaging with multislice spiral CT. *Med Phys* 2003; 30:1683-1693.
19. Smit EJ, Vonken EJ, van der Schaaf IC, et al. Timing-invariant reconstruction for deriving high-quality computed tomography angiography from cerebral CT-perfusion data. *Radiology* 2012; 263:216-225.
20. Habets J, Symersky P, van Herwerden LA, et al. Prosthetic heart valve assessment with multidetector-row CT: imaging characteristics of 91 valves in 83 patients. *Eur Radiol*. 2011; 21:1390-1396.
21. Altman DG. *Practical statistics for medical research*. Chapman & Hall/CRC, 1990.
22. Mercer JL. Movement of the aortic annulus. *Br J Radiol*. 1969; 42:623-626.
23. Beller CJ, Labrosse MR, Thubrikar MJ, et al. Role of aortic root motion in the pathogenesis of aortic dissection. *Circulation* 2004; 109:763-769.
24. Beller CJ, Labrosse MR, Hagl S, et al. Aortic root motion remodelling after aortic valve replacement-implications for late aortic dissection. *Interact Cardiovasc Thorac Surg* 2008; 7:407-411.
25. Kozerke S, Scheidegger MB, Pedersen EM, et al. Heart motion adapted cine phase-contrast flow measurements through the aortic valve. *Magn Reson Med* 1999; 42:970-978.
26. Barrett JF, Keat N. Artifacts in CT: recognition and avoidance. *Radiographics* 2004; 24:1679-1691.
27. Wilting JE, Timmer J. Artefacts in spiral-CT images and their relation to pitch and subject morphology. *Eur Radiol*. 1999; 9:316-322.
28. Slone RM, Foss DH, Whiting BR, et al. Assessment of visually lossless irreversible image compression: comparison of three methods by using an image-comparison workstation. *Radiology* 2000; 215:543-553.



CHAPTER XV

SERIAL COMPUTED  
TOMOGRAPHY IMAGING *of*  
PROSTHETIC HEART VALVE  
ENDOCARDITIS *in a* PEDIATRIC  
PATIENT

J. Habets  
G. van Iperen  
F. Haas  
W.P.Th.M. Mali  
R.P.J. Budde

SUBMITTED



We present a case of a 16 year old boy that was born with a complex congenital heart disease that included a double aortic arch and patent ductus arteriosus, valvular aortic stenosis, valvular pulmonary stenosis, left pulmonary artery origin stenosis, perimembranous ventricular septum defect and patent foramen ovale. The patient had underwent multiple previous cardiac operations the most recent of which included implantation of a 21 mm bileaflet St Jude prosthetic heart valve in the aortic position. The patient presented at the emergency room with persistent fever after initiation of antibiotic treatment (amoxicillin and clavulanate potassium) because of erysipelas of the left upper leg by the general practitioner. Physical examination demonstrated a moderately ill patient with a normal circulation. No new findings were found during cardiac and pulmonary auscultation. Laboratory evaluation revealed an increased C reactive protein level (179 mg/L) but normal leucocyte count ( $4.5 \times 10^9$  mmol/L), hemoglobin (7.9mmol/l), hematocrit (0.37L/L) and thrombocyte count ( $74 \times 10^9$  mmol/L). Four separate blood cultures were positive for staphylococcus aureus. Broad spectrum antibiotic regimen was started (flucloxacillin, rifampicin and gentamycin) intravenously based on the first blood culture result. One day after admission, transthoracic echocardiography demonstrated no signs of endocarditis (vegetations, mycotic aneurysms or abscesses). Two days later, transesophageal echocardiography (TEE) demonstrated a vegetation (8.5x5.8mm) in the left ventricular outflow tract (LVOT) and an irregular aspect of the dorsal aortic wall (Figure 1A). With this findings and the positive blood cultures he met the Duke criteria for endocarditis. Retrospectively ECG-gated cardiac CT angiography (CTA) was performed with a 256 slice computed tomography (CT) system (iCT, Philips Medical Systems, Cleveland, Ohio, USA) on the same day. Acquisition parameters were: tube voltage 120kV; tube current 500mAs; collimation 128x0.625; pitch 0.16 seconds, and gantry rotation time 0.27 seconds. CTA confirmed the presence of the vegetation (Figure 2) but also revealed diffuse thickening of the ascending aortic wall consistent with aortitis (Figure 3). After this CT scan, it was decided to continue the patient management with broad spectrum antibiotic therapy. One week later, clinical deterioration (recurrent fever during antibiotic therapy) occurred. TEE and CTA were repeated and now showed an increased vegetation size (13x8mm) (Figure 1B). TEE now also showed diffuse thickening of ascending aortic

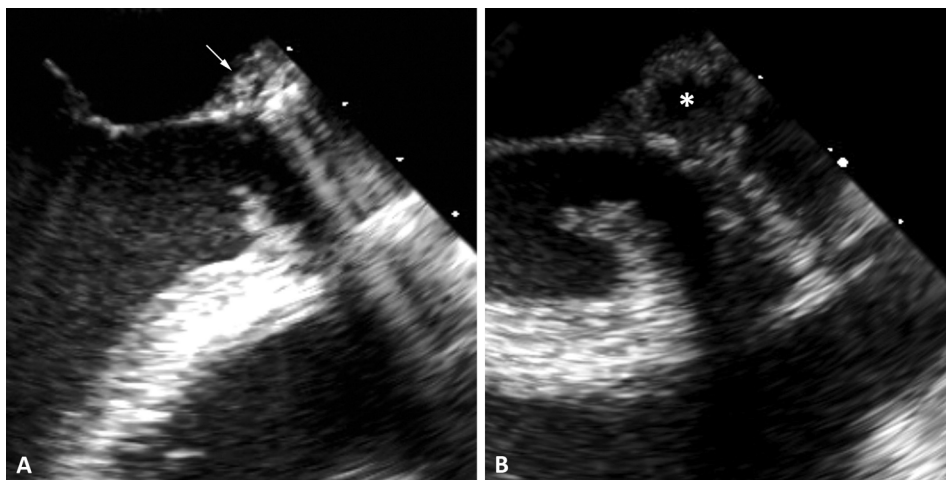


**Figure 1** | Transesophageal echocardiographic long axis view: an echodense mass (vegetation) is present in the left ventricular outflow tract (LVOT). The white arrow indicates the aortitis of the dorsal aortic wall (A) During follow up the vegetation size increased and a echolucent mass (\*) representing the dorsal aortic root mycotic aneurysm appeared (B)

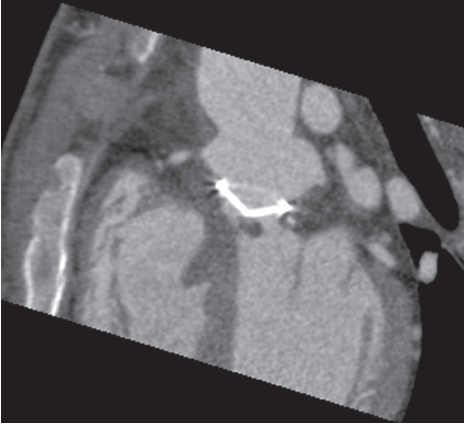


**Figure 2** | CT image of the first CT scan demonstrates a hypodense subvalvular mass that is compatible with a vegetation

wall and a echolucent cavity suspected for mycotic aneurysm (Figure 1B). CTA better delineated an extensive dorsal aortic root mycotic aneurysm (Figure 4). Furthermore, the aortitis was more extensive compared to the previous CTA. CTA also revealed the close relationship of the mycotic aneurysm with the right coronary artery (Figure 5). One day later, the patient was reoperated. Surgical inspection confirmed the dorsal aortic root mycotic aneurysm and the vegetation in the LVOT. The prosthetic heart valve (PHV) was explanted and the aortic root resected. After carefully removing all vegetations from the LVOT, a 22mm aortic homograft was implanted with re-implantation of the coronary arteries. Postoperative recovery was uneventful except for a temporary sick sinus syndrome treated with external cardiac pacing. The antibiotic regimen was continued intravenously for 6 weeks after the reoperation. The patient was discharged home in good condition on the 25th postoperative day.

208

## DISCUSSION

Endocarditis is a feared and potentially devastating disease in patients with a PHV. Echocardiography (TTE and TEE) are the routine imaging techniques to evaluate suspected prosthetic heart valve

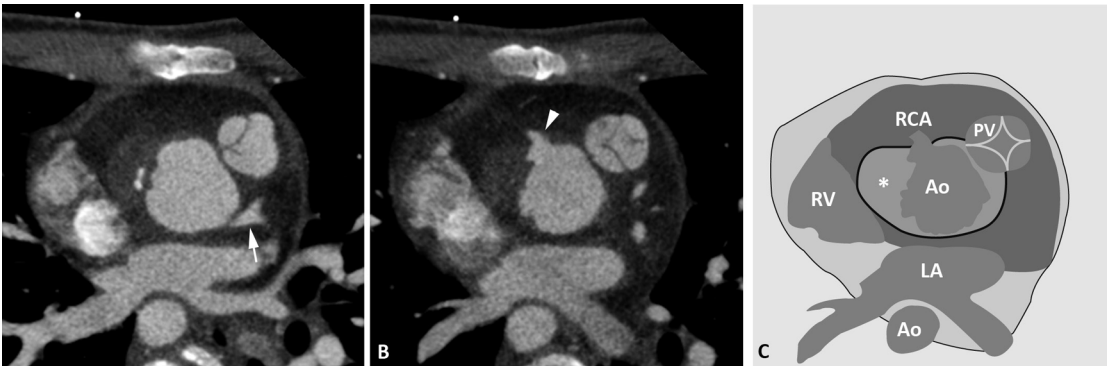


**Figure 3** | CT reconstruction perpendicular to the aortic valve at supra valvular level demonstrating diffuse thickening of the aortic wall at the level of the origin of the left coronary artery (arrow) (A) and the right coronary artery (arrowhead) (B). The black line in the illustration (C) delineates the diffuse area of aortitis (\*). Ao = aorta; LA = left atrium, PV = pulmonary valve; RCA = right coronary artery; and RV = right ventricle



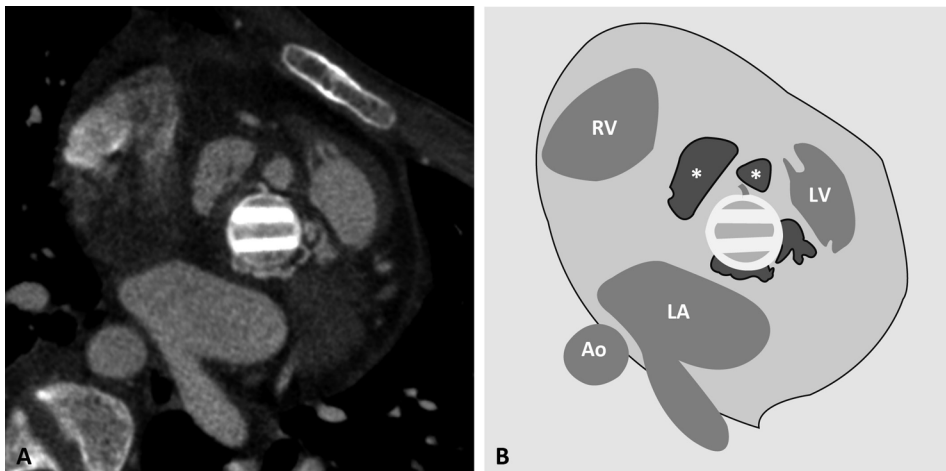


**Figure 4** | CT reconstruction in plane with the prosthetic heart valve (A) and illustration (B) demonstrating the extent of the aortic wall mycotic aneurysm (\*). Ao = aorta; LA = left atrium; LV = left ventricle and RV = right ventricle

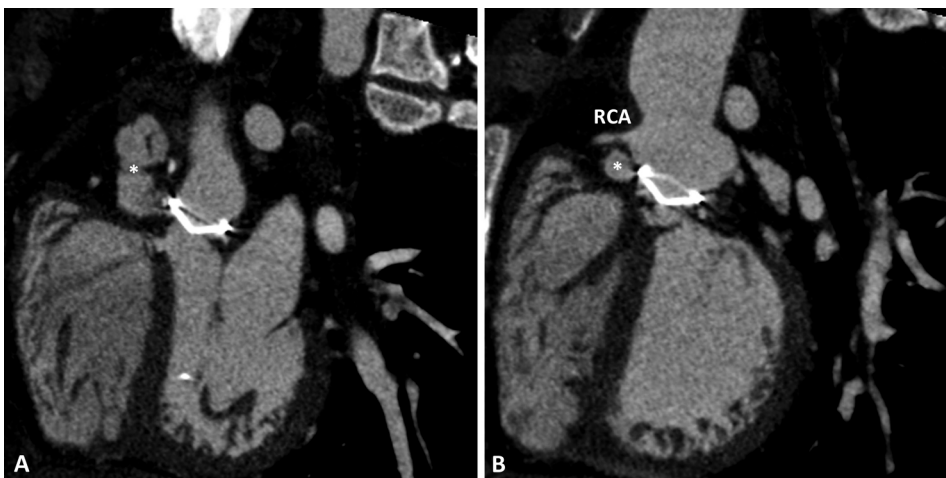


**Figure 5** | CT reconstruction perpendicular to the valve leaflets showing the extent of the aortic root mycotic aneurysm (A, \*) and its close relationship with the right coronary artery (RCA) (B).

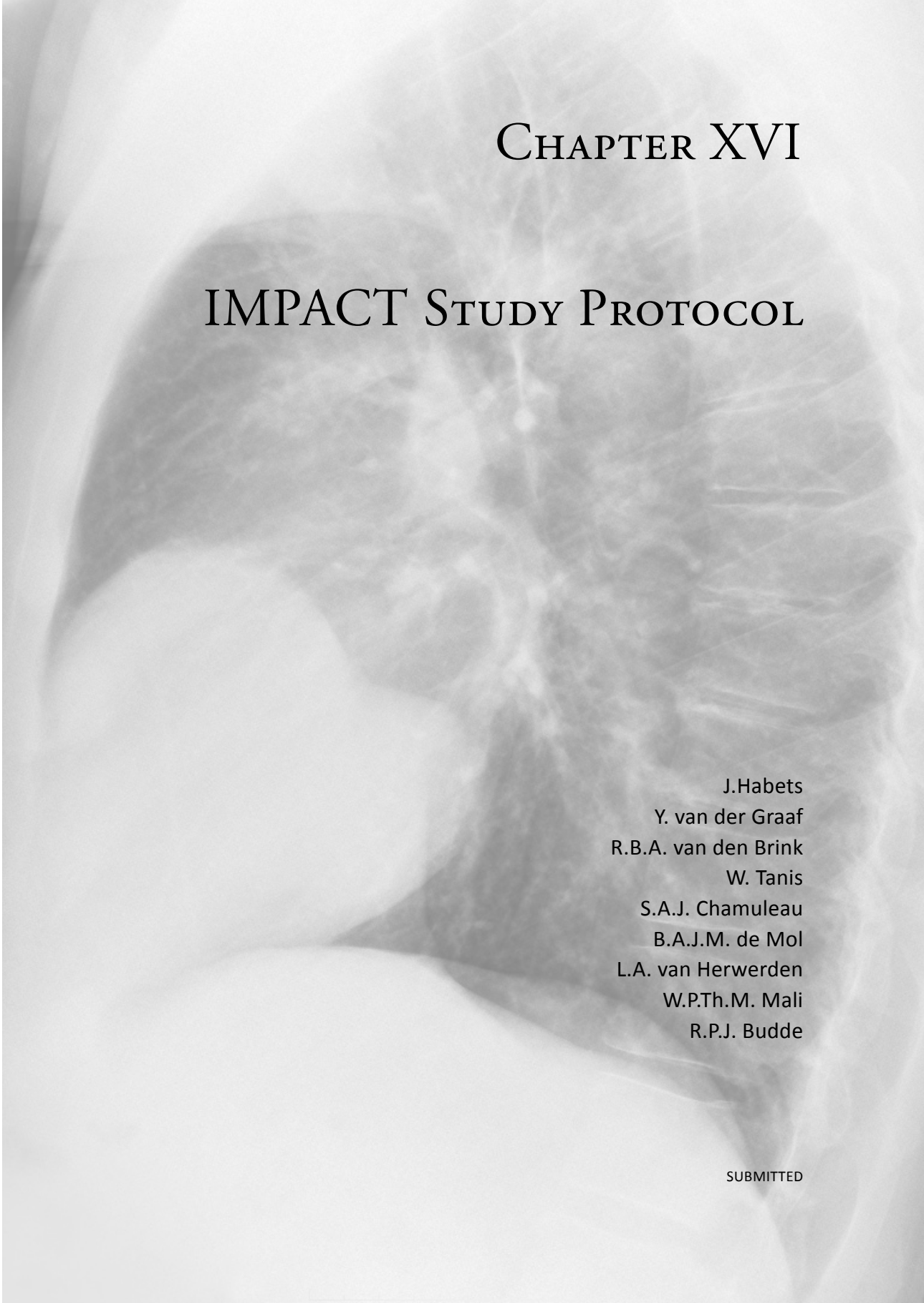
endocarditis.<sup>1</sup> In a previous study in 37 adults with native or prosthetic heart valve endocarditis, CTA detected all vegetations, mycotic aneurysms and abscesses detected by TEE in patients with a prosthetic heart valve. In one patient with a PHV, CTA detected a vegetation that was missed with TEE.<sup>2</sup> Echocardiography may miss signs of PHV infective endocarditis due to acoustic shadowing caused by the prosthesis. Recently, CTA has emerged as an adjunct to echocardiography for PHV assessment and most PHV types generate only limited artifacts on CT.<sup>3</sup> The serial CTA examinations in this patient described in this report nicely demonstrated the clinical course from aortitis to aortic root destruction with mycotic aneurysm formation in PHV endocarditis. CTA is not hampered by acoustic shadowing and echocardiographic windows and can assess the entire area from LVOT to the (ascending) aorta from a single scan. Furthermore, image acquisition and assessment is uncoupled

for CT. Off-line images can be reconstructed in any desired viewing plane, and allow for precise assessment of the extent of the aortic root disease. Besides the assessment of aortic root and the presence of vegetations, CTA can also assess the presence of coronary artery disease without the risk of embolization of vegetations. A major drawback of CT angiography, especially in the pediatric population, is the associated radiation exposure. However, in adults the risk associated with reoperation to replace a dysfunctional PHV is high and overall mortality after aortic PHV reoperation is reported up to 15.3% depending on the cause of PHV dysfunction.<sup>4</sup> Radiation exposure reduction strategies such as dose modulation, prospective triggering and iterative reconstruction have to be considered especially in the pediatric population. In conclusion, we describe a pediatric patient in which serial CT imaging depicted the course from aortitis to aortic root mycotic aneurysm formation and had additional diagnostic value to echocardiography in visualizing the extent of disease.

## REFERENCES

1. Habets J, Budde RP, Symersky P, et al. Diagnostic evaluation of left-sided prosthetic heart valve dysfunction. *Nat Rev Cardiol* 2011; 8:466-78.
2. Feuchtner GM, Stolzmann P, Dichtl W, et al. Multislice computed tomography in infective endocarditis: comparison with transesophageal echocardiography and intraoperative findings. *J Am Coll Cardiol*. 2009; 53:436-44.
3. Habets J, Symersky P, van Herwerden LA, et al. Prosthetic heart valve assessment with multidetector-row CT: imaging characteristics of 91 valves in 83 patients. *Eur Radiol*. 2011; 21:1390-6.
4. Leontyev S, Borger MA, Modi P, et al. Redo aortic valve surgery: Influence of prosthetic valve endocarditis on outcomes. *J Thorac Cardiovasc Surg* 2011; 142:99-105.





CHAPTER XVI

IMPACT STUDY PROTOCOL

J.Habets  
Y. van der Graaf  
R.B.A. van den Brink  
W. Tanis  
S.A.J. Chamuleau  
B.A.J.M. de Mol  
L.A. van Herwerden  
W.P.Th.M. Mali  
R.P.J. Budde

SUBMITTED

## ABSTRACT

**PURPOSE** | Prosthetic heart valve dysfunction is an infrequent but potentially life-threatening disease. In clinical practice, non-invasive imaging modalities (echocardiography and fluoroscopy) play a key role in the establishment of the diagnosis. These imaging techniques may fail to determine the exact cause of prosthetic heart valve dysfunction. Multidetector-row computed tomography is a promising imaging technique to evaluate patients with prosthetic heart valve dysfunction. Further prospective studies are required: (1) to determine normal computed tomography imaging characteristics of prosthetic heart valves and (2) to determine the additional diagnostic value of MDCT to echocardiography and fluoroscopy for assessment of suspected PHV dysfunction and its impact on patient management.

**METHODS/DESIGN** | We propose a diagnostic-cross sectional study to determine (1) normal MDCT imaging characteristics of six commonly implanted mechanical and biological prosthetic heart valves, and (2) complementary diagnostic value of MDCT to clinical routine imaging modalities in patients with suspected PHV dysfunction and its impact as patient management. In this manuscript, we describe in detail the methods and design of the prospective IMPACT study.

**DISCUSSION** | This diagnostic cross-sectional study will be the first large prospective study to determine the complementary value of MDCT in patients with suspected PHV dysfunction. Moreover, this study will provide normal MDCT imaging characteristics of PHVs which are important for MDCT interpretation.

### Abbreviations

DLP = dose length product  
 ECG = electrocardiogram  
 GFR = glomerular filtration rate  
 IMPACT = Imaging of Prosthetic Heart Valves By CT  
 IV = intravenous  
 LV = left ventricle  
 MDCT = multidetector-row computed tomography  
 PACS = Picture and Archiving Systems  
 PHV = Prosthetic Heart Valve  
 ROC = Receiver Operating Curve  
 TTE = transthoracic echocardiography  
 TEE = transesophageal echocardiography

In 2003, approximately 290,000 patients underwent prosthetic heart valve (PHV) replacement using either a biological (porcine or pericardial) or mechanical PHV.<sup>1</sup> Biological PHVs structurally decline in 10-15 years and mechanical PHV carry a per patient-year risk of valve failure and dysfunction of approximately 0.1-0.4%.<sup>2,3</sup> Therefore, patients remain under lifelong surveillance using non-invasive echocardiography which provides both anatomical and functional information, and is especially suited to confirm normal valve function.<sup>4</sup>

PHV dysfunction can be subclassified into three main groups: (1) obstruction, (2) abnormal leakage and (3) endocarditis. PHV obstruction manifests itself as an elevated pressure gradient over the valve on echocardiography and/or decreased prosthetic orifice area. Echocardiography relies on Doppler flow velocities to calculate the pressure drop over the valve and is influenced by the patient's hemodynamic status, localized areas of high flow as well as being operator dependent. Even when an elevated pressure gradient is unequivocally established on echocardiography its anatomical substrate often remains difficult or impossible to determine. Especially, the echocardiographic discrimination between pannus (tissue ingrowth underneath the valve) and thrombus is extremely difficult.<sup>5-7</sup> In the clinical setting, this discrimination is very important as thrombus can be treated with anticoagulation therapy or thrombolysis whereas pannus formation primarily requires a re-operation in symptomatic patients.<sup>6</sup>

All PHVs demonstrate a normal amount of leakage backflow that is needed to close the valve leaflets and each PHV has its own distinct pattern.<sup>4,8</sup> Abnormal leakage inside the valve ring may be seen with leaflet dysfunction. Leakage outside the PHV ring is always pathological. Echocardiography is well suited to demonstrate abnormal leakage. Difficulties may arise in discriminating normal from abnormal leakage inside the valve ring and determining the exact location of paravalvular leaks.

Patients with a PHV are at risk for developing endocarditis. The diagnosis may be extremely challenging and relies on clinical, laboratory and echocardiographic findings. Identifying vegetations on the PHV with echocardiography is often hampered by PHV induced artifacts especially in patients with aortic PHVs. These artifacts may also obscure the adjacent anatomy rendering the identification of abscess and/or mycotic aneurysm formation more difficult.

A high-risk reoperation to replace a dysfunctional prosthetic valve may be required in patients with PHV obstruction, leakage or endocarditis but echocardiography may fail to diagnose the cause of PHV dysfunction in up to 50% of patients.<sup>6</sup> Furthermore, echocardiography can determine the opening and closing angles of bileaflet mechanical valves in only 35% of patients and thus additional fluoroscopy may be needed to assess leaflet motion.<sup>9,10</sup> Echocardiographic assessment of PHV function is particularly difficult in patients with aortic PHVs and patients with double PHV replacements (aortic and mitral PHV) because of acoustic shadowing which hampers appropriate diagnostic assessment.

Consequently, echocardiography and fluoroscopy are best suited (1) to confirm normal PHV function, and (2) to detect the effects of PHV dysfunction but often can not determine the anatomic substrate which is of vital importance to plan a high risk reoperation (mean mortality of 9.4% which rises to 33% in emergency cases)<sup>11-13</sup> and assess the potential gain of such a high-risk and costly procedure.

Multidetector-row computed tomography (MDCT) is a non-invasive cardiac imaging method that has been established for coronary assessment.<sup>14,15</sup> With the current high-resolution scanners a three-dimensional dataset is obtained that can be analyzed in any desired imaging plane. Recently, initial work has shown that MDCT has potential for PHV assessment as well.<sup>8,16-23</sup> We have imaged the most commonly implanted mechanical PHVs in an in vitro perfusion set-up using 64- and 256-detector-row scanners and demonstrated that highly detailed images can be reproducibly

obtained with only few artifacts.<sup>24,25</sup> Although echocardiography is fast, non-invasive and provides anatomical and functional information, several pitfalls and shortcomings exist for visualization of PHVs.<sup>4-6</sup> With cardiac MDCT, a non-invasive imaging technique has entered the clinical arena that is expected to complement echocardiography in the evaluation of patients with suspected PHV dysfunction.

The imaging of prosthetic heart valves with CT (IMPACT) study was designed with a twofold objective: (1) to determine the normal MDCT imaging characteristics of commonly implanted PHV types in our centers and (2) to determine the additional diagnostic value of MDCT to echocardiography and fluoroscopy for assessment of suspected PHV dysfunction and its impact on patient management.

## METHODS/DESIGN

### Primary and secondary endpoints

We expect that MDCT will have complementary diagnostic value to the clinical routine imaging modalities in the diagnosis of the anatomical substrate of PHV dysfunction and its impact on patient management. Since little is known about the MDCT imaging characteristics of patients with normal PHV function, this study aims to determine MDCT normal reference values of six currently implanted PHV types (IMPACT I). This validation of MDCT findings of normally functioning PHVs is essential for interpretation of MDCT findings in patients with suspected PHV dysfunction. Furthermore, we aim to determine the additional diagnostic value of MDCT to routinely used imaging techniques (transthoracic echocardiography (TTE), transesophageal echocardiography (TEE) and fluoroscopy) to diagnose the anatomical substrate in patients with suspected PHV dysfunction and its subsequent impact on patient management (IMPACT II).

### IMPACT I

The primary endpoints in IMPACT I are: (1) percentage of patients in which supra-, peri-, sub- and valvular anatomy could be diagnostically assessed; and (2) percentage of patients in which leaflet motion in cine mode could be diagnostically assessed and opening and closing angles could be measured.

### IMPACT II

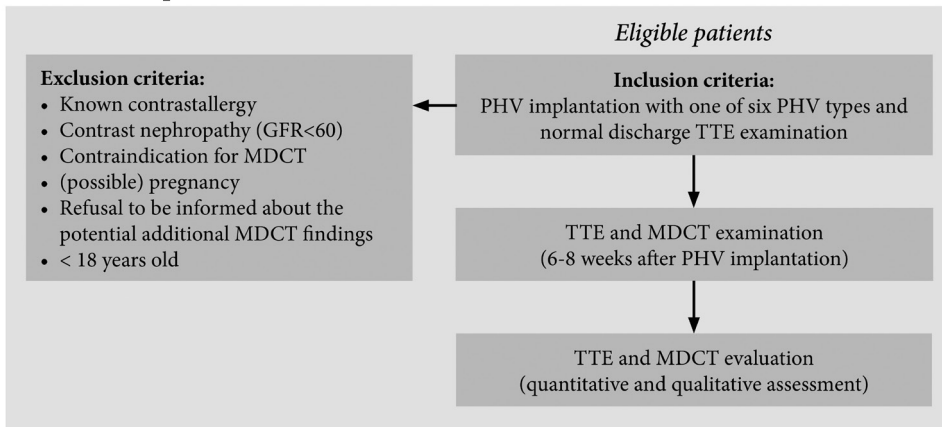
The primary endpoints in IMPACT II are: (1) diagnostic accuracy of echocardiography/fluoroscopy and MDCT for detection of the cause of PHV dysfunction; and (2) percentage of patients in which MDCT imaging provided additional diagnostic information to echocardiography and fluoroscopy and (3) percentage of patients in which MDCT imaging led to a change in patient management.

### DESIGN

Prospective two-centre diagnostic cross-sectional study in a tertiary setting including two academic medical centres, University Medical Centre of Utrecht (UMCU) and the Academic Medical Centre (AMC) Amsterdam, in the Netherlands. This diagnostic cross-sectional study has been approved by the local institutional review board at UMCU and AMC [IRB number 10-008]. This clinical study will be performed according to the DECLARATION OF HELSINKI – Ethical Principles for Medical Research Involving Human Subjects. The study is supported by a grant of the Netherlands Heart Foundation [Grant number 2009B014].



Figure 1 |

**IMPACT I (suspected normal PHV function)**

GFR = glomerular filtration rate; MDCT = multidetector-row CT; PHV = Prosthetic Heart Valve; and TTE = Transthoracic Echocardiography

**IMPACT I**

In Figure 1, the workflow of IMPACT I is shown. In IMPACT I, our aim is to include seventy-two patients who underwent PHV implantation with one of six predefined PHV types and have a normal routine follow-up TTE before hospital discharge. Twelve patients with each PHV type will be included. The six different PHV types that are eligible for inclusion include, 4 mechanical valves (ON-X, On-X Life Technologies Inc, Austin, TX, USA; Carbomedics, Sorin Group USA Inc., Arvada, CO, USA; Sorin, Sorin Biomedica Cardio, Milan, Italy; St Jude, St Jude Medical, St Paul, MN, USA) and 2 biological valves (Mitroflow, Mitroflow, Richmond, Canada; Carpentier Edwards, Carpentier Edwards bovine, Edwards Lifesciences, Irvine, CA, USA). Patients in IMPACT I are informed about the IMPACT study during their hospital stay for PHV implantation. If patients provide informed consent, they are invited to visit the outpatient clinic approximately 6-8 weeks after PHV implantation to undergo a TTE and cardiac CT-scan as described below.

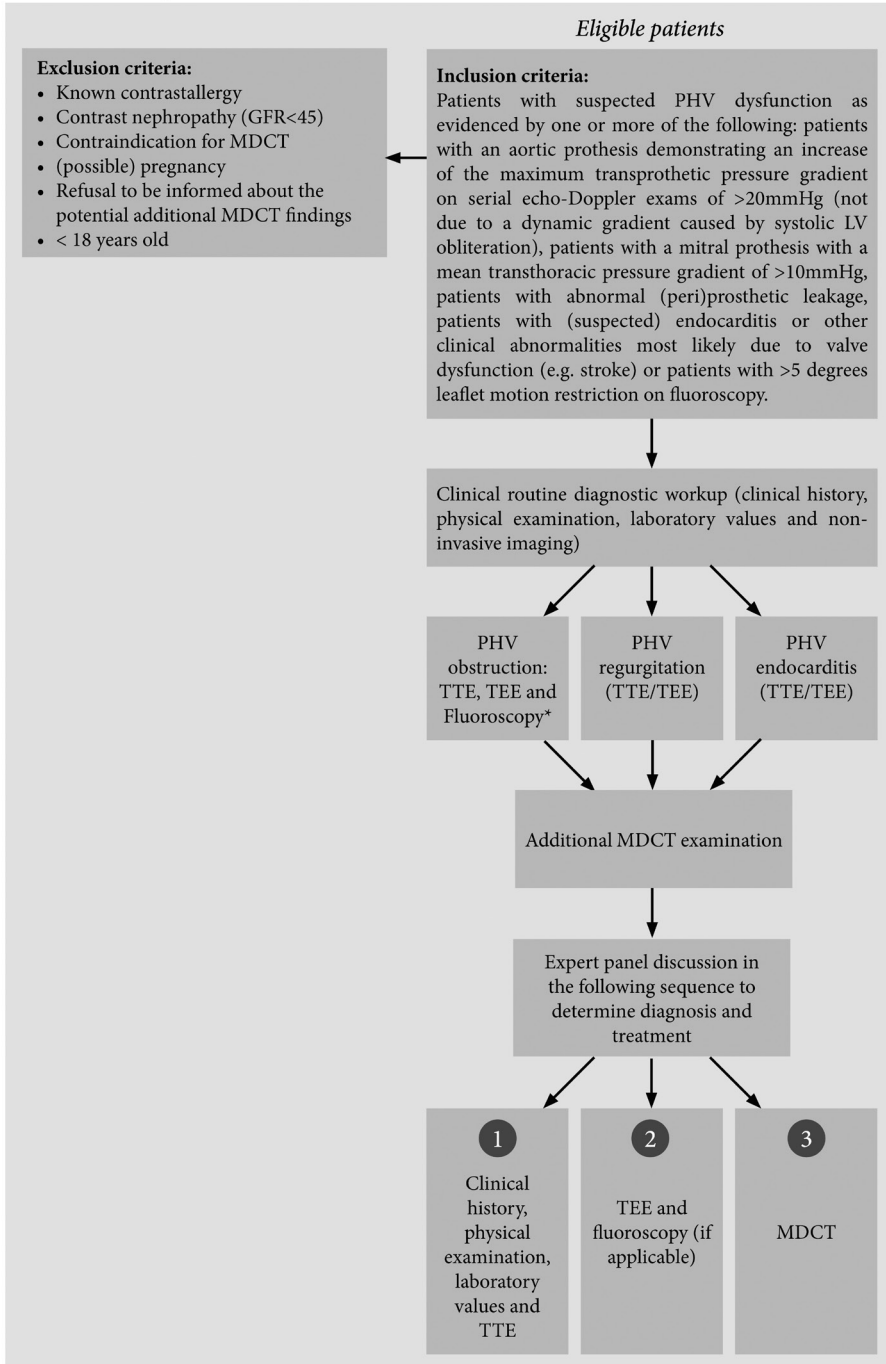
MDCT images are obtained on a MDCT system preferably a 256-slice (iCT, Philips Medical Systems, Cleveland, Ohio, USA) in the UMCU and evaluated and scored for different imaging findings by 2 experienced observers, the most important determinants being: (1) ability to diagnostically assess supra-, sub-, peri- and valvular anatomy; and (2) ability to diagnostically assess leaflet motion in cine mode and measure opening and closing angles. Imaging findings are related to surgical inspection at PHV implantation, intraoperative TEE if performed at PHV implantation, postoperative TTE and manufacturer reference values.

**IMPACT II**

In IMPACT II, we aim to include one hundred patients with suspected PHV dysfunction (Figure 2). PHV dysfunction is defined as: (1) patients with an aortic PHV demonstrating an increase of the maximum transprosthetic pressure gradient on serial echo-Doppler exams of >20mmHg (not due to a dynamic gradient caused by systolic LV obliteration), patients with a mitral prosthesis with a mean transthoracic pressure gradient of >10mmHg, patients with abnormal (para)valvular leakage, patients with (suspected) PHV endocarditis or other clinical abnormalities most likely due to PHV dysfunction (e.g. stroke) or patients with >5 degrees leaflet motion restriction on fluoroscopy. Patients

Figure 2 |

**IMPACT II (suspected PHV dysfunction)**



GFR = glomural filtration rate; MDCT = multidetector-row CT; LV = Left Ventricle; PHV = Prosthetic Heart Valve; TTE = Transthoracic Echocardiography; and TEE = Transesophageal Echocardiography; \* in patients with mechanical PHVs

are informed and included at the outpatient clinic of the Cardiology department where patients with PHV dysfunction are likely to present or at the Cardiology or Cardiothoracic ward if they are admitted or referred to the hospital. In normal daily routine patients suspected of PHV dysfunction usually undergo an extensive workup including (1) TTE, (2) TEE and (3) fluoroscopy (except for biological valves) depending on the type of PHV dysfunction. Three different major groups of PHV dysfunction are differentiated: (1) PHV obstruction, (2) PHV regurgitation and (3) PHV endocarditis. In patients with suspected PHV obstruction, TTE, TEE and fluoroscopy (in patients with mechanical PHVs) have to be performed. In patients with PHV regurgitation or endocarditis, non-invasive evaluation with TTE and TEE is required. After clinical routine non-invasive testing, an additional MDCT acquisition is performed.

The reference standard in this study is the consensus opinion of an expert panel consisting of two experienced imaging cardiologists (RB and SC) and two experienced cardiothoracic surgeons (LvH and BM). In the expert panel consensus meeting, a case is presented in the following sequence: (1) clinical history, physical examination, laboratory testing and TTE; (2) TEE and fluoroscopy (in patients with mechanical PHV obstruction) and (3) MDCT examination. After each of the three assessment moments, the expert panel will determine a consensus on the exact cause of PHV dysfunction and the suggested patient treatment (the main categories being: conservative medical treatment/surgery/"wait and see"/more additional imaging). This results in three consensus scores on the most likely cause of dysfunction and suggested patient management. This expert panel setup will result in determination of: (1) additional value of TEE to TTE in the evaluation of PHV dysfunction and (2) additional diagnostic value of MDCT to the clinical routine diagnostic workup and its implications for patient treatment. The latter is the main purpose of this diagnostic cross-sectional study. Findings on the actual patient management combined with findings at reoperation and/or pathology will be combined to determine the diagnostic accuracy. If they are not available the expert panel consensus combined with clinical follow-up will be used.

## IMAGING MODALITIES

### TTE

In IMPACT I and II, TTE assessment will be performed according to a standardized protocol that includes a full cardiac assessment focusing on the implanted PHV. Anatomical assessment is performed with B-mode imaging. Standardized TTE anatomic assessment includes: two and four chamber apical view, left parasternal long and short axis view and in case of aortic PHV regurgitation also the suprasternal view. The two-dimensional and real-time echocardiography will be combined with functional information obtained with continuous wave (CW), pulsed wave (PW) and color Doppler flow measurements. The detailed TTE protocol is shown in Figure 3.

In IMPACT II, TTE assessment is performed clinically in the referring hospital or AMC/UMCU. In patients with suspected PHV obstruction, mean and maximum transprosthetic gradients are determined using the modified Bernoulli equation.<sup>4</sup> Besides pressure gradient, prosthetic orifice area is obtained using the continuity equation.<sup>4</sup> For mitral PHV assessment, pressure half time is determined in addition to the mean and maximum pressure gradient. PHV assessment will also include the evaluation of (para)valvular regurgitation. In patients with suspected PHV endocarditis, TTE evaluation focuses on the detection of signs of PHV endocarditis (vegetations, abscesses/mycotic aneurysms and PHV dehiscence). Furthermore, increased or novel pathological regurgitation may be a sign of PHV endocarditis.<sup>4</sup>

Figure 3 |

**TTE Protocol IMPACT study**

General	Views
Study number: Date of birth: Type of PHV: Size of PHV: Position of PHV: Date of implantation:	1. Parasternal long axis 2D  2. Parasternal RV inflow 2D  3. Parasternal short axis 2D
Date of echocardiography: Echocardiographer: Type echo device: Length (cm): Weight (kg): BSA: Blood pressure (mm Hg): Heart rate (bpm): Heart rhythm:	<ul style="list-style-type: none"> <li>• LV</li> <li>• Aortic valve</li> <li>• (TV/PV)</li> </ul> 4. Apical 2 CH  5. Apical 3 CH  6. Apical 4 CH  7. Apical 5 CH  8. Subcostal <ul style="list-style-type: none"> <li>• 4 CH</li> <li>• VCI</li> <li>• Abdominal aorta</li> </ul>

BSA: Body Surface Area; CH = Chamber; LV = Left Ventricle; PHV = Prosthetic Heart Valve; PV = Pulmonary Valve; RV = Right Ventricle; TV = Tricuspid Valve; and VCI = Vena Cava Inferior.

**TEE**

TEE is performed with high frequency (5 Mhz) multiplane TEE probes (Philips Medical Systems, Best, the Netherlands) in patients included in the IMPACT-II subgroup as part of the routine clinical work-up of suspected PHV dysfunction in either the referring hospital or the UMCU or AMC. TEE may be omitted in patients with contraindications such as oesophagus pathology (e.g. esophageal spasm, stricture, laceration, perforation, and diverticula). These patients will be excluded. TEE will be performed according to the routine clinical standards of the particular hospital but will at least include standard TEE views (0, 30-60, 90, 120-130 degrees) depending on the PHV position (aortic/mitral).<sup>4</sup> TEE will also include Doppler ultrasound. TEE will focus mainly on the detection of the exact cause of PHV dysfunction. Doppler measurements are often performed because of the superior angulation of the TEE probe compared to TTE for mitral PHV assessment. In Figure 4 detailed information on the TEE protocol is provided.

**Fluoroscopy**

Fluoroscopy may be performed as part of the routine clinical work up in patients with a mechanical PHV and suspected PHV dysfunction (IMPACT II). The X-ray beam is oriented perpendicular to the valve leaflets and images are recorded during several heart beats after appropriate alignment with an appropriate frame rate. Opening and closing angles, and the presence of rocking motion are assessed in each case.

Figure 4 |

## TEE Protocol IMPACT study

General	Views
Study number:	LV and RV (2D images)
Date of birth:	<ul style="list-style-type: none"> <li>• 4 CH view LV/RV (0°)</li> <li>• 2 CH view LV/RV (90°)</li> <li>• 3 CH view LV/RV (120-140°)</li> </ul>
Type of PHV:	Mitral Valve (2D images and color Doppler):
Size of PHV:	<ul style="list-style-type: none"> <li>• Transverse Plane (0°) <ul style="list-style-type: none"> <li>○ Deep (posterior annulus)</li> <li>○ Mid (mid annulus at 4 CH level)</li> <li>○ High (anterior annulus at 5 CH level)</li> </ul> </li> <li>• Commissural View (60°)</li> <li>• Two-chamber View (90°)</li> <li>• Three-chamber View (120-140°)</li> </ul>
Position of PHV:	Aortic valve (2D images and color Doppler):
Date of implantation:	<ul style="list-style-type: none"> <li>• LVOT/AV/Aorta (Long-axis view, 120-140°)</li> <li>• AV SAX (30°-50, mid esophageal)</li> <li>• LVOT/AV/Aorta (5 CH view, 0°)</li> </ul>
Date of echocardiography:	Ascending aorta
Echocardiographer:	<ul style="list-style-type: none"> <li>• SAX views (0°, high esophageal)</li> <li>• Long axis view (120°, )</li> </ul>
Type echo device:	
Length (cm):	
Weight (kg):	
BSA:	
Blood pressure (mm Hg):	
Heart rate (bpm):	
Heart rhythm	
2 D: 3 consecutive beats in sinus rhythm and 5 in atrial fibrillation	

AV = Aortic Valve; BSA: Body Surface Area; CH = Chamber; LV = Left Ventricle; LVOT = Left Ventricular Outflow Tract; PHV = Prosthetic Heart Valve; RV = Right Ventricle; SAX = Short Axis

### MDCT

MDCT imaging is preferably performed on a 256-slice MDCT system in the UMCU. In case a patient is unable to be transported to the UMCU, the CT scan can be performed in the referring hospital provided it is performed on a  $\geq 64$ -slice scanner. Before starting the CT-scan, intravenous access will be secured preferably in an antecubital vein. Heart rate will be optimized by administration of 5-20mg metoprolol (selokeen<sup>®</sup>) intravenously in consultation with the cardiologist in patients without contraindications for  $\beta$ -blockers. In patients with contra-indications (severe aortic stenosis, worse left ventricle dysfunction, severe aortic insufficiency) for  $\beta$ -blocker administration, the acquisition will be performed without the administration of intravenous metoprolol. The target heart rate is 60 beats per minute. A contrast-enhanced retrospectively ECG-gated scan of the target PHV as well as the surrounding cardiac anatomy is performed. Images will be reconstructed at each 10 percent of the R-R interval providing 11 image datasets (including an additional 75% phase). Images are transferred to a workstation and analyzed using dedicated software (Extended Brilliance Workstation, Philips Medical Systems, Philips, Best, the Netherlands). The detailed MDCT acquisition parameters for the 256-slice scanner are presented in Figure 5. The reconstructed images are sent to our picture and archiving system (PACS) for assessment and storage.

### Risk assessment

For this study, in both the IMPACT I and II groups, one additional contrast enhanced MDCT acquisition of the heart is performed in each patient compared to the standard clinical practice.

**Figure 5 IMPACT MDCT acquisition parameters**

MDCT acquisition parameters	Non-contrast enhanced CT	Retrospectively ECG gated CTA 64 slice	Retrospectively ECG-gated CTA 256 slice
Slice thickness	0.9	0.9	0.9
Increment	0.45	0.45	0.45
kV	120	120	120
mAs	30	500-700 <sup>*</sup>	600-700 <sup>**</sup>
Collimation	128x0.625	64x0.625	128x0.625
Pitch	-	0.20	0.16-0.18 <sup>***</sup>
Rotation time	0.27	0.42	0.27-0.33 <sup>****</sup>
FOV	250	250	250
Filter	Cardiac B	Cardiac B	Cardiac B
Matrix	512x512	512x512	512x512
Reconstruction algorithm	FBP	FBP	FBP
Reconstruction phases	75%	10 phases (equally spaced)	10 phases (equally spaced)

<sup>\*</sup> <60kg = 500mAs, 65-80kg = 600mAs, >80kg = 700mAs

<sup>\*\*</sup> 65-80kg = 600mAs, >80kg = 700mAs

<sup>\*\*\*</sup> Heart rate < 72 beats per minute = 0.18, heart rate > 72 beats per minute = 0.16

<sup>\*\*\*\*</sup> Heart rate < 62 beats per minute = 0.33, heart rate > 62 beats per minute = 0.27

CT = Computed Tomography; CTA = Computed Tomography Angiography; FBP = Filtered Back Projection; MDCT = Multidetector-row Computed Tomography

Advice and protocol approval from the department of Radiation protection of the UMC Utrecht has been obtained. The risk assessment will now be discussed in detail. The radiation dose of a CT scan of the heart depends on the type of CT scanner. For the IMPACT study, we intent to scan all patients on a 256-slice scanner in the UMC Utrecht (Brilliance iCT, Philips, Best, the Netherlands). A retrospectively ECG-gated contrast enhanced CT of the heart is obtained using the standard protocol used in clinical practice. The specific protocol used depends on body weight. The protocol with the highest radiation dose to the patient is used for subsequent dose calculation. This protocol uses the following scan parameters: 120 kV, 700mAs, pitch of 0.18 seconds, and a gantry rotation time of 0.27 seconds (Figure 5). Radiation dose also depends on scan length. The scan length is adjusted to include the valve prosthesis of interest and the surrounding cardiac anatomy. It is unlikely that scan length will exceed 15cm, even in very tall patients. In order to calculate the maximum radiation dose a patient may receive by participating in this study we calculate the dose according to a “worst case scenario” that is: a relatively heavy patient and a scan length of 15 cm. Unfortunately no estimated dose calculation using Impac computer software is possible as the parameters for the Brilliance iCT scanner are not available in this software. Estimated dose calculation can also be performed by using the Dose Length Product (DLP) that is displayed on the scanner.<sup>15,26</sup>

Estimated dose for a cardiac CT can be calculated as follows:  $DLP \times 0.017 = \text{estimated dose in mSv}$  and in this formula is 0.017 the conversion factor used for scans of the thorax. A readout of the DLP given by the scanner software for the above described “worst case scenario” is 920.2 mGy-cm. This translates into a maximum dose of 15.6 mSv ( $920.2 \times 0.017 = 15.6 \text{ mSv}$ ) to a single patient participating in this study (which is more than 10mSv placing the patient in category 3. If circumstances dictate the scan may be performed on another type of CT scanner. In this case the radiation exposure to the patient will not increase. Besides radiation exposure, patients will receive additional nonionic contrast media. Rare complications of contrast administration are contrast-induced nephropathy (CIN) and

general (allergic) reactions.<sup>27</sup> The risk is minimized because of adherence to our institutional protocol ‘Prevention of contrast reaction and contrast-induced nephropathy’. A recent glomerular filtration rate (GFR) has to be available in each patient participating in the study. A maximum of approximately 125 ml of contrast agent will be used with most patients receiving less than 100 ml. With non-ionic contrast media severe acute general reactions can occur in 0.04% of patients. Patients with previous severe acute adverse reactions to contrast injection are non-eligible for inclusion in this study. For the administration of contrast agent intravenous access is necessary. An intravenous (IV) access needle will be inserted in each patient.

In addition to the MDCT scan, patients in IMPACT I will undergo an additional TTE which is not associated with any risk.

## STATISTICAL ANALYSIS

### Sample size calculation

Sample size calculation is difficult due to the limited data available on imaging of PHVs with MDCT. The study is a diagnostic cross-sectional study.

**IMPACT I:** With 12 acquisitions of each PHV type after PHV implantation we expect to get a good first indication of the normal MDCT findings of each valve type. Furthermore, little data is available in the literature on the normal CT findings in normally functioning PHVs so the findings will serve as a benchmark for normal CT findings of different commonly implanted PHV types.

**IMPACT II:** Echocardiography may fail to detect the cause of PHV dysfunction in 51% of patients.<sup>4</sup> If we assume echocardiography to be accurate in detecting the cause of PHV dysfunction in 50% of patients in IMPACT II, it will fail to detect the exact cause in the other 50% of the patients. Our preliminary data showed that MDCT provided additional information to echocardiography in 71% of patients in a selected group of patients. For this study, we use a conservative estimate of 30% management change in the 50 patients expected not to have an echo diagnosis. The confidence interval (CI) is 19-43%. Thus with 100 patients a MDCT induced management change of at least 19% (lower limit CI) should be detected. Given the patient heterogeneity, adequate sample size calculation is hardly possible. Independent of the results, we expect 100 patients to give a good estimate of the added value of MDCT that will allow an initial assessment of the utility of this technique. We will perform interim analyses of the results in the group as a whole as well as sub-analysis of the obstruction, leakage and endocarditis groups. The number of included patients may be changed accordingly. Furthermore, separate publications of different patient groups is an option depending on the interim analysis.

### Data analysis

Data is prospectively collected including patient characteristics, laboratory values and non-invasive imaging data. Data is entered into standardized electronic case record forms. Continuous variables will be expressed with means±standard deviation (SD) or medians and interquartile range (IQR) dependent on the data distribution (parametric/non-parametric). The percentage of patients in which supra-, peri-, sub- and valvular anatomy could be diagnostically assessed; and the percentage of patients in which leaflet motion in cine mode could be diagnostically assessed and opening and closing angles could be measured, will be provided (IMPACT I).

In IMPACT II, the accuracy of TTE, TEE and MDCT to diagnose the cause of PHV dysfunction as well as the additional diagnostic value of MDCT to the routine clinical workup and its impact on

patient management are the primary outcomes. In the data analysis of this diagnostic cross-sectional study, the most important question is: Does MDCT have additional diagnostic value to the daily routine clinical work-up in the evaluation of PHV dysfunction? To answer this question Receiver Operating Characteristics (ROC) curves will be performed with the normal clinical routine work-up (relevant patient characteristics/lab values, echocardiography and fluoroscopy) and the same workup including the additional MDCT scan. The comparison of these two ROC curves will answer the above mentioned question (95% CI or  $p$ -values of the difference). Dorfman and Alf maximum likelihood program will be used to produce areas under the ROC curves and standard errors.<sup>28</sup>

The important patient characteristics will be predefined based on the available scientific evidence. An additional univariate analysis of the determinants will be performed to evaluate what patient characteristics are relevant to fit the final model ( $p < 0.20$ ).

In the multivariate model the separate models will be compared in accuracy. Reduced models will be made based on Akaike's information criteria. Furthermore, step backward and forward models will be used to control for multicollinearity. The final model will be checked for calibration (goodness of fit test/calibration plot) and discrimination (ROC-curves, discussed above). Internal validation (control for "overfitting") will be performed using bootstrapping methods. PHV dysfunction is a broad clinical disease including many different pathological entities. If the subgroups are large enough, separate models can be fit for specific pathological entities and a clinical predictive rule will be formulated based on the coefficients resulting from the logistic regression analysis. TEE is a semi-invasive test which may be replaced by MDCT for the evaluation of PHV dysfunction. Additional ROC analyses will be performed including and excluding TEE as determinant.

## DISCUSSION

Non-invasive imaging is the cornerstone of diagnosing PHV dysfunction. The clinical routine imaging techniques may fail to diagnose the exact cause of PHV dysfunction. MDCT has entered the clinical arena, and is a promising imaging technique to detect the exact cause of PHV dysfunction. However, prospective studies with considerable number of patients are lacking. Furthermore, reference values for normal functioning PHV are lacking.

The IMPACT study has two aims: (1) provide normal MDCT reference values of six commonly implanted PHV types (IMPACT I); and (2) determine the complementary diagnostic value of MDCT to the clinical routine imaging modalities in patients with suspected PHV dysfunction and its implications for treatment decisions. We distinguish three main PHV dysfunction groups: PHV obstruction, PHV regurgitation and PHV endocarditis.

For these main groups, the complementary diagnostic and therapeutic value will be explored. At this moment, little data is available on normal MDCT imaging characteristics of PHVs. Previous studies<sup>20,21</sup> demonstrated that MDCT is an accurate imaging technique to assess opening and closing angles of PHVs compared with fluoroscopy and manufacturer data. Konen et al.<sup>20</sup> evaluated the feasibility of MDCT to evaluate bileaflet and tilting disc PHVs. Bileaflet mechanical PHVs had an excellent visibility. In contrast, tilting disc PHVs had a moderate-good visibility. Two patients could not be evaluated because of non-diagnostic image quality. These patients had a Sorin and Björk-Shiley tilting disc that contain a cobalt-chrome alloy ring which caused severe PHV artifacts. Previous work of our group confirmed these findings.<sup>18</sup> However, the Medtronic Hall tilting disc PHV was imaged with good to excellent image quality. These studies were generally all performed on  $\leq 64$ -slice CT systems. MDCT acquisitions for the IMPACT I study will be performed on a 256-slice CT



system with a higher temporal resolution than 64-slice MDCT systems which may improve MDCT image quality. Large prospective studies to provide normal MDCT PHV imaging characteristics are lacking. IMPACT I will provide this normal MDCT imaging data of PHVs.

MDCT is a promising imaging technique to evaluate patients with suspected PHV dysfunction. Tsai et al.<sup>23</sup> prospectively evaluated patients with suspected mechanical PHV dysfunction. In these patients, TTE and MDCT were performed. Twenty-nine patients were evaluated, but only six patients with surgical correlation were included in the data analysis. In these six patients MDCT diagnosis was confirmed by surgical inspection.<sup>23</sup> Important limitations of this study are the small patient numbers and the selection bias. Our previous work also demonstrated that MDCT is a promising imaging technique to evaluate patients with mechanical PHV obstruction.<sup>22</sup> In this small patient population ( $n=13$ ), MDCT was a promising imaging technique to determine the exact cause of PHV obstruction, especially for the detection of pannus formation.<sup>22</sup> Unfortunately, patients with evident thrombosis were excluded in this retrospective study design. This may have resulted in a potential selection bias because the clinician is interested in the diagnostic accuracy of the index test in the unselected suspected population and not in a specific subpopulation. Besides PHV obstruction, MDCT is a promising imaging technique to evaluate patients with suspected PHV endocarditis. Feuchtner et al.<sup>17</sup> compared diagnostic accuracy of MDCT to TEE and intraoperative findings for the diagnosis of infective endocarditis. Only six of 37 patients (16%) were patients with suspected PHV endocarditis. In these 6 patients, MDCT detected all vegetations, pseudoaneurysms and abscesses detected by TEE and intraoperative findings. Moreover, MDCT detected 2 vegetations in a patient with a mechanical aortic PHV which were missed by TEE, but confirmed at surgery.<sup>17</sup> A small case series confirmed these findings.<sup>19</sup>

These initial findings are promising. However, a large diagnostic cross-sectional study is needed to determine the exact complementary diagnostic value of MDCT and its impact on patient management in patients with suspected PHV dysfunction. The IMPACT study is expected to provide an answer to these questions.

### **Limitations**

This study protocol has several limitations. First, an expert panel was chosen as the reference standard. Ideally, surgical and/or pathological confirmation of non-invasive imaging findings are present for each patient for verification. However, in clinical practice, not all patients with suspected PHV dysfunction will undergo surgery. Therefore, we chose for the expert panel to have similar verification for each patient to avoid verification bias. In patients with surgical or pathological data, these data will be recorded. Second, an appropriate power calculation is not possible because of the lack of published data and the heterogeneity of the PHV dysfunction group. Third, only one vendor MDCT system is used for the study for comparability reasons. However, in clinical practice it is important to know if MDCT acquisitions with MDCT systems of different vendors are also possible.

## **CONCLUSION**

The IMPACT study is a diagnostic-cross sectional study that will be the first large prospective study: (1) to determine normal MDCT imaging characteristics of six different commonly implanted PHV types; and (2) to determine the diagnostic accuracy and the additional diagnostic value of MDCT in the evaluation of patients with suspected PHV dysfunction and its impact on patient management.

## REFERENCES

1. Yacoub MH, Takkenberg JJ. Will heart valve tissue engineering change the world? *Nat Clin Pract Cardiovasc Med* 2005; 2:60-61.
2. Grunkemeier GL, Li HH, Naftel DC, et al. Long-term performance of heart valve prostheses. *Curr Probl Cardiol* 2000; 25:73-154.
3. Hammermeister K, Sethi GK, Henderson WG, et al. Outcomes 15 years after valve replacement with a mechanical versus a bioprosthetic valve: final report of the Veterans Affairs randomized trial. *J Am Coll Cardiol* 2000; 36:1152-1158.
4. Zoghbi WA, Chambers JB, Dumesnil JG, et al. Recommendations for evaluation of prosthetic valves with echocardiography and doppler ultrasound: a report from the American Society of Echocardiography's Guidelines and Standards Committee and the Task Force on Prosthetic Valves, developed in conjunction with the American College of Cardiology Cardiovascular Imaging Committee, Cardiac Imaging Committee of the American Heart Association, the European Association of Echocardiography, a registered branch of the European Society of Cardiology, the Japanese Society of Echocardiography and the Canadian Society of Echocardiography, endorsed by the American College of Cardiology Foundation, American Heart Association, European Association of Echocardiography, a registered branch of the European Society of Cardiology, the Japanese Society of Echocardiography, and Canadian Society of Echocardiography. *J Am Soc Echocardiogr*. 2009; 22:975-1014.
5. Barbetseas J, Nagueh SF, Pitsavos C, et al. Differentiating thrombus from pannus formation in obstructed mechanical prosthetic valves: an evaluation of clinical, transthoracic and transesophageal echocardiographic parameters. *J Am Coll Cardiol*. 1998; 32:1410-1417.
6. Girard SE, Miller FA, Jr., Orszulak TA, et al. Reoperation for prosthetic aortic valve obstruction in the era of echocardiography: trends in diagnostic testing and comparison with surgical findings. *J Am Coll Cardiol* 2001; 37:579-584.
7. Lin SS, Tiong IY, Asher CR, et al. Prediction of thrombus-related mechanical prosthetic valve dysfunction using transesophageal echocardiography. *Am J Cardiol* 2000; 86:1097-1101.
8. Habets J, Budde RP, Symersky P, et al. Diagnostic evaluation of left-sided prosthetic heart valve dysfunction. *Nat Rev Cardiol* 2011; 8:466-478.
9. Muratori M, Montorsi P, Teruzzi G, et al. Feasibility and diagnostic accuracy of quantitative assessment of mechanical prostheses leaflet motion by transthoracic and transesophageal echocardiography in suspected prosthetic valve dysfunction. *Am J Cardiol* 2006; 97:94-100.
10. Lee DH, Youn HJ, Shim SB, et al. The measurement of opening angle and orifice area of a bileaflet mechanical valve using multidetector computed tomography. *Korean Circ J* 2009; 39:157-162.
11. Vogt PR, Brunner-LaRocca H, Sidler P, et al. Reoperative surgery for degenerated aortic bioprostheses: predictors for emergency surgery and reoperative mortality. *Eur J Cardiothorac Surg* 2000; 17:134-139.
12. Tang GH, Maganti M, David TE, et al. Effect of prior valve type on mortality in reoperative valve surgery. *Ann Thorac Surg* 2007; 83:938-945.
13. Akins CW, Buckley MJ, Daggett WM, et al. Risk of reoperative valve replacement for failed mitral and aortic bioprostheses. *Ann Thorac Surg* 1998; 65:1545-1551.
14. Meijboom WB, Meijs MF, Schuijf JD, et al. Diagnostic accuracy of 64-slice computed tomography coronary angiography: a prospective, multicenter, multivendor study. *J Am Coll Cardiol* 2008; 52:2135-2144.
15. Prokop M. Radiation Dose and Image Quality. In: Prokop M., Galanski M. (eds). *Spiral and Multislice Computed Tomography of the Body*. Stuttgart, Thieme, 2003.
16. Chenot F, Montant P, Goffinet C, et al. Evaluation of anatomic valve opening and leaflet morphology in aortic valve bioprosthesis by using multidetector CT: comparison with transthoracic echocardiography. *Radiology* 2010; 255:377-385.
17. Feuchtner GM, Stolzmann P, Dichtl W, et al. Multislice computed tomography in infective endocarditis: comparison with transesophageal echocardiography and intraoperative findings. *J Am Coll Cardiol*. 2009; 53:436-444.
18. Habets J, Symersky P, van Herwerden LA, et al. Prosthetic heart valve assessment with multidetector-row CT: imaging characteristics of 91 valves in 83 patients. *Eur Radiol*. 2011; 21:1390-1396.
19. Kim RJ, Weinsaft JW, Callister TQ, et al. Evaluation of prosthetic valve endocarditis by 64-row multidetector computed tomography. *Int J Cardiol* 2007; 120:e27-e29.
20. Konen E, Goitein O, Feinberg MS, et al. The role of ECG-gated MDCT in the evaluation of aortic and mitral mechanical valves: initial experience. *Am J Roentgenol*. 2008; 191:26-31.
21. LaBounty TM, Agarwal PP, Chughtai A, et al. Evaluation of mechanical heart valve size and function with ECG-gated 64-MDCT. *Am J Roentgenol* 2009; 193:W389-W396.
22. Symersky P, Budde RP, de Mol BA, et al. Comparison of multidetector-row computed tomography to echocardiography and fluoroscopy for evaluation of patients with mechanical prosthetic valve obstruction. *Am J Cardiol* 2009; 104:1128-1134.

23. Tsai IC, Lin YK, Chang Y, et al. Correctness of multi-detector-row computed tomography for diagnosing mechanical prosthetic heart valve disorders using operative findings as a gold standard. *Eur Radiol.* 2009; 19:857-867.
24. Symersky P, Budde RP, Westers P, et al. Multidetector CT imaging of mechanical prosthetic heart valves: quantification of artifacts with a pulsatile in-vitro model. *Eur Radiol.* 2011; 21:2103-2110.
25. Symersky P, Budde RP, Prokop M, et al. Multidetector-row computed tomography imaging characteristics of mechanical prosthetic valves. *J Heart Valve Dis* 2011; 20:216-222.
26. Nitt-Gray MF. AAPM/RSNA Physics Tutorial for Residents: Topics in CT. Radiation dose in CT. *Radiographics* 2002; 22:1541-1553.
27. Namasivayam S, Kalra MK, Torres WE. Small WC: Adverse reactions to intravenous iodinated contrast media: a primer for radiologists. *Emerg Radiol* 2006; 12:210-215.
28. Hanley JA, McNeil BJ. A method of comparing the areas under receiver operating characteristic curves derived from the same cases. *Radiology* 1983; 148:839-843.





CHAPTER XVII

GENERAL DISCUSSION

In this thesis, the use of multidetector computed tomography (MDCT) in the evaluation of prosthetic heart valves (PHVs) was investigated. In the first part of this thesis, literature was systematically reviewed to assess the diagnostic role for the different imaging modalities (transthoracic and transesophageal echocardiography, fluoroscopy and MDCT) in the diagnosis of PHV dysfunction. In the *in vitro* part of this thesis, studies were conducted to optimize the MDCT acquisition protocol for PHV evaluation. Strategies were explored to reduce radiation exposure and PHV-related artifacts. In the *in vivo* part of this thesis, the multidisciplinary diagnostic approach (cardiology, cardiothoracic surgery and radiology) was emphasized. Studies were conducted to evaluate the normal CT imaging characteristics of PHVs, and to assess the surrounding cardiac anatomy especially coronary arteries. The last chapter of this thesis presents the IMPACT (Imaging of Prosthetic Heart Valves by CT) study protocol.

**Chapter II and III** review currently available literature on the diagnostic value of different imaging modalities (echocardiography, fluoroscopy and MDCT) to evaluate patients with suspected PHV dysfunction. In patients with suspected PHV obstruction, transthoracic echocardiography (TTE) can often accurately determine the severity of the PHV obstruction by pressure gradient and effective prosthetic orifice area measurements. Transesophageal echocardiography (TEE) can have additional diagnostic value especially in patients with suspected mitral PHV obstruction.<sup>1</sup> However, TEE is not suitable to differentiate between pannus and thrombus formation which is crucial for therapeutic decisions, and may even fail to detect its presence.<sup>2</sup> The additional diagnostic value of three-dimensional TEE has to be explored beyond the presently available case series.<sup>3</sup> In addition to echocardiography, fluoroscopy can provide leaflet opening and closing angles especially in the aortic position. MDCT allows for both dynamic (leaflet opening and closing) and anatomical assessment. In previous publications with small sample sizes, MDCT proved to be a promising imaging technique to determine the exact cause of PHV obstruction.<sup>4,5</sup> Diagnostic assessment can be hampered by mainly hypodense PHV-related artifacts which emphasize the need for tailored MDCT acquisition protocols. The most important causes of PHV obstruction, thrombus and pannus formation, present both as hypodense lesions on MDCT images. For the differentiation between pannus and thrombus, no evidence is present for performing Hounsfield measurements. The morphologic CT differences between both entities in combination with the clinical history (interval between PHV implantation, (in)adequate anticoagulation therapy and clinical course) may be the key to diagnostic differentiation. However, a large prospective diagnostic cross-sectional study is required to determine the exact complementary value of MDCT in patients with suspected PHV obstruction. At this moment, MDCT can be considered in patients with inconclusive diagnostic routine work-up (TTE, TEE and fluoroscopy) (Figure 1).

In patients with PHV regurgitation, TTE and TEE are required to differentiate between physiological and pathologic regurgitation, and to differentiate between pathologic valvular and paravalvular regurgitation. Echocardiography has an important advantage over MDCT because it provides blood flow information including diastolic/systolic flow and its location/severity. This information is important for both diagnostic (differentiating normal closure backflow from pathological leakage) and therapeutic purposes. MDCT may detect the presence of paravalvular regurgitation<sup>6</sup>, but will never replace echocardiography. On MDCT, paravalvular regurgitation presents as contrast-enhanced blood next to the valve prosthesis at annular level. It needs to be differentiated from other hyperdense CT structures (calcifications, polytetrafluorethylene (PTFE) pledgets). **Chapter XI** demonstrated that hyperdense PTFE pledgets have higher Hounsfield values than hyperdense contrast-enhanced blood (paravalvular leakage) without any overlap. However,

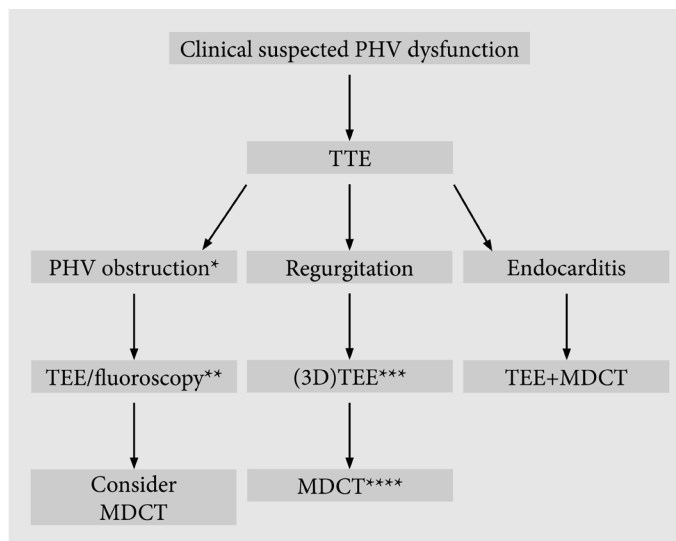


**Figure 1** | Flowchart for a suggested non-invasive imaging protocol in the diagnostic work-up of patients with suspected PHV dysfunction. \*If increased transprosthetic gradient pressure is found on TTE examination. \*\*Consider skipping fluoroscopy when MDCT is performed because of the comparable diagnostic accuracy of MDCT for the evaluation of leaflet motion. Fluoroscopy is not a diagnostic imaging modality for patients with biological PHVs. \*\*\*3D TEE can often be diagnostic for pathologic regurgitation. When TEE is inconclusive, consider MDCT. \*\*\*\*MDCT can have additional diagnostic value after TEE evaluation of regurgitation in case of inconclusive TEE, additional PHV obstruction, questions about leaflet closure, and to identify the exact location of the valvular or paravalvular leakage.

Abbreviations: 3D = three-dimensional; MDCT = multidetector Computed Tomography; PHV = Prosthetic Heart Valve; TEE = transesophageal echocardiography; and TTE = transthoracic echocardiography.

the clinical implication of these findings is restricted to our institutional contrast administration protocol. The conclusion of this study may not be extrapolated using different contrast administration protocols. In patients with paravalvular leakage and suspected endocarditis, MDCT can have additional diagnostic value by evaluating the extent of the aortic root disease. In these patients, MDCT has to be considered (Figure 1).

In patients with suspected PHV endocarditis, non-invasive imaging plays a key role in the diagnosis according to the Duke criteria.<sup>7,8</sup> TEE is superior to TTE in the detection of vegetations and abscesses/mycotic aneurysms especially in the mitral position.<sup>9,10</sup> It is important to keep in mind that the studies reporting on the diagnostic accuracy of TTE and TEE in patients with PHV endocarditis are mainly performed in a selected population (surgically explored population). In the aortic position, echocardiography may miss signs of PHV endocarditis (vegetations, abscesses and mycotic aneurysms) because of acoustic shadowing due to the metal contents in PHVs and annular calcifications.<sup>9,10</sup> MDCT can have complementary diagnostic value in patients with suspected PHV endocarditis especially owing to visualization of the extent of the disease. Moreover, MDCT examinations are suitable for simultaneous assessment of proximal aortic dimensions and the coronary arteries in patients planned for reoperation without the need of invasive coronary angiography with the risk of embolization of vegetations (**Chapter XII**). MDCT has to be considered in patients with suspected PHV endocarditis especially in patients with aortic PHVs (Figure 1).

## IN VITRO PART

In the in vitro part, different studies are presented: (1) to optimize MDCT acquisition parameters; (2) to reduce radiation exposure, and (3) to increase the knowledge on the occurrence of PHV-related artifacts. Retrospectively ECG-gated MDCT acquisition has a considerable radiation exposure. Different strategies to reduce radiation dose were explored: iterative reconstruction (**Chapter IV**) and prospective triggering (**Chapter VI**). **Chapter IV** demonstrates that high-dose retrospectively ECG-gated MDCT acquisition (120kV and 600mAs) reconstructed with filtered back projection (FBP) had similar image noise and PHV-related artifact volumes than low-dose retrospectively ECG-gated MDCT acquisition (120kV, 300mAs) reconstructed with iterative reconstruction (IR) level 4 on a 64 detector-row scanner. In contrast, low-dose acquisitions reconstructed with FBP had significant higher image noise levels and PHV-related artifact volumes compared to high-dose acquisitions reconstructed with FBP. IR reduced PHV-related artifacts both in systole and diastole. Prospectively triggered MDCT acquisition is also suitable for radiation exposure reduction. However, the clinical application of IR and prospective triggering has to be explored.

The use of IR not only has the potential to reduce radiation exposure, but may also reduce streak artifacts. Besides the application of IR, varying tube voltage and the use of a metal artifact reduction filter (MARF) may reduce PHV-related artifacts. The MARF used in our experiments is based on an image-based algorithm which interpolates data to reduce artifacts. In **Chapter V**, these different artifact reduction strategies were evaluated for their effect on the PHV-related artifact volumes. Increased tube voltage (140kV) resulted in decreased hypodense and hyperdense PHV-related artifact volumes. IR had less effect than increasing tube voltage on PHV-related artifact volumes. However, IR significantly decreased image noise. MARF resulted in a substantial decrease in PHV-related artifact volumes compared with other artifact reduction strategies (tube voltage and IR). However, MARF induced interpolation artifacts which preclude current clinical application of MARF. Besides the previously mentioned artifact reduction strategies, prospectively triggered MDCT acquisition is an effective MDCT acquisition technique to reduce PHV-related artifacts at different heart rates (**Chapter VI**).

These in vitro studies have several limitations. First, the absence of cardiac and annular movement which can induce PHV-related artifacts and influence MDCT image quality in the clinical setting. Second, our threshold ( $\leq 50$  Hounsfield units) used for hypodense artifact volumes could have included image noise. Therefore, the measured hypodense artifact volume reduction could have been partially declared due to image noise reduction. The most important limitation was that image quality was not assessed in most in vitro studies. However, in **Chapter VII**, image quality was assessed by two observers independently using a validated randomized blinded image quality assessment method. This chapter demonstrated a superior image quality of low-dose prospectively triggered acquisition protocols at lower heart rates ( $\leq 75$  bpm). At higher heart rates (90 bpm), image quality of prospectively triggered acquisitions protocols was similar to the high-dose helical acquisition. These results advocate for further prospective clinical studies using low-dose prospectively triggered acquisition protocols reconstructed with iterative reconstruction after heart rate reduction to reduce radiation exposure.



## IN VIVO PART

The diagnosis of the exact cause of PHV dysfunction is a complex diagnostic process. A multidisciplinary cooperation between cardiologists, cardiothoracic surgeons and radiologists is crucial (**Chapter VIII and IX**). The cardiologists assesses the patient on the outpatient clinic, ward or emergency department. Clinical history, physical examination and laboratory testing are important. Non-invasive imaging, however, is the keystone for the establishment of the diagnosis PHV dysfunction. Non-invasive imaging techniques (TTE, TEE, fluoroscopy and MDCT) has to be combined to determine the exact cause of PHV dysfunction. Besides diagnostic information, MDCT can provide additional information for the surgical planning in patients scheduled for reoperation: (1) the relation of PHV pathology to relevant surrounding cardiac structures (e.g. coronary arteries), (2) the presence of coronary artery disease in patients with low or intermediate risk of coronary artery disease; and (3) aortic dimensions which can have clinical important implications (e.g. aortic ascendens replacement).

In **Chapter X**, MDCT image quality of different PHV types in 83 patients with 91 PHVs was explored. MDCT image quality of PHVs largely depends on the PHV composition. Most commonly implanted PHVs contain titanium alloy rings which have a good to excellent image quality. St Jude PHVs can contain nickel which causes more artifacts but generally present with a good CT image quality. PHVs containing cobalt-chromium preclude diagnostic assessment because of the occurrence of severe PHV-related artifacts. Biological PHVs generally present with a good to excellent general image quality. However, image quality of the valvular leaflets often was scored moderate in our retrospective study (**Chapter X**). Chenot et al. demonstrated better valvular leaflet visualization using higher tube voltage (140kV instead of 120kV) and effective tube current (714mAs instead of 600mAs).<sup>11</sup> However, 34/54 (63%) patients had biological PHV dysfunction. In biological PHV degeneration, valve leaflets thicken which may explain the improved valvular image quality in this study. **Chapter X** has several limitations because of the retrospective study design. First, eighteen (36%) retrospectively ECG-gated aortic MDCT acquisitions were included. These patients received a scan not tailored for cardiac purposes. Second,  $\beta$ -blockers were not systematically administered to optimize the heart rate before CT acquisition. However, no influence of heart rate was found on CT image quality. It is important to note that this feasibility study was not statistically powered to find this significant difference.

Besides PHV assessment, MDCT examinations are also useful to simultaneously assess the presence of coronary artery disease. In patients with a low or intermediate risk of coronary artery disease and a PHV, MDCT has the diagnostic potential to exclude coronary artery disease because of a high negative predictive value.<sup>12</sup> In **Chapter XII**, a study in 82 patients with 94 PHVs was described to evaluate in which PHVs coronary artery segment assessment is possible, and not hampered by PHV-related artifacts. In most patients with PHVs, coronary artery segments can be assessed without PHV-related artifacts that hamper coronary assessment. St Jude PHVs containing nickel alloy rings may hamper proximal right coronary artery and left circumflex artery (including marginal obtuse branches) assessment depending of PHV position (aortic/mitral). In patients with PHVs containing cobalt-chromium, coronary artery assessment is not possible because of severe artifacts. This study had some limitations. First, almost all MDCT acquisitions were performed for other clinical indications than coronary artery assessment. It could be expected that the high number of non-diagnostic segments (26%) will decrease if optimal dedicated coronary MDCT acquisition with administration of intravenous  $\beta$ -blockers and sublingual nitroglycerin is performed. Second, some PHVs were present in small number. These small numbers impede scientific conclusions for these

specific PHVs. Third, to assess the diagnostic accuracy of MDCT for the detection of coronary artery stenosis, a prospective diagnostic cross-sectional study is required comparing MDCT to the reference standard invasive coronary angiography.

**Chapter XIII** presents a study which was conducted to (1) establish the best systolic and diastolic ECG-gated MDCT imaging reconstruction phase and (2) identify possible imaging phases with lower image quality which are suitable for the application of dose modulation or can be omitted in case of prospectively triggered MDCT acquisition. Image quality was assessed with a blinded randomized side-to-side comparison method.<sup>13</sup> The principle findings of this study were that 30 /40% and 70%/75%/80% are the best systolic and diastolic imaging reconstruction phases, respectively. Moreover, this study justifies dose modulation for imaging phases (10%, 20%, 50% and 60%) with a lower image quality or these imaging phases can be omitted in case of prospectively triggered acquisition to reduce radiation dose exposure.

**Chapter XIV** describes the effect of PHV motion during the cardiac cycle on MDCT image quality in patients with aortic PHVs. This study demonstrated that PHV velocity was least during the following phases of the cardiac cycle: end-systole (30 to 40% of the ECG interval) and mid-diastole (75 to 80% of the ECG interval). Increasing heart rates were associated with an increased mid-diastolic velocity due to non-proportional shortening of the diastole. At >90 beats per minute mid-diastolic velocities were higher than end-systolic velocities. On the other hand, the mid-diastolic image quality remained superior to systolic phases. Clinical implication of these findings is that in patients with higher heart rates (>60 beats per minute),  $\beta$ -blockers have to be considered in patients without contraindications for intravenous  $\beta$ -blocker administration. The limitations of this study were relative small number of patients in the three frequency subgroups, and a vendor specific algorithm for correction for non-proportional shortening. Therefore, these results could not be extrapolated to patients scanned with MDCT systems of other vendors.

## FUTURE PERSPECTIVES

Prospective diagnostic cross-sectional studies have to determine the exact diagnostic value of MDCT in patients with suspected PHV dysfunction.

The IMPACT study (**Chapter XVI**) was designed to determine (1) normal MDCT imaging characteristics of PHVs, and (2) the complementary diagnostic value of MDCT to echocardiography and fluoroscopy in the evaluation of patients with suspected PHV dysfunction and its impact on patient management. In patients with PHV endocarditis, MDCT may have complementary diagnostic value to TTE and TEE especially in patients with aortic PHVs. However, TEE remains important because of the better spatial and temporal resolution for the detection of small vegetations and the differentiation between valvular and paravalvular leakage. Besides complementary value, MDCT might also replace a part of the clinical routine workup. In patients with PHV obstruction, the current diagnostic algorithm (TTE, TEE and fluoroscopy) might be replaced with TTE and MDCT because TEE is not suitable for the differentiation between pannus and thrombus formation.<sup>2</sup> Finally, MDCT might have no complementary diagnostic value and can be omitted. This might be the case in patients with PHV regurgitation without signs of PHV endocarditis. However, MDCT as well as three-dimensional TEE may have additional diagnostic value by measuring the diameter and surface area of the paravalvular leakage. These measurements may be important for appropriate planning and selection of patients for percutaneous closure of paravalvular leakage in the future. Prospective studies to evaluate the exact value of these novel imaging techniques in this patient group are warranted.

In previous studies, image quality of most PHVs was good to excellent. MDCT acquisition was performed with relatively high dose retrospectively ECG-gated acquisitions.<sup>4,5,11,14-18</sup> In this thesis, low-dose MDCT acquisition protocols were evaluated under pulsatile in vitro conditions. These low-dose MDCT acquisition protocols are not inferior to the high-dose helical acquisition protocols. In patients with mechanical PHVs, a low-dose unenhanced helical acquisition (80kV, 40mAs) for dynamic leaflet motion assessment followed by a systolic and diastolic prospectively triggered acquisition for diagnostic anatomical assessment is promising. At this moment, in patients with biological PHVs, retrospectively ECG-gated acquisition remains the acquisition protocol of first choice because of the radiolucent aspect of the valvular leaflets. Iterative reconstruction may decrease radiation exposure in this subgroup. Prospective clinical feasibility studies are required to validate these low-dose MDCT acquisition protocols. When these low-dose MDCT acquisition protocols are validated, these protocols will allow for MDCT evaluation of PHVs in the direct postoperative phase. MDCT examination can reveal relevant diagnostic findings in the direct postoperative phase. However, further studies are needed to evaluate if a standard baseline low-dose MDCT scan after normal PHV implantation is required.

Patients with PHV dysfunction may have an altered hemodynamic circulation which may influence contrast passage. Optimal contrast-enhancement is important to detect small abnormalities (e.g. thrombus or pannus formation). For optimal MDCT acquisition, studies are needed with individually tailored contrast administration protocols (e.g. test bolus contrast administration before contrast injection).

Besides the current clinical routine imaging techniques and MDCT, other imaging modalities may have diagnostic value in the evaluation of patients with PHV dysfunction. At the moment, cardiac MRI has no role in the evaluation of mechanical PHVs owing to metal-induced imaging artifacts. In patients with biological PHVs without a supporting metal framework, cardiac MRI may assess transvalvular flow and prosthetic orifice area.<sup>19,20</sup> The development of new MRI acquisition sequences, which are less susceptible to metal artifacts, is needed to make MRI worthwhile for clinical PHV assessment. Hybrid imaging (combination of anatomical and functional imaging modalities), may be the key to diagnostic success in patients with PHV dysfunction. For example, in patients with suspected PHV endocarditis, it remains difficult to diagnose active PHV endocarditis with the present imaging modalities (TTE/TEE/MDCT). Hybrid imaging techniques may improve the diagnostic accuracy in the future, and may predict clinical outcome.

The following case represents an example of a potential new hybrid imaging technique (diagnostic MDCT and PET) for the evaluation of patients with suspected PHV endocarditis.

*A 65-year-old male with a St. Jude aortic prosthetic heart valve (PHV) implanted 20 years ago presented with fever, four consecutive positive blood cultures (Staphylococcus Aureus) and progressive PR prolongation. Transthoracic and transesophageal echocardiography (TTE/TEE) and CT angiography (CTA) (Figure 2A) were unremarkable. However, low carbohydrate diet 18F-fluorodeoxyglucose positron emission tomography (FDG-PET) fused with CTA demonstrated high uptake around the PHV near the proximal right and left coronary artery (RCA/LCA) (Figure 2B, \* = crista terminalis). Surgical inspection six days after presentation did not reveal signs of endocarditis and the PHV remained in situ (Figure 2C). However, because of clinical deterioration CTA and TEE were repeated eight days after surgery and revealed a mycotic aneurysm beneath the RCA origin (Figure 2D), and two abscesses around the LCA (Figure 2E), confirmed by urgent re-operation (Figure 2F). Retrospectively, the FDG-PET abnormalities around the PHV predicted the occurrence and location of PHV endocarditis complications.*



Figure 2 |

This case presents the potential value of FDG-PET fused with CTA in the diagnosis of active PHV endocarditis. FDG-PET may predict abscess and mycotic aneurysm formation in patients with suspected PHV endocarditis. Further prospective diagnostic cross-sectional studies have to determine the diagnostic and prognostic value of hybrid imaging (diagnostic MDCT combined with PET) in patients with suspected PHV endocarditis.

Non-invasive imaging of prosthetic heart valves is a research field in which new imaging techniques (3D TEE, MDCT and hybrid imaging) can improve diagnostic accuracy in patients with suspected PHV dysfunction in the future.

## REFERENCES

1. Chaudhry FA, Herrera C, DeFrino PF, et al. Pathologic and angiographic correlations of transesophageal echocardiography in prosthetic heart valve dysfunction. *Am Heart J* 1991; 122:1057-1064.
2. Girard SE, Miller FA, Jr., Orszulak TA, et al. Reoperation for prosthetic aortic valve obstruction in the era of echocardiography: trends in diagnostic testing and comparison with surgical findings. *J Am Coll Cardiol* 2001; 37:579-584.
3. Singh P, Inamdar V, Hage FG, et al. Usefulness of live/real time three-dimensional transthoracic echocardiography in evaluation of prosthetic valve function. *Echocardiography* 2009; 26:1236-1249.
4. Tsai IC, Lin YK, Chang Y, et al. Correctness of multi-detector-row computed tomography for diagnosing mechanical prosthetic heart valve disorders using operative findings as a gold standard. *Eur Radiol.* 2009; 19:857-867.
5. Symersky P, Budde RP, de Mol BA, et al. Comparison of multidetector-row computed tomography to echocardiography and fluoroscopy for evaluation of patients with mechanical prosthetic valve obstruction. *Am J Cardiol* 2009; 104:1128-1134.
6. Hara M, Nishino M, Taniike M, et al. Impact of the 64 multi-detector computed tomography for the evaluation of aortic paraprosthetic regurgitation. *J Cardiol* 2011; 58:294-299.
7. Durack DT, Lukes AS, Bright DK. New criteria for diagnosis of infective endocarditis: utilization of specific echocardiographic findings. *Duke Endocarditis Service. Am J Med* 1994; 96:200-209.
8. Li JS, Sexton DJ, Mick N, et al. Proposed modifications to the Duke criteria for the diagnosis of infective endocarditis. *Clin Infect Dis* 2000; 30:633-638.
9. Daniel WG, Mügge A, Martin RP, et al. Improvement in the diagnosis of abscesses associated with endocarditis by transesophageal echocardiography. *N Engl J Med* 1991; 324:795-800.
10. Daniel WG, Mügge A, Grote J, et al. Comparison of transthoracic and transesophageal echocardiography for detection of abnormalities of prosthetic and bioprosthetic valves in the mitral and aortic positions. *Am J Cardiol* 1993; 71:210-215.
11. Chenot F, Montant P, Goffinet C, et al. Evaluation of anatomic valve opening and leaflet morphology in aortic valve bioprosthesis by using multidetector CT: comparison with transthoracic echocardiography. *Radiology* 2010; 255:377-385.
12. Meijboom WB, Meijs MF, Schuijf JD, et al. Diagnostic accuracy of 64-slice computed tomography coronary angiography: a prospective, multicenter, multivendor study. *J Am Coll Cardiol.* 2008; 52:2135-2144.
13. Smit EJ, Vonken EJ, van der Schaaf IC, et al. Timing-Invariant Reconstruction for Deriving High-Quality CT Angiographic Data from Cerebral CT Perfusion Data. *Radiology* 2012; 263:216-225.
14. Feuchtner GM, Stolzmann P, Dichtl W, et al. Multislice computed tomography in infective endocarditis: comparison with transesophageal echocardiography and intraoperative findings. *J Am Coll Cardiol* 2009; 53:436-444.
15. Habets J, Symersky P, van Herwerden LA, et al. Prosthetic heart valve assessment with multidetector-row CT: imaging characteristics of 91 valves in 83 patients. *Eur Radiol.* 2011; 21:1390-1396.
16. Konen E, Goitein O, Feinberg MS, et al. The role of ECG-gated MDCT in the evaluation of aortic and mitral mechanical valves: initial experience. *Am J Roentgenol.* 2008; 191:26-31.
17. LaBounty TM, Agarwal PP, Chughtai A, et al. Evaluation of mechanical heart valve size and function with ECG-gated 64-MDCT. *Am J Roentgenol* 2009; 193:W389-W396.
18. Teshima H, Hayashida N, Fukunaga S, et al. Usefulness of a multidetector-row computed tomography scanner for detecting pannus formation. *Ann Thorac Surg.* 2004; 77:523-526.
19. von Knobelsdorff-Brenkenhoff F, Rudolph A, Wassmuth R, et al. Assessment of mitral bioprostheses using cardiovascular magnetic resonance. *J Cardiovasc Magn Reson* 2010; 12:36.
20. von Knobelsdorff-Brenkenhoff F, Rudolph A, Wassmuth R, et al. Feasibility of cardiovascular magnetic resonance to assess the orifice area of aortic bioprostheses. *Circ Cardiovasc Imaging* 2009; 2:397-404.





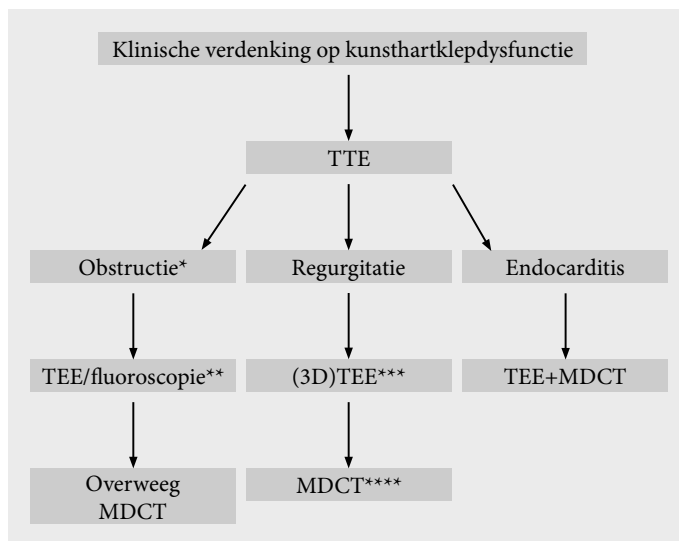
# NEDERLANDSE SAMENVATTING

In dit proefschrift wordt het gebruik van multidetector computed tomography (MDCT) bij het onderzoeken van patiënten met kunsthartkleppen beschreven. In het eerste gedeelte werd de literatuur systematisch bekeken met als doel de diagnostische waarde van de verscheidene beeldvormende technieken (echocardiografie, klepdoorlichting en MDCT) in de diagnostiek van patiënten met een verdenking op kunsthartklepdysfunctie vast te stellen. In het in-vitro gedeelte van dit proefschrift werden studies verricht ter optimalisatie van het MDCT scan protocol voor de beoordeling van kunsthartkleppen. Verscheidene methoden om de stralingsbelasting en kunsthartklepartefacten te verminderen werden onderzocht. In het in-vivo gedeelte van het proefschrift staat de multidisciplinaire samenwerking met de afdeling Cardiologie en Cardiothoracale chirurgie centraal. Studies werden verricht om de normale CT beeldkarakteristieken van kunsthartkleppen vast te stellen. Tevens werd onderzocht of de kransslagaders bij patiënten met een kunsthartklep kunnen worden beoordeeld zonder het optreden van belemmerende artefacten. In het laatste hoofdstuk van dit proefschrift, wordt het IMPACT (Imaging of Prosthetic Heart Valves by CT) studieprotocol beschreven.

In **Hoofdstuk II en III** wordt de huidige beschikbare literatuur over de diagnostische waarde van verschillende beeldvormende technieken in de evaluatie van patiënten met een verdenking op kunsthartklepdysfunctie beoordeeld. Bij patiënten met een verdenking op kunsthartklepdysfunctie kan transthoracale echocardiografie (TTE) vaak betrouwbaar de ernst van de kunsthartklepobstructie vaststellen. Slokdarmechocardiografie (TEE) kan additionele diagnostische waarde hebben met name voor patiënten met een mitraliskunstklep.<sup>1</sup> TEE is echter niet geschikt om te differentiëren tussen pannus en trombus weefsel. Deze differentiatie is cruciaal voor het bepalen van het behandelplan. TEE kan echter falen om zelfs een massa vast te stellen in deze patiëntencategorie.<sup>2</sup> De additionele diagnostische waarde van 3D TEE zal nog verder onderzocht moeten worden aangezien er slechts enkele kleine patiëntenseries beschreven zijn.<sup>3</sup> Aanvullend op de echocardiografie kan de klepdoorlichting informatie verschaffen over de openings- en sluitingshoeken van met name kunsthartkleppen in de aortapositie. Uit eerdere publicaties met kleine patiëntenaantallen is gebleken dat MDCT een veelbelovende beeldvormende techniek is om de precieze oorzaak van kunsthartklepobstructie vast te stellen.<sup>4,5</sup> Diagnostische beoordeling kan verstoord worden door kunsthartklepartefacten. Daarom is het belangrijk dat er scanprotocollen ontwikkeld worden speciaal voor kunsthartkleppen. De meest voorkomende oorzaken van kunstklepobstructie, pannusweefsel en trombus, presenteren zich beiden als hypodense afwijkingen op de MDCT beelden. De huidige literatuur levert geen bewijs dat deze twee entiteiten onderscheiden kunnen worden op basis van Hounsfield metingen. De morfologische CT verschillen tussen beiden entiteiten in combinatie met de anamnese (interval tussen kunsthartklepimplantatie en presentatie, (in)adequate antistollingstherapie en de klinische presentatie) zijn wellicht de sleutel naar de diagnostische differentiatie. Een grote prospectieve diagnostische cross-sectionele studie is echter vereist om de exacte toegevoegde waarde van CT in patiënten met kunsthartklepobstructie vast te stellen. Op dit moment kan MDCT overwogen worden in patiënten met een inconclusieve diagnostiek (Figuur 1).

TTE and TEE zijn noodzakelijk voor de differentiatie tussen normale en pathologische lekkage (paravalvulair/valvulair) bij patiënten met een lekkage van de kunsthartklep. Echocardiografie heeft als belangrijk voordeel dat het in tegenstelling tot MDCT informatie verschaft over de bloedstroom inclusief diastolische/systolische bloedstroomsnelheid en de locatie/ernst van de lekkage. MDCT kan de aanwezigheid van paravalvulaire lekkage vaststellen<sup>6</sup>, maar zal voor deze indicatie nooit de echocardiografie vervangen. Op de MDCT beelden presenteert een paravalvulaire lekkage zich als contrastrijk bloed naast de hartklepprothese ter hoogte van de annulus, en moet gedifferentieerd worden van andere hyperdense CT structuren zoals calcificaties en polytetrafluorethylene (PTFE)





**Figuur 1** | Een stroomdiagram waarin een niet-invasieve beeldvormend protocol wordt weergegeven voor patiënten met een verdenking op kunsthartklepdyfunctie. \*Wanneer een toegenomen drukgradiënt gevonden wordt tijdens het TTE onderzoek. \*\*Overweeg klepdoorlichting te schrappen als MDCT wordt uitgevoerd vanwege de vergelijkbare diagnostische betrouwbaarheid van MDCT en klepdoorlichting voor de beoordeling van klepbewegingen. Klepdoorlichting is niet een diagnostische beeldvormende techniek voor patiënten met biologische kunsthartkleppen. \*\*\*3D TEE kan vaak diagnostisch zijn voor het vaststellen van pathologische lekkage. Wanneer TEE inconclusief is, overweeg MDCT. \*\*\*\*MDCT kan additionele diagnostische waarde hebben na TEE evaluatie van pathologische lekkage: inconclusieve TEE, additionele kunstklepobstructie, vragen omtrent de klepopening, en voor het vaststellen van de precieze locatie van de (para)valvulaire lekkage. Afkortingen: 3D = drie-dimensionaal; MDCT = multidetector Computed Tomography; TEE = slokdarmechocardiografie; en TTE = transthoracale echocardiografie.

pledgets. **Hoofdstuk XI** toont dat hyperdense PTFE pledgets een hogere Hounsfield waarde hebben dan hyperdense contrastrijk bloed zonder enige overlap. Deze bevindingen zijn echter alleen klinisch toepasbaar wanneer ons contrastprotocol gebruikt wordt. In patiënten met een paravalvulaire lekkage en een verdenking op een endocarditis kan MDCT toegevoegde diagnostische waarde hebben door het evalueren van de uitgebreidheid van de ziekte van de aortawortel. In deze patiënten moet MDCT overwogen worden (Figuur 1).

Niet-invasieve beeldvorming speelt een sleutelrol in de diagnose kunsthartklependocarditis en is daarom een belangrijk onderdeel van de Duke criteria.<sup>7,8</sup> TEE is superieur in het opsporen van vegetaties en abscessen/mycotisch aneurysmata met name in de mitraliskleppositie.<sup>9,10</sup> Het is belangrijk om in gedachten te houden dat de studies die rapporteren over de diagnostische betrouwbaarheid van TTE en TEE in patiënten met een kunsthartklependocarditis vooral gebaseerd zijn op studies uitgevoerd in een geselecteerde populatie. In de aortapositie kan de echocardiografie tekenen van endocarditis missen met name ten gevolge van echografische artefacten en annulaire calcificaties.<sup>9,10</sup> MDCT kan aanvullende diagnostische waarde hebben bij patiënten met verdenking op een kunsthartklependocarditis met name door het afbeelden van de uitgebreidheid van de endocarditis. Tevens is MDCT geschikt om tegelijkertijd ook de kransslagaders en de aortawortel in patiënten met kunsthartklependocarditis die voor een reoperatie gepland staan af te beelden zonder dat er het risico van systemische embolisatie van vegetaties bestaat (**Hoofdstuk XII**). MDCT moet overwogen worden in patiënten met een verdenking op kunstklependocarditis met name in patiënten met een aortakunstklep (Figuur 1).

## HET IN VITRO GEDEELTE

In het in vitro gedeelte worden verschillende studies beschreven met als doel: (1) het optimaliseren van MDCT scan parameters; (2) het reduceren van de stralingsbelasting voor de patiënt; en (3) het laten toenemen van de kennis omtrent het optreden van kunstklepartefacten.

Retrospectieve ECG-gated MDCT scans hebben een aanzienlijke stralingsbelasting. Verschillende strategieën om de stralingsdosis te verlagen werden onderzocht: iteratieve reconstructie

(**Hoofdstuk IV**) en prospectieve ECG-triggering (**Hoofdstuk VI**). **Hoofdstuk IV** laat zien dat een hoge dosis retrospectieve ECG-gated scan (120kV, 600mAs) gereconstrueerd met filtered back projection (FBP) vergelijkbare ruis en kunstklepartefactvolumes heeft als lage dosis retrospectieve ECG-gated MDCT scans (120kV, 300mAs) gereconstrueerd met iteratieve reconstructie (IR) niveau 4 op een 64 detectoren CT scanner. De lage-dosis scans gereconstrueerd met FBP hebben daarentegen een significant hoger ruisniveau en kunstklepartefactvolumes vergeleken met de hoge dosis scans gereconstrueerd met FBP. IR vermindert kunstklepartefacten zowel in systole als in diastole. Prospectieve ECG-triggering is ook geschikt voor het verlagen van stralingsbelasting. De klinische toepassing van deze technieken moeten echter nog in patiënten onderzocht worden.

Het gebruik van IR heeft niet alleen het potentieel om de stralingsbelasting te verlagen, maar kan mogelijk ook CT artefacten verminderen. Naast het gebruik van IR zou het verhogen van de buisspanning en het gebruik van een metaalartefactenfilter de kunstklepartefacten kunnen verminderen. In **hoofdstuk V** wordt de effectiviteit van deze artefactreductie strategieën onderzocht. Verhoogde buisspanning (140kV) leidde tot een afname van zowel hypodense als hyperdense kunstklepartefacten. IR had minder effect op de artefacten dan de verhoging van de buisspanning. IR verlaagde wel het ruisniveau in het CT beeld. MARF was de meest effectieve methode om kunstklepartefacten te reduceren. MARF induceerde echter interpolatieartefacten die op dit moment klinische toepasbaarheid van deze techniek belemmeren. Naast deze technieken is prospectieve ECG-triggering ook een effectieve manier om kunstklepartefacten te verminderen (**Hoofdstuk VI**).

Deze in vitro studies hadden verscheidene beperkingen. Ten eerste waren de cardiale en annulaire bewegingen, die kunstklepartefacten kunnen induceren en de MDCT beeldkwaliteit kunnen beïnvloeden, afwezig in de gebruikte perfusieopstelling. Ten tweede zouden de gemeten hypodense artefactvolumes ruis kunnen bevatten door de gekozen drempelwaarde ( $\leq 50$  Hounsfield eenheden). Daardoor zou een deel van de vermindering van hypodense artefacten verklaard kunnen worden door ruisvermindering. De meest belangrijke beperking was dat de beeldkwaliteit in meeste studies niet onderzocht werd. In **hoofdstuk 7** werd echter de beeldkwaliteit door 2 beoordelaars onderzocht gebruik makend van een gevalideerde gerandomiseerde geblindeerde beoordelingsmethode. Dit hoofdstuk laat zien dat de lage dosis prospectieve ECG getriggerde scans een superieure beeldkwaliteit hebben bij hartfrequenties van 60 en 75 slagen per minuut. Bij hogere hartfrequenties (90 slagen per minuut) hadden prospectieve ECG getriggerde en retrospectieve ECG-gating een vergelijkbare beeldkwaliteit. De resultaten uit deze studie pleiten voor prospectieve klinische studies waarin gebruik gemaakt wordt van prospectieve ECG-triggering en iteratieve reconstructie om de stralingsbelasting te verlagen.

## HET IN VIVO GEDEELTE

De diagnose van de precieze oorzaak van de kunsthartklepdyshctie is een complex diagnostisch proces waarin multidisciplinaire samenwerking tussen cardiologen, cardiothoracale chirurgen en radiologen essentieel is (**Hoofdstuk VIII en IX**). De cardioloog beoordeelt de patiënt op de polikliniek, verpleegafdeling of de spoedeisende hulp. Anamnese, lichamelijk onderzoek en laboratoriumonderzoek zijn hierbij belangrijk. De niet-invasieve beeldvorming speelt echter een sleutelrol in het stellen van de diagnosis kunsthartklepdyshctie. De verschillende beeldvormende technieken (TTE, TEE, klepdoorlichting en MDCT) moeten worden gecombineerd om de oorzaak van de kunsthartklepdyshctie vast te stellen. Naast deze diagnostische informatie kan MDCT bij patiënten gepland voor een reoperatie toevoegende informatie verschaffen over: (1) de relatie tussen de kunsthartkleppathologie en relevante cardiale structuren (bijv. de kransslagaders); (2) de aanwezigheid van kransslagaderlijden in patiënten met een laag of intermediair risico op kransslagaderlijden; en (3) de aortadimensies.

In **Hoofdstuk X** werd de MDCT beeldkwaliteit van verschillende kunsthartkleptypen onderzocht in 83 patiënten met 91 kunsthartkleppen. MDCT beeldkwaliteit van kunsthartkleppen hangt met name van de kunstklepsamenstelling. De meeste kunsthartkleppen die een titanium legering bevatten in de klepring hebben een goede tot uitstekende beeldkwaliteit. St Jude kunsthartkleppen kunnen een nickel legering bevatten die artefacten kan veroorzaken. Echter, in het algemeen zijn de beelden van goede kwaliteit. Kunsthartkleppen die een cobalt-chroom legering bevatten veroorzaken ernstige kunstklepartefacten die klinische beoordeling verhinderen. Biologische kunsthartkleppen hebben in het algemene een goede tot uitstekende beeldkwaliteit. De beeldkwaliteit van biologische klepbladen is daarentegen vaak matig (**Hoofdstuk X**). Chenot en co-auteurs hebben in een andere studie laten zien dat het verhogen van de buisspanning en de buisstroom resulteerde in betere visualisatie van de klepbladen.<sup>11</sup> In deze studie hadden echter 34/54 (63%) van de patiënten biologische klepdyshctie. Bij biologische degeneratie verdikken de klepbladen en deze verdikking verklaart wellicht de relatief betere beeldkwaliteit van de klepbladen in deze studie. **Hoofdstuk X** heeft verscheidene beperkingen vanwege de retrospectieve studieopzet. Ten eerste werden 18 (36%) patiënten met een retrospectieve ECG-gated aorta MDCT scans geïnccludeerd. Deze patiënten ondergingen een scan die niet speciaal verricht werd voor cardiale beeldvorming. Ten tweede werden  $\beta$ -blockers niet systematisch toegediend om de hartslag te optimaliseren voor CT beeldvorming. In deze studie werd geen correlatie gevonden tussen CT beeldkwaliteit en hartslag, maar deze studie was echter ook niet opgezet om dit verschil aan te tonen.

Naast de kunsthartklepbeoordeling kunnen de kransslagaders op dezelfde scan beoordeeld worden. In patiënten met een laag of intermediair risico op kransslagaderlijden kan MDCT met een grote mate van zekerheid kransslagaderlijden uitsluiten.<sup>12</sup> **Hoofdstuk XII** beschrijft een studie in 82 patiënten met 94 kunstkleppen waarin wordt aangetoond dat de meeste kleppen de coronair beoordeling niet belemmeren. St Jude kunsthartkleppen bevatten een nikkel legering in de klepring die beoordeling van de proximale rechter coronair arterie en de ramus circumflexus (inclusief MOrtakken) kunnen belemmeren afhankelijk van de kleppositie (aorta/mitraal). Coronair beoordeling is onmogelijk in patiënten met een cobalt-chroom legering in de klepring vanwege ernstige artefacten in bepaalde segmenten. Deze studie had enkele beperkingen. Ten eerste werden de meeste MDCT scans verricht voor een andere klinische indicatie dan coronair beeldvorming. Het systematisch toedienen van intraveneuze  $\beta$ -blockers en sublinguale nitroglycerine had de beeldkwaliteit van de kransslagaders in deze patiëntengroep kunnen verbeteren. Ten tweede waren sommige kunsthartkleppen in een gering aantal aanwezig. Deze kleine aantallen belemmeren wetenschappelijke conclusies voor deze

specifieke kunsthartkleppen. Ten derde werd de diagnostische betrouwbaarheid van MDCT voor het opsporen van kransslagadervernouwingen niet onderzocht in deze studie en is er een prospectieve studie noodzakelijk waarin vergeleken wordt met coronair angiografie, de huidige referentie standaard.

**Hoofdstuk XIII** beschrijft een studie die werd uitgevoerd om: (1) de beste systolische en diastolische ECG-gated MDCT reconstructie fase vast te stellen en (2) de reconstructie fasen vast te stellen met een lagere beeldkwaliteit die mogelijk geschikt zijn voor dosismodulatie of niet gescand hoeven te worden wanneer men gebruikt maakt van prospectieve ECG-triggering. Beeldkwaliteit werd in deze studie onderzocht gebruikmakend van een gerandomiseerde geblindeerde paarsgewijze vergelijkingsmethode.<sup>13</sup> De voornaamste bevindingen van deze studie waren dat 30/40% en 70%/75%/80% de beste systolische en diastolische reconstructiefasen zijn. Deze studie rechtvaardigt het gebruik van dosismodulatie in de volgende fasen met een relatief lagere beeldkwaliteit (10%, 20%, 50% en 60%) of deze fasen hoeven niet gescand te worden (prospectieve ECG-triggering) om de stralingsbelasting te verminderen.

**Hoofdstuk XIV** beschrijft het effect van de beweging van de kunstklep gedurende de hartcyclus op de MDCT beeldkwaliteit in patiënten met aortakunstkleppen. Deze studie laat zien dat de snelheid van de kunstklep het geringste was in de eind-systolische (30-40%) en mid-diastolische fasen (75%-80%) van het ECG interval. Hogere hartfrequenties zijn geassocieerd met een toegenomen mid-diastolische snelheid vanwege niet-evenredige verkorting van de diastole. Bij een hartslag boven de 90 slagen per minuut waren mid-diastolische snelheden hoger dan de eind-systolische snelheden. De beeldkwaliteit bleef echter beter in de mid-diastolische fasen vergeleken met de eind-systolische fasen. De klinische implicaties van deze bevindingen is dat  $\beta$ -blockers overwogen moeten worden in patiënten met een hogere hartslag. De beperkingen van deze studie waren de relatieve kleine patiëntenaantallen in de drie hartfrequentie subgroepen en het gebruik van een scanner specifiek algoritme voor het corrigeren van de niet-evenredige verkorting. Daarom kunnen de resultaten uit deze studie niet geëxtrapoleerd worden naar patiënten die op andere scanners gescand worden.

## TOEKOMSTPERSPECTIEVEN

Prospectieve diagnostische cross-sectionele studies zijn vereist om de precieze diagnostische waarde van MDCT te kunnen bepalen in patiënten met een verdenking op kunsthartklepdysfunctie. De IMPACT studie (**Hoofdstuk XVI**) is opgezet om de normale MDCT beeldkarakteristieken van kunsthartkleppen te bepalen en de aanvullende diagnostische waarde van MDCT in vergelijking met echocardiografie en klepdoorlichting in de evaluatie van patiënten met een verdenking op kunsthartklepdysfunctie te bepalen. MDCT zou aanvullende diagnostische waarde kunnen hebben boven TTE en TEE in patiënten met een verdenking op kunsthartklep-endocarditis. Dit geldt met name voor patiënten met een aortakunstklep. TEE blijft echter belangrijk vanwege de betere spatiele en temporele resolutie vergeleken met MDCT voor het opsporen van vegetaties en het differentiëren tussen valvulaire en paravalvulaire lekkage.

Naast aanvullende diagnostische waarde zou MDCT eventueel een gedeelte van de huidige klinische diagnostische beeldvorming kunnen vervangen. In patiënten met een kunsthartklepobstructie zou MDCT de TEE kunnen vervangen aangezien TEE niet in staat is om de differentiëren tussen de aanwezigheid van pannus en trombus weefsel.<sup>2</sup> Tenslotte zou MDCT wellicht bij patiënten met een para(valvulaire) lekkage zonder aanwijzingen voor een endocarditis achterwege gelaten kunnen worden. MDCT en driedimensionale TEE zou echter in een selectieve populatie meerwaarde kunnen hebben door het meten van de grootte en het oppervlak van de paravalvulaire lekkage voor de planning van percutane procedures voor het sluiten van een paravalvulaire lekkage in de toekomst. Prospectieve studies zullen verricht moeten worden om de waarde van deze nieuwe technieken in deze populatie aan te tonen.

Uit eerdere studies is gebleken dat de CT beeldkwaliteit van de meeste kunsthartkleppen goed tot uitstekend is. MDCT scans werden in deze studies verricht met een hoge dosis retrospectief ECG-gated scan protocol.<sup>4,5,11,14-18</sup> In dit proefschrift werden lage dosis MDCT scan protocols onderzocht in een pulsatiele perfusieopstelling. Deze lage dosis MDCT scan protocollen zijn niet inferieur aan de hoge dosis retrospectief ECG-gated scan protocollen. In patiënten met een mechanische kunsthartklep kan een lage dosis spiraal scan (80kV, 40mAs) zonder contrast gebruikt worden voor de beoordeling van de dynamische klepbeweging gevolgd door een prospectieve ECG-getriggerde systolische en diastolische scan. Bij patiënten met biologische kunsthartkleppen blijft retrospectieve ECG-gating het scanprotocol van eerste keuze vanwege het feit dat de klepblaadjes niet zichtbaar zijn bij röntgenbeeldvorming. Iteratieve reconstructie zou in deze subgroep de stralingsdosis nog kunnen verminderen. Prospectieve klinische studies zijn noodzakelijk om deze scanprotocollen verder te onderzoeken. Wanneer deze lage dosis scan protocollen klinisch gevalideerd zijn, staan deze scanprotocollen MDCT evaluatie van patiënten met kunsthartkleppen toe in de vroege postoperatieve fase. Meer studies zijn echter nodig om te bepalen of het zinvol is om een standaard uitgangsscan te maken na een normale kunsthartklepimplantatie.

Patiënten met een kunsthartklepdysfunctie kunnen een veranderde hemodynamische circulatie hebben die de contrastpassage kan beïnvloeden. Optimaal contrastaanbod is belangrijk voor het opsporen van kleine afwijkingen zoals trombus en pannus weefsel. Studies zijn noodzakelijk om te kijken naar het effect van contrastprotocollen die op het individu aangepast worden.

Naast de huidige klinische beeldvormende technieken en MDCT zouden andere beeldvormende technieken diagnostische waarde kunnen hebben bij de evaluatie van patiënten met kunsthartklepdysfunctie. Op dit moment is er geen plek voor het gebruik van MRI bij de evaluatie van mechanische kunsthartkleppen vanwege de metaalartefacten. In patiënten met biologische kleppen zonder metalen omhuizing is cardiale MRI in staat om de bloedstroom langs de klep en

het kunstklepopeningsoppervlakte te bepalen.<sup>19,20</sup> De ontwikkeling van nieuwe MRI sequenties, die minder gevoelig zijn voor metaalartefacten, is noodzakelijk om MRI een interessant alternatief te laten zijn. Hybride beeldvorming (combinatie van anatomische en functionele beeldvormende technieken) zou de sleutel kunnen zijn tot diagnostisch succes in patiënten met kunsthartklepdyfunctie. Het blijft lastig om vast te stellen of een patiënt een actieve kunsthartklependocarditis heeft met de huidige beeldvormende technieken. Hybride beeldvorming kan mogelijk de diagnostische betrouwbaarheid in de toekomst verbeteren en het wellicht mogelijk maken om de klinische uitkomst te voorspellen.

De volgende casus toont een voorbeeld van een potentiële nieuwe hybride beeldvormende techniek (diagnostische MDCT en PET) voor de evaluatie van patiënten met een verdenking op een kunsthartklependocarditis.

*Een 65-jarige oude man met een 20 jaar geleden geïmplanteerde St Jude mechanische aortakunsthartklep (PHV) presenteerde zich met koorts, vier positieve bloedkweken voor Staphylococcus aureus, en progressieve toename van het PRinterval. TTE, TEE en CTA toonden geen aanwijzingen voor kunsthartklependocarditis (Figuur 2A). Additionele 18F-fluorodeoxyglucose positron emissie tomographie (FDG-PET) met cardiale voorbereiding gefuseerd met CTA toonde een verhoogde opname rondom de kunsthartklep in de regio van de RCA en de linker coronair arterie (LCA) (Figuur 2B, \* = crista terminalis). Chirurgische inspectie 6 dagen na presentatie onthulde geen tekenen van endocarditis en de kunsthartklep bleef in situ (Figuur 2C). Wegens klinische verslechtering, werden CTA en TEE 8 dagen na initiële operatie herhaald en toonden een mycotisch aneurysma onder de RCA en twee abscessen rondom de LCA (Figuur 2E). Deze bevindingen werden bevestigd bij de daarop volgende reoperatie (Figuur 2F). In retrospect voorspelden de FDG-PET afwijkingen (Figuur 2B) rondom de kunsthartklep het optreden en de locatie van de complicaties van de kunsthartklependocarditis.*

**Figuur 2 |**



Deze casus presenteert de potentiële waarde van FDG-PET gefuseerd met CTA voor de diagnose van een actieve kunstklependocarditis. FDG-PET zou in de toekomst misschien het optreden van abcesvorming en mycotische aneurysmata kunnen voorspellen. Prospectieve diagnostische cross-sectionele studies moeten bepalen wat de diagnostische en prognostische waarde van deze hybride beeldvorming is in patiënten met een verdenking op kunsthartklependocarditis.

Niet-invasieve beeldvorming van kunsthartkleppen is een onderzoeksveld waarin nieuwe beeldvormende technieken (3D TEE, MDCT en hybride beeldvorming) de diagnostische betrouwbaarheid van de diagnose bij patiënten met een verdenking op kunsthartklepdysfunctie kunnen verbeteren.

## REFERENTIES

1. Chaudhry FA, Herrera C, DeFrino PF, et al. Pathologic and angiographic correlations of transesophageal echocardiography in prosthetic heart valve dysfunction. *Am Heart J* 1991; 122:1057-1064.
2. Girard SE, Miller FA, Jr., Orszulak TA, et al. Reoperation for prosthetic aortic valve obstruction in the era of echocardiography: trends in diagnostic testing and comparison with surgical findings. *J Am Coll Cardiol* 2001; 37:579-584.
3. Singh P, Inamdar V, Hage FG, et al. Usefulness of live/real time three-dimensional transthoracic echocardiography in evaluation of prosthetic valve function. *Echocardiography* 2009; 26:1236-1249.
4. Tsai IC, Lin YK, Chang Y, et al. Correctness of multi-detector-row computed tomography for diagnosing mechanical prosthetic heart valve disorders using operative findings as a gold standard. *Eur Radiol.* 2009; 19:857-867.
5. Symersky P, Budde RP, de Mol BA, et al. Comparison of multidetector-row computed tomography to echocardiography and fluoroscopy for evaluation of patients with mechanical prosthetic valve obstruction. *Am J Cardiol* 2009; 104:1128-1134.
6. Hara M, Nishino M, Taniike M, et al. Impact of 64 multi-detector computed tomography for the evaluation of aortic paraprosthetic regurgitation. *J Cardiol* 2011; 58:294-299.
7. Durack DT, Lukes AS, Bright DK. New criteria for diagnosis of infective endocarditis: utilization of specific echocardiographic findings. Duke Endocarditis Service. *Am J Med* 1994; 96:200-209.
8. Li JS, Sexton DJ, Mick N, et al. Proposed modifications to the Duke criteria for the diagnosis of infective endocarditis. *Clin Infect Dis* 2000; 30:633-638.
9. Daniel WG, Mügge A, Martin RP, et al. Improvement in the diagnosis of abscesses associated with endocarditis by transesophageal echocardiography. *N Engl J Med* 1991; 324:795-800.
10. Daniel WG, Mügge A, Grote J, et al. Comparison of transthoracic and transesophageal echocardiography for detection of abnormalities of prosthetic and bioprosthetic valves in the mitral and aortic positions. *Am J Cardiol* 1993; 71:210-215.
11. Chenot F, Montant P, Goffinet C, et al. Evaluation of anatomic valve opening and leaflet morphology in aortic valve bioprosthesis by using multidetector CT: comparison with transthoracic echocardiography. *Radiology* 2010; 255:377-385.
12. Meijboom WB, Meijs MF, Schuijf JD, et al. Diagnostic accuracy of 64-slice computed tomography coronary angiography: a prospective, multicenter, multivendor study. *J Am Coll Cardiol.* 2008; 52:2135-2144.
13. Smit EJ, Vonken EJ, van der Schaaf IC, et al. Timing-Invariant Reconstruction for Deriving High-Quality CT Angiographic Data from Cerebral CT Perfusion Data. *Radiology* 2012; 263:216-225.
14. Feuchtner GM, Stolzmann P, Dichtl W, et al. Multislice computed tomography in infective endocarditis: comparison with transesophageal echocardiography and intraoperative findings. *J Am Coll Cardiol* 2009; 53:436-444.
15. Habets J, Symersky P, van Herwerden LA, et al. Prosthetic heart valve assessment with multidetector-row CT: imaging characteristics of 91 valves in 83 patients. *Eur Radiol.* 2011; 21:1390-1396.
16. Konen E, Goitein O, Feinberg MS, et al. The role of ECG-gated MDCT in the evaluation of aortic and mitral mechanical valves: initial experience. *Am J Roentgenol.* 2008; 191:26-31.
17. LaBounty TM, Agarwal PP, Chughtai A, et al. Evaluation of mechanical heart valve size and function with ECG-gated 64-MDCT. *Am J Roentgenol* 2009; 193:W389-W396.
18. Teshima H, Hayashida N, Fukunaga S, et al. Usefulness of a multidetector-row computed tomography scanner for detecting pannus formation. *Ann Thorac Surg.* 2004; 77:523-526.
19. von Knobelsdorff-Brenkenhoff F, Rudolph A, Wassmuth R, et al. Assessment of mitral bioprostheses using cardiovascular magnetic resonance. *J Cardiovasc Magn Reson* 2010; 12:36.
20. von Knobelsdorff-Brenkenhoff F, Rudolph A, Wassmuth R, et al. Feasibility of cardiovascular magnetic resonance to assess the orifice area of aortic bioprostheses. *Circ Cardiovasc Imaging* 2009; 2:397-404.





DANKWOORD

**D**aar zit je dan op de luchthaven van Kuala Lumpur in Maleisië, op weg naar een internationaal congres in Melbourne, Australië. Dit zijn de momenten waar je het gehele jaar hard voor werkt. Het is prachtig om de wetenschappelijke bevindingen met de rest van de wereld te mogen delen...

Het schrijven van een proefschrift is alleen maar mogelijk met een groep van geweldige mensen om je heen en in dit dankwoord wil ik dan ook alle mensen van harte bedanken die dit mede mogelijk gemaakt hebben.

Professor dr. Willem P.Th.M. Mali, mijn promotor, ik wil u bedanken voor uw enthousiaste begeleiding en de ruimte die u mij gaf om mijn eigen wetenschappelijke ideeën te mogen ontplooiën. Ik hoop dat ik aan u verwachtingen heb kunnen voldoen.

Dr. Ricardo P.J. Budde, mijn copromotor, Beste Ricardo ik wil jou bedanken voor de prettige manier waarop wij samengewerkt hebben de afgelopen 2,5 jaar. Jouw enthousiasme stimuleerde mij alleen maar meer. Ik heb veel waardering voor je toewijding voor het wetenschappelijk onderzoek. Daarnaast is het begeleiden van meerdere promovendi als arts-assistent ook geen makkelijke klus. Hulde daarvoor! Hoop dat we de komende jaren deze goede samenwerking kunnen voortzetten en dat het nog tot mooie gezamenlijke publicaties mag leiden!

Dr. Petr Symersky, Beste Petr ik wil jou bedanken voor de succesvolle samenwerking en je bijdrage aan een deel van de artikelen in dit proefschrift. Eerder dit jaar mocht jij jouw proefschrift verdedigen en hadden we een geweldige boottocht over de prachtige Amsterdamse grachten. Verder zal ik ook ons Bourgondisch dinertje in Parijs nooit vergeten, ga zeker terug wanneer ik weer in Parijs ben. Jouw chirurgische expertise en je verkregen radiologische kennis is een goed voorbeeld van de geneeskunde anno 2012: multidisciplinair denken leidt tot vooruitgang!

Drs. Linda de Heer, Beste Linda ik wil je bedanken voor de prettige samenwerking tijdens onze gezamenlijke promotieperiode. Jij was altijd welwillend om mij te helpen als er zaken op de afdeling Cardiothoracale Chirurgie afdeling in het UMC Utrecht geregeld moesten worden. Daar ben ik je erg dankbaar voor! Ik kijk nu al uit naar jouw verdediging eind dit jaar.

Prof. dr. Lex A. van Herwerden, ik wil u bedanken voor uw gastvrijheid op de afdeling Cardiothoracale Chirurgie van het UMC Utrecht. Tijdens het wekelijkse kleppenteam heb ik erg veel van u geleerd over hartklepaandoeningen en de chirurgische presentatie van deze aandoeningen. De correlatie van onze imaging bevindingen met uw intraoperatieve bevindingen op de operatiekamer was voor mij een van de meest waardevolle onderdelen van mijn promotieonderzoek. Ik kan elke (aanstaande) radioloog adviseren om eens wat vaker op de operatiekamer te gaan kijken hoe imaging bevindingen zich tijdens chirurgische inspectie presenteren.

Prof. dr. Bas A.J.M. de Mol, ik wil u bedanken dat ik de gelegenheid kreeg op uw afdeling Cardiothoracale Chirurgie in het AMC wetenschappelijk onderzoek uit te voeren. Zou mooi zijn om deze samenwerking voort te zetten!



Dr. Renee B.A. van den Brink, Beste Renee, Ik wil u bedanken voor het verruimen van mijn kennis over echocardiografie. Ik heb respect voor uw cardiologische kennis. Het is erg leuk om met u te discussiëren over cardiale imaging. Ben elke keer bij de IMPACT meetings weer onder de indruk van uw scherpe oog voor kleine subtiele echocardiografische afwijkingen.

251

Dr. Steven A.J. Chamuleau, Beste Steven, jij hebt altijd geloofd in het slagen van de IMPACT studie. Je hebt ook altijd gezorgd voor een maatje voor mij vanuit de cardiologie. Eerst Ruben, later Wilco. Jouw enthousiasme en behulpzaamheid zijn voor mij erg waardevol en hoop dat we deze samenwerking in de toekomst succesvol kunnen voortzetten.

Prof. dr. Mathias Prokop, Beste Mathias, ik wil u via deze weg bedanken voor de waardevolle bijdrage aan de manuscripten die Petr Symersky en ik samen geschreven hebben. Tevens wil ik u bedanken voor het plaatsnemen in de leescommissie.

Prof. dr. Guido de Wert, Beste Guido, ik wil je via deze weg bedanken dat je tijd genomen hebt om in de oppositie plaats te nemen. Je bent voor mij een bijzondere opponent aangezien je mij al vanaf mijn geboorte kent. Een aantal jaren geleden hield je een speech toen ik mijn artsdiploma ontving en nu mag je me die gewilde kritische vraag stellen....

Prof. dr. Max A. Viergever en Prof. dr. Pieter A. Doevendans, Prof. dr. A. de Roos, ik wil u via deze weg bedanken dat u tijd vrij gemaakt heeft om mijn manuscript kritisch te beoordelen.

Dr. Anje M. Spijkerboer, Beste Anje, ik wil jou bedanken voor jouw medewerking aan de totstandkoming van twee manuscripten in mijn thesis. Het was altijd erg prettig met jou samenwerken in het AMC.

Dr. J.B. Reitsma, Beste Hans, ik ontmoette jou voor de eerste keer als docent van een vak voor de postgraduate master epidemiology. Ik heb veel respect voor jouw kennis en kunde aangaande diagnostische studies. Dank voor je bijdrage aan de meta-analyse. Hoop in de toekomst op het raakvlak van de Radiologie en klinische epidemiologie nog mooie papers samen te schrijven.

Drs. Ewoud Smit, Beste Ewoud, ik wil je bedanken voor jouw bijdrage aan mijn proefschrift. Verheug me al op jouw promotie in de nabije toekomst.

Drs. T. Susan Meijer, Beste Susan, ik wil je bedanken voor jouw bijdrage aan mijn proefschrift. Was gezellig om met jou samen te werken. Veel succes in jouw verdere carrière!

Dr. Paul Westers, Beste Paul, ik wil je bedanken voor de statistische hulp die je mij in het begin van mijn promotietraject geboden hebt.

Prof. dr. Yolanda van der Graaf, Beste Yolanda, ik wil u via deze weg bedanken voor uw hulp bij het opzetten van de IMPACT studie. Ik heb genoten van onze pittige discussies over de epidemiologische aspecten van deze studie. Hoop dat onze samenwerking dit jaar resulteert in het succesvol afronden van de postgraduate master Clinical Epidemiology. Ik vind deze master een erg waardevol onderdeel van mijn promotie aangezien ik echt geleerd heb aan welke voorwaarden goed wetenschappelijk onderzoek moet voldoen.

Prof. dr. Maurice A.A.J. van den Bosch, Beste Maurice, ik wil je graag bedanken voor de leerzame discussies die ik met jou gehad heb over de ontwikkelingen binnen het radiologische vak en hoop de komende tijd onder jouw supervisie samen met dr. Tim Leiner, een mooi nieuw project binnen de vasculaire interventieradiologie op te zetten.





Dr. Tim Leiner, Beste Tim, Ik wil je via deze weg bedanken voor je bijdrage aan een aantal manuscripten in mijn thesis. Het is voor mij elke keer weer een genoegen om weer te sparren over nieuwe wetenschappelijke ideeën (liefst onder het genot van een goed glas wijn). Hoop de komende jaren met jou nog vele mooie wetenschappelijke projecten op te zetten.

253

Drs. Ruben Uijlings, Beste Ruben, ik wil je via deze weg bedanken voor de energie die jij samen met mij gestoken hebt in het opzetten van de IMPACT studie. In het bijzonder je hulp bij het plannen en verrichten van de cardiale echo-onderzoeken en fluoroscopie-onderzoeken. Je bent voor mij een graag geziene deelnemer aan de IMPACT consensus meetings en hoop je daar in de toekomst nog vaak te treffen.

Drs. Wilco Tanis, Beste Wilco, we hebben de laatste periode vrij intensief samengewerkt. Ik wil je bedanken voor jouw bijdrage aan dit proefschrift. Hoop dat je eigen wetenschappelijke inspanningen ook nog tot een proefschrift gaan leiden. Naast onze werkrelatie, zijn we echte vrienden geworden. Ik heb genoten van onze etentjes en je rondleiding door Gouda. Door onze toewijding voor de IMPACT studie, vergaten we wel eens de tijd. Joëlle, excuses daarvoor. Hoop dat de risotto laatst een kleine pleister op de wonde was...

Dr. Brigitta K. Velthuis, Brigitta, Dr. Evert-Jan P.A. Vonken, Evert-Jan, Hein, Cees, Lilian hartelijk dank voor jullie hulp bij het verslaan van de patiënten gescand voor de IMPACT-studie, en de leerzame cardiobesprekingen.

Alle arts-assistenten, fellows en stafleden van de afdelingen Radiologie, Cardiologie en Cardiothoracale chirurgie in het UMC Utrecht en AMC wil ik bedanken voor de hulp bij het uitvoeren van de IMPACT studie.

De laboranten van de Radiologie UMC Utrecht, in het bijzonder Monique Eulink, Anne Manders en Karin Thijn wil ik bedanken voor de hulp bij het scannen van de patiënten voor de IMPACT studie en het verrichten van de in-vitro experimenten. Het is altijd prettig samenwerken met jullie. Kijk al uit naar onze samenwerking tijdens mijn opleiding tot radioloog.

De laboranten van de echoafdeling van het UMC Utrecht en AMC Amsterdam, in het bijzonder wil ik Jeannette Bakker en Rianne de Bruin bedanken voor de hulp bij de planning en uitvoering van de benodigde echo-onderzoeken voor de IMPACT studie.

Trial bureau Radiologie, Anneke/Cees/Saskia/Shanta/Lenny, bedankt voor de bijdrage die jullie leveren aan de logistiek van de IMPACT studie.

Fotografie, Eugene, Karin, Roy en Jan, bedankt voor de hulp bij het bewerken van de vele figuren en filmpjes die gedurende mijn promotieonderzoek gemaakt zijn. Een illustratief plaatje zegt vaak meer dan vele woorden. Ik had op sommige momenten nog net geen vaste stoel bij jullie. Erg genoten!

Karin van Rijnbach, Beste Karin, bedankt voor je hulp en ondersteuning bij de totstandkoming van mijn proefschrift. Ik wil je in het bijzonder bedanken voor de moeite die je in de layout geïnvesteerd hebt.

Ingrid G.J. Janssen, Beste Ingrid, bedankt voor een aantal illustraties die jij voor mijn manuscripten gemaakt hebt. Een radiologisch proefschrift kan in mijn opinie niet zonder deze illustraties.

Stafsecretariaat Radiologie, Marja, Petra, Marion, Linda, Amanda, bedankt voor de hulp met het oplossen van allerlei praktische zaken gedurende mijn promotietraject. In het bijzonder wil ik Marja bedanken voor alle praktische zaken die je geregeld hebt tijdens mijn promotieperiode (in het bijzonder voor het symposium en de verdediging).

Het gehele technische cluster voor het oplossen van alle technische problemen gedurende mijn promotieperiode. Zonder jullie, was er heleboel waardevolle data verloren gegaan. Dank!

Arthur Adams, Beste Arthur, we begonnen een jaar of 2 geleden als kamergenoot maar al snel groeide dit uit tot een hechte vriendschap. Je bent net zoals ik een erg ondernemend persoon en dit resulteerde al snel in het gezamenlijke idee voor de Axcie. Dit leidde tot de introductie van het ski-uitje voor arts-onderzoekers. Zou mooi zijn om dit tot een traditie te laten uitgroeien. Verder delen we de passie van het wielrennen. Op dit moment zijn we samen met collega/vriend Nolan en vriendin Tjitske in training voor de Alpen waar we gaan fietsen voor het WKZ. Naast deze gezamenlijke sociale activiteiten, waardeer ik jouw gedrevenheid als wetenschapper en kijk ik al uit naar de artistieke omslag van jouw proefschrift.

Mijn research collega's, Nolan, Jan Willem, Reinoud, Beatrijs, Marianne, Arthur, Thomas, Suzanne, Laura, Malou, Ewoud, Onno, Anne, Mandy, Charlotte, Tom, Hamza, Martijn, Maarten & Maarten, Stan, Tim, Anja, Puspha, Jill, Martin, Anouk, Josephine, Merel, Joris, Marlijne, Joost, Hanke, Bertine, Alexandra, Annemarie, Mies, Marleen en Cécile, wil ik bedanken voor de gezellige activiteiten die we samen ondernomen hebben en jullie steun gedurende mijn promotieperiode. Allen veel succes gewenst met jullie promotietraject danwel met de opleiding tot medisch specialist. We komen elkaar vast weer tegen...



Beste familie, vrienden en vriendinnen, ik heb de afgelopen 2,5 jaar hard gewerkt, maar naast mijn drukke leven altijd geprobeerd tijd voor jullie te maken. Ik wil jullie allen bedanken voor jullie steun en zonder alle gezellige etentjes, sportactiviteiten, reisjes, avondjes stappen en drankjes drinken had ik deze promotie nooit kunnen afronden. Jullie zijn geweldig!

255

Beste paranimfen, Arthur&Tim, Dank voor jullie hulp bij het mogelijk maken van deze dag. Jullie zijn twee artsen waar ik waardering voor heb, maar nog veel meer goede vrienden die altijd voor mij klaarstaan. Dank!

Pap, mam, Kay en David, dit is voor mij een belangrijke dag maar deze dag is alleen maar mogelijk dankzij onze hechte familieband. We zijn net samen naar Venetië geweest, in 1 woord geweldig! Pap, mam, jullie hebben mij geleerd te genieten van de kleine dingen. Samen heerlijk buiten dineren met een goed glas wijn in de avondzon. Puur genieten! Bedankt voor jullie liefde, steun en vertrouwen!







CURRICULUM VITAE



Jesse Habets was born on the 17<sup>th</sup> of May 1985 in Beek, the Netherlands. In Beek, he learned to talk and explore the world. He graduated from grammar school (Gymnasium) in 2003 at the Graaf Huyn College, Geleen. In 2003, he started studying Medicine at the University of Maastricht. In June 2009, he graduated from medical school and started as resident Pediatric Surgery at Erasmus Medical Center, Rotterdam. In January 2010, he started as a PhD student at the University Medical Center Utrecht on a project concerning imaging of prosthetic heart valves by multidetector-row CT under supervision of prof. dr. W.P.Th.M. Mali and dr. R.P.J. Budde. This project was supported by a grant of the Dutch Heart Foundation [DHF-2009B014]. In September 2010, he started with a postgraduate master Clinical Epidemiology at the University of Utrecht. In August 2012, he will start as a resident in Radiology at the Gelre Ziekenhuizen under supervision of dr. J.W. Gratama.





LIST *of* PUBLICATIONS

## PUBLICATIONS

**Habets J**, Buth J, Cuypers PW, Nienhuijs SW, de Hingh IH. Infraarenal Abdominal Aortic Aneurysm with Concomitant Urological Malignancy: Treatment Results in the Era of Endovascular aneurysm Repair. *Vascular* 2010; 18(1):14-19.

**Habets J**, Symersky P, van Herwerden LA, de Mol BA, Spijkerboer AM, Mali WP, Budde RP. Prosthetic Heart Valve Assessment with Multidetector-row CT: Imaging Characteristics of 91 Valves in 83 Patients. *Eur Radiol.* 2011; 21(7):1390-1396.

**Habets J**, Budde RP, Symersky P, van den Brink RB, de Mol BA, Mali WP, van Herwerden LA, Chamuleau SA. Diagnostic Evaluation of Left-sided Prosthetic Heart Valve Dysfunction. *Nat Rev. Cardiol* 2011; 8(8):466-78.

**Habets J**, Symersky P, de Mol BA, Mali WP, Leiner T, Budde RP. A Novel Iterative Reconstruction Algorithm Allows Reduced Dose Multidetector-row CT Imaging of Mechanical Prosthetic Heart Valves. *Int J Cardiovasc Imaging* 2011; DOI: 10.1007/s10554-011-9954-7.

**Habets J**, van den Brink RB, Uijlings R, Spijkerboer AM, Mali WP, Chamuleau SA, Budde RP. Coronary Artery Assessment by Multidetector Computed Tomography in Patients with Prosthetic Heart Valves. *Eur Radiol.* 2011; DOI: 10.1007/s00330-011-2360-7.

Symersky P, **Habets J**, Westers P, de Mol BA, Mali WP, Prokop M, Budde RP. Prospective ECG Triggering Reduces Prosthetic Heart Valve-induced Artefacts Compared with Retrospective ECG gating on 256-slice CT. *Eur Radiol.* 2011; DOI 10.1007/s00330-011-2358-1.

de Heer LM, **Habets J**, Chamuleau SA, Mali WP, van Herwerden LA, Kluin J, Budde RP. Multidetector Row Computed Tomography Assessment of the Native Aortic and Mitral Valve: A Call for Routine Assessment of Left-sided Heart Valves during Coronary Computed Tomography. *Cardiol Rev.* 2012; DOI: 10.1097/CRD.0b013e318250eaaa.

**Habets J**, Symersky P, Leiner T, de Mol BA, Mali WP, Budde RP. Artifact reduction strategies for prosthetic heart valve CT imaging. *Int J Cardiovasc Imaging* 2012; DOI: 10.1007/s10554-012-0041-5.

**Habets J**, Meijer TS, Meijer RC, Mali WP, Vonken EP, Budde RP. Computed Tomography attenuation measurements are valuable to discriminate pledgets used in prosthetic heart valve implantation from paravalvular leakage. *The British Journal of Radiology* 2012; DOI: 10.1259/bjr/29602784.

**Habets J**, Mali WP, Budde RP. MDCT Angiography in the Evaluation of Prosthetic Heart Valve Dysfunction. *Radiographics* 2012 (Accepted).

**Habets J**, Tanis W, Mali WP, Chamuleau SA, Budde RP. Imaging of Prosthetic Heart Valve Dysfunction: Complementary Diagnostic Value of Transesophageal Echocardiography and Multidetector Computed Tomography. *JACC Cardiovasc Imaging.* 2012 (Accepted).

Tanis W, **Habets J**. "A Real Heart Sign" *J Am Coll Cardiol.* 2012 (Accepted).

Zandvoort HJA, **Habets J**, Leiner T, Moll FL, van Herwaarden JA. Review of Type 2 endoleaks. Chapter in *Vascular and Endovascular Controversies Update*. Charing Cross 2012. ISBN 978-0-9570419-0-5. Editor: Roger M Greenhalgh.

## CONFERENCE PROCEEDING | ORAL PRESENTATIONS

*Radiologendagen 2010, Veldhoven:*

**Habets J**, Symersky P, van Herwerden LA, de Mol BA, Mali WP, Budde RP. Prosthetic Heart Valve Assessment by Multislice-CT: Image Quality of Different PHV Types.

*European Congress of Radiology (ECR) 2011, Vienna:*

**Habets J**, Meijer TS, Meijer RC, Vonken EP, Mali WP, Budde RP. Imaging Characteristics of PTFE felt Pledgets Used in Prosthetic Heart Valve Implantation on 256-slice CT: Helpful in the Detection of Paravalvular Leakage?

*Radiologendagen 2011, Maastricht:*

**Habets J**, Symersky P, de Mol BA, Mali WP, Leiner T, Budde RP. A Novel Iterative Reconstruction Algorithm Allows Reduced Dose Multidetector-row CT Imaging of Mechanical Prosthetic Heart Valves.

Symersky P, **Habets J**, de Mol BA, Prokop M, Budde RP. Radiation Dose and Artifacts Are Reduced by Prospective ECG-triggering Relative to Retrospective ECG-gating for Imaging of Prosthetic Heart Valves with 256-slice CT.

**Habets J**, van den Brink RB, Uijlings R, Spijkerboer AM, Mali WP, Chamuleau SA, Budde RP. Coronary Artery Assessment with Multislice Computed Tomography in Patients with a Prosthetic Heart Valve: Is Coronary Assessment Hampered by Valve Related Artifacts?

*European Society of Cardiac Radiology 2011, Amsterdam:*

**Habets J**, Symersky P, Leiner T, de Mol BA, Mali WP, Budde RP. The Influences of Scan Parameters, a Novel Metal Artifact Reduction Filter and Iterative Reconstruction on the CT Image Quality of Mechanical Prosthetic Heart Valves.

*97th Scientific Assembly and Annual Meeting Radiological Society of North America 2011, Chicago:*

**Habets J**, Symersky P, de Mol BA, Mali WP, Leiner T, Budde RP. A Novel Iterative Reconstruction Algorithm Allows Reduced Dose Multidetector-row CT Imaging of Mechanical Prosthetic Heart Valves.

**Habets J**, Van den Brink RB, Uijlings R, Spijkerboer AM, Mali WP, Chamuleau SA, Budde RP. Coronary Artery Assessment with Multislice Computed Tomography in Patients with a Prosthetic Heart Valve: Is Coronary Assessment Hampered by Valve Related Artefacts?

*European Congress of Radiology (ECR) 2012, Vienna:*

De Heer LM, **Habets J**, Kluin J, Mali WP, Stella PR, van Herwerden LA, Budde RP. In-vivo Imaging Characteristics of a Transcatheter Heart Valve Prosthesis with Multislice Computed Tomography.

## CONFERENCE PROCEEDING | POSTER PRESENTATIONS

*European Congress of Radiology (ECR) 2011, Vienna:*

**Habets J**, Symersky P, van Herwerden LA, de Mol BA, Spijkerboer AM, Mali WP, Budde RP. Commonly Implanted Prosthetic Heart Valves Can Be Adequately Assessed by Multidetector-row CT.

*European Society of Cardiology Congress 2011, Paris:*

**Habets J**, van den Brink RB, Uijlings R, Spijkerboer AM, Mali WP, Chamuleau SA, Budde RP. . Coronary Artery Assessment with Multislice Computed Tomography in Patients with a Prosthetic Heart Valve: Is Coronary Assessment Hampered by Valve Related Artefacts? *European Heart Journal* 2011; 32 SUPPL. 1:1010-1011.

*97th Scientific Assembly and Annual Meeting Radiological Society of North America 2011, Chicago:*

**Habets J**, van den Brink RB, Uijlings R, Spijkerboer AM, Mali WP, Chamuleau SA, Budde RP. Coronary Artery Assessment with Multislice Computed Tomography in Patients with a Prosthetic Heart Valve: Is Coronary Assessment Hampered by Valve Related Artefacts?

*International Society for Magnetic Resonance in Medicine 20th Annual Meeting & Exhibition 2012, Melbourne:*

Van Stralen M, **Habets J**, Driessen MM, El Aïdi H, Pluim JP, Leiner T. Dual Breath-hold 3D Whole Heart Cine Cardiac MRI: Feasibility and Initial Experience.

**Habets J**, Zandvoort HJ, Cornelissen SA, Moll FL, Bartels LW, van Herwaarden JA, Leiner T. MR Imaging Improves Endoleak Detection in Patients after Endovascular Abdominal Aneurysm Repair.

**Habets J**, Zandvoort HJ, Reitsma JB, Moll FL, Bartels LW, van Herwaarden JA, Leiner T. Magnetic Resonance Imaging is More Sensitive than Computed Tomography Angiography for the Detection of Endoleaks after Endovascular Abdominal Aortic Aneurysm Repair: A Systematic Review.





# APPENDIX

CHAPTER III - APPENDIX I  
CHAPTER XIII/ XIV - APPENDIX I T/M VIII

**Appendix I** | Exact search string**Pubmed**

((“heart valve”[tiab] OR “heart valves”[tiab] OR “prosthetic heart valve”[tiab] OR “prosthetic heart valves”[tiab] OR “PHV”[tiab] OR “biological valve”[tiab] OR “biological valves”[tiab] OR “mechanical valve”[tiab] OR “mechanical valves”[tiab] OR “mechanical prosthesis”[tiab] OR “mechanical prostheses”[tiab] OR “biological prosthesis”[tiab] OR “biological prostheses”[tiab] OR “prosthetic mitral”[tiab] OR “prosthetic aortic”[tiab] OR “prosthetic”[tiab])) AND (“echocardiography”[tiab] OR “transthoracic echocardiography”[tiab] OR “transoesophageal echocardiography”[tiab] OR “ultrasound”[tiab] OR “ultrasonography”[tiab] OR “TTE”[tiab] OR “TEE”[tiab] OR “fluoroscopy”[tiab] OR “cine-fluoroscopy”[tiab] OR “computed tomography”[tiab] OR “CT”[tiab] OR “multislice computed tomography”[tiab] OR “multidetector-row computed tomography”[tiab] OR “MSCT”[tiab] OR “MDCT”[tiab] OR “computed tomography angiography”[tiab] OR “CTA”[tiab] OR “computed assisted tomography angiography”[tiab] OR “imaging”[tiab])

**Embase**

[embase]/lim NOT [medline]/lim AND ('heart'/exp OR heart AND valve:ab,ti OR ('heart'/exp OR heart AND valves:ab,ti) OR (prosthetic AND ('heart'/exp OR heart) AND valves:ab,ti) OR (prosthetic AND ('heart'/exp OR heart) AND valve:ab,ti) OR phv:ab,ti OR (biological AND valve:ab,ti) OR (biological AND valves:ab,ti) OR (mechanical AND valve:ab,ti) OR (mechanical AND valves:ab,ti) OR (mechanical AND prosthesis:ab,ti) OR (mechanical AND prostheses:ab,ti) OR (biological AND prosthesis:ab,ti) OR (biological AND prostheses:ab,ti) OR (prosthetic AND mitral:ab,ti) OR (prosthetic AND aortic:ab,ti) OR prosthetic:ab,ti) AND (echocardiography:ab,ti OR (transthoracic AND echocardiography:ab,ti) OR (transoesophageal AND echocardiography:ab,ti) OR tee:ab,ti OR (transesophageal AND echocardiography:ab,ti) OR tte:ab,ti OR fluoroscopy:ab,ti OR 'cine fluoroscopy':ab,ti OR (computed AND tomography:ab,ti) OR ct:ab,ti OR (multislice AND computed AND tomography:ab,ti) OR ('multidetector row' AND computed AND tomography:ab,ti) OR msct:ab,ti OR mdct:ab,ti OR (computed AND ('tomography'/exp OR tomography) AND angiography:ab,ti) OR cta:ab,ti OR ('computer'/exp OR computer AND assisted AND ('tomography'/exp OR tomography) AND angiography:ab,ti) OR imaging:ab,ti)

**Appendix I | Best PHV ECG-gated imaging phase (paired comparison, mean percentage better (range))**

	0%	10%	20%	30%	40%	50%	60%	70%	75%	80%	90%
0% better	X	<b>95.3</b> (93.0-97.7)	<b>81.4</b> (79.1-83.7)	59.9 (55.8-62.8)	65.7 (58.1-79.1)	72.7 (67.4-79.1)	<b>48.3</b> (44.2-55.8)	<b>37.8</b> (37.2-39.5)	<b>29.7</b> (27.9-30.2)	<b>33.1</b> (30.2-34.9)	47.1 (37.2-60.5)
10% better	4.7 (2.3-7.0)	X	<b>32.0</b> (23.3-37.2)	<b>16.3</b> (11.6-18.6)	<b>16.9</b> (14.0-23.3)	24.4 (16.3-32.6)	<b>12.8</b> (7.0-16.3)	<b>10.5</b> (4.7-14.0)	<b>9.9</b> (7.0-11.6)	<b>7.6</b> (4.7-11.6)	<b>17.4</b> (16.3-20.9)
20% better	<b>18.6</b> (16.3-20.9)	<b>68.0</b> (62.8-76.7)	X	29.7 (23.3-32.6)	<b>30.8</b> (23.3-34.9)	39.0 (37.2-44.2)	<b>23.8</b> (18.6-27.9)	<b>19.8</b> (16.3-23.3)	<b>20.3</b> (18.6-23.3)	<b>15.1</b> (9.3-18.6)	<b>17.4</b> (11.6-20.9)
30% better	40.1 (37.2-44.2)	<b>83.7</b> (81.4-88.4)	70.3 (67.4-76.7)	X	<b>54.1</b> (44.2-60.5)	59.9 (41.9-69.8)	43.0 (32.6-53.5)	<b>29.7</b> (25.6-34.9)	<b>27.9</b> (23.3-32.6)	<b>27.9</b> (16.3-34.9)	34.3 (18.6-51.2)
40% better	34.3 (20.9-41.9)	<b>83.1</b> (76.7-86.0)	<b>69.2</b> (65.1-69.8)	<b>45.9</b> (39.5-55.8)	X	52.9 (41.9-69.8)	36.0 (27.9-44.2)	<b>30.8</b> (20.9-39.5)	<b>29.7</b> (20.9-37.2)	<b>28.5</b> (11.6-41.9)	<b>38.4</b> (30.2-44.2)
50% better	27.3 (20.9-32.6)	75.6 (67.4-83.7)	61.0 (55.8-65.1)	40.1 (30.2-58.1)	47.1 (30.2-58.1)	X	<b>26.7</b> (16.3-32.6)	<b>26.7</b> (25.6-30.2)	<b>25.6</b> (23.3-30.2)	<b>20.3</b> (14.0-27.9)	<b>26.7</b> (23.3-30.2)
60% better	<b>51.7</b> (44.2-55.8)	<b>87.2</b> (83.7-93.0)	<b>76.2</b> (72.1-81.4)	57.0 (46.5-67.4)	64.0 (55.8-72.1)	<b>73.3</b> (67.4-83.7)	X	<b>32.0</b> (27.9-37.2)	<b>26.2</b> (20.9-30.2)	<b>31.4</b> (20.9-37.2)	<b>48.8</b> (44.2-55.8)
70% better	<b>62.2</b> (60.5-62.8)	<b>89.5</b> (86.0-95.3)	<b>80.2</b> (76.7-83.7)	<b>70.3</b> (65.1-74.4)	<b>69.2</b> (60.5-79.1)	<b>73.3</b> (69.8-74.4)	<b>68.0</b> (62.8-72.1)	X	34.9 (27.9-41.9)	<b>44.2</b> (39.5-51.2)	<b>53.5</b> (51.2-58.1)
75% better	<b>70.3</b> (69.8-72.1)	<b>90.1</b> (88.4-93.0)	<b>79.7</b> (76.7-81.4)	<b>72.1</b> (67.4-76.7)	<b>70.3</b> (62.8-79.1)	<b>74.4</b> (69.8-76.7)	<b>73.8</b> (69.8-79.1)	65.1 (58.1-72.1)	X	51.2 (44.2-60.5)	<b>58.7</b> (53.5-65.1)
80% better	<b>66.9</b> (65.1-69.8)	<b>92.4</b> (88.4-95.3)	<b>84.9</b> (81.4-90.7)	<b>72.1</b> (65.1-83.7)	<b>71.5</b> (65.1-88.4)	<b>79.7</b> (72.1-86.0)	<b>68.6</b> (62.8-79.1)	<b>55.8</b> (48.8-60.5)	48.8 (39.5-55.8)	X	<b>64.5</b> (60.5-69.8)
90% better	52.9 (39.5-62.8)	<b>82.6</b> (79.1-83.7)	<b>82.6</b> (79.1-88.4)	65.7 (48.8-81.4)	<b>61.6</b> (55.8-69.8)	<b>73.3</b> (69.8-76.7)	<b>51.2</b> (44.2-55.8)	<b>46.5</b> (41.9-48.8)	<b>41.3</b> (34.9-46.5)	<b>35.5</b> (30.2-39.5)	X

Percentages better are depicted in bold when inter- and intraobserver κ statistics ≥0.6

**Appendix II** | Intraobserver agreement for Best PHV ECG-gated imaging phase evaluation (mean  $\kappa$ , (range))

	0%	10%	20%	30%	40%	50%	60%	70%	75%	80%	90%
0% better	X	<b>1.0 (0.9-1.0)</b>	<b>0.6 (0.6-0.7)</b>	0.5 (0.5-0.6)	<b>0.6 (0.5-0.7)</b>	<b>0.7 (0.6-0.7)</b>	<b>0.7 (0.6-0.7)</b>	<b>0.8 (0.8-0.8)</b>	<b>0.8 (0.7-0.9)</b>	<b>0.8 (0.7-0.9)</b>	<b>0.7 (0.7-0.8)</b>
10% better	<b>1.0 (0.9-1.0)</b>	X	<b>0.7 (0.6-0.7)</b>	<b>0.7 (0.7-0.8)</b>	<b>0.7 (0.7-0.8)</b>	<b>0.6 (0.6-0.6)</b>	<b>0.9 (0.9-0.9)</b>	<b>0.8 (0.7-0.9)</b>	<b>0.8 (0.8-0.9)</b>	<b>0.9 (0.8-1.0)</b>	<b>0.8 (0.8-0.8)</b>
20% better	<b>0.6 (0.6-0.7)</b>	<b>0.7 (0.6-0.7)</b>	X	<b>0.6 (0.4-0.7)</b>	<b>0.7 (0.7-0.8)</b>	<b>0.6 (0.4-0.7)</b>	<b>0.8 (0.8-0.8)</b>	<b>0.9 (0.8-1.0)</b>	<b>0.9 (0.9-1.0)</b>	<b>0.9 (0.8-0.9)</b>	<b>0.8 (0.8-0.9)</b>
30% better	0.5 (0.5-0.6)	<b>0.7 (0.7-0.8)</b>	<b>0.6 (0.4-0.7)</b>	X	<b>0.8 (0.8-0.8)</b>	<b>0.6 (0.5-0.7)</b>	<b>0.6 (0.6-0.7)</b>	<b>0.8 (0.8-0.8)</b>	<b>0.7 (0.5-0.9)</b>	<b>0.8 (0.6-0.9)</b>	<b>0.7 (0.6-0.8)</b>
40% better	<b>0.6 (0.5-0.7)</b>	<b>0.7 (0.7-0.8)</b>	<b>0.7 (0.7-0.8)</b>	<b>0.8 (0.8-0.8)</b>	X	0.4 (0.3-0.5)	<b>0.8 (0.7-0.9)</b>	<b>0.8 (0.8-0.8)</b>	<b>0.8 (0.8-0.8)</b>	<b>0.7 (0.7-0.8)</b>	<b>0.8 (0.7-0.8)</b>
50% better	<b>0.7 (0.6-0.7)</b>	<b>0.6 (0.6-0.6)</b>	<b>0.6 (0.4-0.7)</b>	<b>0.6 (0.5-0.7)</b>	0.4 (0.3-0.5)	X	<b>0.7 (0.6-0.9)</b>	<b>0.8 (0.6-0.9)</b>	<b>0.8 (0.7-0.9)</b>	<b>0.8 (0.8-0.8)</b>	<b>0.6 (0.6-0.6)</b>
60% better	<b>0.7 (0.6-0.7)</b>	<b>0.9 (0.9-0.9)</b>	<b>0.8 (0.8-0.8)</b>	<b>0.6 (0.6-0.7)</b>	<b>0.8 (0.7-0.9)</b>	<b>0.7 (0.6-0.9)</b>	X	<b>0.7 (0.7-0.7)</b>	<b>0.7 (0.6-0.8)</b>	<b>0.7 (0.7-0.7)</b>	<b>0.7 (0.7-0.8)</b>
70% better	<b>0.8 (0.8-0.8)</b>	<b>0.8 (0.7-0.9)</b>	<b>0.9 (0.8-1.0)</b>	<b>0.8 (0.8-0.8)</b>	<b>0.8 (0.8-0.8)</b>	<b>0.8 (0.6-0.9)</b>	<b>0.7 (0.7-0.7)</b>	X	0.4 (0.3-0.6)	<b>0.7 (0.6-0.7)</b>	<b>0.9 (0.8-1.0)</b>
75% better	<b>0.8 (0.7-0.9)</b>	<b>0.8 (0.8-0.9)</b>	<b>0.9 (0.9-1.0)</b>	<b>0.7 (0.5-0.9)</b>	<b>0.8 (0.8-0.8)</b>	<b>0.8 (0.7-0.9)</b>	<b>0.7 (0.6-0.8)</b>	0.4 (0.3-0.6)	X	0.5 (0.4-0.6)	<b>0.8 (0.7-0.9)</b>
80% better	<b>0.8 (0.7-0.9)</b>	<b>0.9 (0.8-1.0)</b>	<b>0.9 (0.8-0.9)</b>	<b>0.8 (0.6-0.9)</b>	<b>0.7 (0.7-0.8)</b>	<b>0.8 (0.8-0.8)</b>	<b>0.7 (0.7-0.7)</b>	<b>0.7 (0.6-0.7)</b>	0.5 (0.4-0.6)	X	<b>0.7 (0.6-0.8)</b>
90% better	<b>0.7 (0.7-0.8)</b>	<b>0.8 (0.8-0.8)</b>	<b>0.8 (0.8-0.9)</b>	<b>0.7 (0.6-0.8)</b>	<b>0.8 (0.7-0.8)</b>	<b>0.6 (0.6-0.6)</b>	<b>0.7 (0.7-0.8)</b>	<b>0.9 (0.8-1.0)</b>	<b>0.8 (0.7-0.9)</b>	<b>0.7 (0.6-0.8)</b>	X

$\kappa$  statistics  $\geq 0.6$  are depicted in bold

**Appendix III** | Interobserver agreement for best PHV ECG-gated imaging phase evaluation (mean  $\kappa$ , (range))

	0%	10%	20%	30%	40%	50%	60%	70%	75%	80%	90%
0% better	X	<b>1.0 (1.0-1.0)</b>	<b>0.7 (0.6-0.8)</b>	0.5 (0.4-0.6)	0.4 (0.3-0.6)	0.5 (0.4-0.7)	<b>0.6 (0.5-0.7)</b>	<b>0.7 (0.6-0.8)</b>	<b>0.7 (0.7-0.8)</b>	<b>0.6 (0.4-0.7)</b>	0.5 (0.4-0.7)
10% better	<b>1.0 (1.0-1.0)</b>	X	<b>0.7 (0.5-0.7)</b>	<b>0.8 (0.6-0.9)</b>	<b>0.6 (0.4-0.7)</b>	0.5 (0.4-0.6)	<b>0.9 (0.8-1.0)</b>	<b>0.8 (0.7-0.8)</b>	<b>0.8 (0.8-0.9)</b>	<b>0.9 (0.8-1.0)</b>	<b>0.9 (0.8-0.9)</b>
20% better	<b>0.7 (0.6-0.8)</b>	<b>0.7 (0.5-0.7)</b>	X	0.4 (0.3-0.5)	<b>0.6 (0.5-0.6)</b>	0.3 (0.2-0.4)	<b>0.8 (0.7-0.8)</b>	<b>0.7 (0.6-0.7)</b>	<b>0.7 (0.6-0.7)</b>	<b>0.7 (0.6-0.8)</b>	<b>0.8 (0.8-0.9)</b>
30% better	0.5 (0.4-0.6)	<b>0.8 (0.6-0.9)</b>	0.4 (0.3-0.5)	X	<b>0.7 (0.6-0.7)</b>	0.4 (0.3-0.4)	0.5 (0.3-0.6)	<b>0.7 (0.6-0.8)</b>	<b>0.7 (0.5-0.8)</b>	<b>0.7 (0.6-0.8)</b>	0.4 (0.3-0.5)
40% better	0.4 (0.3-0.6)	<b>0.6 (0.4-0.7)</b>	<b>0.6 (0.5-0.6)</b>	<b>0.7 (0.6-0.7)</b>	X	0.3 (0.2-0.5)	0.5 (0.4-0.6)	<b>0.6 (0.5-0.7)</b>	<b>0.6 (0.5-0.6)</b>	<b>0.6 (0.4-0.7)</b>	<b>0.7 (0.5-0.9)</b>
50% better	0.5 (0.4-0.7)	0.5 (0.4-0.6)	0.3 (0.2-0.4)	0.4 (0.3-0.4)	0.3 (0.2-0.5)	X	<b>0.6 (0.5-0.6)</b>	<b>0.7 (0.6-0.7)</b>	<b>0.6 (0.6-0.7)</b>	<b>0.7 (0.6-0.9)</b>	<b>0.6 (0.4-0.7)</b>
60% better	<b>0.6 (0.5-0.7)</b>	<b>0.9 (0.8-1.0)</b>	<b>0.8 (0.7-0.8)</b>	0.5 (0.3-0.6)	0.5 (0.4-0.6)	<b>0.6 (0.5-0.6)</b>	X	<b>0.7 (0.5-0.8)</b>	<b>0.7 (0.5-0.8)</b>	<b>0.7 (0.7-0.7)</b>	<b>0.7 (0.6-0.8)</b>
70% better	<b>0.7 (0.6-0.8)</b>	<b>0.8 (0.7-0.8)</b>	<b>0.7 (0.6-0.7)</b>	<b>0.7 (0.6-0.8)</b>	<b>0.6 (0.5-0.7)</b>	<b>0.7 (0.6-0.7)</b>	<b>0.7 (0.5-0.8)</b>	X	0.3 (0.3-0.4)	<b>0.6 (0.5-0.7)</b>	<b>0.7 (0.7-0.8)</b>
75% better	<b>0.7 (0.7-0.8)</b>	<b>0.8 (0.8-0.9)</b>	<b>0.7 (0.6-0.7)</b>	<b>0.7 (0.5-0.8)</b>	<b>0.6 (0.5-0.6)</b>	<b>0.6 (0.6-0.7)</b>	<b>0.7 (0.5-0.8)</b>	<b>0.7 (0.5-0.8)</b>	X	0.4 (0.1-0.6)	<b>0.7 (0.6-0.8)</b>
80% better	<b>0.6 (0.4-0.7)</b>	<b>0.9 (0.8-1.0)</b>	<b>0.7 (0.6-0.8)</b>	<b>0.7 (0.6-0.8)</b>	<b>0.6 (0.4-0.7)</b>	<b>0.7 (0.6-0.9)</b>	<b>0.7 (0.7-0.7)</b>	<b>0.6 (0.5-0.7)</b>	0.4 (0.1-0.6)	X	<b>0.6 (0.4-0.8)</b>
90% better	0.5 (0.4-0.7)	<b>0.8 (0.8-0.9)</b>	<b>0.8 (0.8-0.9)</b>	0.4 (0.3-0.5)	<b>0.7 (0.5-0.9)</b>	<b>0.6 (0.4-0.7)</b>	<b>0.7 (0.6-0.8)</b>	<b>0.7 (0.7-0.8)</b>	<b>0.7 (0.6-0.8)</b>	<b>0.6 (0.4-0.8)</b>	X

$\kappa$  statistics  $\geq 0.6$  are depicted in bold

**Appendix IV | Mechanical PHVs: Best PHV ECG-gated imaging phase (paired comparison, mean percentage better (range))**

	0%	10%	20%	30%	40%	50%	60%	70%	75%	80%	90%
0% better	X	<b>95.4</b> (92.6-96.3)	<b>80.6</b> (77.8-85.2)	<b>58.3</b> (55.6-63.0)	72.2 (66.7-85.2)	75.9 (66.7-81.5)	<b>46.3</b> (40.7-55.6)	<b>37.0</b> (33.3-40.7)	<b>27.8</b> (22.2-29.6)	<b>25.9</b> (22.2-29.6)	42.6 (29.6-55.6)
10% better	4.6 (3.7-7.4)	X	<b>30.6</b> (18.5-37.0)	<b>13.0</b> (11.1-14.8)	<b>20.4</b> (18.5-25.9)	25.9 (14.8-37.0)	<b>10.2</b> (7.4-11.1)	<b>8.3</b> (3.7-11.1)	<b>8.3</b> (3.7-11.1)	4.6 (3.7-7.4)	13.9 (11.1-14.8)
20% better	19.4 (14.8-22.2)	69.4 (63.0-81.5)	X	28.7 (22.2-33.3)	<b>37.0</b> (25.9-48.1)	45.4 (40.7-48.1)	<b>21.3</b> (18.5-22.2)	<b>21.3</b> (18.5-22.2)	<b>22.2</b> (22.2-22.2)	<b>11.1</b> (3.7-18.5)	13.9 (7.4-18.5)
30% better	41.7 (37.0-44.4)	87.0 (85.2-88.9)	71.3 (66.7-77.8)	X	<b>64.8</b> (55.6-70.4)	64.8 (48.1-70.4)	44.4 (29.6-55.6)	36.1 (33.3-40.7)	25.9 (14.8-33.3)	21.3 (11.1-25.9)	36.1 (18.5-55.6)
40% better	27.8 (14.8-33.3)	79.6 (74.1-81.5)	<b>63.0</b> (51.9-74.1)	<b>35.2</b> (29.6-44.4)	X	48.1 (37.0-63.0)	<b>26.9</b> (14.8-37.0)	<b>25.0</b> (18.5-29.6)	<b>22.2</b> (14.8-29.6)	<b>17.6</b> (7.4-29.6)	24.1 (11.1-33.3)
50% better	24.1 (18.5-33.3)	74.1 (63.0-85.2)	54.6 (51.9-59.3)	35.2 (25.9-51.9)	51.9 (37.0-63.0)	X	24.1 (11.1-29.6)	<b>27.8</b> (22.2-29.6)	<b>21.3</b> (14.8-29.6)	<b>13.0</b> (7.4-18.5)	20.4 (14.8-25.9)
60% better	53.7 (44.4-59.3)	89.8 (88.9-92.6)	78.7 (77.8-81.5)	55.6 (44.4-70.4)	73.1 (63.0-85.2)	75.9 (70.4-88.9)	X	<b>31.5</b> (29.6-33.3)	<b>21.3</b> (18.5-22.2)	<b>23.1</b> (11.1-29.6)	45.4 (40.7-51.9)
70% better	63.0 (59.3-66.7)	91.7 (88.9-96.3)	78.7 (77.8-81.5)	63.9 (59.3-66.7)	75.0 (70.4-81.5)	72.2 (70.4-77.8)	<b>68.5</b> (66.7-70.4)	X	25.9 (22.2-29.6)	<b>35.2</b> (29.6-40.7)	56.5 (48.1-63.0)
75% better	72.2 (70.4-74.1)	91.7 (88.9-96.3)	77.8 (77.8-77.8)	74.1 (66.7-85.2)	77.8 (70.4-85.2)	78.7 (70.4-85.2)	<b>78.7</b> (77.8-81.5)	74.1 (70.4-77.8)	X	49.1 (44.4-51.9)	66.7 (59.3-70.4)
80% better	74.1 (70.4-77.8)	95.4 (92.6-96.3)	88.9 (81.5-96.3)	78.7 (74.1-88.9)	82.4 (70.4-92.6)	87.0 (81.5-92.6)	<b>76.9</b> (70.4-88.9)	<b>64.8</b> (59.3-70.4)	50.9 (48.1-55.6)	X	68.5 (63.0-81.5)
90% better	57.4 (44.4-70.4)	86.1 (85.2-88.9)	86.1 (81.5-92.6)	63.9 (44.4-81.5)	75.9 (66.7-88.9)	79.6 (74.1-85.2)	<b>54.6</b> (48.1-59.3)	43.5 (37.0-51.9)	33.3 (29.6-40.7)	<b>31.5</b> (18.5-37.0)	X

Percentages better are depicted in bold when inter- and intraobserver κ statistics ≥0.6

**Appendix V | Biological PHVs: Best PHV ECG-gated imaging phase (paired comparison, mean percentage better (range))**

	0%	10%	20%	30%	40%	50%	60%	70%	75%	80%	90%
0% better	X	<b>95.3</b> (93.8-100.0)	<b>82.8</b> (75.0-87.5)	62.5 (56.3-68.8)	54.7 (43.8-68.8)	<b>67.2</b> (56.3-68.8)	<b>51.6</b> (43.8-56.3)	<b>39.1</b> (37.5-43.8)	<b>32.8</b> (25.0-37.5)	45.3 (31.3-56.3)	<b>54.7</b> (37.5-68.8)
10% better	4.7 (0.0-6.3)	X	<b>34.4</b> (31.3-37.5)	21.9 (12.5-31.3)	<b>10.9</b> (6.3-18.8)	21.9 (18.8-31.3)	17.2 (6.3-25.0)	14.1 (6.3-18.8)	12.5 (6.3-18.8)	12.5 (6.3-18.8)	<b>23.4</b> (18.8-31.3)
20% better	<b>17.2</b> (12.5-25.0)	<b>65.6</b> (62.5-68.8)	X	31.2 (25.0-37.5)	<b>20.3</b> (12.5-25.0)	28.1 (18.8-37.5)	<b>28.1</b> (18.8-37.5)	<b>17.2</b> (12.5-25.0)	<b>17.2</b> (12.5-25.0)	<b>21.9</b> (12.5-37.5)	<b>23.4</b> (18.8-25.0)
30% better	37.5 (31.3-43.8)	78.1 (68.8-81.3)	68.8 (62.5-75.0)	X	<b>35.9</b> (25.0-43.8)	51.6 (31.3-62.5)	40.6 (25.0-50.0)	<b>18.8</b> (12.5-25.0)	31.2 (18.8-37.5)	<b>39.1</b> (25.0-50.0)	<b>31.2</b> (18.8-43.8)
40% better	45.3 (31.3-56.3)	<b>89.1</b> (81.3-93.8)	<b>79.7</b> (75.0-87.5)	<b>64.1</b> (56.3-75.0)	X	60.9 (50.0-81.3)	51.6 (43.8-62.5)	40.6 (18.8-56.3)	42.2 (31.3-56.3)	46.9 (18.8-62.5)	<b>62.5</b> (62.5-62.5)
50% better	<b>32.8</b> (25.0-43.8)	78.1 (68.8-81.3)	71.9 (62.5-81.3)	48.4 (37.5-68.8)	39.1 (18.8-50.0)	X	<b>31.2</b> (25.0-37.5)	25.0 (18.8-31.3)	<b>32.8</b> (25.0-37.5)	<b>32.8</b> (31.3-43.8)	37.5 (31.3-43.8)
60% better	<b>48.4</b> (43.8-56.3)	<b>82.8</b> (75.0-93.8)	<b>71.9</b> (62.5-81.3)	59.4 (50.0-75.0)	48.4 (37.5-56.3)	<b>68.8</b> (62.5-75.0)	X	32.8 (25.0-43.8)	34.4 (25.0-43.8)	45.3 (37.5-50.0)	<b>54.7</b> (50.0-62.5)
70% better	<b>60.9</b> (56.3-62.5)	<b>85.9</b> (81.3-93.8)	<b>82.8</b> (75.0-87.5)	<b>81.2</b> (75.0-87.5)	59.4 (43.8-81.3)	75.0 (68.8-81.3)	<b>67.2</b> (56.3-75.0)	X	50.0 (25.0-68.8)	<b>59.4</b> (50.0-68.8)	<b>48.4</b> (37.5-62.5)
75% better	<b>67.2</b> (62.5-75.0)	<b>87.5</b> (81.3-93.8)	<b>82.8</b> (75.0-87.5)	68.8 (62.5-81.3)	57.8 (43.8-68.8)	<b>67.2</b> (62.5-75.0)	<b>65.6</b> (56.3-75.0)	50.0 (31.3-75.0)	X	54.7 (31.3-75.0)	<b>45.3</b> (37.5-56.3)
80% better	54.7 (43.8-68.8)	<b>87.5</b> (81.3-93.8)	<b>78.1</b> (62.5-87.5)	<b>60.9</b> (50.0-75.0)	53.1 (37.5-81.3)	<b>67.2</b> (56.3-75.0)	<b>54.7</b> (50.0-62.5)	<b>40.6</b> (31.3-50.0)	45.3 (25.0-68.8)	X	57.8 (50.0-68.8)
90% better	<b>45.3</b> (31.3-62.5)	<b>76.7</b> (68.8-81.3)	<b>76.7</b> (75.0-81.3)	<b>68.8</b> (56.3-81.3)	<b>37.5</b> (37.5-37.5)	62.5 (56.3-68.8)	<b>45.3</b> (37.5-50.0)	<b>51.6</b> (37.5-62.5)	<b>54.7</b> (43.8-62.5)	42.2 (31.3-50.0)	X

Percentages better are depicted in bold when inter- and intraobserver κ statistics ≥0.6

**Appendix VI** | PHV scans with a heart rate <60 bpm (paired comparison, mean percentage better (range))

	Average image quality	0%	10%	20%	30%	40%	50%	60%	70%	75%	80%	90%
0% better	45	X	97.7 (90.9-100.0)	70.5 (63.6-72.7)	45.5 (36.4-63.6)	56.8 (45.5-72.7)	65.9 (54.5-72.7)	43.2 (27.3-63.6)	25.0 (18.2-27.3)	11.4 (9.1-18.2)	20.5 (9.1-36.4)	43.2 (27.3-54.5)
10% better	11	2.3 (0.0-9.1)	X	34.1 (18.2-45.5)	6.8 (0.0-9.1)	27.3 (18.2-36.4)	11.4 (9.1-18.2)	13.6 (0.0-27.3)	4.5 (0.0-18.2)	0.0 (0.0-0.0)	0.0 (0.0-0.0)	6.8 (0.0-9.1)
20% better	26	29.5 (27.3-36.4)	65.9 (54.5-81.8)	X	31.8 (27.3-36.4)	36.4 (36.4-36.4)	22.7 (9.1-27.3)	27.3 (9.1-45.5)	13.6 (0.0-27.3)	11.4 (0.0-18.2)	13.6 (9.1-18.2)	6.8 (0.0-18.2)
30% better	49	54.5 (36.4-63.6)	93.2 (90.9-100.0)	68.2 (63.6-72.7)	X	75.0 (54.5-90.9)	61.4 (36.4-81.8)	47.7 (27.3-72.7)	18.2 (9.1-36.4)	22.7 (9.1-36.4)	20.5 (0.0-36.4)	29.5 (9.1-63.6)
40% better	38	43.2 (27.3-54.5)	72.7 (63.6-81.8)	63.6 (63.6-63.6)	25.0 (9.1-45.5)	X	38.6 (27.3-54.5)	40.9 (27.3-63.6)	22.7 (9.1-36.4)	20.5 (9.1-36.4)	20.5 (0.0-36.4)	27.3 (18.2-36.4)
50% better	41	34.1 (27.3-45.5)	88.6 (81.8-90.9)	77.3 (72.7-90.9)	38.6 (18.2-63.6)	61.4 (45.5-72.7)	X	38.6 (18.2-54.5)	22.7 (18.2-27.3)	15.9 (9.1-27.3)	18.2 (9.1-36.4)	18.2 (0.0-36.4)
60% better	48	56.8 (36.4-72.7)	86.4 (72.7-100.0)	72.7 (54.5-90.9)	52.3 (27.3-72.2)	59.1 (36.4-72.7)	61.4 (45.5-81.8)	X	13.6 (0.0-18.2)	9.1 (0.0-18.2)	15.9 (9.1-27.3)	56.8 (45.5-72.7)
70% better	71	75.0 (72.7-81.8)	95.5 (81.8-100.0)	86.4 (72.7-100.0)	81.8 (72.7-90.9)	77.3 (63.6-90.9)	77.3 (72.7-81.8)	86.4 (81.8-100.1)	X	38.6 (9.1-54.5)	40.9 (18.2-63.6)	54.5 (45.5-63.6)
75% better	79	88.6 (81.8-90.9)	100.0 (100.0-100.0)	88.6 (81.8-100.0)	77.3 (63.6-90.9)	79.5 (63.6-90.9)	84.1 (72.7-90.9)	90.9 (81.8-100)	61.4 (45.5-90.9)	X	61.4 (36.4-81.8)	61.4 (54.5-81.8)
80% better	75	79.5 (63.6-90.9)	100.0 (100.0-100.0)	86.4 (81.8-90.9)	79.5 (63.6-100.0)	79.5 (63.6-100.0)	81.8 (63.6-100)	84.1 (72.7-90.9)	59.1 (36.4-81.8)	38.6 (18.2-63.6)	X	65.9 (54.5-81.8)
90% better	63	56.8 (45.5-72.7)	93.2 (90.9-100.0)	93.2 (81.8-100.0)	70.5 (36.4-90.9)	72.7 (63.6-81.8)	81.8 (63.6-100)	43.2 (27.3-54.5)	45.5 (36.4-54.4)	38.6 (18.2-45.5)	34.1 (18.2-45.5)	X



**Appendix VII** | PHV scans with a heart rate 60-90 bpm (paired comparison, mean percentage better (range))

	Average image quality										
	0%	10%	20%	30%	40%	50%	60%	70%	75%	80%	90%
0% better	X	99.0 (96.0-100.0)	86.0 (84.0-92.0)	66.0 (56.0-76.0)	70.0 (60.0-88.0)	79.0 (72.0-84.0)	49.0 (44.0-56.0)	40.0 (36.0-44.0)	35.0 (32.0-40.0)	39.0 (32.0-44.0)	51.0 (40.0-64.0)
10% better	1.0 (0.0-4.0)	X	31.0 (24.0-40.0)	17.0 (12.0-20.0)	13.0 (8.0-20.0)	27.0 (16.0-40.0)	10.0 (4.0-16.0)	6.0 (4.0-12.0)	8.0 (4.0-12.0)	7.0 (4.0-12.0)	21.0 (20.0-24.0)
20% better	14.0 (8.0-16.0)	69.0 (60.0-76.0)	X	25.0 (16.0-32.0)	27.0 (16.0-36.0)	42.0 (36.0-44.0)	22.0 (16.0-28.0)	19.0 (16.0-20.0)	21.0 (16.0-28.0)	9.0 (0.0-12.0)	21.0 (16.0-28.0)
30% better	34.0 (24.0-44.0)	83.0 (80.0-88.0)	75.0 (68.0-84.0)	X	45.0 (36.0-52.0)	59.0 (44.0-68.0)	41.0 (32.0-52.0)	33.0 (32.0-36.0)	25.0 (24.0-28.0)	28.0 (20.0-36.0)	37.0 (24.0-52.0)
40% better	30.0 (12.0-40.0)	87.0 (80.0-92.0)	73.0 (64.0-84.0)	55.0 (48.0-64.0)	X	55.0 (40.0-68.0)	33.0 (24.0-44.0)	31.0 (24.0-40.0)	30.0 (20.0-36.0)	27.0 (8.0-44.0)	40.0 (28.0-48.0)
50% better	21.0 (16.0-28.0)	73.0 (60.0-84.0)	58.0 (56.0-64.0)	41.0 (32.0-56.0)	45.0 (32.0-60.0)	X	21.0 (8.0-28.0)	24.0 (20.0-28.0)	27.0 (20.0-32.0)	18.0 (16.0-20.0)	28.0 (24.0-32.0)
60% better	51.0 (44.0-56.0)	90.0 (84.0-96.0)	78.0 (72.0-84.0)	59.0 (48.0-68.0)	67.0 (56.0-76.0)	79.0 (72.0-96.0)	X	37.0 (36.0-40.0)	31.0 (24.0-36.0)	34.0 (24.0-48.0)	45.0 (40.0-56.0)
70% better	60.0 (56.0-64.0)	94.0 (88.0-96.0)	81.0 (80.0-84.0)	67.0 (64.0-68.0)	69.0 (60.0-76.0)	76.0 (72.0-80.0)	63.0 (60.0-64.0)	X	33.0 (32.0-36.0)	43.0 (40.0-44.0)	59.0 (56.0-64.0)
75% better	65.0 (60.0-68.0)	92.0 (88.0-96.0)	79.0 (72.0-84.0)	75.0 (72.0-76.0)	70.0 (64.0-80.0)	73.0 (68.0-80.0)	69.0 (64.0-76.0)	67.0 (64.0-68.0)	X	48.0 (44.0-52.0)	62.0 (60.0-68.0)
80% better	61.0 (56.0-68.0)	93.0 (88.0-96.0)	91.0 (88.0-100.0)	72.0 (64.0-80.0)	73.0 (56.0-92.0)	82.0 (80.0-84.0)	66.0 (52.0-76.0)	57.0 (56.0-60.0)	52.0 (48.0-56.0)	X	67.0 (56.0-80.0)
90% better	49.0 (36.0-60.0)	79.0 (76.0-80.0)	79.0 (72.0-84.0)	63.0 (48.0-76.0)	60.0 (52.0-72.0)	72.0 (68.0-76.0)	55.0 (44.0-60.0)	41.0 (36.0-44.0)	38.0 (32.0-40.0)	33.0 (20.0-44.0)	X

**Appendix VIII | PHV scans with a heart rate >90 bpm (paired comparison, mean percentage better (range))**

	Average image quality	0%	10%	20%	30%	40%	50%	60%	70%	75%	80%	90%
0% better	56	X (14.3-28.6)	78.6 (71.4-85.7)	82.1 (71.4-85.7)	60.7 (57.1-71.4)	64.3 (57.1-71.4)	60.7 (42.9-53.6)	53.6 (28.6-71.4)	50.0 (42.9-57.1)	39.3 (28.6-42.9)	32.1 (28.6-42.9)	39.3 (28.6-57.1)
10% better	26	21.4 (14.3-28.6)	X	32.1 (14.3-42.9)	28.6 (14.3-42.9)	14.3 (0.0-28.6)	35.7 (28.6-42.9)	21.4 (0.0-42.9)	35.7 (14.3-42.9)	32.1 (14.3-42.9)	21.4 (14.3-28.6)	21.4 (14.3-42.9)
20% better	34	17.9 (14.3-28.6)	67.9 (57.1-85.7)	X	42.9 (28.6-57.1)	35.7 (28.6-42.9)	53.6 (28.6-71.4)	25.0 (0.0-42.9)	32.1 (28.6-42.9)	32.1 (28.6-42.9)	39.3 (28.6-42.9)	21.4 (14.3-28.6)
30% better	48	39.3 (28.6-42.9)	71.4 (57.1-85.7)	57.1 (42.9-71.4)	X	53.6 (42.9-57.1)	60.7 (42.9-71.4)	42.9 (28.6-57.1)	35.7 (28.6-42.9)	46.4 (42.9-57.1)	39.3 (28.6-57.1)	32.1 (14.3-57.1)
40% better	52	35.7 (28.6-42.9)	85.7 (71.4-100.0)	64.3 (57.1-71.4)	46.4 (42.9-57.1)	X	67.9 (42.9-100)	39.3 (28.6-57.1)	42.9 (28.6-57.1)	42.9 (28.6-57.1)	46.4 (42.9-57.1)	50.0 (42.9-57.1)
50% better	40	39.3 (28.6-57.1)	64.3 (57.1-71.4)	46.4 (28.6-71.4)	39.3 (28.6-57.1)	32.1 (0.0-57.1)	X	28.6 (0.0-57.1)	42.9 (28.6-57.1)	35.7 (28.6-42.9)	32.1 (28.6-57.1)	35.7 (14.3-57.1)
60% better	56	46.3 (28.6-71.4)	78.6 (57.1-100.0)	75.0 (57.1-100.0)	57.1 (42.9-71.4)	60.7 (42.9-71.4)	71.4 (42.9-100)	X	42.9 (28.6-57.1)	35.7 (28.6-42.9)	46.4 (28.6-57.1)	50.0 (28.6-71.4)
70% better	54	50.0 (42.9-57.1)	64.3 (57.1-85.7)	67.9 (57.1-71.4)	64.3 (57.1-71.4)	57.1 (42.9-71.4)	57.1 (42.9-71.4)	57.1 (42.9-71.4)	X	35.7 (14.3-42.9)	53.6 (42.9-57.1)	32.1 (14.3-42.9)
75% better	59	60.7 (57.1-71.4)	67.9 (57.1-85.7)	67.9 (57.1-71.4)	53.6 (42.9-57.1)	57.1 (42.9-71.4)	64.3 (57.1-71.4)	64.3 (57.1-71.4)	64.3 (57.1-85.7)	X	46.4 (42.9-57.1)	42.9 (28.6-57.1)
80% better	60	67.9 (57.1-71.4)	78.6 (71.4-85.7)	60.7 (42.9-71.4)	60.7 (42.9-71.4)	53.6 (42.9-57.1)	67.9 (42.9-71.4)	53.6 (42.9-71.4)	46.1 (42.9-56.0)	53.6 (42.9-57.1)	X	53.6 (42.9-57.1)
90% better	62	60.7 (42.9-71.4)	78.6 (57.1-85.7)	78.6 (71.4-85.7)	67.9 (42.9-85.7)	50.0 (42.9-57.1)	64.3 (42.9-85.7)	50.0 (28.6-71.4)	67.9 (57.1-71.4)	57.1 (42.9-71.4)	46.4 (42.9-57.1)	X